

# DSIE | 16

PROCEEDINGS OF  
THE DOCTORAL SYMPOSIUM IN  
INFORMATICS AND TELECOMMUNICATIONS  
ENGINEERING

PORTO | PORTUGAL  
FEBRUARY 3RD  
2016

EDITORS:  
EUGÉNIO OLIVEIRA  
A. AUGUSTO SOUSA  
ANÍBAL FERREIRA  
HENRIQUE SALGADO

**Deloitte.**  
**Digital**

**iT GROW**



**HEALTHY SYSTEMS**  
**DOLCE VITA**  
SHOPPING PORTO

**Primavera**  
BUSINESS SOFTWARE SOLUTIONS

**SIEMENS**

**FARFETCH**

**U.PORTO**  
FEUP FACULDADE DE ENGENHARIA  
UNIVERSIDADE DO PORTO

**U.PORTO**

**DEI** Departamento de  
Engenharia Informática

# **Copyright**

Personal use of this material is permitted. However, permission to reprint/re-publish this material for advertising or promotional purposes or for creating new collective works for resale or redistribution to servers or lists, or to reuse any part of this work in other works must be obtained from the editors.

1<sup>a</sup> Edição / 1<sup>st</sup> Edition 2016

Editors: Eugénio Oliveira; A. Augusto Sousa; Aníbal Ferreira; Henrique Salgado

Publisher: FEUP Edições - <http://feupedicoes.fe.up.pt>

ISBN:978-972-752-196-8

Proceedigns Design: Ana Reis

Graphical Design: Carlos Costa, Valter Costa and Ana Reis

Website: Carlos Costa, Valter Costa and Hugo Antunes

Faculdade de Engenharia da Universidade do Porto

Rua Dr. Roberto Frias, 4200-465 Porto

## **DSIE|16 SECRETARIAT:**

Faculdade de Engenharia da Universidade do Porto

Rua Dr. Roberto Frias, s/n

4200-465 Porto, Portugal

Telephone: +351 22 508 21 34

Fax: +351 22 508 14 43

E-mail: [dsie16@fe.up.pt](mailto:dsie16@fe.up.pt)

Symposium Website: <http://www.fe.up.pt/dsie16>



---

## Foreword

The 11<sup>th</sup> Edition of DSIE – Doctoral Symposium in Informatics Engineering, an event usually organized by PhD students of the FEUP Doctoral Program in Informatics Engineering (ProDEI) includes, in the current edition, PhD students of MAP–tele, the Doctoral Program in Telecommunications at the Universities of Minho, Aveiro and Porto.

All the synergies brought by different, however closed related Doctoral Programs, can be seen as an added value to the expected quality of this scientific meeting.

DSIE meetings have been held since the scholar year 2005/06 and the main goal has always been to provide a forum for discussion on, and demonstration of, the practical application of a variety of scientific research issues, particularly in the context of information technology, computer science, computer engineering plus, in the current edition, telecommunications. DSIE symposium comes out as a natural conclusion of mandatory ProDEI course called "Methodologies for Scientific Research" (MSR) leading to a formal assessment of the students learned competencies.

The above mentioned specific course (MSR) aims at giving students the opportunity to learn the processes, methodologies and best practices related to scientific research, particularly in the referred areas, as well as to improve their own capability to produce adequate scientific texts. With a mixed format based on theoretical lessons on the meaning of a scientific approach to knowledge together with multidisciplinary seminars and tutorials, the course culminates with the realization of the DSIE meeting, seen as a kind of laboratory test for the concepts learned by students. In the scope of DSIE, students are expected to play various roles, such as authors of the submitted articles, members of both scientific and organization committees, as well as reviewers, duly guided by senior lecturers and professors.

DSIE event is then seen as a "leitmotif" for the students to be exposed to all facets of a scientific meeting associated with relevant research activities in the areas under consideration. Although still at an embryonic stage, and despite some of the papers still lack of maturity, we already can find some interesting research work or promising perspectives about future work. At this moment, it is not yet essential, nor even possible, for most of the students in the first semester of their PhD, to produce strong and deep research results. However, we hope that the basic requirements for publishing an acceptable scientific paper have been fulfilled.

Each year DSIE Proceedings include papers addressing different topics according to the current students' interests, both from Informatics and Telecommunications Engineering. This year, the tendency is on Smart Sensors and Robotics, Informatics for Health, Data Acquisition & Information Retrieval, Wireless Networks and Optical Communications.

The complete DSIE|16 meeting lasts one day with 5 sessions and includes also one invited talk by an outstanding researcher in Computer Networks security.

---

Professors responsible for the current edition of both ProDEI and MAP–tele Doctoral Programs, are proud to participate in DSIE|16 meeting and would like to acknowledge all the students who have been deeply involved in the success of this event that, hopefully, will not only contribute for a better understanding of the themes that have been addressed during the above referred course, but also promote the best scientific research methods and the good practices for writing scientific papers and conveying novel ideas.

February 03, 2016  
Porto

**Eugénio Oliveira and A. Augusto Sousa (ProDEI)**  
**Aníbal Ferreira and Henrique Salgado (MAP–tele)**

---

## **Foreword – Organization and Scientific Committees**

The organization and scientific committees welcome you to the 11th Edition of the Doctoral Symposium in Informatics Engineering – DSIE|16. This edition is a joint effort of both the students of the Doctoral Program in Informatics Engineering (ProDEI) and the Doctoral Program in Telecommunications (MAP-tele). The symposium is very relevant for the students, since it provides the opportunity to be involved in all the steps of a scientific conference organization, namely its conception, preparation, scientific papers writing, evaluation and presentation. We would like to thank all the Professors that have helped us through all this process, namely the members of the Steering Committee and the senior members of the Scientific Committee. We would also like to thank the sponsors, as well as Pedro Silva and Sandra Reis of the Department of Informatics Engineering of FEUP for their priceless help in all the logistic support. Last but not least, we want to thank all the participants in DSIE|16.

February 03, 2016  
Porto

**Bruno Lima, Jaime Silva**  
(Organization Committee Chairs)  
**André Pilastri, Orangel Azuaje and Rui Pinto**  
(Scientific Committee Chairs)



---

# Conference Committees

**Steering Committee**

Eugénio Oliveira  
A. Augusto Sousa

**Organization Committee Co-Chairs**

Bruno Lima  
Jaime Silva

**Scientific Committee Co-Chairs**

André Pilastri  
Orangel Azuaje  
Rui Pinto

**Organization Committee**

Carlos Costa  
Hugo Antunes  
Jonas Queiroz  
Luís Neto  
Rui Sarmento  
Valter Costa

---

### **Scientific Committee**

Abel Costa	Alex Araújo
Ana Aguiar	André Pilastri
Ana Paiva	Asad Rehman
Ana Rocha	Bruno Lima
Carlos Soares	Carlos Costa
Daniel Silva	Carlos Gulo
Francisco Vasques	Celestino Martins
Henrique Cardoso	Danilo Jodas
Henrique Salgado	Eduardo Almeida
João Cardoso	Emanuel Lima
João Sousa	Hugo Antunes
João Tavares	Jaime Silva
Jorge Barbosa	Joana Tavares
Jorge Silva	Jonas Queiroz
José Baptista	Luís Neto
Luís Almeida	Orangel Azuaje
Luís Pessoa	Roberta Oliveira
Manuel Ricardo	Rui Pinto
Miguel Monteiro	Rui Sarmento
Paulo Costa	Sherif Busari
Paulo Portugal	Stephen Ogodo
Pedro Brandão	Thiago Rúbio
Ricardo Morla	Valter Costa
Rosaldo Rossetti	
Rui Maranhão	
Sérgio Crisóstomo	

---

# Invited Speaker

## Luis Filipe Antunes

Luis Filipe Coelho Antunes, Associate Professor and Chair of the Computer Science Department at Faculty of Sciences, University of Porto (FCUP). Director of the Competence Centre for Cybersecurity and Privacy, University of Oporto. Senior researcher at INESC Tec. Member of the Scientific Council of FCUP and member of the Council for Electronic Administration at the University of Porto. Develops research activity in the field of computer security has several scientific publications, successfully guided 5 PhD students and belongs to several research projects funded by FCT. Has exercised consultancy activity in the area of computer security for the Ministry of Health and the Portuguese Data Protection Commission, is accredited by the National Security Cabinet and is expert at ENISA (European Union Agency for Network and Information Security) in the area of eID and eGovernment eHealth. Luis Antunes appears regularly on TV program as information security expert. In 2013 co-founded a spin-off from the University, called HealthySystems that centers its activity in the area of information security with a strong focus on auditing, eID and anonymization techniques. Recently co-founded the University of Porto spin-off Adyta. Adyta main objective is to promote specialized security solutions tailored to the needs of sovereign bodies dealing with sensitive or classified information and large business groups. Adyta focuses its activity in the defense field and securing communications through innovative solutions and adjusted to each customer. This spin-off is the result of several years of collaboration with the Portuguese National Security Agency.

### Invited Talk:

#### Cyber–sovereignty: sovereignty in a world without borders

**Abstract:** The internet is global by nature and unhindered by physical borders, network technologies challenge the existing concept of sovereignty, where each sovereign jurisdiction regulates communication that takes place in its territory. Bypassing geographical and jurisdictional restraints, the internet is a serious concern for the traditional notion of sovereignty. In cyberspace it is technically possible to operate anonymously threatening interconnected targets around the globe, there is extensive discussion as to whether the concept of borders is relevant to the challenges of cyber security as they define the territory in which national governments can employ sovereign measures. In this talk we will cover technological aspects of cyber-sovereignty that should be considered in any nation cyber-security strategy.



---

# Contents

Implementation of Reconfigurable and Adaptive TDMA for Multi-Hop Ad Hoc Networks .....	1
Eduardo Nuno Almeida and João Dias	
An Architecture Solution for Calculating and Monitoring Radiation Dose in Healthcare Area .....	13
Hugo Miguel Silva Antunes	
Analysis of End-to-End Delay in Fading Channels using Stochastic Network Calculus .....	27
Orangel Azuaje	
Zigbee and Arduino-Based Data Acquisition System for Precision Agriculture.....	39
Sherif A. Busari, Abibat F. Dunmoye and Kayode F. Akingbade	
Real-Time Vision System for Lane Tracking and Semaphore Recognition .....	49
Valter Costa	
A Model-Driven Approach for Components Testing.....	61
Bruno Lima and João Pascal Faria	
DisToNet: Disconnection Tolerant Mobile Ad Hoc Networks .....	73
Emanuel Lima, Pedro Brando, Orangel Azuaje, Ana Aguair	
Digital Chromatic Dispersion Equalization in Coherent Optical System .....	85
Celestino Martins, Fernando P. Guiomar and Armando N.Pinto	
Recognition of Banknotes in Multiple Perspectives Using Selective Feature Matching and Shape Analysis .....	95
Carlos M. Costa	
Optimizing Network Calls by Minimizing Variance in Data Availability Times .....	107
Luis Neto	

---

Visible Light Communication – A Brief Survey .....	117
Stephen O. Ogodo	
Reconstruction Algorithms in Compressive Sensing; An Overview .....	127
André Luiz Pilastri and João Manuel R. S. Tavares	
Robot Self-Localization Based on Sensor Fusion of GPS and iBeacons Measurements .....	139
Rui Pinto, Filipe Neves dos Santos, Armando Sousa	
A Multi-Agent System for Micro Grids Energy Production Management Supported by Predictive Data Analysis .....	151
Jonas Queiroz, Paulo Leitão and Artur Dias	
Cooperative Spectrum Sensing with Energy Detection in Cognitive Radio Networks .....	163
A. U. Rehman	
Topic Modeling – A Case Study with Scientific Production .....	175
Rui Sarmento	
A Review of Recent Developments in Abstractive Summarization Techniques .....	187
Jaime Reis Silva	
Phase Conjugated Twin Waves Based Transmission in Few-mode Fibers .....	197
J. S. Tavares, L. M. Pessoa and H. M. Salgado	

# Implementation of Multi-Hop Routing in Reconfigurable and Adaptive TDMA for Ad Hoc Networks

Eduardo Nuno Almeida and João Dias

Faculdade de Engenharia da Universidade do Porto, Porto, Portugal  
{ee10136, ee10126}@fe.up.pt

**Abstract.** Small teams of cooperating robots, organized in ad hoc networks, are being deployed in many applications, where frequently nodes are sending live video streams to a remote station. In order to reduce the end-to-end delay and jitter, an optimization to the Reconfigurable and Adaptive Time-Division Multiple Access (RATDMA) was proposed, enabling multi-hop routing within TDMA time-slots. To complement and validate the results obtained in the simulation, we propose an implementation of the optimization in real devices, based on a previous implementation provided by the authors of the original paper, in addition to a testbed to evaluate the results obtained. The results of this implementation show a reduction of the end-to-end delay and jitter between end nodes, thus enabling the transmission of live video streams with acceptable quality.

**Keywords:** Wireless networks · Reconfigurable and Adaptive TDMA · Multi-hop routing · Video streaming

## 1 Introduction

Teams of cooperating robots are being used in many applications, such as civil and military operations [6]. Due to the mobility of the robots, these teams are organized in small decentralized mesh networks, presenting significant advantages, such as extended range of communications and greater flexibility in its operation. In some applications, it is necessary for one robot to send multimedia content in real-time to another node in the network. One popular example includes robots sending live video streams of their cameras to a remote operator conducting the mission [4]. In order for the video streams to have good quality, the end-to-end delay between the end nodes, as well as the jitter between consecutive video frames, must be kept at a minimum level. However, due to the mobility of the robots within the ad hoc network, the links between them are constantly being changed, which affects the topology of the network and, consequently, the routes followed by the packets, thereby affecting these metrics throughout the course of the mission.

In order to minimize this problem, in [5] a novel Time-Division Multiple Access (TDMA) protocol is proposed – Reconfigurable and Adaptive TDMA (RATDMA). This protocol consists in an adaptive TDMA scheduling algorithm, which is able to automatically reconfigure the TDMA round according to the number of nodes in a small ad hoc network, in a fully distributed way without requiring clock synchronization. Using this approach, the probability of collisions between nodes is minimized, at the cost of a larger end-to-end delay [1]. This work is further extended in [2], where the authors propose a global synchronization protocol for RATDMA, while also disseminating the network topology information among all nodes, using a RF ranging mechanism and without global knowledge, namely clock synchronization. In [1], a novel approach for multi-hop routing in ad hoc networks within TDMA slots is proposed. Contrary to traditional TDMA, where each node only transmits / forwards packets in its own slot (single-hop per time-slot), in this approach every node in the network can forward received packets in the time-slot of the node that initiated the transmission. On the other hand, the routing protocol is based on the Dijkstra's algorithm, where the network topology is sent within the synchronization messages [2]. This approach reduces the end-to-end delay in a multi-hop ad hoc network, as proved by the simulation results, while preserving the benefits of TDMA scheduling algorithm, hence enabling the streaming of multimedia content between 2 nodes [1].

To complement and validate the results obtained in the simulation, we propose an implementation of the multi-hop per time-slot optimization in the RATDMA protocol in real devices, based on an previous implementation provided by the authors of the original paper [1]. This optimization enables a reduction in both the average end-to-end delay and jitter between consecutive video frames, which allows the transmission of live video streams in a small ad hoc network with acceptable video quality. Additionally, in order to validate the implementation and collect results regarding its performance in real use-case scenarios, an experimental testbed was also developed.

The remainder of this article is organized as follows. Section 2 describes the implementation of the optimized protocol. Section 3 presents the implemented testbed to validate and analyze the performance of the developed protocol. The analysis of the obtained results is performed in Section 4. Finally, Section 5 concludes the paper and presents future work guidelines.

## 2 Implementation of RATDMA Multi-Hop per Time-Slot Optimization

In order to implement the optimization of multi-hop routing within TDMA time-slots in the RATDMA protocol proposed in [1], we started with a previous implementation that already contained some adaptations for the multi-hop scenario, provided by the authors of the original paper [1]. This includes the constant update of the connectivity matrix, where the update is performed during the protocol's synchronization stage in the beginning of each time-slot. Our contribution consisted in the implementation of the routing protocol, along with

the necessary corrections detected in the existing implementation. Both of these topics will be explored in the following subsections.

The interaction between the RATDMA protocol and both the physical interfaces and the application is described in Fig. 1. The protocol creates a virtual interface TAP that communicates with the application through sockets, and with the routing protocol through the `read()` and `write()` UNIX system calls. Then, the protocol communicates with the wireless physical interface using raw sockets. Additionally, the TAP interface shares a direct link with the physical interface using a set of predefined functions contained in the developed TAP2ETH class.

After this initial configuration, the protocol acquires full control of all traffic passing through the Wireless Local Area Network (WLAN), processing it and deciding the interface where the packet should be forwarded to. Packets generated by and destined to the application are forwarded to the TAP interface, whereas packets received by the node that should be forwarded to another node are only processed by the routing protocol.

The following sections present the changes made to the original implementation, with the objective of finishing the implementation of the solution proposed in [1].

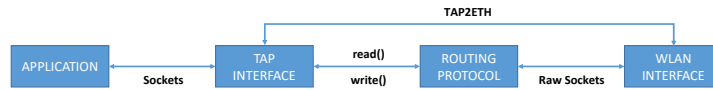


**Fig. 1.** Internal communication architecture of the implemented protocol.

## 2.1 Forwarding

In the ad hoc mode, each node must calculate the route of a given packet to its destination. In order to avoid collisions when using the multi-hop communication mechanism in the same time-slot, the node must also determine, for each packet sent, the time interval needed for the packet to reach its final destination. Therefore, the node can only send a new packet after this time interval, since at each moment only one packet may be transmitted / forwarded in the entire network. As a consequence, each node must, not only know the next-hop, but also the total number of hops to reach a given destination. Thus, each node needs to maintain an updated routing table containing the next-hop for any packet sent by a given node and destined to another node in the network. As such, this routing table is a  $N \times N$  matrix, in which  $N$  is the total number of nodes in the network, built based on the informations collected by each node about the network topology.

The network topology informations are stored in a  $N \times N$  connectivity matrix, which contains a boolean value representing the status of a direct link between any pair of nodes in the network. In order for the routing protocol to correctly

update its routing table, this matrix is updated by the RATDMA protocol in the beginning of each time-slot, after the synchronization between all network nodes. Using this information, we implemented the Dijkstra's algorithm, in order to update the routing table with the shortest path between any pair of nodes in the network. Therefore, when processing a packet, it is possible to inform the protocol about the next-hop where the packet should be forwarded to, so that it can reach its final destination using the shortest path. Another alternative to solve this routing problem without an auxiliary routing table was also considered. Instead of running the Dijkstra's algorithm in the beginning of each time-slot to build / update the node's routing table – proactive routing –, for each packet sent by the node, the Dijkstra's algorithm is executed to determine the shortest path to reach the packet's final destination – reactive routing.

However, since the total number of nodes in the network is generally very small, we chose the proactive routing approach, due to the low memory usage by the routing table and a decreased latency when forwarding the packets, as a result of a simple lookup table instead of the execution time of a full Dijkstra's algorithm. Additionally, since the routing table is only recalculated if the connectivity matrix changes, which generally should not occur very often (as such situation would significantly decrease the performance of the whole protocol), the overhead of updating the routing table is minimized.

## 2.2 Multi-hop Communication in the Same Time-slot

To solve the latency problem, the mechanism proposed in [1] indicates that a given node, when receiving a packet to forward, should use the current time-slot of the packet's transmitter node to forward it to the next-hop. In this way, a packet can be forwarded through multiple hops, using just one time-slot, hence significantly reducing the end-to-end delay. For this mechanism to be correctly implemented, when receiving a message to forward, the node needs to know when the current time-slot began, when will it end and the time interval needed to reach the packet's next-hop. Using this information, it is possible to determine if the node still has sufficient available time in the current time-slot to forward the packet to the correspondent next-hop, or, if it should be queued and scheduled to be retransmitted in the node's own time-slot.

The main challenge in the implementation of this solution consisted in the determination of the current time-slot at the moment a new packet arrived at the node. Due to the fact that every node may forward the packet in the current time-slot or queue it, if there is not sufficient available time to transmit it in that time-slot, two cases must be considered. In the first case, when the received packet was transmitted in the packet's original transmitter time-slot, the current time-slot corresponds to the packet's original transmitter, which is determined by the source IP address. However, when an intermediate node transmits a previously queued packet in its own time-slot, there is no available information in the packet to determine the intermediate's node, and thus its time-slot, since the packet's source IP address corresponds to the original node

(which remains the same) and the source MAC address is always equal to the previous node's address.

One possible solution to solve this problem consists determining the current time-slot using the informations that are always available to every node, namely the current time, the initial time of the node's own time-slot and the duration of a time-slot. However, this solution does not provide sufficient accuracy and, hence, reduces the protocol's efficiency. Therefore, the solution we implemented consisted in the insertion of a byte in the Ethernet frame, indicating the global ID (last byte of the IP address) of the node that started the transmission or retransmission of the given packet, within a given time-slot. This additional field is, thus, inserted in the frame when it is received by the protocol, originated in the application, and it is removed when the message reaches its final destination, before being sent to the application. Hence, the value of this field is only updated in two situations: i) when the node that originated the message sends it for the first time and ii) when an intermediate node queues the packet and schedules it to transmit in the node's own time-slot. Therefore, this solution solves the mentioned problem, while maintaining the transparency of the protocol. Using this extra byte, every node can immediately determine the node that started the (re)transmission of a given received packet and, therefore, the current time-slot. Using this information, the node can then determine if the current time-slot still has sufficient available time to forward the packet or if it should be queued and scheduled to be retransmitted in the node's own time-slot.

**Determination of the Packet's Transmission Time:** The time interval needed to transmit a given packet is presented in Eq. (1) [1], where  $t_{DIFS}$  represents the DCF Inter Frame Spacing (DIFS), which is the period of time in which the node senses if the medium is free,  $t_{Backoff}$  is the random backoff time (applied when the medium is sensed busy), and  $t_{Preamble}$  is the preamble of the frame, which signals the beginning of the frame. With the exception of the  $FrameSize$ , all of the remaining values are constant and were taken from [1], which correspond to the typical parameters of IEEE 802.11g. Therefore, every wireless interface was configured to use a fixed bitrate of 11 Mbit/s.

Although the Linux Operating System (OS) internally handles every frame as an IEEE 802.3 (Ethernet) frame, the OS correctly converts the frame to the correspondent protocol, depending on the physical interface to which the frame is sent, immediately before the frame's transmission. Therefore, the  $FrameSize$  field consists, in addition to the frame's payload size, to the size of the IEEE 802.11 (Wi-Fi) header, instead of the IEEE 802.3 (Ethernet) header.

$$t_{Frame}(Frame\ Size, Bitrate) = t_{DIFS} + t_{Backoff} + t_{Preamble} + \frac{Frame\ Size \times 8}{Bitrate} \quad (1)$$

### 3 Testbed

To validate our implementation and collect statistical results regarding its performance in a real scenario and measure the achieved gains, relative to the non-optimized version of the protocol in these networks, it was also necessary to design and implement a testbed.

In that sense, 6 PCs running the Debian 7.1 Wheezy OS, equipped with a IEEE 802.11 (Wi-Fi) wireless card and an IEEE 802.3 (Ethernet) network card were used. These 6 stations establish between them a wireless ad hoc network – using the wireless interfaces –, whilst being also connected in a Local Area Network (LAN) to a switch. Since these PCs have a good-quality link to every other PC, the network topology was implemented configuring every PC's firewall (e.g., IPTables) to only allow direct communication with neighbor PCs. This was achieved through a bash script, that dynamically blocks all MAC addresses from non-neighbor PCs and allows only the MAC addresses of neighbor PCs, according to a specified topology.

#### 3.1 Test Application

In order to evaluate the protocol's performance in the considered scenarios, a test application was developed in Java. This application, divided in client (i.e., transmitter) and server (i.e., receiver), creates 2 sockets connecting the transmitter to the receiver. One socket is established using the LAN interfaces, whereas the other socket connects both PCs using the wireless interfaces, which were previously joined in the same ad hoc network. Since different PCs have different clocks, in order to improve the accuracy of the hop-to-hop time interval, every packet exchanged by the nodes is transmitted through the wireless socket, while simultaneously sending a duplicate of the same packet through the LAN socket. Since the LAN connections between any pair of PCs uses FastEthernet (100 Mbit/s) interfaces and cables, the transmission time through the LAN socket is considered to be approximately 0. Therefore, the transmission time of a given packet is approximately equal to the time when that packet was received in the LAN socket. On the other hand, the transport protocol used for both sockets is UDP, since it does not add additional overheads, due to flow-control mechanisms and retransmissions, which may affect the accuracy of the results obtained.

In every test scenario, the objective of the client is to send an image (i.e., a video frame) at a given frequency (i.e., framerate (FR)), in order to simulate the transmission of a video stream between the client and the server. Since the transport protocol is UDP, it is the client application's responsibility to fragment the image in several smaller packets (if needed), being reconstructed and reordered by the server application. During the video transmission, the server application saves the ID of each packet received in the LAN socket and the respective timestamp in a Hash Table. Another Hash Table saves the IDs of the packets received with no errors by the wireless socket, along with the correspondent timestamp. By comparing both tables, it is possible to calculate relevant metrics to analyze the performance of the protocol, as described in

Section 3.2. To correctly identify each frame, as well as each composing fragment, a specific protocol for the exchanged frames was developed for the exchange of the video frame's fragments between the client and the server, which consists in the payload (1495 Bytes), in addition of the video frame ID (2 Bytes) and the fragment ID (2 Bytes), which is presented in Fig. 2.

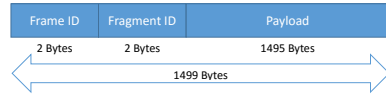


**Fig. 2.** Message protocol between the client and server test applications.

### 3.2 Performance Evaluation Metrics

To evaluate the performance of the protocol, 3 metrics were used.

- Frame's error rate.
- Packet's Propagation Delay (PPD): calculated through the difference between each pair of video frame's fragment timestamps (TS) received in both sockets, represented in Eq. (2). This calculation assumes that the server application correctly orders the received frames, since the UDP protocol does not ensure this property.

$$PPD = TS_{Frame \#i_{WLAN}} - TS_{Frame \#i_{LAN}} \quad (2)$$

- Delay between Consecutive Frames (DCF) (i.e., jitter): calculated as the difference between the timestamps (TS) of consecutive frames received in the wireless socket relative to the transmitter's frame-rate (FR). This calculation is performed after the reconstruction of the entire video frame by the server application, as represented in Eq. (3). As such, positive values indicate that the frames arrived later than the theoretically expected, whereas negative values indicate that the frames arrived earlier than expected.

Using this data, it is also possible to obtain additional metrics, such as the percentage of video frames received with a delay greater than: i) 2 FPS - "Bad" quality, ii) 10 FPS - "Acceptable" quality and iii) 18 FPS - "Good" quality (minimum framerate for a fluid video quality perceived by the human eye) [3].

$$DCF = \frac{TS_{Frame \#i+1} - TS_{Frame \#i}}{Transmitter FR} \quad (3)$$

### 3.3 Tests

The tests conducted to evaluate the performance of the implemented protocol are based on real use-case scenarios, using a TDMA round of 500 ms and a bit-rate of 11 Mbit/s. Despite transmitting a (simulated) video stream in every test, these could also be applied to generic multimedia content, since their stream quality is susceptible to network delays. Moreover, we chose to transmit in every test a video stream, since this multimedia content has stricter quality limits. The tests are explained in the following sections.

**Test 1 - Performance vs. Number of Hops:** The first test's main objective is to compare the developed protocol – RATDMA optimized for ad hoc networks (multi-hop / time-slot) – against the RATDMA without optimization – single-hop / time-slot. Therefore, a transmitter separated by  $n$  hops to the receiver sends 1000 equal images, which are fragmented in 4 separate fragments, at a framerate (FR) of 25 Frames Per Second (FPS). This scenario simulates the transmission of a video stream with a FR greater than the minimum FR necessary for the human eye not to perceive lag (18 FPS). Two series of tests will be conducted: one using the optimized and another using the non-optimized version of the protocol. The results of the tests allow the determination of the FR received in the server and, thus, the evaluation of the perceived video quality on the server, for both versions of the protocol.

**Test 2 - Performance vs. FR of Transmitter:** The objective of the second test is to evaluate the behavior of the optimized version of the protocol, according to the FPS used in the transmitter and its distance to the receiver (i.e., number of hops). In that sense, a transmitter, separated by  $n$  hops to the receiver, sends 100 equal images, which are fragmented in 4 packets, at a variable FR of 2, 5, 10 and 25.

**Test 3 - Performance vs. Network Load:** The third test enables the evaluation of the behavior of the optimized version of the protocol according to the load imposed on the network, that is, the number of clients simultaneously transmitting. In that sense,  $n$  transmitters sending 200 equal images, which are fragmented in 4 packets, are deployed according to a linear topology.

## 4 Test Results

After performing the tests described in Section 3, the correspondent results are analyzed in the following sections. In these analyzes, all presented delays were measured at the application layer of the OSI reference model. Additionally, each test was only run once. On the other hand, in almost all tests the frame's error rate is approximately 0, as expected, since these tests were performed in a controlled environment.

#### 4.1 Test 1 - Performance vs. Number of Hops

Analyzing the results from test 1, presented in Fig. 3, it is possible to verify that the average delay of the received frames increases with the number of hops, as theoretically expected. Indeed, in an ad hoc network with linear topology, where the transmitter and the receiver are located in the extremities of the network, the packets sent by the transmitter need to be forwarded by all intermediate nodes (i.e., relays), thus increasing the end-to-end delay measured at the application layer. Therefore, for 1 hop, both versions of the protocol display similar results, since in both cases the final destination of the packet is a neighbor of the transmitter, hence not revealing any influence of the optimization implemented in the protocol. On the contrary, starting with 2 hops, a significant reduction of the packet's end-to-end delay in the optimized version of the protocol relative to the non-optimized one is observed, which is explained by the forwarding of the packet in the same time-slot of the original transmitter, instead of waiting for the intermediate node's time-slot. Moreover, beginning with 2 hops, the delay of the optimized version increases, due to the fact that some frames do not fit within the time-slot and, thus, have to be queued in intermediary nodes.

The results obtained in this test confirm the results obtained in the computational simulation presented in [1]. In fact, analyzing the results of [1], where the solution is originally presented, we can conclude that, for 1-hopped transmissions, the behavior of the protocol with and without the optimization is very similar, showing small performance increases with the optimization, as we verified experimentally. The difference observed in the delays between both approaches hits its maximum value for 2 hops in simulation, just as our experimental test. For 3 and 4 hops, that difference decreases, while the optimized version of the protocol still exhibits significantly smaller delays relative to the non-optimized version, which is confirmed by the results obtained in our experimental testbed.

The analysis of the average delay of consecutive frames, measured relative to the FR used in the transmitter (25 FPS), indicates that the implemented optimization of the protocol provides, in average, higher delays relative to the non-optimized version of the protocol. This effect is due to the algorithm used by the optimized protocol, which allows the transmission of several packets through multiple hops during the same time-slot, which, not only reduces the end-to-end delay, but also reduces the amount of packets circulating in the network at the same time (i.e., throughput). As a consequence, the receiver receives less frames per time-unit (smaller FPS), although with a smaller end-to-end delay. In fact, in the optimized version of the protocol's worst case scenario, the FR of the received video is  $FR = 1 / ((1/25 \text{ FPS}) \times (1 + 2.60\%)) = 24.37 \text{ FPS}$ , which occurs for 3 hops, whereas in the non-optimized version's worst case scenario, the FR is given by  $FR = 1 / ((1/25 \text{ FPS}) \times (1 + 2.45\%)) = 24.40 \text{ FPS}$ . This analysis allows the conclusion that both protocols provide a fluid video quality.

In Fig. 4 the percentage of consecutive frames that were received with a delay greater than the equivalent time interval to 18 FPS, that is, with  $FR = 1/18 \text{ FPS} = 55.56 \text{ ms}$  are presented.

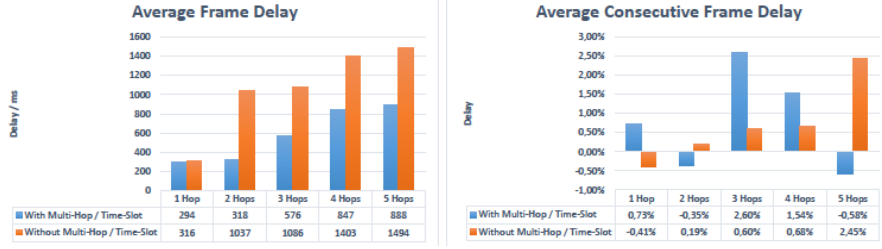


**Fig. 3.** Comparison of the protocol's performance with and without optimization, according to the number of hops.

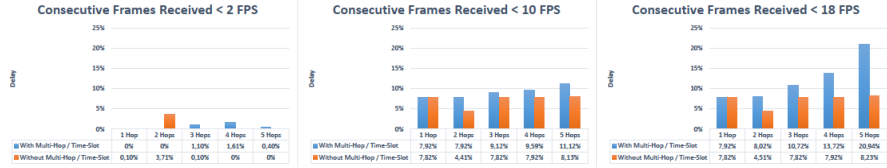


**Fig. 4.** Comparison of the protocol's performance with and without optimization, regarding the percentage of frames received with a FR less than a given threshold.

#### 4.2 Test 2 - Performance vs. FR of Transmitter

Analyzing the results of test 2, presented in Fig. 5, it is possible to observe that, as in test 1, the packet's average end-to-end delay increases with the distance separating the transmitter and the receiver, as well as the transmitter's used FR, as theoretically expected. In fact, until 10 FPS, the delay is similar to all distances (i.e., number of hops), showing a significant difference for 25 FPS. The analysis of the results for the average consecutive frame's reveal that, for FRs lower than 10 FPS, the delay relative to the transmitter's FR is negative, indicating that these are received before being played. On the contrary, starting from 10 FPS, the average delay is positive, indicating a delay in the reception of the frames relative to the time instant that these should be played, being 25 FPS the worst case of the test.

#### 4.3 Test 3 - Performance vs. Network Load

The results obtained on test 3 are presented in Fig. 6. Analyzing them, it is possible to verify that, as theoretically expected, the packet's average end-to-end delay increases with the increase of the load imposed on the network (i.e., the number of simultaneous transmitters). In fact, since the ad hoc network is configured in a line topology, the increase of the load imposed on the network implies that each intermediate node will have a greater number of packets to forward, both on the current time-slot and the own node's time-slot. On the other hand, since in this protocol only 1 packet can circulate on the network in

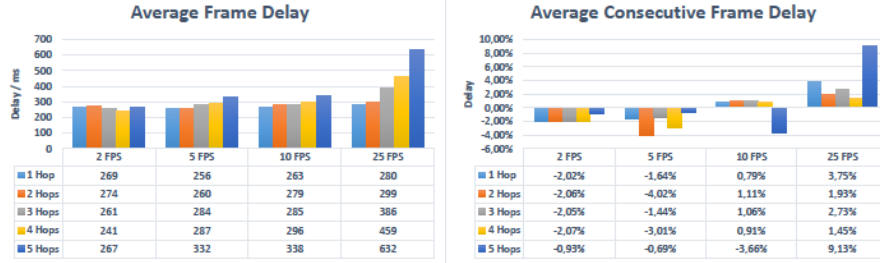


**Fig. 5.** Comparison of the optimized protocol's performance, according to the transmitter's FR and for different number of hops.

each instant, the remaining packets will suffer an increased delay in the internal buffers of each node, translating into a generalized increase in the average end-to-end delay.

Similarly, the average delay of consecutive frames, relative to the FR of the original transmitter, increases with the number of clients simultaneously transmitting, since, for the same reason, the frames (i.e., packets) can be queued in the buffers of the intermediate nodes, due to not being able to be transmitted in the current time-slot. This effect results in an increased frame's average delay, translated into a smaller FR relative to the original transmitter. However, observing the average consecutive frame delay, we can conclude that, with the exception of the case with 5 transmitters with 20 FPS, the delay is globally negative, indicating that the received FR is similar to the original transmitter's.

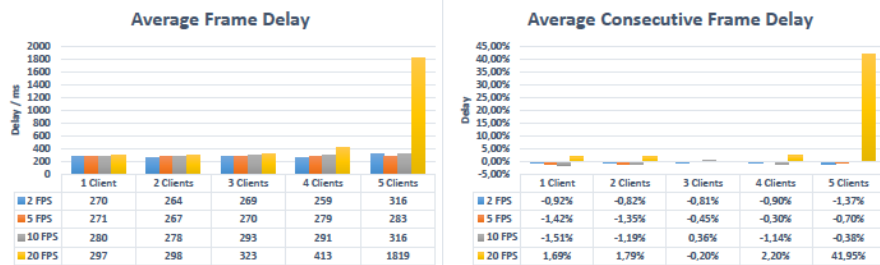


**Fig. 6.** Comparison of the optimized protocol's performance, according to the transmitter's FR and the number of clients simultaneously transmitting.

## 5 Conclusion

In this paper, we implemented the optimization of multi-hop routing within TDMA time-slots on real devices, based on a previous implementation provided

by the authors of the original paper. The results showed that the multi-hop per time-slot approach provides lower end-to-end delays, measured at the application layer, relative to the single-hop per time-slot approach. However, the delay between received consecutive frames is higher, since some packets may be queued by intermediate nodes. As a result, the packets are received with a lower latency, but in bursts, instead of a continuous stream. Thus, this approach can be used in real use-case scenarios, such as the transmission of a live video stream with an acceptable quality, between two nodes in the network, in small robot teams of no more than 10 robots. As future work, we propose the execution of the tests in an experimental testbed, using mobile PCs / Raspberry Pi to actually generate the required network topology without the use of firewall rules.

## References

1. Oliveira, L., Almeida, L., Lima, P.: Multi-hop routing within tdma slots for teams of cooperating robots. In: Factory Communication Systems (WFCS), 2015 IEEE World Conference on. pp. 1–8. IEEE (2015), [Based on a 2014 draft]
2. Oliveira, L., Almeida, L., Santos, F.: A loose synchronisation protocol for managing rf ranging in mobile ad-hoc networks. In: RoboCup 2011: Robot Soccer World Cup XV, pp. 574–585. Springer (2012)
3. Read, P., Meyer, M.P.: Restoration of motion picture film. Butterworth-Heinemann (2000)
4. Rosário, D., Zhao, Z., Braun, T., Cerqueira, E., Santos, A., Alyafawi, I.: Opportunistic routing for multi-flow video dissemination over flying ad-hoc networks. In: A World of Wireless, Mobile and Multimedia Networks (WoWMoM), 2014 IEEE 15th International Symposium on. pp. 1–6. IEEE (2014)
5. Santos, F., Almeida, L., Lopes, L.S.: Self-configuration of an adaptive tdma wireless communication protocol for teams of mobile robots. In: Emerging Technologies and Factory Automation, 2008. ETFA 2008. IEEE International Conference on. pp. 1197–1204. IEEE (2008)
6. Wang, J., Lewis, M., Scerri, P.: Cooperating robots for search and rescue. In: Agent Technology for Disaster Management Workshop at AAMAS. vol. 6 (2006)

## An Architecture Solution for Calculating and Monitoring Radiation Dose in Healthcare Area

Hugo Miguel Silva Antunes<sup>1</sup>

<sup>1</sup>Faculty of Engineering, University of Porto  
Rua Dr. Roberto Frias, s/n 4200-465 Porto, Portugal  
hugoantunes@hotmail.com

**Abstract.** The radiation dose values calculation and monitoring that come from the Imaging equipments, has suffered over the past few years a few iterations. Currently, it is through objects named DICOM Structured Reports (DICOM SR) and Dose Reports, created by the equipments, that is possible to extract this information. The aim of this paper is to propose and analyze a tool based on DICOM standard principles, which retrieve DICOM SRs from Picture Archive and Communication System (PACS), process the content of this objects and provides respective radiation dose values. This tools was tested in a real hospital environment, retrieving Computed Tomography SRs from local PACS institution. From the tests and analysis performed, it was possible to realize that the architecture proposed presents excellent results and accuracy comparing with the techniques traditionally used. It was possible to understand that the proposed architecture solution based on interaction between PACS and the developed tool is the newest and more efficiently mode of monitoring and calculating the radiation dose values in the radiology examinations.

**Keywords:** DICOM · Radiation Dose · Medical Informatics · Radiation Dose Structured Reports · Dose Reports

### 1 Introduction

Radiation dose for diagnostic medical imaging examinations has recently come under intense scrutiny, triggered by media coverage of overexposures in Computed Tomography (CT) by some newspapers and by recent epidemiological studies on radiation dose and risks[1].

The health industry is moving toward safer and more effective diagnostic imaging by using optimized acquisition protocols, implementing dose-reduction technologies, measuring and reporting dose indices, participating in dose registries, identifying reference dose standards, and providing feedback to identify outliers and optimize the utilization of ionizing radiation. The goals are to reduce corresponding risks of radiation, choose the most appropriate exam, render an accurate diagnosis, and provide the best patient care as safely as possible. Part of this effort involves raising awareness of imaging examination dose metrics on the part of the interpreting physician, referring phy-

sicians, technologists, medical physicist, caregivers, administrators, and others involved in the oversight of medical imaging. Retrieving and using this information is an informatics challenge, which requires knowledge of the Digital Imaging and Communications in Medicine (DICOM) standards[2]. In addition, an understanding of the corresponding relevant metadata and structured reporting objects is required, as well as of efforts of the Integrating the Healthcare Enterprise (IHE) organization in describing the radiation exposure monitoring (REM) profile to identify the relevant parameters and information to be extracted [3].

Informatics plays a crucial role in providing information on radiation dose delivered to patients during an exam, the dose distributions for specific protocols, and identifying and comparing the current delivered dose to the mean dose at an institution, local area, or in regional and national registry databases. Many challenges arise in the area of informatics, including measuring and extracting radiation dose metrics per exam; using standards to gather/store information (DICOM metadata and DICOM Structured Reports) and template information; tracking patient radiation dose histories; accumulating dose per patient; decision making for future imaging exams[4].

## 2 State of the Art

In recent years, various methods of dose monitoring and analyzing have been introduced, for example, DICOM Structured Reports, DICOM modality performed procedure step (MPPS) messages, and image recognition and usage of the DICOM header. The DICOM standard was introduced in 1993. It was initially established to store and share medical images and image-related data and to provide a structured way to organize radiological reports. Despite ongoing discussions regarding the value and utility of the DICOM Structure Reports (SR), the DICOM standard is today an essential part of almost every medical devices using ionizing radiation [7]. The DICOM radiation dose structured report (DICOM RDSR) provides radiation dose parameters within the DICOM SR allowing for automated analysis of dose related data. CT related dose parameters (volume computed tomography dose index – CTDI<sub>vol</sub> and dose length product – DLP) for all examinations are stored in the DICOM SR [8].

### 2.1 Dose Reports Optical Character Recognition

One of the more familiar ways for radiologists to access CT radiation output data is via dose reporting screen – secondary capture images in the DICOM CT object where the volume CT dose index and the Dose Length Product values for the study have been “burned in”. These images are assigned a unique series number, and have a DICOM header associating them with the imaging study. Unfortunately neither the layout nor the information displayed in the image is standardized among vendors. Getting this information out of the image and into a database presents a challenge. Optical Character Recognition (OCR) is typically required to extract useful information, a difficult process which requires error correction algorithms to account for split-text and misidentifi-

fied characters, resulting in a data set that may not be 100% accurate. The lack of structured content, information sparseness and difficulty of accurate data extraction make this avenue of data collection far from ideal [9]. Fig. 1 shows an example of a CT Dose Report.

Patient Name:	xam no: 30312				
Accession Number:	Sep 01 2010				
Patient ID:	LightSpeed VCT				
Exam Description:	CT CTA CHEST WO & W CO				
<b>Dose Report</b>					
Series	Type	Scan Range (mm)	CTDIvol (mGy)	DLP (mGy·cm)	Phantom cm
1	Scout	-	-	-	-
2	Scout	-	-	-	-
200	Axial	\$223.250-\$223.250	4.72	2.36	Body 32
3	Helical	\$348.250-\$13.250	25.72	980.67	Body 32
3	Helical	\$519.000-\$284.000	10.90	306.58	Body 32
Total Exam DLP:		<b>1289.61</b>			

**Fig. 1.** Example of Computed Tomography Dose Report

## 2.2 DICOM Image Headers

Medical images contain a DICOM header describing technical parameters and device attributes associated with the creation of an image, e.g. x-ray generator energy setting (kVp), exposure (mAs), collimation width, pitch factor and slice location. This information can be collected to gain a detailed understanding of the acquisition process. However, the image header is not as ideal place for the storage of dose information. Images may be sent to PACS prior to study completion, original thin-slice data may never be sent, but rather reconstructed into thicker slices or other viewing planes, and others can result in under or over counting of dose, particularly when data is retrieved from PACS and there is no other available DICOM source for dose information [10].

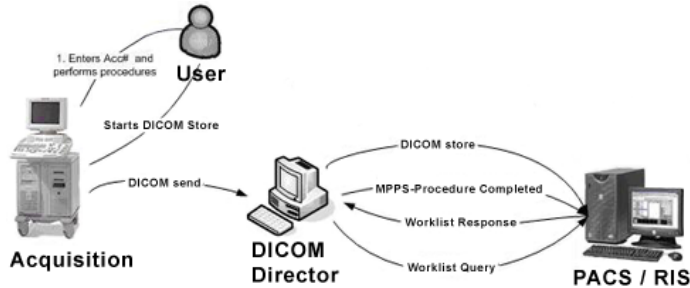
DICOM Tags			
Group Tag	Element Tag	Tag Description	Value
0010	0011	Private Tag	HUMAN
0010	0020	Patient ID	12345
0010	0030	Patient's Birth Date	00000000
0010	0040	Patient's Sex	M
0010	1030	Patient's Weight	0.
0010	2165	Private Tag	Male
0010	2166	Private Tag	None
0010	4000	Patient Comments	
0018	0015	Body Part Examined	THORAX
0018	1000	Device Serial Number	00000000
0018	1020	Software Version(s)	1.0.120
0018	1164	Imager Pixel Spacing	0.1.120
0018	1508	Positioner Type	COLUMN
0018	5100	Patient Position	ANTERIOR - POSTERIOR
0018	7004	Detector Type	DIRECT
0018	7006	Detector Description	
0018	7011	Detector Binning	1:1
0020	0000	Study Instance UID	1.2.826.0.1.3680043.2.1330.1000001.3.2213256752.2712337979
0020	000E	Series Instance UID	1.2.826.0.1.3680043.2.1330.1000001.4.2213256752.2712318977
0020	0010	Study ID	Thorax
0020	0011	Series Number	1
0020	0013	Instance Number	29
0020	0020	Patient Orientation	\
0020	0060	Laterality	L
0020	0062	Private Tag	U
0020	4000	Image Comments	
0028	0002	Samples per Pixel	1

Fig. 2. Example of a DICOM image header information

### 2.3 DICOM Modality Performed Procedure Step

Images and image headers are not the only source of dose data. The DICOM standard introduced a network transaction that is typically initiated by modalities at the beginning and end of imaging acquisitions. The transaction, called Modality Performed Procedures Step (MPPS), is sent to the PACS and/or Radiology Information System (RIS), although other systems requiring information about acquisition status may also receive the message. The transaction allows efficient workflow management of radiology subprocess such as image processing and reporting. MPPS may contain organizational and medical details related to the procedure, as well as billing data, material management data in some cases radiation dose metrics [11].

Although MPPS may contain dose information not directly available from image headers, two significant drawbacks exist with respect to the use of MPPS in dose management. First, MPPS is essentially a transient message – the supplied data is not maintained in a DICOM object for storage, query or retrieval. Second, there is no standardization of CT dose information in MPPS, making the available dose and acquisition information highly variable across devices. Fig. 3 illustrates the usual workflow for MPPS messages in an integrated system with Radiology Information System (RIS) and PACS.



**Fig. 3.** Modality performed procedure step message workflow

#### 2.4 DICOM Structured Reporting

DICOM structured reporting bridge the gap between medical devices and information systems, allowing for transmission and storage of relevant clinical documents, free-text reports and structured information. The Radiation Dose SR template accommodates the recording and storage of dose information and related metrics from imaging modalities, described in DICOM PS 3.16-2011 (template ID 10011, 10012, 10013 and 10014 for CT). The RDSR provides detailed information which may be missing from image header data or not included as part of MPPS. It is also persistent, unlike MPPS which was designed for workflow. Like other DICOM objects, the RDSR may be created, archived, anonymized, queried and retrieved. As a result these reports may be stored on PACS together with images [12]. Table 1 shows the structure of CT DICOM Structured Reports.

**Table 1.** Computed tomography radiation dose structured report - DICOM object structure

CT Radiation Dose – TID 10011	
CT Accumulated Dose Data – TID 10012	Provides information on dose value accumulations over several irradiation events from the same equipment over the scope of accumulation defined by the report.
CT Irradiation Event Data – TID 10013	Dose and equipment parameters for a single irradiation event, including the anatomical target region and CTDI <sub>vol</sub> .
CT Scanning Length – TID 10014	Contains information regarding the exposed range scanned length and length of reconstructable volume.

Not all CT devices support structured reporting. Where RDSR is supported, the data available in the report will vary by make and model described in the device's DICOM conformance statement. In other words while the RDSR template provides a location and framework for information, certain fields may not be populated by a particular device. As an example, “CT Effective Dose Total” is a data field in the RDSR template,

but it is not typically provided by the CT Scanner [13]. Fig. 4 shows the usual content of a DICOM CT RDSR

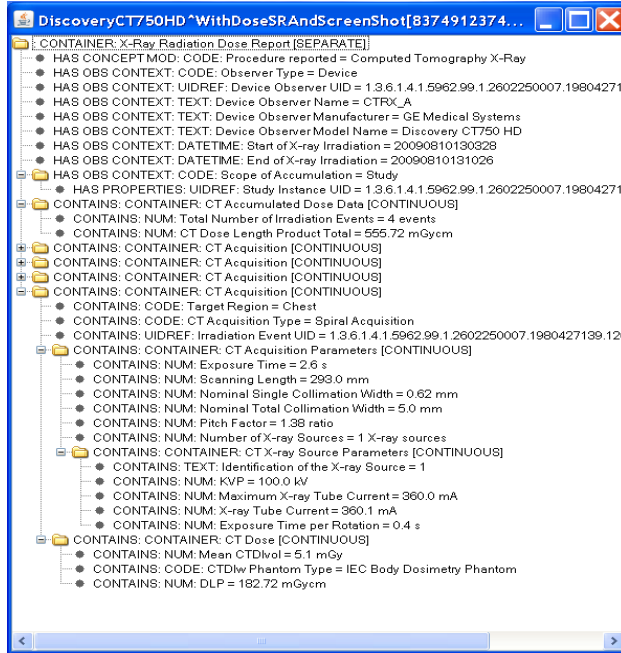


**Fig. 4.** Computed tomography radiation dose structured report - Content information

## 2.5 Dose Datamed Project

The project Dose Datamed, is a project promoted by the European Commission, which Portugal is associated. This project aims is evaluating the relative exposure of the population to medical examinations of diagnostic radiology and nuclear medicine, in the European Union [14].

The latest version of this design - Dose Datamed 2 (DDM 2), conducted in 2010, emerged as a continuation of the previous project, the Dose Datamed 1 (DDM 1), held between 2004 and 2007, in which several European countries with experience in conducting national surveys, often conducted studies and dose estimation received by patients in the context of several tests of diagnostic radiology and nuclear medicine. The project DDM 2 resulted in a proposal for a common methodology, and the recommendation for its use in conducting future surveys of this type - in order to promote strength in the collection and analysis of data and the inter-comparison of results obtained in different European countries.

The proposed methodology [15] is being adopted and implemented in Portugal.

The report's final recommendations on project results Dose Datamed2 in Portugal, refers some topics that is important to refer:

- The project represents the first time that Portugal has managed to compile, evaluate and present comprehensive and representative data (with respect to amounts of radiation doses) of the national situation to an international organization;
- It recommends the creation of a consortium of "stakeholders" (organisms, establishing actions with clear interest in this type of evaluations), to promote and make a periodic assessment of the effective collective dose in the Portuguese population due to medical activities;
- The consortium should take steps to enable the effective collective dose estimation work in the Portuguese population is enhanced and optimized, in diagnostic radiology component, and carrying out more pilot studies, and drawings studies and data collection to reduce the uncertainty in the estimate of collective dose for the Portuguese population.

It should be noted that the average amount of data by type of examination and X-ray room, which Portugal provided for this study were drawn from academic papers and studies presented at conferences or published studies. Here, it can be seen how difficult is to obtain these values in any health institution of our country [14].

### 3 Related Work

There are some initiatives that make use of RDRS for analyzing and extracting radiation dose information. We can mention DoseUtility [16], a tool developed by Dr. David Clunie which is a free open source tool with a user interface to query, retrieve, import and extract report radiation dose information from a screen save or localizer image using the proprietary Standard Extended SOP Class Exposure Dose Sequence information in the "header". It also generates RDSRs from such extracted dose information. It is written in pure Java, will run on any platform and can be started from the web without local installation. The goal of this tool is to show how to work and manage radiation dose information provided by RDSR.

Radiance is another open-source software designed to automatically extract and archive CT dose-related parameters from the dose sheets produced by CT Scanners [17]. It was designed by a team of radiologists interested in dose monitoring and quality assurance. This tool is based on character recognition program that processes each dose sheet. The power of Radiance is its ability to extract information from dose sheets produced by legacy CT scanners that cannot generate DICOM Dose SR reports.

MPPS converter is another existent tool that receives MPPS messages through the RIS, which allow to analyze DICOM MPPS messages and create DICOM SR objects [18]. There are some different commercial tools like DoseWatch from GE, AuntMinnie from Bayer or TeamPlay from Siemens. But all these solution are vendor dependent.

### 3.1 Integrating Healthcare Enterprise

Integrating Healthcare Enterprise (IHE) is an initiative promoting the use of standards to achieve interoperability of health IT systems and effective use of electronic health records through the publication of implementation guidelines. Under a well-defined process, stakeholders, developers and volunteer committees in clinical and operational domains reach consensus on standards-based solutions, called IHE profiles, which go through various levels of testing and real word deployment. After the profile is sufficiently verified, it is incorporated into the IHE Technical Framework, which provides a resource for developers and users of health IT systems to address common interoperability challenges.

Purchasers can specify conformance with appropriate IHE profiles as a requirement in requests for proposals. The pertinent for this article is REM Profile [19].

The REM profile (Fig. 6) specifies communications between systems that generate reports of irradiation events (the acquisition modalities) and systems that receive, store or process those reports. The profile defines how DICOM Structured Reports for CT and projection X-Ray dose objects are created, stored, queried, retrieved, and how they may be processed and displayed. Use of the IHE REM Profile in specifying requirements for radiation dose software and database capabilities is a highly recommended step in developing local informatics standards and tools for the ultimate achievement of personalized dose tracking.

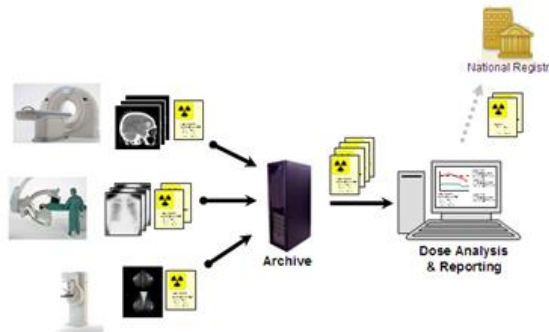


**Fig. 5.** IHE profile for Radiation Dose Monitoring and Reporting

Some reasons that make IHE so relevant and important:

- Provides a means for vendors to state explicitly their products integration capabilities
- Allows users to be informed and to hold vendors to their commitment
- Improves service to patients and referring physicians
- Improves efficiency and workflow
- Promotes systems integration
- Enables interaction among multiple systems

- Improves the use of industry communication standards by removing excessive flexibility [20]

The concept referred in Fig. 6 as "National Registry", does not exist in Portugal. This term refers to the Index Registry Dose (DIR), which is an existing dose of registration information in the United States of America, which is based on receive regulate mind the radiation dose values performed at each institution, then be able to give feedback to institutions comparing the results obtained with other institutions. Since this information is always grouped by type of examination and body parts. This registration system, has been classified by the American College of Radiology (ACR) as suitable for the improvement of the quality criteria of the practice performed.

#### 4 Objectives and Challenges

The main objective and the aim of this work was to design and implement a system/toolkit, capable to communicate with PACS, and extract the radiation dose information from all (or selected) CT's, through RDSR's. This information should be processed and transformed in a clear output report showing the radiation dose values, as Fig. 6 explains.

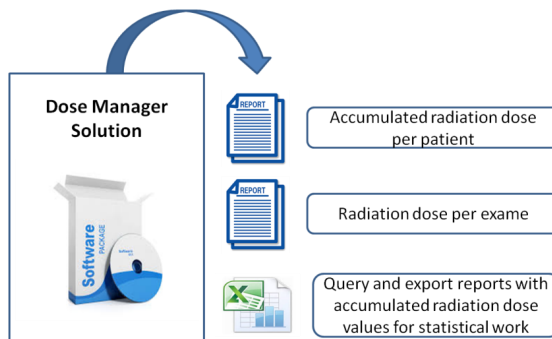


**Fig. 6.** Expected output from proposed tool

As we can observe in the IHE REM profile, the system responsible for communicating with the equipments is the PACS system, and this one should be queried by the toll that would interpret, process and obtain the radiation dose values. However, most of current existent solutions is not respecting this workflow. In most cases, the Dose Report Manager, communicates directly with the equipments, leaving the PACS system out of the solution. The main understandable reason for that, it that it is easier to retrieve and configure a system to communicate in that way, and sometimes, when exists equipments from different vendors, it is really complicated to query and process SRs from PACS, that are coming with different contents. However the structure should be compliant with the DICOM conformance statement, and in that way, there is no reason for

do not apply the IHE REM Profile in an architecture solution do obtain the radiation dose values.

Another challenge is the known DICOM inconsistencies that appear in some DICOM objects, which always require some workarounds to overtake them.

## 5 Methods

The implementation proposal was to provide a generic, user-friendly application for communicate with PACS, with the main goal of retrieving and processing the radiation dose information from CT studies through RDSRs, in order to produce reports with that information.

Fig. 8 shows the overall architecture of the solution. It consists in the following modules with the described functionalities:

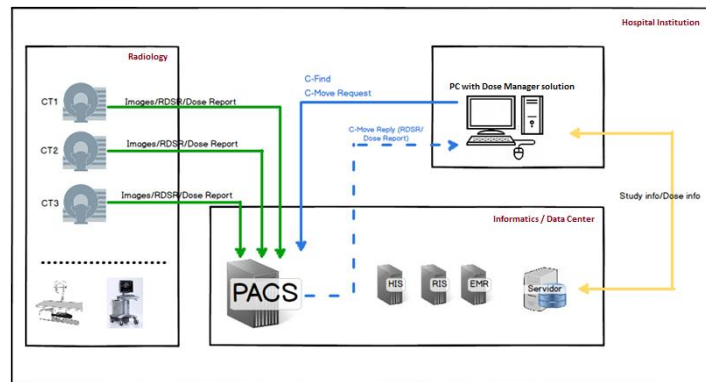


**Fig. 7.** Architecture design of proposed solution

### 5.1 Tool Description and Features

As the image describes, the solution is based on DICOM services and DICOM communication protocol.

The Dose Manager solution, communicate directly with PACS system, gathering all Structured Reports regarding the patients that was requested by the end user. The request can be only one or more examinations from the same patient, or can be different examinations from different patients.

The goal is to have the possibility of retrieve the dose information from different patients at the same time.

With this architecture we are not dependent from any radiology equipment. We are only dependent of the communication with the local PACS system, which should always be available and working as it is supposed to be in a normal scenario.

This tool at the end, should allow end user to generate reports with Accumulated radiation dose per patient and examinations radiation dose values. It should also allow the possible or querying those values and export them to a file in a structured way. The developed solution was built using Microsoft Visual Studio 2013, which easily allowed to integrate some .NET additional modules. It was also used framework .NET and Offis DICOM Toolkit version 3.6.0 to grant SR processing.

### 5.2 Tool Testing Process

The test objectives for this tool was to verify it it was capable to successfully make a retroactive analysis of CT studies to retrieve radiation dose values from SR objects existent in a local PACS solution (independent vendor).

The tool was tested in a real hospital environment with the informatics and radiology department support. It was installed in an existent computer in the Radiology department which was already configured to allow communication with PACS.

After the configuration process, it was successfully queried and retrieved information from PACS through SR objects.

First step was to retrieve some randomized CT RDSRs to analyze the existent information in those objects. It could happen that SRs objects could not be in compliant with DICOM conformance statement. By this analysis it was concluded that only 2 CT scanners (from total of 3) was sending SR objects to PACS.

After this analysis it was decided to query and retrieve fifty DICOM RDSRs individually, to process and generate report with radiation dose values. It was also queried thirty patients for all existent RDSRs to allow processing accumulated radiation dose values. After this steps, and to conclude the test process it was done a PACS query of all CT studies during a randomized week.

All this tasks was successfully done and completed.

## 6 Results

The tasks performed in the test process, are shown below:

**Table 2.** Results obtained in test process

Action	Number of tests	Action status	Average time
CT radiation Dose Value	50 studies	Completed	1'10"
CT accumulated radiation dose value	30 patients	Completed	3'25"
Query/export accumulated radiation dose values	1 week (7 days)	Completed	20"15"

This results represents outcomes from tests actions. We can verify that all features were successfully executed. Table below also show us the mean time of execution for each action. This time is important, because in that way we can evaluate the performance of this tool. The presented times, were measured considering that the start of action was done when front end tool received command to execute the operation, and the end time, was considered when solution showed or presented the required values.

As we can see the times are relatively high. However, the principle objective was not to obtain and demonstrate a good performance, but show that the best way to gather the radiation dose values in a real hospital environment is the proposed architecture.

## 7 Conclusions

The process of radiation dose calculation, from the radiology equipment in hospitals, has undergone enough changes due to changing technologies, and at the same time due to updates of the standard DICOM.

Nowadays DICOM Structured Reports objects, allow to query and retrieve large amounts of structured information, including the amounts of radiation dose from imaging tests. This requires providing a tool capable to communicate with the PACS system, which is the system responsible for storing this type of objects.

A solution with this architecture, brings many advantages compared to other solutions that do not fully guarantee the accuracy of the data or the efficiency in obtaining the required information.

Actually, by the lecture and projects that was read and analyzed in Portugal, there is no Institutions in Portugal, with tool(s) or system able to provide the radiation dose values according with the recommendations of the last European project in this area - Dose Datamed 2.

Comparing this tool, with previous solutions referred, and by the tests which was done, we can mention some considerable advantages:

- Instead of consider MPPS messages or Dose Reports through OCR process, information based on Structured Reports is 100% reliable.
- Based on DICOM Structured Reporting, can communicate with all devices that respect DICOM standards.
- It is not dependent from radiology equipments.
- Allow Radiology department, to evaluate dose values from same type of equipments.

## 8 References

1. Morin, R.L., Seibert, J.A., Boone, J.M.: Radiation Dose and Safety: Informatics Standards and Tools. *J. Am. Coll. Radiol.* 11, 1286–1297 (2014).
2. ACR-NEMA: National Electrical Manufacturers Association: The Dicom Standard 2015, <http://dicom.nema.org/standard.html>.
3. Donnell, K.O.: IHE & Radiation Exposure Monitoring. (2010).
4. Supanich, M.P., Ph, D.: Radiation Dose Index Monitoring Practical Advice on

- Configuration Informatics Informatics Informatics Informatics : Dose Metric Acquisition RDIM Informatics Requirements. 257, 1–8 (2015).
- 5. Europeias, J.O. das C.: DIRECTIVA 97/43/EURATOM. 22–27 (1997).
  - 6. Gray, J.E., Archer, B.R., Butler, P.F., Hobbs, B.B., Mettler, F. a, Pizzatiello, R.J., Schueler, B. a, Strauss, K.J., Suleiman, O.H., Yaffe, M.J.: Reference values for diagnostic radiology: application and impact. Radiology. 235, 354–358 (2005).
  - 7. Noumeir, R.: Benefits of the DICOM Structured Report. J. Digit. Imaging. 19, 295–306 (2006).
  - 8. Clunie, D.A.: DICOM structured reporting: Overview and characteristics. 891–896 (2000).
  - 9. Li, X., Zhang, D., Liu, B.: Automated extraction of radiation dose information from CT dose report images. Am. J. Roentgenol. 196, 781–783 (2011).
  - 10. Dandu Ravi Varma: Managing DICOM images: Tips and tricks for the radiologist. Indian J. Radiol. Imaging.
  - 11. ACR-NEMA: Digital Imaging and Communications in Medicine (DICOM) - Supplement 17: Modality Performed Procedure Step.
  - 12. Clunie, D.A.: DICOM structured reporting. (2000).
  - 13. Sluis, D., Lee, K., Mankovich, N.: DICOM SR-Integrating structured data into clinical information systems. Medicamundi. 31–36 (2002).
  - 14. Teles, P., Sousa, M.C., Paulo, G., Santos, J., Pascoal, A., Lança, I., Matela, N., Janeiro, L., Sousa, P., Carvoeiras, P., Santos, a I., Simãozinho, P., Neves, M., Vaz, P.: Relatório sobre os resultados do projecto Dose Datamed 2 Portugal. Image Wisely. 1–40 (2012).
  - 15. Wall, B., Hart, D., Mol, H., Lecluyse, A., Aroua, A., Trueb, P., Griebel, J., Nekolla, E., Gron, P., Waltenburg, H., Beauvais-March, H., Aubert, B., Scanff, P., Pirard, P., Sinno-Tellier, S., Shannoun, F., Brugmans, M., Meeuwesen, E., Stoop, P., Olerud, H., Borretzen, I., Leitz, W.: RADIATION PROTECTION N ° 154 European Guidance on Estimating Population Doses from Medical X-Ray Procedures. Environ. Hazards. 1–123 (2008).
  - 16. Clunie, D.A.: DoseUtility, <http://www.dclunie.com/pixelmed/software/webstart/DoseUtilityUsage.html>.
  - 17. Cook, T.S., Zimmerman, S.L., Steingall, S.R., Maidment, a. D. a, Kim, W., Boonn, W.W.: Informatics in Radiology: RADIANCE: An Automated, Enterprise-wide Solution for Archiving and Reporting CT Radiation Dose Estimates. Radiographics. 31, 1833–1846 (2011).
  - 18. Mildnerger, P.: New concepts for dose registration and analysis – including IHE REM and Radiance. (2013).
  - 19. IHE REM profiles, [http://wiki.ihe.net/index.php?title=Radiation\\_Exposure\\_Monitoring](http://wiki.ihe.net/index.php?title=Radiation_Exposure_Monitoring).
  - 20. Boochever, S.S.: HIS/RIS/PACS integration: getting to the gold standard. Radiol. Manage. 26, 16–24; quiz 25–27 (2004).



# Analysis of End-to-End Delay in Fading Channels using Stochastic Network Calculus

Orangel Azuaje

Faculdade de Engenharia da Universidade do Porto (FEUP), Porto, Portugal  
up201307429@fe.up.pt

**Abstract.** Stochastic network calculus is a theory that allows to compute performance guarantees in communication networks that can be violated with certain violation probability. Based on a service process that describes fading channels, this work studied the end-to-end delay in a multi-hop wireless ad-hoc network through two scenarios: first, it was incremented the number of nodes with just one flow in the network and second, it was added new traffic each time a node joined to the network. Results show the way the end-to-end delay is affected by the number of nodes and new traffic for the specific case of an emergency wireless ad-hoc network and the possibility to apply network calculus for real case scenarios.

**Keywords:** network calculus · fading · wireless · delay

## 1 Introduction

The use of Wireless Ad-Hoc Networks (WANETs) has increased in the last years, mainly due to the amount of connected sensors to monitor physical or environmental variables such as pressure, sound, temperature or even electrical activity of the heart (electrocardiogram), giving life to the new Internet of Things (IoT) and wearable technology [1]. WANETs are principally deployed in areas such as emergency, research and military scenarios.

Every application running on top of a WANET has different requirements and the analysis of the network performance is done after the whole deployment of the nodes and applications. However, obtaining some analysis of performance guarantees by theoretical means allows the saving of deployment cost (money as well as man-work) of the whole network, studying different network topologies and identifying points of interest.

Network Calculus is a theoretical framework for performance guarantees analysis of communication networks. It is based on using alternate algebras, particularly the min-plus and max-plus algebra, to transform complex non-linear network systems into analytically tractable linear systems [8]. A service guarantee is either deterministic or stochastic but as the wireless channel is an unreliable medium, we will focus on stochastic service guarantee, where the Quality of Service (QoS) objectives specified by a flow can be violated a certain violation probability ( $\epsilon$ ).

A stochastic network calculus using moment generating functions (MGFs) and the Chernoff bound was proposed in [2] and elaborated in more detailed in [5] but it was in [6] where was derived a service curve model for Gilbert-Elliott channels with memory. This service curve was implemented in the present work to analyze the impact of topologies changes in the end-to-end delay bound of a wireless network for an emergency scenario, specifically the Project Vital Responder 2.0 - Intelligent management of critical events of stress, fatigue and smoke intoxication in forest firefighting<sup>1</sup>, which has as main purpose to design a system for decision support in ground-based firefighting operations.

The remainder of this paper is organized as follows: Section 2 gives a brief introduction to Stochastic Network Calculus and its use to analyze the end-to-end delay bound, Section 3 introduces the modeling of fading channels using Markov Channel model, Section 4 explains the concepts of scheduling discipline and leftover service, Section 5 provides the explored scenarios and corresponding results and Section 6 presents the conclusions and future work.

## 2 End-to-End Delay Bound

Network calculus can be seen as the system theory that applies to computer networks. Fig. 1 depicts the network calculus representation of a network element. Applying the previous analogy, the input function of system theory can be seen as the arrival process of a traffic source, the transfer function as the service offered for the network and the output function is the departure process of the network.



**Fig. 1.** Network calculus representation

### 2.1 Min-Plus Algebra Basics

In min-plus algebra, the addition and multiplication of conventional algebra becomes computation of the infimum and addition, respectively. This work does not cover all of the properties of this “new” algebra but, continuing with the analogy of system theory, we will present the definition of the min-plus convolution and deconvolution because these two operations will allow us further on, to concatenate server in series and to compute service guarantees. Min-plus convolution of real-valued, bivariate functions  $x(s, t)$  and  $y(s, t)$  and corresponding min-plus deconvolution are defined for  $t \geq s \geq 0$  as

<sup>1</sup> <http://vitalresponder.web.ua.pt/>

$$(x \otimes y)(s, t) = \inf_{\tau \in [s, t]} [x(s, \tau) + y(\tau, t)] \quad (1)$$

$$(x \oslash y)(s, t) = \sup_{\tau \in [0, s]} [x(\tau, t) - y(\tau, s)] \quad (2)$$

where inf is the infimum and sup is the supremum.

In the following sections, this algebra will be applied to data flows and network elements, using the concepts of arrival, server and departures processes.

## 2.2 Stochastic Network Calculus

Arrival and departures process are defined as  $A(0, t)$  and  $D(0, t)$ , respectively. These functions are real-valued cumulative functions, therefore, are nonnegative and increasing in  $t$  and represent the amount of data detected in the interval  $(0, t]$  with  $t \in \mathbb{N}_0$ . In addition, we can represent the amount of data detected in the interval  $(s, t]$  by the bivariate functions  $A(s, t) = A(0, t) - A(0, s)$  and  $D(s, t) = D(0, t) - D(0, s)$ .

From [2], we used the following definition: Assume  $A(0, t)$  and  $D(0, t)$  are the arrival and departure process of a lossless server, respectively. Let  $S(s, t)$  for  $t \geq s \geq 0$  be a random process that is nonnegative and increasing in  $t$ . The server is called a dynamic server  $S(s, t)$  if for any fixed sample path it holds for all  $t \geq 0$  that

$$D(0, t) \geq (A \otimes S)(0, t) \quad (3)$$

## 2.3 Moment Generating Function

In [5] a network calculus with moment generating function (MGF) is developed using the concept of dynamic servers. Throughout this work we assume that arrival and service are described by statistically independent, stationary random process. Under this assumption  $A(s, s + t)$  equals  $A(0, t)$  in distribution for all  $s = 0$ . The MGF of a stationary random process  $A$  is defined as

$$M_A(\theta, t) = E e^{\theta A(0, t)} \quad (4)$$

where  $E$  is the expected value of a random variable.

We use the same notation as [5] to define  $\bar{M}_S(\theta, t) = M_S(-\theta, t)$ . MGFs have some interesting properties. For additive and multiplicative constants  $a$  and  $b$  it is known for all  $\theta$  that

$$M_{a+bA}(\theta, t) = e^{\theta a} M_A(b\theta, t) \quad (5)$$

and for the addition of two statistically independent random processes  $A$  and  $B$  it holds that

$$M_{A+B}(\theta, t) = M_A(\theta, t)M_B(\theta, t) \quad (6)$$

**Theorem 1 (Concatenation):** Consider  $S_1(s, t)$  and  $S_2(s, t)$  dynamic servers in series as depicted in Fig. 2. There exist an equivalent, single dynamic server  $S(s, t)$  for  $t \geq s \geq 0$  where

$$S(s, t) = (S_1 \otimes S_2)(s, t) \quad (7)$$

Assuming as [6] that  $S_1(s, t)$  and  $S_2(s, t)$  are statistically independent, stationary and have MGF  $\overline{M}_{S_1}(\theta, t)$  and  $\overline{M}_{S_2}(\theta, t)$  respectively. The MGF of the equivalent server is upper bounded for  $t \geq 0$   $\theta$  according to

$$\overline{M}_S(\theta, t) \leq \sum_{\tau=0}^t \overline{M}_{S_1}(\theta, t)\overline{M}_{S_2}(\theta, t-\tau) \quad (8)$$

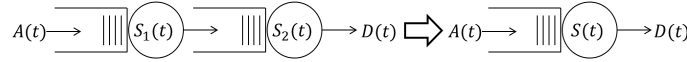


**Fig. 2.** Equivalent server - Server in series

**Delay:** Let  $A(0, t)$  and  $D(0, t)$  be the arrival and departures process of a lossless server, respectively. Assuming first-come first-served ordering the delay at time  $t \geq 0$  is upper bounded according to

$$d(t) = \inf[s \geq 0 : A(0, t) - D(0, t+s)] \leq 0 \quad (9)$$

**Theorem 2:** Consider a dynamic server  $S(s, t)$  with arrival process  $A(s, t)$ . Assuming first-come first-served ordering the delay at time  $t \geq 0$  is upper bounded according to

$$d(t) \leq \inf[s \geq 0 : (A \oslash S)(t+s, t)] \leq 0 \quad (10)$$

and the departure process is upper bounded for any  $t \geq s \geq 0$  according to

$$D(s, t) \leq (A \oslash S)(s, t) \quad (11)$$

Performance bounds [5] follow with Chernoff's theorem. Consider a dynamic server  $S(t)$  with arrival process  $A(t)$ , which are statistically independent, stationary and have MGF  $M_S(\theta, t)$  and  $M_A(\theta, t)$ , respectively. Assuming first-come first-served ordering an upper delay bound that are violated at most with probability  $\epsilon \in (0, 1]$  are

$$d = \inf_{\theta \geq 0} \left[ \inf[\tau : \frac{1}{\theta} (\log \sum_{s=\tau}^{\infty} M_A(\theta, s-t) \overline{M}_S(\theta, s) - \log \epsilon) \leq 0] \right] \quad (12)$$

Given this framework, obtaining the delay bound for a specific network topology boils down to selecting the violation probability, modeling the arrival and service process through corresponding MGFs and searching the infimum values of  $\theta$  and  $\tau$  for which the previous equation holds.

### 3 Fading Channels

The use of network calculus and the derivation of quality of service guarantees for wireless systems has not been an easy problem to address because of the modeling of the wireless medium. In order to apply the network calculus theory, it is crucial to present probabilistic service curves that describe fading channels.

One of the traditional techniques for modeling fading channel consists in the use of Markov chain. Markov chain permits to consider memory between consecutive transmissions, which is a key factor for high-layer models, that is, models that do not represent the received signal strength or related process at the physical layer. One of these models is the classical Gilbert-Elliott model [7] [3], which is based on a discrete time 2-state Markov chain, in which the data can be decoded error-free if the channel is in “on state”, or cannot be decoded correctly at the receiver if the channel is in “off state”.

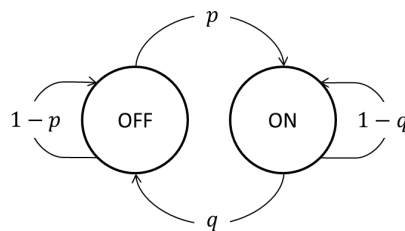


**Fig. 3.** Gilbert-Elliott model

The Gilbert-Elliott model of Fig. 3 is used to describe a random process  $S(s, t)$  that is defined as the service offered by a fading channel in the interval  $(s, t]$ .

Assuming that the service is non-idling and uses the entire available service to serve backlogged data (i.e. work-conserving server), it can be seen as dynamic server.

From [6] we used the following definition: Consider an irreducible, homogeneous Markov chain with  $n$  states and stationary distribution  $\pi$ . Workload is process with rate  $h_i$  when in state  $i$ . Let  $H(\theta)$  be the diagonal matrix  $\text{diag}(e^{\theta h_1}, e^{\theta h_2}, \dots, e^{\theta h_n})$  and  $Q$  be the transition probability matrix, where  $q_{ij}$  is the transition probability from state  $i$  to state  $j$  and  $\mathbf{1}$  is a column vector of ones. For all  $t \geq 0$  and all  $\theta$  the MGF of the corresponding random process  $S$  is

$$\overline{M}_S(\theta, t) = \pi(H(-\theta)Q)^{t-1}H(-\theta)\mathbf{1} \quad (13)$$

At this point, we have a characterization of the fading channel with a packet-base model that depends of the transition probabilities between the states and the rate at which the channel processes the workload. The expression (13) will be used on (12) to determine delay bound.

#### 4 Scheduling Discipline and Leftover Service Characterization

The analysis of performance bounds to multiplexed flow is also possible inside the network calculus framework. However, as we want to analyze the end-to-end delay per-flow, we will consider a single system with stationary service curve  $S(t)$ , stationary through-traffic arrival  $A^t(t)$ , stationary cross-traffic arrivals  $A^c(t)$  and corresponding departures  $D^t(t)$  and  $D^c(t)$ , respectively as shown in Fig. 4.

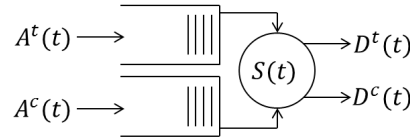


**Fig. 4.** Queuing system with through and cross traffic

To analyze the delay of a through-flow is important to isolate the remaining service that is left over by cross-traffic at each of the systems, that is, the service curve that actually would see the through-flow (Fig. 5). Then, we can use the concatenation theorem with the so-called leftover service curve of each subsystem to obtain the equivalent network service curve for the through-traffic flow [4]. The left over service is strongly related with the scheduling model that is implemented in the network. Following are the expressions of left over service using the General Scheduling Model.

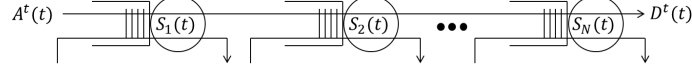


**Fig. 5.** Server in series with cross-traffic

**General Scheduling Model:** Suppose flows with stationary arrival process  $A_1(t)$  and  $A_2(t)$ , which are scheduled at a stationary work-conserving server with service process  $S(t)$ .  $A_2(t)$  sees a dynamic server [5]

$$S_2(t) = \max[0, S(t) - A_1(t)] \quad (14)$$

Assuming  $A_1(t)$  and  $S(t)$  are statistically independent and have MGF  $M_{A_1}(\theta, t)$  and  $\bar{M}_S(\theta, t)$ , respectively. The MGF of the server seen by  $A_2(t)$  is upper bounded for  $\theta \geq 0$  by

$$\bar{M}_{S_2}(\theta, t) \leq \min[1, \bar{M}_S(\theta, t)M_{A_1}(\theta, t)] \quad (15)$$

It is important to note that the general scheduling model “does not make any assumptions about the order in which flows are served with respect to each other”, in other words, as we do not have any other information of the system, the bound that we can find is actually for a priority scheduler where flow  $A_2(t)$  has low priority respect to  $A_1(t)$ .

## 5 Numerical Results

To derive the service guarantees we had to define the traffic source of the nodes in the network and the properties of the channel described by the discrete-time Markov model of Fig. 3. In this work, we used an independent periodic traffic source to model the data that will be generated by the network device attached to the firemen. This type of source generates  $\sigma$  units of workload at times  $UT + nT, n = 0, 1, \dots$  where  $T$  is the period of the source and  $U$  is the initial start time which is uniformly distributed in the interval  $[0, 1]$ . For all  $t \geq 0$  and  $\theta \geq 0$  it is known that the MGF is given by [9]

$$M_A(\theta, t) = e^{\theta\sigma\lfloor\frac{t}{T}\rfloor} \left(1 + \left(\frac{t}{T} - \lfloor\frac{t}{T}\rfloor\right)(e^{\theta\sigma} - 1)\right) \quad (16)$$

Analyzing the traffic properties of the Project Vital Responder 2.0, we have that the data rate is 30kbps and the block of sensor data consists on 3600 bytes. Assuming a physical layer data rate of 1Mbps for the 802.11 ad-hoc network and a workload of 600 bytes, we have that the wireless channel can process this workload in 4.8 ms, which it is considered as the time slot of the discrete time model. Consequently, the rate  $h = 1$  used for the channel model corresponds

to one unit of workload served in each time slot. Simultaneously, for the traffic source, the time to transmit 3600 bytes at 30kbps is 960 ms, which leads to a period of the source  $T = 200$  and units of workload  $\sigma = 6$ .

The channel model is specified by the transition rate from OFF to ON state  $p$  and the steady state error rate  $q/(p + q)$ , where for a given  $p$ , the transition rate from ON to OFF  $q$  can be obtained. As discussed in [10], we modeled the slowly fading channel choosing  $p = 0.1$  and  $q/(p + q) = 0.1$ . Table 1 shows the complete set of parameters used for the source and channel models.

**Table 1.** Source and channel model parameters

Parameter	Description	Value
$q/(p + q)$	Steady state block error probability	0.1
$p$	Transition probability from OFF to ON	0.1
$h$	Channel rate	1
$T$	Period of the source	200
$\sigma$	Burst size	6

In the first scenario, we examined the delay bound of a chain of node while changing the number of nodes in the network until a maximum of five (5) wireless links, that is, five (5) servers (Fig. 6) through the stochastic delay bound of equation 12 with the values of the Table 1. It was established a maximum of five servers because is the usual number of firemen in a firemen squad according to the Vital Responder 2.0 details. To solve this scenario, we used the concatenation property of equation 8. It is also important to say we assumed that the channel conditions between the network elements are all alike.

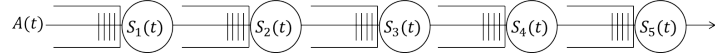


**Fig. 6.** First scenario - One flow in a chain of servers

Fig. 7 depicts the delay bound up to five server in series. As expected, while increasing the number of servers, the higher the delay bound for the arrival process. We can identify the lowest delay bound curve for the one-server case 264 – 696 ms for the different violation probabilities and the higher curve 801 – 1291 ms for the five-server case. One interesting behavior is that the difference between the  $(n+1)$ -server case and the  $n$ -server case for any  $n = [1, 2, 3, 4]$  seems constant due to the fact that the channels are alike.

In the second scenario, we explored the end-to-end delay of the flow  $A_1$  in a more real WANET case, where each new node in the network does not only forwards data from previous nodes but also generates its own (Fig. 8). To solve this scenario, we used first the leftover service of equation 15 and then the

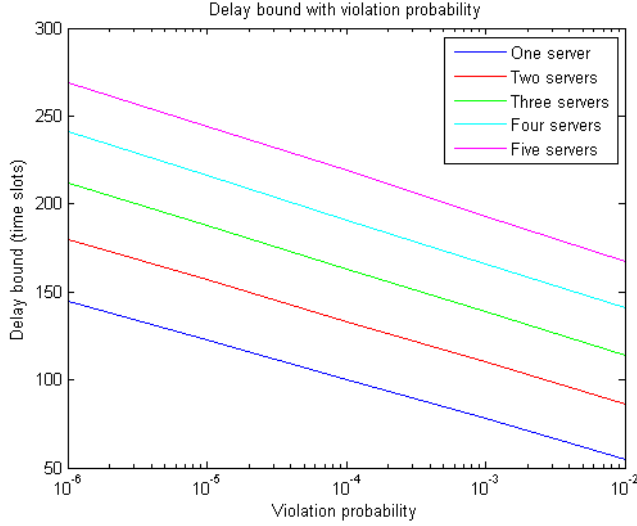


**Fig. 7.** Delay bound - One flow in a chain of servers

concatenation property. Again, we limited the network up to five servers due to the aforementioned reason.

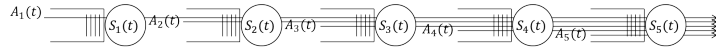


**Fig. 8.** Second scenario - Generate and Forward

Fig. 9 depicts the delay bound up to five server for the ad-hoc network case. As expected, while increasing the number of servers, the higher the delay bound for the arrival process  $A_1$ , however, given that this time each new server is not only a channel but also a source of cross-traffic the difference between the  $(n+1)$ -server case and the  $n$ -server case for any  $n = [1, 2, 3, 4]$  is not constant. We can identify the delay bound for the one-server case 264 – 696 ms for the different violation probabilities and the maximum 1324 – 1963 ms for the five-server case.

## 6 Conclusions

Network calculus proved to be a complex tool that allows the systematic study of the end-to-end delay in a wireless network. In this work, we were able to use the service curve described by a Gilbert-Elliott model to analyze the end-to-end delay in a multi-hop ad-hoc network while changing its topology in the scope of a specific wireless emergency network. A further development of this research

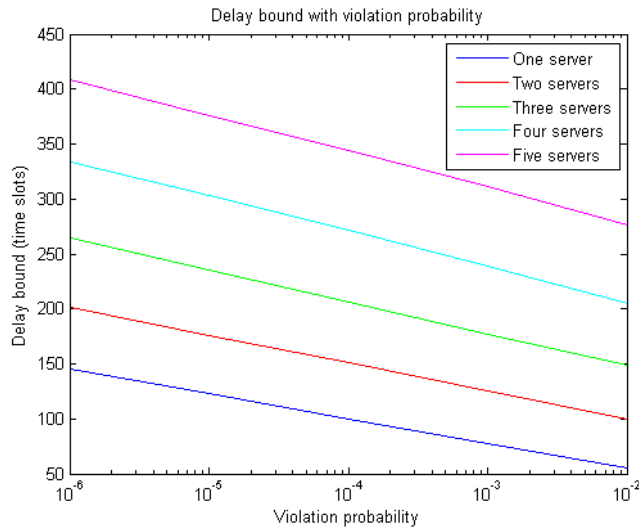


**Fig. 9.** Delay bound - Generate and Forward

is the application of others scheduling discipline such as Priority Scheduling or Generalized Processor Sharing to tight more the delay bounds and also considering wireless channels with different conditions, however, this will require a considerable amount of computational resources to solve the delay bound equation.

## References

1. Atzori, L., Iera, A., Morabito, G.: The internet of things: A survey. *Computer networks* 54(15), 2787–2805 (2010)
2. Chang, C.S.: Performance Guarantees in Communication Networks. *Performance Guarantees in Communication Networks*, Springer London (2000), <https://books.google.pt/books?id=u-2IiZO3rlgC>
3. Elliott, E.O.: Estimates of Error Rates for Codes on Burst-Noise Channels (1963)
4. Fidler, M.: Survey of deterministic and stochastic service curve models in the network calculus. *Communications Surveys Tutorials, IEEE* 12(1), 59–86 (2010)
5. Fidler, M.: An End-to-End Probabilistic Network Calculus with Moment Generating Functions. In: *Quality of Service, 2006. IWQoS 2006. 14th IEEE International Workshop on*. pp. 261–270 (2006)
6. Fidler, M.: WLC15-2: A Network Calculus Approach to Probabilistic Quality of Service Analysis of Fading Channels. *IEEE Globecom 2006* pp. 1–6 (2006), <http://ieeexplore.ieee.org/lpdocs/epic03/wrapper.htm?arnumber=4151329>
7. Gilbert, E.N.: Capacity of a burst-noise channel. *Bell System Technical Journal*, The 39(5), 1253–1265 (1960)
8. Jiang, Y., Liu, Y.: Stochastic Network Calculus. *Computer Communications and Networks*, Springer (2009), <https://books.google.pt/books?id=zj7JkPymkGIC>

9. Kelly, F.: Notes on Effective Bandwidths. Stochastic networks: theory and applications pp. 141–168 (1996)
10. Zorzi, M., Rao, R.R., Milstein, L.B.: Error Statistics in Data Transmission over Fading Channels. IEEE Transactions on Communications 46(11), 1468–1477 (1998)



## ZigBee and Arduino-Based Data Acquisition System for Precision Agriculture

Sherif A. Busari<sup>1</sup>, Abibat F. Dunmoye<sup>2</sup> and Kayode F. Akingbade<sup>2</sup>

<sup>1</sup>Faculdade de Engenharia da Universidade do Porto, Porto, Portugal

<sup>2</sup>The Federal University of Technology, Akure, Nigeria

sherif.busari@fe.up.pt  
dunmoyefeyisayo@yahoo.co.uk, kfakingbade@futa.edu.ng

**Abstract.** Precision Agriculture (PA) is an information-based management of farmlands for optimal performance. It relies on abundant mass of data for decision-making purposes in order to improve yield and make informed forecasts. Data Acquisition Systems (DAS) can provide the much-needed information for these purposes. This paper presents the design of a DAS which employs a wireless sensor network (WSN) approach using Arduino microcontroller for signal processing and ZigBee-based transceivers operating on the 2.4 GHz license-free ISM band for communication. Streams of temperature, pressure and relative humidity data from sensors and GPS data from an onboard module, are transmitted from the farmland to a receiver system interfaced with an LCD for display and with a PC for data logging and analysis. An SD card is incorporated in the design for data storage. The test results show that the system is capable of providing real-time and site-specific data for precision agriculture.

**Keywords:** Precision Agriculture · DAS · WSN · Arduino · ZigBee · 2.4 GHz band

### 1 Introduction

Precision agriculture is a farming practice which integrates technology and agronomy principles to manage farmlands with the aim of improving the performance of crops. Acquired data can be relayed to the farmers and farm managers in order to analyze and consequently take appropriate actions [1].

Precision Agriculture uses information-driven technologies for the monitoring and management of spatial (in-field) and temporal (over time) variabilities associated with agricultural production activities for enhanced production and reduced environmental pollution [2]. Wireless sensor technologies are increasingly being applied in precision agriculture using data acquisition systems (DAS).

The purpose of data acquisition systems is to gather useful measurement data for characterization, monitoring or control. They interface between the real world of physical parameters, which are analogue, and the artificial world of digital

computation and control [3] and are used for a variety of system monitoring operations in agricultural, military, industrial, commercial and medical applications [4].

Advances in hardware technologies (such as microcontrollers) and low-power wireless communication have revolutionized the development of Data Acquisition Systems such that application-specific systems can now be developed with enhanced capabilities for accurate and real-time gathering, logging, viewing and analysis of data, at low cost and with optimal performance [5].

In order to promote sustainable agriculture for improved food production and economic development by farmers, particularly peasant farmers in rural communities, data acquisition systems that can help make informed decisions are indispensable. A multi-functional farm monitoring system designed to provide soil, crop and environmental data from sensors and a point-to-multipoint communication of acquired data to several receivers at designated points using WSN approach is thus proposed. The central transmitter unit is envisioned to be carried by a tethered Helium-filled balloon.

This paper therefore presents the development of a Data Acquisition System using Arduino microcontroller and ZigBee technology for monitoring temperature, pressure and relative humidity on the farms, as part of the proposed monitoring system, towards a data-driven management of farmlands (i.e. precision agriculture). Being site-specific, real-time, automated and user-friendly, the developed DAS is aimed at replacing the laborious, manual and traditional methods of recording farm data by combining data logging and storage, visual display, location tracking, signal processing and wireless communication capabilities using an SD card, an LCD, a GPS module, two Arduino Uno microcontroller boards and two ZigBee transceivers respectively.

The Arduino Uno<sup>1</sup> is a microcontroller board based on Atmel's ATmega328P<sup>2</sup>. It has 14 digital input/output pins (of which 6 can be used as PWM outputs), 6 analogue inputs, a 16MHz quartz crystal, a USB connection, a power jack, an ICSP header and a reset button. Power to the board can be through the computer with a USB cable, through an AC-to-DC adapter or a battery. It can switch automatically between USB and DC power and supports both the 3.3V and 5V power supply. The Atmel ATmega328P microcontroller operates at 5 V with 2KB of RAM, 32KB of flash memory for storing programs and 1KB of EEPROM for storing parameters. With a clock speed of 16MHz, it can execute around 300,000 lines of C source code per second. The Arduino Uno is well-suited for processing in data acquisition systems.

ZigBee is a low-cost, low-power, low-data rate wireless mesh technology standard for Low-Rate, Wireless Personal Area Network (LR-WPAN). The ZigBee standard defines only the networking, application, and security layers of the OSI model and adopts IEEE 802.15.4 PHY and MAC layers as part of the ZigBee networking protocol. It takes full advantage of a powerful IEEE 802.15.4 physical radio standard

---

<sup>1</sup> <https://www.arduino.cc/en/Main/ArduinoBoardUno>

<sup>2</sup> <http://www.atmel.com/devices/atmega328p.aspx>

and operation in unlicensed bands worldwide at 2.4GHz (global), 915MHz (Americas) and 868MHz (Europe).

Raw data throughput rates of 250kbps can be achieved at 2.4GHz (16 channels), 40kbps at 915MHz (10 channels) and 20kbps at 868MHz (1 channel). Transmission distances range from 10 to 100 meters up to a few kilometers, depending on power output and environmental characteristics, and uses CSMA/CA network. ZigBee is well suited for sensing, monitoring and control applications among inexpensive devices such as Data Acquisition Systems.

The rest of the paper is organized as follows: Section 2 gives a brief survey of related works Section 3 details the system development approach. Results are presented and discussed in Section 4. The conclusions and direction for future works are presented in Section 5.

## 2 Related Works

Several works on the use of data acquisition systems for precision agriculture have been published. In [1], a DAS for monitoring temperature, water content, moisture content, electrical conductivity and pH of the soil together with weed seeker and wind speed was developed using WSN approach. [2] monitored the soil moisture's electric resistance using watermark sensor while [6] deployed a supervisory data acquisition system for monitoring temperature and humidity in oil palm tissue culture. [7] deployed smart sensing platform for monitoring temperature, relative humidity, pressure and sunlight data and [8] developed a system for the acquisition of environmental temperature, relative humidity, noise and water leakage using ZigBee technology.

In [9], temperature, pH, humidity and soil moisture were monitored with the incorporation of a GSM module in the design. An implementation of DAS for precision agriculture using remote sensing was developed in [10] while [11] investigated only temperature and humidity.

These works have shown that crop performance could be enhanced by making plant management decisions based on acquired data. Depending on the intended application, the technologies used by these acquisition systems differed and the parameters monitored are varied but could largely be classified into three sets of parameters: soil, plant/crop and environmental parameters.

In this work, the design focuses on acquisition of environmental data. Several modules were integrated to give unique features yet maintaining a simple system with sensing, tracking, wireless communication, display and storage capabilities. The system provides remote access to site-specific and real-time data for farm management system towards precision agricultural practice.

### 3 System Development

The design approach and development phases are detailed in this section. The system development includes principally hardware integration of the modules, coding of the Arduino board for processing and configuration of the transceivers.

#### 3.1 System Architecture

The schematic diagram of the developed system is shown in Fig. 1. It is divided into two units: the transmitter and the receiver units. The transmitter end consists of sensors to monitor temperature, pressure and relative humidity, a GPS module to acquire date, time, location (latitude and longitude) and altitude data, an Arduino Uno-based microcontroller as processing unit and a ZigBee transmitter for wireless communication.

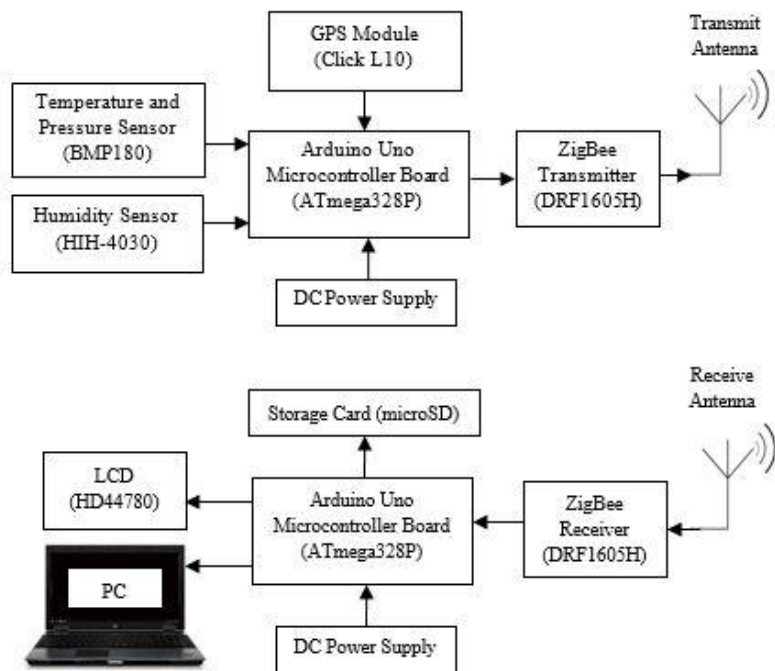


**Fig. 1.** Schematic Diagram of the developed Data Acquisition System

The receiver unit, on the other hand, comprises a ZigBee receiver, an Arduino-Uno microcontroller for processing, a microSD card for data storage and display via an

LCD or alternately through a PC using virtual terminals such as PuTTY or Tera Term. Each of the Arduino Uno microcontroller boards is powered with a 9V dc battery or alternatively from a PC via USB. Other components are supplied with either 3.3V or 5V from the regulated 3.3V and 5V from the Arduino board based on their respective operating voltages. The features of the various components of the system are summarized in Table 1.

Arduino communication with the sensors and microSD is via I<sup>2</sup>C and SPI respectively. Communication with the PC (via USB), and with the ZigBee and GPS modules is through UART at baud rates of 9600bps, 38400bps and 9600bps respectively.

**Table 1.** Summary of Components<sup>c</sup> features

Component	Current (mA)	Voltage (V)	Features
TPS <sup>3</sup> (BMP180)	0.005	3.3	Digital sensor
RHS <sup>4</sup> (HIH-4030)	5	5	Analogue sensor
Arduino Uno (ATmega 328P)	50	5	32KB (Flash memory), 2KB (SRAM), 1KB (EEPROM)
GPS Click L10 (with antenna)	38	3.3	4Mb (Flash memory), 5Hz (update rate), -165dBm (tracking sensitivty)
DRF1605H Transceiver (with antenna)	80 (Tx) 45 (Rx)	3.3	2.4 GHz, 1.6 km (max. range), 250 kbps (max. data rate), -110dBm (receiver sensitivity), ZigBee 2007/PRO
LCD (HD44780)	4	5	16*2 LCD
microSD Click		3.3	2 GB
Ni-MH Battery	....	9	350mAh

### 3.2 System Implementation

**Data Processing with Arduino.** Coding of the Arduino Uno microcontroller is done in the Arduino Software (IDE) v1.0. The connections of the various components of the system with the Arduino board are shown in Tables 2 and 3 for the transmitter and receiver units respectively.

<sup>3</sup> Temperature and Pressure Sensor (TPS)

<sup>4</sup> Relative Humidity Sensor (RHS)

Temperature and pressure data from the BMP 180 digital sensor, relative humidity data from the analogue HIH-4030 sensor together with the date, time, location (latitude and longitude) and altitude data are processed and sent to the transmitter at intervals of 10s. The relative humidity being analogue, 10-bit digitization/quantization of the acquired values is done using (1).

$$RH = 100 - (\text{humidityValue} * 5) / 1024 \quad (1)$$

The microcontroller on the Arduino Uno board at the receiver unit formats the received streams of data and sends to the PC (running virtual terminal) and the LCD for display, and to the SD card using FAT16 file system for storage and future analysis.

**Table 2.** Components<sup>5</sup> pin connections with Arduino at the transmitter unit

Arduino Pin <sup>5</sup>	Component Pin
3.3V	J2-12 (Zigbee), +3.3V (GPS), + (TPS)
5V	5V (RHS)
GND	GND (Battery)
GND	J2-11 (ZigBee), GND (GPS), - (RHS), - (TPS)
Vin	(+9V) (Battery)
A3	OUT (RHS)
D4	IO (TPS)
D6	J2-4 Rx (ZigBee)
D7	J2-5 Tx (ZigBee)
D8	Tx (GPS)
D9	Rx (GPS)

---

<sup>5</sup> Pins on the Arduino or other components that are not shown had no connections

**Table 3.** Components' pin connections with Arduino at the receiver unit

Arduino Pin	Component Pin
3.3V	J2-12 (Zigbee), +3.3V (microSD)
5V	5V (LCD)
GND	GND (Battery)
GND	J2-11 (ZigBee), GND (LCD)
Vin	(+9V) (Battery)
D0 (Rx)	PC (via USB)
D1 (Tx)	PC (via USB)
D2, D3, D4, D5	LCD
D6	J2-4 Rx (ZigBee)
D7	J2-5 Tx (ZigBee)
D8, D9	LCD
D10, D11, D12, D13	CS, SDI, SDO, SCK (microSD)

**Data Communication with ZigBee.** The DRF1605H<sup>6</sup> transmitter and receiver modules is based on TI's CC2530F256 chip running ZigBee2007/PRO<sup>7</sup> agreement. It has all the features of the ZigBee protocol. It transmits data via the serial port and nodes can join the network automatically. It can support 1 coordinator node and up to 6^6 nodes as routers as full function devices (FFD) and supports transmission of variable length of packets (256 bytes per packet maximum).

Communication can be either in the point-to-point mode or transparent mode using the 2.4GHz license-free ISM (2400 – 2483.5MHz) band with 16 channels spaced at 5MHz. Configuration of the transceivers is done using the ZigBee Module Configure V5.1 software by DTK Electronics. For this application, the transceivers were configured to transmit and receive in the point-to-point operation mode on channel 14 (2.42GHz) according to (2). At this frequency, the transceivers can communicate up to a distance of 1.6km apart.

$$f_c = 2405 + 5(k - 11) \text{ MHz} \quad (2)$$

where  $k = 11, 12, \dots, 26$  is the channel number and  $f_c$  is the center frequency.

<sup>6</sup> <http://www.made-in-china.com/showroom/yihua20092010/product-detailGojEyXCLGscF/China-Zigbee-Module-DRF1605H-.htm>

<sup>7</sup> <http://www.zigbee.org/zigbee-for-developers/network-specifications/zigbeepro/>

## 4 Results and Discussion

Following system development, tests and analyses were carried out. These are presented as follows.

### 4.1 Sample Field Tests

Sample field tests were carried out using the developed system at the Federal University of Technology, Akure, Nigeria (lat.  $7.303^{\circ}$ N, long.  $5.135^{\circ}$ E) for three consecutive days (7<sup>th</sup> – 9<sup>th</sup> October, 2014) and at the hilly area of Idanre, Ondo State, Nigeria (lat.  $7.106^{\circ}$ N, long.  $5.106^{\circ}$ E) on 22<sup>nd</sup> October, 2014. Samples of results obtained are given in Table 4.

The transmitter was configured to send data at intervals of 10s. From Table 4, it can be seen that consecutive data were received at intervals of approximately 11s. The end-to-end latency of the system is thus 1s. Also, data streams received at the LCD, at the virtual terminal (Tera term on PC) and on the SD card were consistent across board. Consecutive data also do not vary significantly.

**Table 4.** Sample data retrieved from the SD card for analysis

Date d/m/y	Time h:m:s	Lat. ( $^{\circ}$ )	Long. ( $^{\circ}$ )	Alt. (m)	RH (%)	Temp. ( $^{\circ}$ C)	Pres. (mbar)
7/10/2014	14:36:38	7.3030	5.1355	441.6	98	28.24	968.97
7/10/2014	14:36:49	7.3030	5.1355	441.6	98	28.28	968.88
7/10/2014	14:37:00	7.3030	5.1355	441.6	98	28.41	968.55
8/10/2014	13:31:33	7.3026	5.1355	435.2	98	28.55	969.05
8/10/2014	13:35:53	7.3026	5.1354	435.2	98	28.51	968.89
8/10/2014	13:36:04	7.3026	5.1354	435.2	98	28.53	968.98
9/10/2014	10:27:53	7.3027	5.1358	430.7	97	26.80	971.20
9/10/2014	10:28:05	7.3027	5.1357	430.7	97	26.78	971.20
9/10/2014	10:28:16	7.3027	5.1357	430.7	97	26.75	971.23
22/10/2014	10:30:23	7.1059	5.1059	430.5	97	25.39	967.23
22/10/2014	10:30:34	7.1058	5.1058	431.0	97	25.22	966.96
22/10/2014	10:30:46	7.1058	5.1057	431.7	97	25.21	966.89

### 4.2 Battery Life Analysis

The current drain from the transmitter modules and the receiver modules are summarized in Tables 5 and 6 respectively.

**Table 5.** Current drain at transmitter unit

Component	Current Drain (mA)
TPS	0.005
RHS	0.5
Arduino	50
GPS	38
ZigBee Tx	80
<b>Total</b>	<b>169</b>

**Table 6.** Current drain at receiver unit

Component	Current Drain (mA)
Arduino	50
ZigBee Rx	45
LCD	4
<b>Total</b>	<b>99</b>

The life of the batteries can be calculated using (3)

$$L_{\text{batt}} = \text{battery capacity (mAh)} / \text{current drain (mA)} \quad (3)$$

where  $L_{\text{batt}}$  is the battery life.

With battery capacity of 350 mAh, it can be estimated that the battery at the transmitter and receiver units would last approximately 2 hours and 4 hours respectively if on continuous mode. To increase battery life, the systems have to be run on higher capacity batteries and more importantly on batteries rechargeable using solar power or other energy harvesting methods.

## 5 Conclusion

A data acquisition system with real-time sensing, data logging and wireless communication was developed for the environmental monitoring of farmlands. With the incorporation of a GPS module, users (farmers) are able to determine the exact location, data, time and altitude at which measurements were taken, alongside the monitored environmental parameters (temperature, pressure and relative humidity).

The deployment of this technology-based device may increase productivity of the farm field by providing the opportunity to make informed decisions from acquired data for the appropriate time and place and to model general trends and make accurate forecasts for places with similar characteristics thereby encouraging precision agriculture.

With this system deployed and with the acquired data, appropriate decisions and actions can be taken on the farms based on expert knowledge of the effects of studied parameters on plant yield.

Further works will require the incorporation of soil and crop monitoring sensors, alongside the environmental sensors, for better and improved farm management system. Also, optimization of the system's power and transmission to multiple receivers are the next lines of action for further work.

## References

1. Kodali, R.K.; Rawat, N.; Boppana, L.: WSN sensors for precision agriculture. In: Region 10 Symposium, pp.651-656, IEEE Press (2014)
2. Tagarakis, A.; Liakos, V.; Perlepes, L.; Fountas, S.; Gemtos, T.: Wireless Sensor Network for Precision Agriculture. In: 15th Panhellenic Conference on Informatics (PCI), pp.397-402, IEEE Press (2011)
3. Heintz D.: Essential Components of Data Acquisition Systems Application Note 1386. Agilent Technologies, USA. Available online at <http://cp.literature.agilent.com/litweb/pdf/5988-5386EN.pdf> (2002)
4. Saima M.; Ulya S.: Arising Issues in Wireless Sensor Networks: Current Proposals and Future Developments. IOSR Journal of Computer Engineering (IOSR-JCE), vol. 8, issue 6, pp 56-73 (2013)
5. Deepika D.: Designing a Microcontroller-Based Temperature Data Logger. Master of Engineering Thesis, Department of Electrical and Instrumentation Engineering, Thapar Institute of Engineering and Technology, Deemed University, Patiala, India (2006)
6. Noor H. A.; Suzi S. S.; Kama A. O.; Norfishah W.; Norzatina M.; Ahmad T. H.: Supervisory Data Acquisition of Temperature and Humidity in Oil Palm Tissue Culture Laboratory". International Conference on Computational Intelligence, Modelling and Simulation, pp 470-475, IEEE Press (2010)
7. Haefke, M.; Mukhopadhyay S. C; Ewald H.: A ZigBee-Based Smart Sensing Platform for Monitoring Environmental Parameters. Instrumentation and Measurement Technology Conference (I2MTC), IEEE (2011)
8. Guha, S. K.; Nabhiraj, P. Y.; Bhattacharjee T. K.; Mallik C.: Design and Implementation of an IEEE 802.15.4 / ZigBee Based Star Network for Data Acquisition and Monitoring. India Software and Hardware Technology, pp 160-162, Kolkata, India (2012)
9. Kassim, M.R.M.; Mat, I.; Harun, A.N.: Wireless Sensor Network in precision agriculture application. In: 2014 International Conference on Computer, Information and Telecommunication Systems (CITS), vol., no., pp.1-IEEE Press (2014)
10. Qingyuan M.; Qiang C.; Qingsheng S.; Chao Z.: The Data Acquisition for Precision Agriculture Based on Remote Sensing. In: IGARSS 2006. IEEE International Conference Geoscience and Remote Sensing Symposium, pp.888-891, IEEE Press (2006)
11. Santoshkumar; Udaykumar, R.Y.: Development of WSN system for precision agriculture. In: 2015 International Conference Innovations in Information, Embedded and Communication Systems (ICIECS), pp.1-5, IEEE Press (2015)

## Real-Time Vision System for Lane Tracking and Semaphore Recognition

Valter Costa

Faculty of Engineering University of Porto,  
Rua Dr. Roberto Frias, s/n 4200-465 Porto, Portugal  
[ee09115@fe.up.pt](mailto:ee09115@fe.up.pt)

**Abstract.** The interest in autonomous vehicles has steadily increased in recent years. A number of tasks, like lane tracking and semaphores detection and decoding, are key features for an self-driving robot. This paper presents a path detection and tracking algorithm using the Inverse Perspective Mapping and Hough Transform methods compounded with real-time vision techniques and a semaphore recognition system based on color segmentation. An evaluation of the proposed algorithm is performed and a comparison between the results using real-time techniques is also presented. The suggested architecture has been put to test on autonomous driving robot who competed in the Portuguese autonomous vehicle competition called "Festival Nacional de Robótica". Regarding to the lane tracking algorithm, the usage of the real-time vision premises lead to significantly faster results, with computation time of 1.4ms, almost 60 times faster than the first algorithm tested and a good accuracy, in this context, showing a translation error below 0.03m and a rotation error below 5 degrees. On the subject of semaphore recognition algorithm, it has shown zero false positives but it relies on the quality of the color calibration, making it very dependent of the ambient lighting.

**Keywords:** Real Time Vision · Image Processing · Autonomous Driving · Inverse Perspective Mapping · Lane Tracking · Semaphore Recognition

### 1 Introduction

Autonomous vehicles (AVs) represent a major innovation for the automotive industry; self-driving cars pave the way for a myriad relevant applications across multiple fields. In such a dynamic context, work and research in this area has grown greatly over the last years. Many car makers are developing prototype vehicles. Vehicles like the BMW-Series 5, the Mercedes-Benz-Series 500, the Nissan Leaf EV, the General Motors Cadillac SRX and the Prius and Lexus from Google, already provide interesting key technologies [7].

This topic has even raised interest within the robotics community and was the target focus of many robotic competitions around the world [6].

An autonomous intelligent vehicle has to perform a number of tasks, sometimes in a limited amount of time [4]. The most critical task is the perception

and mapping of the surrounding environment. This involves being capable of identifying and tracking road lanes, being able to process traffic lights and road signs, and being consistent at identifying and avoiding obstacles [5, 8, 13, 2].

Although many solutions exist, one of the most common approaches to tackle these problems is the use of one or more cameras on the robot's body.

This paradigm allows the robot to identify its surroundings and even create a map with its localization. Usually, when extracting information from an image, one holds some prior knowledge on the state of the system (that is, some notion on the state of the surrounding environment) and, therefore, more detailed measurements can be obtained. Often, however, in autonomous driving, little information is known about the environment because no previous or overall structure is present [1]. Therefore, it's not only important to get accurate results, but also to do it in an adequate timing - real-time.

And while real time is often described as "a level of computer responsiveness that a user senses as sufficiently immediate or that enables the computer to keep up with some external process" [3], it is more accurately defined as the sufficient time the robot needs to process external data and actuate without causing any harm to himself or to others.

Some authors [11] have proposed offline-online strategies with a well defined trade off between accuracy and computational cost to the perception of the real world.

A known real-time vision technique is the application of the "zero copy, one pass" technique used in [12]. Using this technique, it is only needed to read the input image only once, taking all the necessary information (which is organized into smaller vectors). This approach guarantees that the objective is reached without creating copies of the input image, saving processing time.

Another technique useful to obtain relevant features for road estimation algorithms is the inverse perspective mapping (IPM) [9, 10]. IPM is a geometrical transformation technique that projects each pixel of the 2D camera perspective view of a 3D object and re-maps it to a new position, constructing a rectified image on a new 2D plane. Mathematically, IPM can be described as a projection from a 3D manifold ,  $W = \{(x, y, z)\} \in E^3$  (real life input space) onto a 2D plane,  $I = \{(u, v)\} \in E^2$ . The result is the desired bird's eye view of the image, thus removing the perspective effect. This is achieved using information from the camera's position and orientation in relation to the road.

The work presented in this paper aims to contribute to this thematic by presenting a line detection and tracking algorithm using real-time vision techniques. This algorithm have been tested on the 2015 Portuguese autonomous driving competition called "Festival Nacional de Robótica". An evaluation of the proposed algorithm is also described.

The remainder of this paper is organized as follows. In Section 2 all the steps and methods followed in designing the algorithm are presented. Section 3 presents the real time results obtained from the algorithm. Finally, Section 4 draws conclusions from the obtained data.

## 2 Methodologies

This section presents all the methods and methodologies used to produce the results presented in the next chapter. All the tasks ranging from the development of the vision system till the building of the autonomous driving robot are presented too. The autonomous driving competition consists of a robot completely devoid of human input during its runtime, which runs on a track, detects vertical signs and traffic lights (projected on two monitors) and avoids obstacles. The vision system developed uses two cameras, being able to: (i) detect and calculate the distance and angle to the right line in the robot referential and (ii) identify and detect semaphores. The cameras used are 2 PLAYSTATION Eye™ running with a resolution 320x240 @ 30Hz.

The choice of two cameras is due to the fact that it makes possible the detection of traffic signs and the track simultaneously, which is normally impossible with only one camera.

### 2.1 Tracking Lines Algorithm

The tracking algorithm used is exemplified in Fig. 1. The first step is to capture a RGB frame from the camera. Then this image is converted to grayscale. The third step is the removal of the distortion due to the lens used (which raises the field of view of the camera). Afterwards, it is applied a kernel to calculate the horizontal derivative of the undistorted image, thus choosing points considered as being part of a line. The IPM transform (explained in the following subsection) is applied only to the aforementioned points. Next, the Probabilistic Hough Transform is employed to detect the lines. From the detected lines returned by the transform, only the "best" one is retained (the line that has the minimum distance between the actual line and the one before).

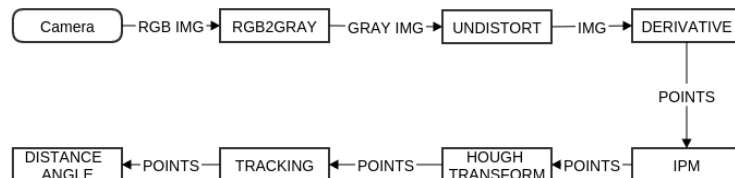


**Fig. 1.** Block diagram for the tracking algorithm.

**Inverse Perspective Mapping** is a geometrical transform that projects each pixel from the 2D view of 3D objects with perspective and maps them to a new position, building a new image on a new inverse 2D plane (this perspective is normally called bird's eye view). In this case, the strategy used was calculating

the transform from the camera referential to the chessboard referential, represented by T1, then calculating the transform from the chessboard to the robot referential, represented by T2, in Fig. 2b. The Fig. 2a shows the setup used to calculate T1 and T2.

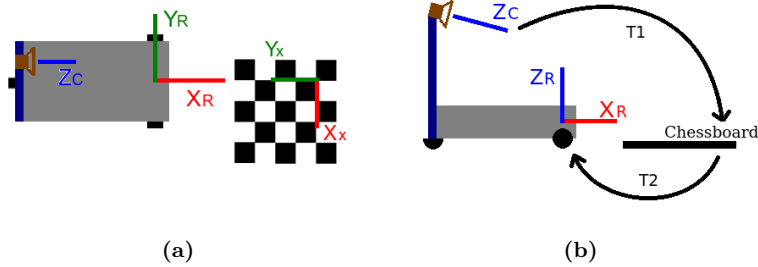


**Fig. 2.** IPM - Transformations used: top view (a) and side view (b).

The T1 transform was obtained using the camera extrinsic parameters and T2 was calculated measuring the distances between the chessboard/robot references and the rotation matrix between them. To apply the IPM transform it is necessary to perform the transformation described in 1. Eq. 2, Eq. 3 and Eq.4 are intermediate steps leading to IPM transform.

$$\begin{bmatrix} X \\ Y \\ Z \\ w \end{bmatrix} = \begin{bmatrix} p_{11} & p_{12} & p_{13} & -x \\ p_{21} & p_{12} & p_{23} & -y \\ p_{31} & p_{32} & p_{33} & -1 \\ a & b & c & 0 \end{bmatrix}^{-1} \times \begin{bmatrix} -t_1 \\ -t_2 \\ -t_3 \\ -d \end{bmatrix} \quad (1)$$

$$P = K * T2_R * T1_R = \begin{bmatrix} p_{11} & p_{12} & p_{13} \\ p_{21} & p_{12} & p_{23} \\ p_{31} & p_{32} & p_{33} \end{bmatrix} \quad (2)$$

$$t = K * T_t = \begin{bmatrix} t_1 \\ t_2 \\ t_3 \end{bmatrix} \quad (3)$$

$$K = \begin{bmatrix} \alpha_x & \beta & x_0 \\ 0 & \alpha_y & y_0 \\ 0 & 0 & 1 \end{bmatrix} \quad (4)$$

$$a * X + b * Y + c * Z + d = 0 \quad (5)$$

Wherein  $\alpha_x$  and  $\alpha_y$  are the focal length in pixels along x and y, respectively,  $x_0$  and  $y_0$  the principal point coordinates in pixels and  $\beta$  the skew factor in matrix K.  $T1_R$  and  $T2_R$  are the rotation matrices from the transformations

$T_1$  and  $T_2$ .  $x$  and  $y$  are the coordinates from the input image pixel.  $T_t$  is the vector of translation resulting of the  $T_1$  and  $T_2$  multiplication.  $a, b, c, d$  define a geometric plane for the application of the IPM (equation 5).  $X$  and  $Y$  are metrical coordinates on the robot's referential.

After we obtain  $X$  and  $Y$ , in order to achieve a visual representation of the IPM, the last step is to map these points. An example of the result can be seen in Fig. 3.

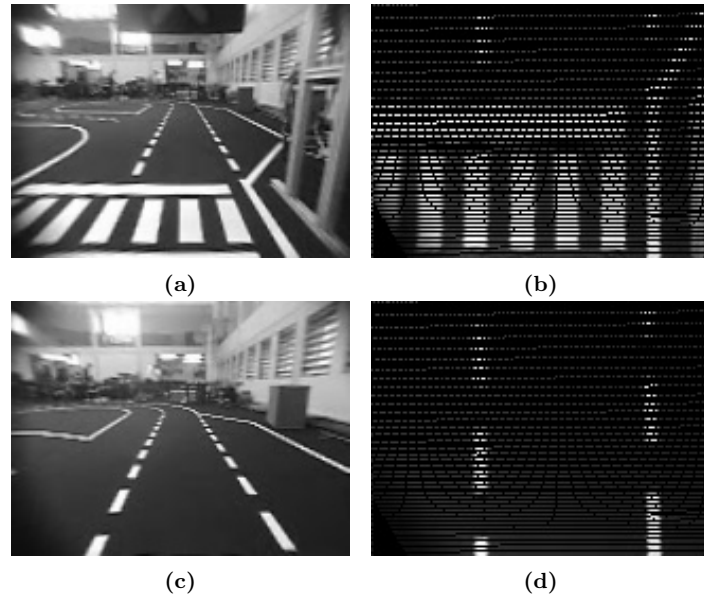


**Fig. 3.** Two examples of the IPM transform. Images (a) and (c) are the original ones taken from the camera, while (b) and (d) are obtained by the IPM transform.

This algorithm has the advantage of allowing, from the input image, the direct calculation of the position ( $x, y$ ) in meters on the robot's referential. Another advantage is the possibility to delimit a window of interest on the robot's referential, allowing an optimized processing of the relevant information.

**Tracking algorithm** After the IPM transform, the next step is the detection of the lines drawn on the IPM transformed image. The strategy used is the application of the Hough Transform variant for line detection. This transform is available in OpenCV in two alternatives: *HoughLines()* and *HoughLinesP()*. The major difference between them is on the choice of the pixels to use on the

calculation of the Hough space. The first one resorts to every pixel on the image and the second uses random pixels to calculate the transform, making it more faster than the previous one mentioned.

The Hough Transform function returns a vector of lines detected. After that, the algorithm chooses the "best" line from the received vector, which is the line nearest to the previous one detected (inside a limited range). If no line fulfills this condition, the previous one is maintained. The last step is to calculate the distance from the robot's referential to the point chosen. As we have used the IPM strategy, this step is simplified, making its computation direct.

## 2.2 Semaphore Detection

The detection of the semaphore is achieved via another camera installed on the robot (pointed up). The competition ruling defines a specific dataset of semaphores used, showed in Fig. 4.

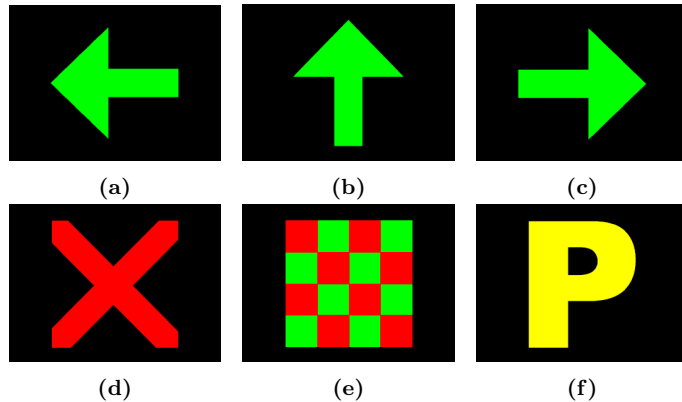


**Fig. 4.** Semaphores used in the 2015 autonomous driving competition.

**Semaphore algorithm** As the semaphores are characterized by three main different colors and shapes (red, yellow and green), the detection algorithm is based on color segmentation in the HSV color space. Basically, it searches for a blob of the mentioned colors possessing a defined minimum area (to filter irrelevant information). A calibration to the hue component thresholds has to be done beforehand to ensure a correct classification.

The stop semaphore (Fig. 4d) was detected by looking for an area of red in the input image, the parking semaphore (Fig. 4f) was detected by looking for an area of yellow and the arrow semaphores (Fig. 4a, 4b and 4c) for an area of green color. The green semaphores need an additional step was to differentiate them. The green region (bounded by a rectangle) is divided into four regions,

and the area ratios between these regions are tested in order to identify the type of arrow.

The red and green flag semaphore, Fig. 4e, although not employed in the competition, is used to test the robustness of the proposed algorithm.

### 3 Results

This section presents the results obtained from the application of real time vision philosophy. Table 1 and 2 shows a comparison between the same tracking algorithm, one version using the real-time vision premise "zero copy, one pass" (Fast) and another version without (Slow). The accuracy of the distance and angle measures obtained from the tracking system is displayed in Fig. 5, and some image results for the tracking lines algorithm are also presented. Regarding to the semaphore recognition algorithm some laboratory results are presented.

**Table 1.** Average execution time of IPM algorithm

PC	Slow IPM Time (ms)	Fast IPM Time (ms)	Ratio (%)
ROG	80.74	0.4854	16634
EeePC	587.7	3.100	18960
RaspberryPi	2970	15.52	19131
RaspberryPi2	1344	7.174	18741

**Table 2.** Average execution time of the tracking algorithm showed in Fig. 1.

PC	Slow Tracking Time (ms)	Fast Tracking Time (ms)	Ratio (%)
ROG	84.56	1.424	5936
EeePC	604.2	8.599	7025
RaspberryPi	3209	45.60	7037
RaspberryPi2	1366	22.98	5946

Looking at Table 1 and 2, it is evident the significant time reduction on the tracking lines algorithm. In the case of the ROG, the execution time became 59 times faster and on the EeePC and in the Raspberry was 70 times faster. This time does not take into account the data transfer time on the USB. The characteristics of PCs used on the tests are in Appendix 1.

Another important result is the accuracy of the distance and angle returned by the tracking algorithm. Fig. 5c and 5b shows a comparison between the real-life measurements and the ones obtained from the algorithm. The blue line represents the ideal case where the real-life measurements equals the calculated ones (a null error). Observing Fig. 5a and Fig. 5b, it can be seen that the obtained

distance and angle are precise enough for the application at hand, showing an distance error below 0.03m, Fig. 5c, and an angle error below 5 degrees, Fig. 5d.

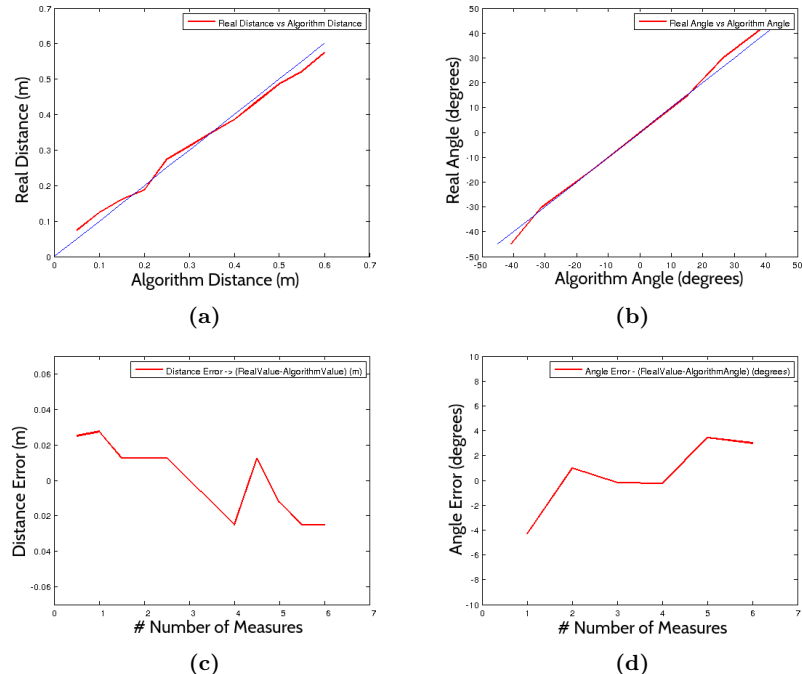


**Fig. 5.** Distance accuracy tests results (a) and related absolute error (c); angle accuracy tests results (b) and related absolute error (d).

The accuracy results were obtained by placing the robot in different known positions on the track, measuring the real distance and angle between the robot's referential and the intersection point to the right line.

In Fig. 6a, it is shown the detected lines returned by the Probabilistic Hough Lines Transform function drawn on top of the IPM image (Fig. 6b).

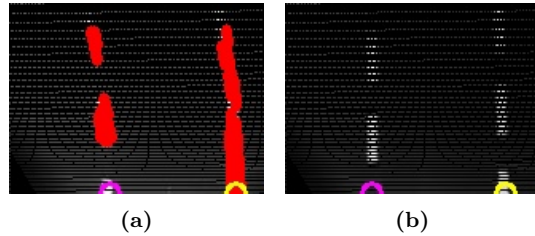


**Fig. 6.** Hough Transform detected lines (a) drawn on top of the IPM transformed image (b).

The yellow and purple circles are the result<sup>1</sup> of the tracking lines system. The distance and angle measures needed are calculated from the yellow circle (which is the correct line to be tracked).

The semaphore recognition algorithm was also tested into the autonomous driving competition. In the context of the robotics competition, this technique is precise enough, ensuring zero false positives in both the tests made and the competition. For a more robust implementation, some additional image processing is required and more complex tests are needed. In Fig. 7 it is showed a laboratory application result for each semaphore of the competition.

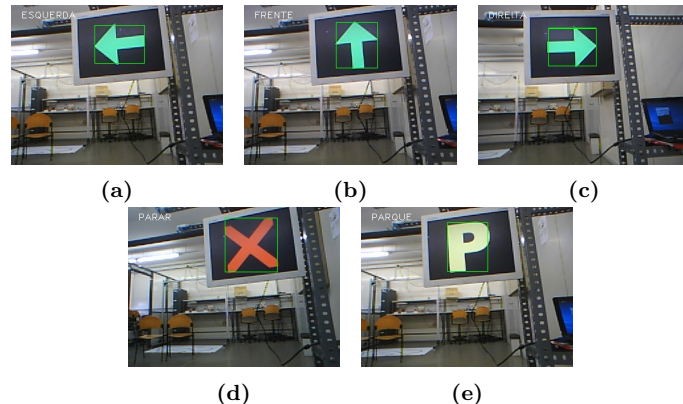


**Fig. 7.** Example of the application of the proposed semaphore detection algorithm.

---

<sup>1</sup> More representative results showing the proposed tracking system can be found in:  
<https://www.youtube.com/watch?v=6XN29PRc5Eg>

As it can be seen from Fig. 7, all semaphores are correctly detected<sup>2</sup>.

#### 4 Conclusions

This paper presented a real-time vision tracking algorithm applied to an autonomous driving robot.

The evaluation of the proposed system is performed in two different ways: measurement and comparison of the algorithm's execution time on different platforms and measurement of the accuracy of the distance and angle calculation.

The proposed system has advantages over existing implementations. After a correct calibration of the camera, the usage of Inverse Perspective Mapping allows to precisely calculate the distance and angle using real world coordinates. Also, the use of the "zero copy, one pass" principles were very important to make this system faster, enabling the possibility of running this algorithm in low-cost embedded platforms.

There are also limitations in the overall architecture. The use of IPM, associated with the removal of the perspective, causes a projection of the 3D objects in the 2D image, making it harder to correctly detect the objects, since connecting pixels in the original image do not correspond to connecting features in the real world image. This implies that, in order to avoid obstacles, another strategy has to be employed, like the use of complementary sensors or more image processing (likely in the original image). Another limitation is that the line following algorithm has to be initialized to start tracking lines.

The developed algorithm can be applied in real-life scenarios, such as a real car, particularly on highways, because it is, usually, a more controlled environment, mostly containing lines.

A proposed semaphore detection algorithm was also presented on the context of the autonomous driving competition. In this case a quantitative evaluation was made. This semaphore recognition algorithm has shown zero false positives but it relies on the quality of the color calibration, making it very dependent of the ambient lighting. To apply this algorithm in another scenarios some additional image processing is required to guarantee robustness to objects with same color range.

As future work it is suggested the creation of a routine that initializes the tracking line system autonomously. This will allow a more flexible way to start the robot at any point and orientation.

Other alternatives include taking manual control of the hardware camera parameters in order to obtain better color image quality in semaphore recognition.

---

<sup>2</sup> More results showing the proposed semaphore recognition system can be found in:  
<https://www.youtube.com/watch?v=KaPIKzncMd8>

## References

1. Chen, N.: A vision-guided autonomous vehicle: an alternative micromouse competition. *IEEE Transactions on Education* 40(4), 253–258 (1997), <http://ieeexplore.ieee.org/lpdocs/epic03/wrapper.htm?arnumber=650837>
2. Della Vedova, M., Facchinetti, T., Ferrara, a., Martinelli, a.: Visual Interaction for Real-Time Navigation of Autonomous Mobile Robots. *2009 International Conference on CyberWorlds* pp. 211–218 (2009), <http://ieeexplore.ieee.org/lpdocs/epic03/wrapper.htm?arnumber=5279610>
3. Group, E.S.: Real Time - ESP Solutions Group (2015), <http://www.espsolutionsgroup.com/glossary/real-time/>
4. Hager, G.D., Toyama, K.: X Vision: A Portable Substrate for Real-Time Vision Applications. *COMPUTER VISION AND IMAGE UNDERSTANDING* 69(1), 23–37 (1998), <http://www.sciencedirect.com/science/article/pii/S1077314297905865>
5. Kardkov, Z.T.: Real-time Traffic Sign Recognition System
6. Kawatsu, C., Li, J., Chung, C.J.: Robot Intelligence Technology and Applications 2012, vol. 208 (2012)
7. MIT: MIT Technology Review (2015), <http://www.technologyreview.com/featuredstory/520431/driverless-cars-are-further-away-than-you-think/>
8. Mu, G., Xinyu, Z., Deyi, L., Tianlei, Z., Lifeng, A.: Traffic light detection and recognition for autonomous vehicles. *The Journal of China Universities of Posts and Telecommunications* 22(1), 50–56 (2015), <http://www.sciencedirect.com/science/article/pii/S1005888515606240>
9. a.M. Muad, Hussain, a., Samad, S., Mustaffa, M., Majlis, B.: Implementation of inverse perspective mapping algorithm for the development of an automatic lane tracking system. *2004 IEEE Region 10 Conference TENCON 2004. A*, 207–210 (2004)
10. Oliveira, M., Santos, V., D.Sappa, A.: Multimodal inverse perspective mapping. *International Journal of Computer Vision* 24(1), 108–121 (2004), <http://www.sciencedirect.com/science/article/pii/S1566253514001031>
11. Ros, G., Ramos, S., Granados, M., Bakhtiyari, A., Vazquez, D., Lopez, A.M.: Vision-Based Offline-Online Perception Paradigm for Autonomous Driving. *2015 IEEE Winter Conference on Applications of Computer Vision* pp. 231–238 (2015), <http://ieeexplore.ieee.org/lpdocs/epic03/wrapper.htm?arnumber=7045892>
12. Sousa, A., Santiago, C., Malheiros, P., Costa, P., Moreira, A.P.: Using Barcodes for Robotic Landmarks. *New Trends in Artificial Intelligence* pp. 300–311 (2009), <http://epia2009.web.ua.pt/onlineEdition/NewTrendsInArtificialIntelligence.pdf>
13. Wahyono, Kurnianggoro, L., Hariyono, J., Jo, K.H.: Traffic sign recognition system for autonomous vehicle using cascade SVM classifier. *IECON 2014 - 40th Annual Conference of the IEEE Industrial Electronics Society* (1), 4081–4086 (2014), <http://ieeexplore.ieee.org/lpdocs/epic03/wrapper.htm?arnumber=7049114>

## Appendix 1: PCs Characteristics

**Table 3.** PCs characteristics used on test of the tracking algorithm.

Model	CPU	Memory
Raspberry Pi B 512MB	ARM1176JZF-S 700 MHz	512MB
Raspberry Pi 2 B	900MHz quad-core ARM Cortex-A7 CPU	1GB
Asus EeePC 1005HA	1.66GHz Intel Atom N280	2GB
Asus ROG GL550JK	Intel Core i7-4700HQ 2.5GHz	16GB

# A Model-Driven Approach for Components Testing

Bruno Lima<sup>1,2</sup> and João Pascoal Faria<sup>1,2</sup>

<sup>1</sup> INESC TEC,

FEUP campus, Rua Dr. Roberto Frias, s/n 4200-465 Porto, Portugal

<sup>2</sup> Faculty of Engineering, University of Porto,  
Rua Dr. Roberto Frias, s/n 4200-465 Porto, PORTUGAL  
`{bruno.lima,jpf}@fe.up.pt`

**Abstract.** In a growing number of domains, such as ambient-assisted living (AAL) and e-health, the provisioning of end-to-end services to the users depends on the proper interoperation of multiple products (devices, applications, etc.) from different vendors, forming a digital ecosystem. To ensure interoperability and the integrity of the ecosystem, it is important that candidate products are independently tested and certified against applicable interoperability requirements. Based on the experience acquired in the AAL4ALL project, we propose in this paper a model-based approach to systematize and automate such testing and certification activities. The approach encompasses the construction of several models: a feature model, an interface model, a product model, and unit and integration test models. The abstract syntax and consistency rules of these models are specified by means of metamodels written in UML and Alloy and automatically checked with Alloy Analyzer. Examples of concrete models from the AAL4ALL project are also presented.

**Keywords:** Test Models · Metamodel · Certification · Ambient-Assisted Living

## 1 Introduction

In the area of e-health, Ambient-Assisted Living (AAL) technologies [8] are being increasingly used in response to problems caused by the increasing age of the population, but these first answers are monolithic, incompatible and thus expensive and potentially not sustainable (e.g. [13]). The AAL4ALL project [1] tried to answer those problems through the development of an ecosystem of interoperable products and services for AAL, associated to a business model and validated through a large scale trial. One goal of this project was to ensure that any supplier of AAL products and services, whether they are physical devices or software, can enter the ecosystem easily and independently, whilst assuring their interoperability with the rest of the ecosystem. In this way customers can acquire a first AAL basic solution (e.g. a fall alert system) and later adding other types of products or services according to their needs, with the assurance that

the products they already have and the new products are able to communicate together. To that end, the AAL4ALL project encompasses the specification of a set of reference models and requirements for products and services, against which candidate products and services can be certified and subsequently integrated as components of the ecosystem. The project also encompasses the definition of a testing and certification methodology for these new components, which can be found in [6].

Recently the use of Model-Driven Engineering (MDE) techniques as a response to deal with complex problems (like the previously described), has been increasing [11]. One of the MDE technologies are the Domain-Specific Modeling Languages (DSMLs) [11]. These languages allow the formalization of the application structure, behavior, and requirements within particular domains, such as software-defined radios, avionics mission computing, online financial services, warehouse management, or even the domain of middleware platforms. DSMLs are described using metamodels, which define the relationships among concepts in a domain and precisely specify the key semantics and constraints associated with these domain concepts. Developers use DSMLs to build applications using elements of the type system captured by metamodels and express design intent declaratively rather than imperatively.

In this article, using DSMs, we propose a set of templates and integrity rules for defining products and their functionality within a specific domain thereby allowing the automatic generation of certification testing for candidate products. For better comprehension of the proposed models, are presented application examples in the field of the AAL4ALL project.

The rest of the paper is organized as follows: section 2 presents the overall approach and architecture; section 3 presents the proposed metamodels; in section 4 are presented application examples; related work is presented in section 5; conclusions and future work are presented in section 6.

## 2 Overall Approach and Architecture

The models proposed in this paper support an incremental process that enables the automatic test case generation for certification. This approach is based on traditional OMG Modeling Infrastructure [2] that consists of a hierarchy of model levels, each (except the top) being characterized as “an instance” of the level above. The bottom level, also referred to as M0 is said to hold the “user data”, i.e., the actual data objects the software is designed to manipulate. The next level, M1, is said to hold a “model” of the M0 user data. This is the level at which user models reside. Level M2 is said to hold a “model” of the information at M1. Since it is a model of a (user) model, it is often referred to as a metamodel. Finally, level M3 is said to hold a model of the information at M2, and hence is often characterized as the meta-metamodel. For historical reasons it is also referred to as the Meta Object Facility (MOF) [9]. Fig. 1 show the global perspective of the models proposed.

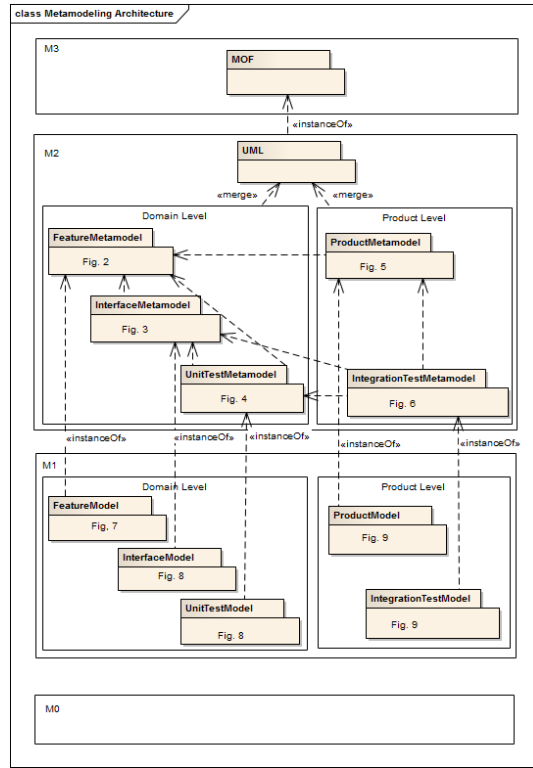


**Fig. 1.** Proposed Metamodels

In M2 we propose a set of metamodels divided in two different levels, Domain Level and Product Level. The Domain Level represents the specific features related with a specific domain, the interfaces and the unit tests related with these features. Inside this level we propose three different metamodels, FeatureMetamodel, InterfaceMetamodel and UnitTestMetamodel. The Product Level represents candidate products and integration test scenarios used for certification, that envolve other products (already certified). Inside of this level we propose two different metamodels, ProductMetamodel and IntegrationTestMetamodel.

In M1 we propose a set of models (“a instances” of the metamodels above) also divided in two different levels. Inside the Domain Level we propose a FeatureModel, InterfaceModel and UnitTestModel. Inside the Product Level we propose a ProductModel and IntegrationTestModel. The next section present the metamodels, by means of UML class diagrams and associated constraints. The constraints and data types are written in Alloy, in order to support the automated analysis and validation of the metamodels with Alloy Analyzer.

### 3 Metamodels

#### 3.1 Feature Metamodel

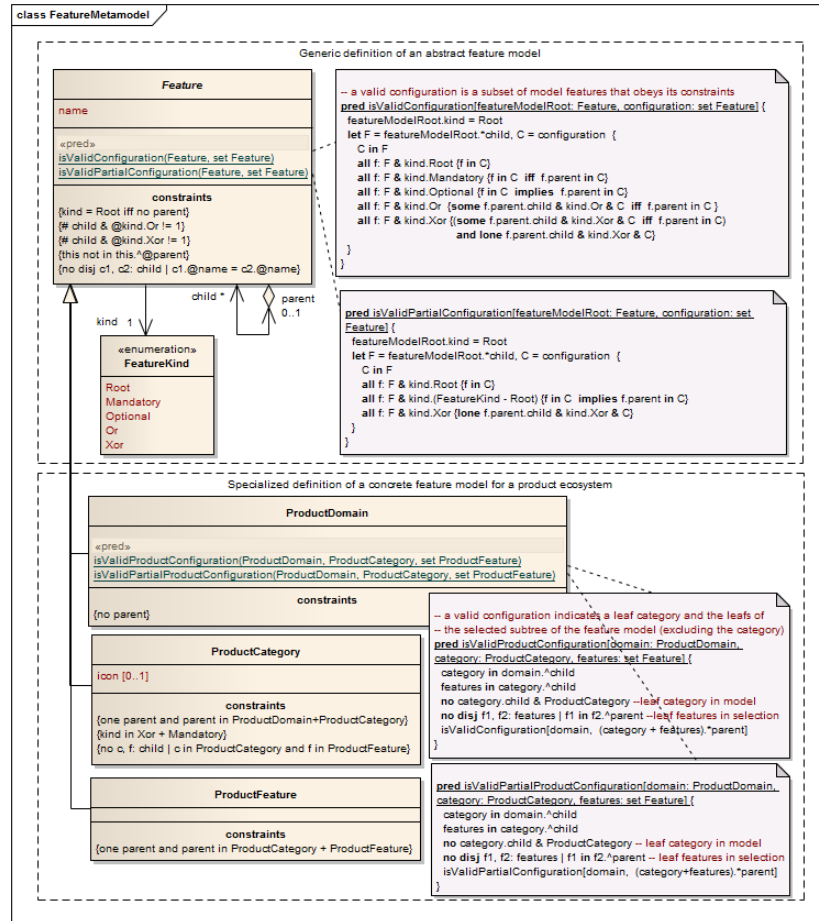


Fig. 2. Feature Metamodel

In some ecosystems, such as in the AAL field, there is a wide variety of products with a great features variability. It is therefore very important to limit the scope of the certification of such products within a ecosystem. For this, based on the formalism of Feature Models [3], we propose a metamodel that allows represent the variability of products and their features within an ecosystem.

Firstly, in the upper layer of Fig. 2, we define the structure and semantics of general purpose feature models. A feature model is a hierarchically arranged set of features where relationships between a parent (or compound) feature and its child features (or subfeatures) are categorized as:

- And – all subfeatures must be selected
- Alternative – only one subfeature can be selected
- Or – one or more can be selected
- Mandatory – features that are required
- Optional – features that are optional

The semantics of these constructs is formalized by the auxiliary predicate `isValidConfiguration` in Fig. 2, which checks if a configuration (a particular selection of features in the feature model) is valid. Some well formedness rules of feature models are specified in Fig. 2 by constraints (facts) written in Alloy.

The lower layer of Fig. 2 contains specialized definitions for our purpose. A Feature Model is created for a specific domain (represented by `root`), where the model is composed of categories (`ProductCategory`) that may or may not have subcategories (`ProductCategory` with a `ProductCategory` as a parent). The product categories have features (represented by `ProductFeature`).

### 3.2 Interface Metamodel

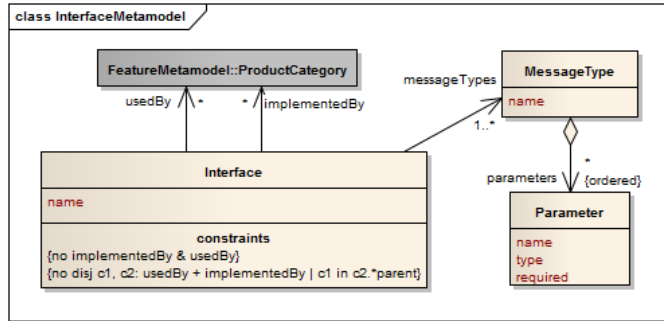


**Fig. 3.** Interface Metamodel

To test a particular feature of a product it is important that the messages exchanged for this product are specified according to a certain format. To allow this we propose the `InterfaceMetamodel` shown in Fig. 3, containing the set of rules necessary to message specification for a particular domain. To ensure interoperability, the ecosystem products have to communicate by exchanging “standardized” messages via “standardized” interfaces. An interface defines the types of messages that can be sent or received through it, by product categories that use or implement the interface, respectively.

### 3.3 Unit Test Metamodel

Our proposal is based on the principle that the features of the FeatureModel (see subsection 3.1) have one or more associated unit tests; these tests allow the verification if a product implement this feature according to the ecosystem rules. To describe the unit tests we propose the UnitTestMetamodel shown in Fig. 4.

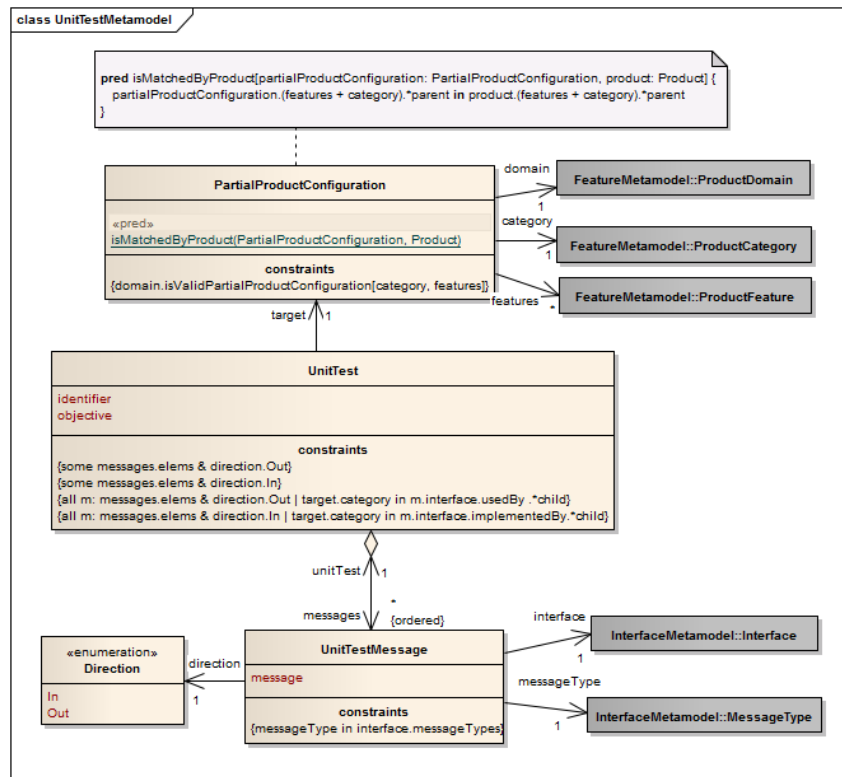


**Fig. 4.** Unit Test Metamodel

A unit test refers to a sequence of messages sent (output) or received (input) by a unit under test through interfaces it uses or implements, respectively. The unit under test is any product that matches (in the sense formalized by the predicate `isMatchedByProduct` in Fig. 4) a `PartialProductConfiguration` specified as the target of the `UnitTest`.

### 3.4 Product Metamodel

The Product Metamodel proposed (See Fig. 5) allows the description of a product. In this context a product belongs to a domain and a specific (sub)category and can have multiple features. The product also has a name and a flag indicating if it is a certified product or not.

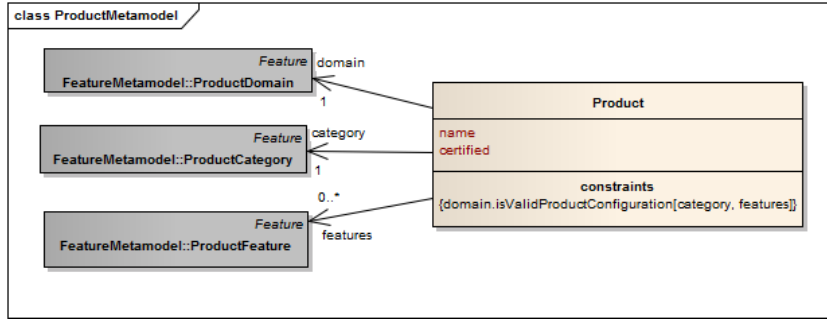


**Fig. 5.** Product Metamodel

### 3.5 Integration Test Metamodel

To obtain certification, products may be submitted to a series of end-to-end integration tests in a scenario that include other products (already certified), in order to ensure that it is able to communicate according to the message specification defined by the ecosystem.

To describe integration tests, we propose the IntegrationTestMetaModel shown in Fig. 6. An integration test refers to a sequence of messages exchanged among a set of participants, including the product under test (not yet certified), zero or more products already certified, and actors. The participants are connected through defined interfaces; for each connection, messages flow from the participant that uses the interface (the source of the message) to the participant that implements the interface (the destination of the message).

Integration tests are generated by instantiating and composing unit tests previously defined. The instantiation is defined by two mappings: a mapping of unit test targets (partial product configurations) to actual products in the integration test (targetMapping); and a mapping of unit test messages to integration test messages (messageMapping). To ensure proper composition and instantiation, several consistency rules or constraints apply for these mappings, as described in the attached note in Fig. 6. Message coupling (synchronization) between unit tests is achieved by mapping a pair of unit test messages - a message sent in the scope of one unit test and a message received in the scope of another unit test - to a single integration test message.

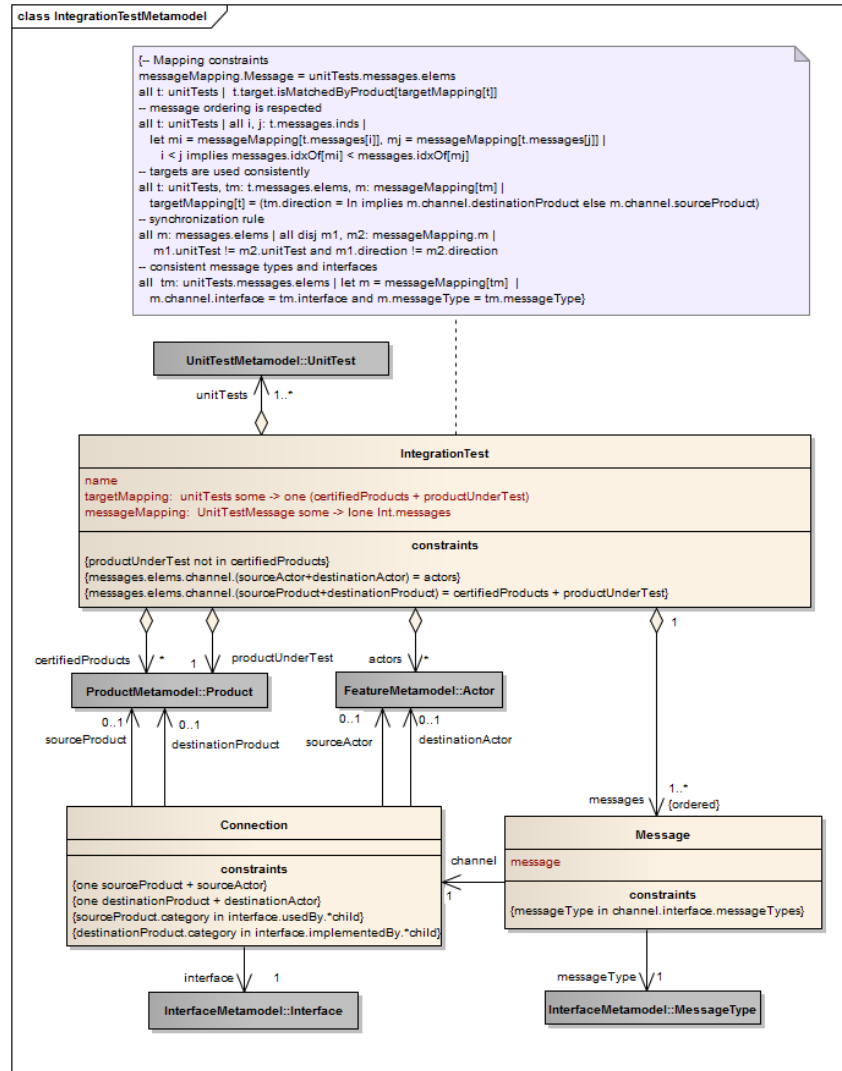
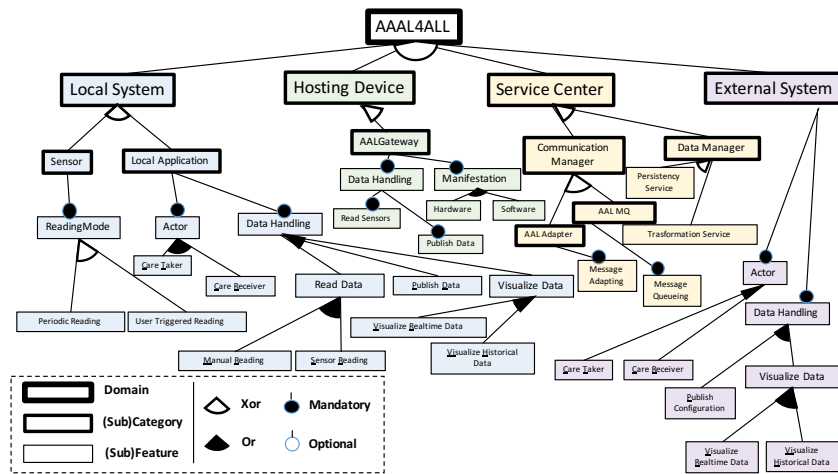


Fig. 6. Integration Test Metamodel

The actual mechanisms of test execution are not specified in the models, but it is assumed that the actors' behavior (send messages to the system and monitor and check messages received from the system) will be simulated by a tester or a test script. Messages exchanged between products in the system may or not be monitored and checked.

#### 4 Example Models for the AAL Domain

The certification process defined in the AAL4ALL project comprises four main categories of products for which candidate products could be certified. Within some of these main categories it were defined product subcategories, taking into account the features that the product must possess. Taking into account the rules described in the FeatureMetamodel proposed in section 3.5 the feature model for the AAL4ALL domain containing the categories, subcategories and features can be observed in Fig. 7.



**Fig. 7.** Feature Model of the AAL4ALL Ecosystem

This categorization process allowed the definition of generic unit tests that were specified for each of these main categories / subcategories. These tests are later instantiated for the candidate product.

Suppose that a manufacturer is interested in getting AAL4ALL certification for a new sensor (Chestband). Looking at the feature model, we realize that a sensor falls into the Local System category (represented in blue in Fig. 7). To obtain certification, the sensor will be submitted to a series of tests in a scenario that includes other products (already certified) in order to ensure that it is able to communicate according to the message specification defined by the ecosystem. For this, the first step is to select products from others categories to create a complete test scenario. For this specific example we need to select one Local Application, one AALMQ and one External System. Unit test models for these product categories are represented in Fig. 8.

After selecting the products and composing the unit tests presented in Fig. 8, we obtain the integration test model shown in Fig. 9, so the next step is start

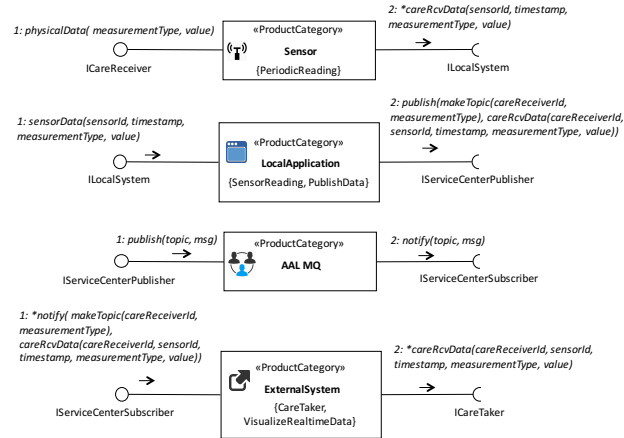


**Fig. 8.** Example of Unit Test Models for some Product Categories and Features

the test injecting messages in one point of the scenario and check the evidences in other point of the scenario (End-to-end testing).

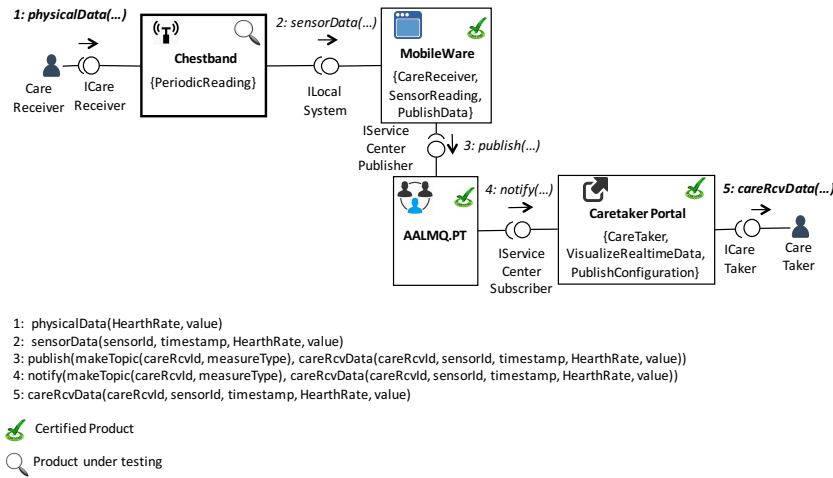


**Fig. 9.** Example of Integration Test Model

In this certification process, a candidate product can be certified in one category.

## 5 Related Work

Integration testing aims to discover faults that are due to incorrect interactions between different software based products. Even if each product is correct and delivers the specified functionality, when integrated into a ecosystem, the interactions between products can lead to incorrect results, for example because different products interpret data processed by other products incorrectly, or do not follow the same interaction protocol [14]. The purpose of integration testing is to find such faults that are difficult if not impossible to find when testing products independently. However, and despite unit test case generation been explored extensively in the literature, there is still little work on the generation of integration test cases [10]. One of these approach to generate integration test cases from simple unit test cases can be found in [10]. Although this work is more related to the test code and interactions between objects, the authors use unit tests composition for the generation of integration testing, as our proposal.

In the area of health the use of models to solve problems is not a recent innovation. For example, to ensure the integration of medical information from various sources (public hospitals, private hospitals, etc.), Eggebraaten [5], proposed a health-care data model based on the HL7 Reference Information Model [7]. The main goal of this model is to enable the health-care industry to tap into this data by providing a solution for integrating data from various sources for the purpose of analytical studies that can help discover new treatments and improve patient care. In our work these medical data structures models could be harnessed and used as mandatory message structure exchanged between the various components of the ecosystem. Other similar work for ensuring the good integration between medical devices is based on ISO/IEEE 11073 standard [12]. The standard is based on an object-oriented system management paradigm. An object oriented data model, the domain information model (DIM), defined in ISO 1173-10201, is used to specify objects, attributes, attribute groups, event reports, and communication services, that may be used to communicate device data and to configure medical devices and functionalities. The standardized nomenclature (ISO 11073-10101) comprises a set of numeric codes that identify every item that is communicated between systems. Related to the general domain information model, there exist device specializations for several medical devices, which provide guidelines for how the DIM should be constrained for application to specific devices. These standards were adopted by the Continua Health Alliance [4], a industry consortium that aims at enabling end-to-end system interoperability in the personal telehealth market by leveraging and integrating existing standards for all layers of the communications stack and for all parts of the overall system ranging from the patients-end to the service providers-end.

## 6 Conclusions and Future Directions

In this article we presented metamodels and associated integrity rules for the description of products within a specific domain so that integration tests can be

automatically generated for certification of its products to enter the ecosystem. For better understanding of the models were presented examples of application based on the AAL4ALL project. As future work we will need to create a set of tools that support the creation of these models automatically with the aim of facilitating its implementation.

**Acknowledgments.** This work is financed by the ERDF - European Regional Development Fund through the Operational Programme for Competitiveness and Internationalisation - COMPETE 2020 Programme, and by National Funds through the FCT - Fundação para a Ciência e a Tecnologia (Portuguese Foundation for Science and Technology) within project INESC - EEA/50014.

## References

1. AAL4ALL: AAL4ALL - Official Website (2015), <http://www.aal4all.org/>
2. Atkinson, C., Kühne, T.: Model-driven development: a metamodeling foundation. Software, IEEE 20(5), 36–41 (2003)
3. Batory, D.: Feature models, grammars, and propositional formulas. Springer (2005)
4. Continua: Continua - Official Website (Dec 2015), <http://www.continuaalliance.org/>
5. Egggebraaten, T.J., Tenner, J.W., Dubbels, J.C.: A health-care data model based on the hl7 reference information model. IBM Systems Journal 46(1), 5–18 (2007)
6. Faria, J.P., Lima, B., Sousa, T.B., Martins, A.: A testing and certification methodology for an open ambient-assisted living ecosystem. International Journal of E-Health and Medical Communications 5(4), 90–107 (2014)
7. Gunther SCHADOW, C.N.M.: The hl7 reference information model under scrutiny. In: Ubiquity: technologies for better health in aging societies: proceedings of MIE2006. vol. 124, p. 151. IOS Press (2006)
8. Hill, C., Grant, R., Yeung, I.: Ambient assisted living technology. An interactive qualifying project report submitted to the Faculty of Worcester Polytechnic Institute (2013)
9. OMG: Meta Object Facility (MOF) Specification. Tech. rep., Object Management Group (2005)
10. Pezze, M., Rubinov, K., Wuttke, J.: Generating effective integration test cases from unit ones. In: Software Testing, Verification and Validation (ICST), 2013 IEEE Sixth International Conference on. pp. 11–20. IEEE (2013)
11. Schmidt, D.C.: Guest editor's introduction: Model-driven engineering. Computer 39(2), 0025–31 (2006)
12. Schmitt, L., Falck, T., Wartena, F., Simons, D.: Novel iso/ieee 11073 standards for personal telehealth systems interoperability. In: High Confidence Medical Devices, Software, and Systems and Medical Device Plug-and-Play Interoperability, 2007. HCMDSS-MDPnP. Joint Workshop on. pp. 146–148 (June 2007)
13. tcare: tcare - Conhecimento e saude SA (November 2015), <http://www.tcare.pt/>
14. Young, M.: Software testing and analysis: process, principles, and techniques. John Wiley & Sons (2008)

## DisToNet: Disconnection Tolerant Mobile Ad Hoc Networks

Emanuel Lima<sup>1</sup>, Pedro Brandão<sup>1</sup>, Orangel Azuaje<sup>1</sup>, Ana Aguiar<sup>1</sup>

<sup>1</sup> Instituto de Telecomunicações, Porto Portugal  
*{emanuellima, up201307429, ana.aguiar}@fe.up.pt*  
*pbrandao@dcc.fc.up.pt*

**Abstract.** Applications running over mobile ad-hoc networks (MANET) often can trade-off some delay versus reliability in case of sporadic disconnection periods. However, existing solutions for network partition usually focus on settings for which disconnection is at least as normal as connection. We propose Disconnection Tolerant Networking (DisToNet) as a transparent, routing protocol agnostic solution to support sporadic and time-limited network partitioning on battery-limited devices, at the cost of some duplicate packets. We conducted a first assessment of DisToNet's system performance experimentally on an RPi B+ platform. The results show that DisToNet has a negligible impact in the nodes' resources like CPU, which makes this solution an efficient approach for increasing communication reliability in nodes' with energy constraints.

**Keywords:** Ad-Hoc Networks · Disconnection Tolerance · implementation

### 1 Introduction

Mobile ad-hoc networks (MANET) have become increasingly popular, to provide connectivity and allow mobility even when there is no network infrastructure. They enable communication between vehicles, in remote areas, disaster zones, social movements distrusting authorities, sensor data gathering, etc. Due to nodal mobility, the network topology may change rapidly and unpredictably over time. Numerous dedicated routing protocols were developed to establish and maintain reachability between communicating nodes in such dynamic environments [1]. In addition, nodes mobility can cause them to go out of neighbors' coverage range, originating disconnection periods from the rest of the network. These periods, even if short, will cause a negative performance impact on applications. Approaches following the concept of delay-tolerant networking (DTN) have been proposed to solve this problem [2]. In fact, numerous proposals have been developed that use asynchronous hop-by-hop communications to avoid the need for a persistent end-to-end path. However, these

usually force the applications into the DTN-inherent asynchronous communication paradigm and often require specific application protocols designed for this purpose [2]. These approaches do not suit the needs of a large variety of MANET applications where the connection between nodes is nearly constant and the disconnection periods are sporadic. This is the case of MANETs where the nodes are always inside the coverage range of at least one neighbor, but exceptionally lose the connection for short periods. Many applications do not have real-time requisites but they want to receive all the data, including the data that should be sent during the disconnection periods. Vehicle networks where their position is monitored, groups of people on a cross-country walk, vital monitoring of first responders, are scenarios that realize these settings.

This work proposes and implements a disconnection tolerant network (DisToNet) that is transparent for applications and suitable for nodes with battery constraints. The proposed solution clearly increases the reliability of data delivery allowing a better application performance. We evaluate our proposal in metrics that influence battery resources and node's performance.

## 2 State of Art

Despite the intense research in the field, mobile ad-hoc networks encompasses many challenges and still open issues. This section focus on routing schemes for mobile ad-hoc networks regarding disconnection periods.

### 2.1 Mobile ad-hoc Networks

In MANETs, the routing protocols can be roughly divided into three groups: proactive, reactive and hybrid [1]. The pro-active protocols such as DSDV [2] and OLSR [3] always maintain link information about the complete topology of the network at each node. This involves periodic updates or notifications of connectivity changes. These protocols update the paths between nodes constantly, improving routing delays at the cost of high overhead for control packets. Reactive routing protocols such as DSR [4] and AODV [5] do not maintain complete topology of the network at each node. Instead, they only search for a path between nodes when there is data to send. This method has the advantage of not wasting network bandwidth with control messages when data transmission is not required, but increases the forwarding delay due to the route discovery process. Hybrid routing protocols such as ZRP [6] exhibit both reactive and proactive properties. These protocols define an area or zone, defined by a number of hop counts surrounding each node. They use a proactive routing approach inside the zone and a reactive one outside.

The main advantage of MANETs' routing protocols is that they allow communication even with a topology that is constantly changing due to nodes mobility and churn. However, this mobility could force the node to go beyond the cover range of its neighbors leading to disconnection periods. During these periods, even if short, all the data that the node should receive or send is lost.

## 2.2 Delay Tolerant Networks

Delay Tolerant Networks (DTN) constitute an emerging subclass of MANETs referring to a network with an intermittent connectivity where there is often no simultaneous path from the source to the destination node. DTN introduces an overlay protocol that interfaces with either the transport layer or lower layers [7]. Each node of the DTN architecture can store information for a long time before forwarding it. In contrast to MANETs, routing in DTNs is more difficult due to the lack of the most recent network topology information. Many routing schemes have been proposed for DTNs and they can be partitioned in three categories: mule-based, opportunity-based and prediction-based.

In mule-based methods [8-9], systems usually employ extra mobile nodes as “mules” for message delivery. The systems control the trajectory of these “mules” to improve delivery performance. However, this control leads to extra cost and overhead.

In opportunity-based schemes [10], nodes forward messages randomly hop by hop with the expectation of an eventual delivery, but with no guarantees. With this approach, multiple copies of the same message are flooded in the network to increase the chance of delivery.

In prediction-based schemes [11], routing protocols make relay selections by estimating metrics relative to successful delivery, such as delivery probability or expected delay based on a history of observations [12]. Most of these protocols focus on whether two nodes will have a contact and when such contact will happen.

In DTNs, the disconnection periods are the majority while the connection periods are only sporadic. Current DTN routing methods aim for a mostly connectionless scenario, which is not suitable for networks where disconnections are inevitable but sparse.

There are some proposals such as [13-14] that use MANET and DTN routing protocols together. The authors divide a MANET into clusters and use MANET’s routing protocols for intra-cluster communication and DTN’s routing protocols for communication between clusters. However, none of these solutions deals with the disconnection periods inside a MANET that albeit not long can affect the applications’ performance.

## 3 Disconnection Tolerant Net-working

The goal of this work is to provide a solution for scenarios where sporadic disconnections between nodes in a MANET affect application performance. The main motivating difference between DTN and DisToNet is that, in our case, disconnection is not the normal network status. Additionally, the solution should be transparent to the application, independent of the MANET routing protocol, and target battery powered nodes, which have energy constraints.

Under these conditions, DTN protocols are neither transparent to the applications, nor efficient solutions if nodes are battery limited. DTNs create an overlay network that supports end-to-end networking through store-and-forward of bundles, created from groups of packets, of which the application must be aware. Moreover, DTN

sends announcement packets to detect connectivity, which consume battery and network resources in a not negligible amount when disconnection is sporadic.

The proposed solution requires the following components: (1) detecting the disconnection; (2) storing locally generated and “to be forwarded” packets during disconnection; and (3) detecting reconnection; and (4) re-inserting the buffered packets onto the network queue. Since the common state of the network nodes is to be connected, we target a solution that is as unnoticeable as possible to applications and to the network. DisToNet thus uses information available only at each node to detect the connection state for points 1 and 3 above, namely the routing table. After detecting disconnection, all packets are stored locally until reconnection, when packet reinsertion starts, interleaved with regular packet flows. Because there is a time lapse between the actual disconnection and the time when the routing table of a node reflects that topology change, packets may be lost. To avoid this, we added an additional first in first out (FIFO) storage stage, where copies of all packets are stored on their regular network path. This approach is represented in Fig. 1.

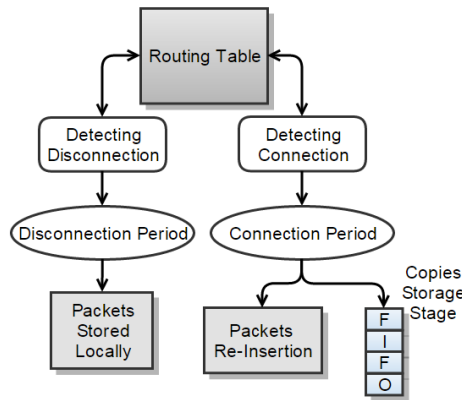


**Fig. 1.** Approach diagram

#### 4 DisToNet Implementation

To achieve efficiency and transparency, we implemented the solution in a Linux kernel-space and not in user-space. We did this through a Loadable Kernel Module (LKM), which is an object code that acts like a kernel extension and can be load at both boot and run-time. User-space processes can only access a small part of the kernel via an interface exposed by the kernel, i.e. using system calls. These calls are requests, in a Unix-like operating system, by an active process for a service performed by the kernel, such as input/output (I/O) or process creation. If a process performs a system call, a software interrupt is sent to the kernel, which then dispatches the appropriate interrupt handler and continues its work after the handler has finished. Working directly in kernel-space, makes the whole process more efficient allowing direct ac-

cess to resources like memory and CPU, without software interrupt handling and user – kernel context switching.

#### 4.1 Using the Netfilter Framework

To access the Linux TCP/IP stack from the LMK we used the Netfilter framework<sup>1</sup>. This framework allows packet mangling outside the normal Berkeley socket interface, among other things. It defines "hooks" for each protocol family (IPv4 defines 5), which are well-defined points in a packet's traversal of the protocol stack (see Fig. 2). After simple sanity checks, the packets received by the network interface are passed to the Netfilter framework's through NF\_IP\_PRE\_ROUTING hook. Next, they enter the routing code, which decides if the packet is destined for forwarding, or for local delivery. The routing code may drop packets for which there is no route. If the packet is destined for local delivery, the Netfilter framework is called again for the NF\_IP\_LOCAL\_IN hook, before the packet is handed over to the process. If the packet is destined for forwarding, the netfilter framework is called for the NF\_IP\_FORWARD hook. Packets generated by the local host go through the NF\_IP\_LOCAL\_OUT. Finally, all packets before being sent to the network interface pass a final Netfilter hook, the NF\_IP\_POST\_ROUTING hook.

At each of these points, the Netfilter framework will call all registered callbacks for that hook and protocol with the packet and the hook number. Parts of the kernel can register to listen to the different hooks for each protocol. Therefore, when the system hands a packet to the Netfilter framework, it checks to see if anyone has registered for that protocol and hook. If this is the case, they get a chance to examine (and possibly alter) the packet. In that context they can also discard the packet (NF\_DROP), allow it to pass (NF\_ACCEPT), tell Netfilter to forget about the packet (NF\_STOLEN), or ask Netfilter to queue the packet for user-space (NF\_QUEUE).

For DisToNet, we implement an LKM that filters the packets coming from the network device for forwarding from other nodes and from the local host. These packets are captured at the NF\_IP\_PRE\_ROUTING or NF\_IP\_LOCAL\_OUT hooks, before making any routing decision. Considering this approach, it is possible to manage the decision of when our LKM should buffer a packet or send it, based on the node's connectivity towards the packet's destination. This solution only works for datagrams. The framework cannot cope currently with streams, such as TCP connections, as it does not maintain flow state.

---

<sup>1</sup> See <http://netfilter.org/>

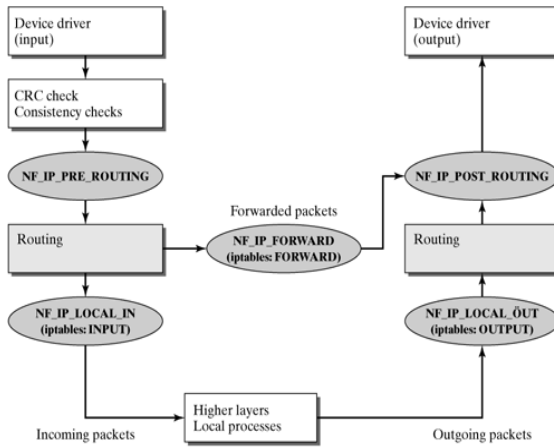


**Fig. 2.** Netfilter hooks on Linux kernel TCP/IP stack [15]

#### 4.2 Buffering

In DisToNet, two types of buffers are used: i) Small Buffers (SB) that store a copy of all packets that pass the stack (both locally originated and forwarded), and ii) Large Buffers (LB) that store packets during the disconnection periods. The SBs are much smaller than the LBs, because they just need to accommodate copies of the packets that are sent during the period between actual disconnection moment and disconnection detection by the routing protocol, i.e. packets that may be undeliverable because the destination becomes unreachable. Notwithstanding, the implementation of the buffers is similar.

**Which Packets to Buffer.** We allow filtering which packets to buffer. Our LKM can filter each packet collected by destination IP address and port number, thus only buffering a sub-set of the packets. All the remaining traffic follows its normal course through the stack. For each packet that matches the filter, we make a routing table lookup to validate the end-to-end path to the destination. If there is a route to the destination, we copy the packet to the SB and then it flows its normal course through the stack. However, if the destination is unreachable the packet is deviated to the LB.

The filtering strategy allows separating the traffic to buffer during the disconnections periods. In a MANET can exist applications for which it is useless to support disconnection periods, even with buffering, e.g. real-time applications, and therefore buffering would be a waste of resources. The ability to select which traffic to buffer allows an efficient use of node resources when multiple types of applications are using the same MANET.

**Filling the Buffers.** The buffers are placed in RAM through dynamic memory allocation. The LB are implemented as linked lists and will allocate memory only during the disconnections periods, which are not frequent. When the buffers achieve their

maximum capacity, our LKM adopts a FIFO policy, and as soon as the packets in the LB are transmitted, the memory is freed. SBs are implemented as circular queues, which means that they store the last packets sent before detecting a disconnection to the destination. This way, the queue is recycled without the need for any timeout.

Every packet sent or received in Linux is handled using socket buffers (SKB). These data structures are the most fundamental data structures in the Linux networking code. Since the LKM created is collecting packets in different points of the stack through the Netfilter hooks, the SKBs that contain the packets have different characteristics. It is necessary to distinguish packets collected in different points of the stack since they will be handed back to the stack in different places as well. For this reason, we divided SB and LB in two extra buffers each to accommodate the packets from each hook: Small Buffer Forwarder (SBf) and Large Buffer Forwarder (LBf) for the packets collected in NF\_IP\_PRE\_ROUTING; and Small Buffer Local (SBl) and Large Buffer Local (LBl) for the packets collected in NF\_IP\_LOCAL\_OUT. The reinjection of these packets in the stack will occur immediately after the point where they were collected. This ensures that the stack makes all the necessary verifications and operations as it would without the collection and buffering process, ensuring transparency.

**Emptying the Buffers.** The packets from LB are sent when their destinations become reachable. Before the packets reinsertion in the stack, all packets from SBs are transferred to the respective LB, local or forwarder. As mentioned, the SBs store copies from the packets sent during the time where a destination becomes disconnected and the routing protocol reflects that, thus we assume that all packets sent during that period are lost and they should be sent again when connection is regained. This may lead to duplicate packets, with which the receiving application should deal.

An independent thread manages the process of sending packets from the buffers. Its main function is to ensure that all the packets from the buffers are placed in the stack to be sent. The transmission rate for the LB packets is controlled using a leaky bucket algorithm. When the maximum number of tokens sent is reached the thread that manages the sending is put in sleep mode saving CPU processing power. We use a timer interrupt, activated each second, to reset the number of tokens to zero and wake the thread so it can verify the packets' destination state and re-start to send the LB packets if it is reachable. We only interrupt this transmission process if the LBs are empty or if the packets' destination becomes unreachable. Note that before sending each packet, a routing table lookup is made to ensure that there is a route to the destination.

The usage of a timer interrupt and an independent thread together with a routing table lookup allows managing the packet transmission rate and at the same time ensure that only the packets that have end-to-end path to the destination are sent. Fig. 3 depicts the buffers emptying process.

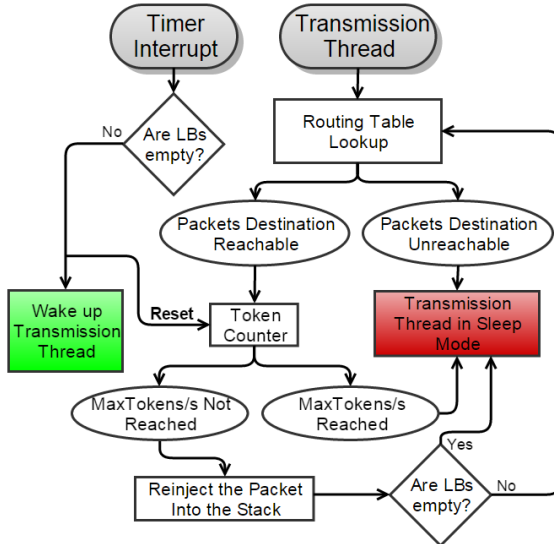


**Fig. 3.** Buffer Emptying Diagram

**Tunable parameters.** We defined a set of tunable parameters read through the Sysfs<sup>2</sup> file system. The parameters that the user can tune are: i) the packets destination IP address and port number for filtering, ii) the buffers' sizes, and iii) the buffers' transmission rate. These tunable parameters allow the adaptation of the solution proposed to many MANETs scenarios and protocols, achieving a high degree of flexibility.

The buffers' transmission rate can be adapted to the capabilities of a MANET. In a scenario where the bandwidth available is abundant, the buffer transmission rate can be set to use all the available bandwidth. However, in scenarios where this is not the case, the buffers' transmission rate could be limited to ensure that the data will eventually reach the destination. Either way, currently our approach requires some knowledge about the MANET and application to efficiently parameterize DisToNet.

<sup>2</sup> Sysfs is a mechanism for representing kernel objects, their attributes, and their relationships with each other. It provides a kernel programming interface for exporting these items, and a user interface to view and manipulate these items that maps back to the kernel objects which they represent

## 5 Performance Evaluation

We implemented and tested our proposed solution on a Raspberry PI B+ using the Raspbian<sup>3</sup> operating system. The disconnection periods were emulated by manipulating the routing table information using static routes. The metrics used to evaluate the solution were CPU and memory usage monitored using sysstat<sup>4</sup>.

We created a controlled test environment with a sequence as follows: 1 minute after the test begins, the node starts to send traffic for 1 minute; then it waits another minute during which our LKM is loaded into the node's kernel, afterwards it starts a second sending session. The second sending session lasts 3 minutes, but after one minute, the node loses connection to the packets' destination. One minute after the second sending session finishes, the node regains connectivity to the packets' destination. The traffic for the tests was generated at 1Mbit/s, with packets of 1470 bytes of payload, using iperf<sup>5</sup>. We defined the size of the SBs as 750 KB, the size of LBs as 26 Mbytes and the transmission rate for the packets in the buffers was set to 1 Mbit/s.

### 5.1 System Resource Consumption

Fig. 4 shows the CPU usage for when the traffic is generated locally. The two initial spikes of the CPU usage in the figure correspond to traffic transmission periods when the node has connectivity to the destination packets. The CPU usage is approximately the same when the node is transmitting traffic normally and when it is transmitting traffic with the LKM loaded and using SBI. When the node loses connectivity to the packets' destination ( $t = \pm 04$ ) and starts buffering, the CPU usage decreases. This happens because the LKM is deviating the packets to the LBI not allowing them to proceed their normal flow through the stack. When the node regains connectivity with the destination ( $t = \pm 07$ ), it starts to send the buffered packets (LBI). Since the packets are queued in the exact same point from where they were deviated to the buffers, the CPU usage during the buffer emptying process is less than the previous traffic transmissions.

We made the exact same test but only forwarding traffic that another machine is generating. This scenario uses the SBf and LBf. As can be seen also in 4, the CPU usage increases slightly but follows the same pattern seen previously. In fact, during the first traffic transmission, when the LKM is not being used, the mean CPU usage is 9,91% (SD=3,53%) when the traffic is generated locally and 12,7% (SD= 5%) when the node is forwarding traffic. Thus, forwarding traffic is more CPU expensive than locally transmitting independently of our LKM usage.

---

<sup>3</sup> See: <https://www.raspberrypi.org/downloads/>

<sup>4</sup> See <http://sebastien.godard.pagesperso-orange.fr/>

<sup>5</sup> See: <https://iperf.fr/>

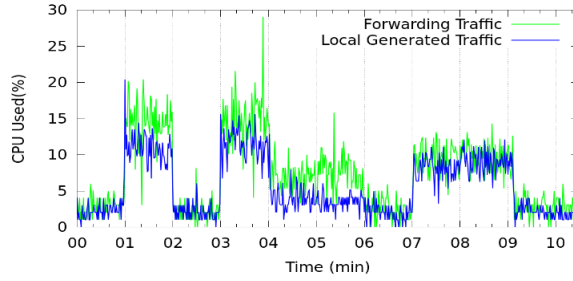


**Fig. 4.** Node's CPU usage

Fig. 5 shows the memory usage when the node is locally generating the traffic and when the node is in a forwarding mode. In both cases, the memory used increases during the disconnection period and decreases when the buffer emptying process starts. However, during the forwarding process, the amount of memory used is almost four times more than when the node is locally generating the traffic. We observed that the difference in memory used is caused by the different sizes of the SKBs used by the Linux stack for forwarded or locally generated traffic. Moreover, the memory usage is mostly influenced not by the packets' payload size but by the number of packets that need to be stored.

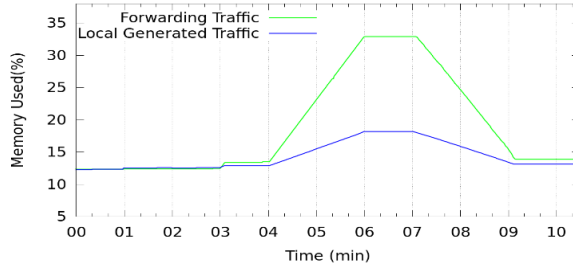


**Fig. 5.** Memory usage during local traffic generation

## 5.2 Network Performance

We assume that all packets sent during the time taken by the routing protocol to detect that a destination is disconnected are lost and need to be sent again. This will cause possible duplicates since some packets sent during this period could still reach the destination. This amount of duplicates will be directly related to the routing protocol reaction time to topology change, i.e. longer reaction time will lead to more possible duplicates. However, since routing protocols are created to rapidly respond to topologies changes these detection periods are usually small. For example, OLSR by default takes 6 seconds to detect a topology change. In a period where a disconnection takes 2 minutes, the amount of duplicates sent until the node regains connectivity

would correspond only to 5% of the total data sent. Considering other metrics like delay and jitter, it will depend on the parameterization of the transmission rate of the buffered packets. On the other hand, a significantly improvement is seen in packets losses, since we are buffering the packets during the disconnection periods for re-sending after connectivity is regained. There may be losses due to the SB not being able to accommodate all traffic during large periods of disconnection, but this may be configured by the user in the parameterization of DisToNet.

## 6 Conclusion

We proposed DisToNet to transparently support periods of network partitioning in MANETs. We describe the solution and implementation using the Netfilter framework. Finally, we evaluate the impact in the system's performance experimentally, using an RPi platform. We conclude that the DisToNet can improve reliability across periods of disconnection at the cost of some duplicate packets, and the implementation causes very little impact on system resource consumption.

Further work includes designing algorithms that can learn parameterization of the buffer sizes and transmission rates from MANET behavior, more extensive testing of the implementation in varied networking scenarios, improving support to larger disconnection periods, and quantifying the dependence of duplicates on the number of hops between origin and destination.

## 7 References

1. Abolhasan, M., Wysocki, T., Dutkiewicz, E.: A review of routing protocols for mobile ad hoc networks. *Ad hoc networks.* 2, 1–22 (2004).
2. Perkins, C.E., Bhagwat, P.: Highly dynamic destination-sequenced distance-vector routing (DSDV) for mobile computers. In: *ACM SIGCOMM Computer Communication Review.* pp. 234–244. ACM (1994).
3. Clausen, T., Jacquet, P., Adjih, C., Laouiti, A., Minet, P., Muhlethaler, P., Qayyum, A., Viennot, L.: Optimized link state routing protocol (OLSR). (2003).
4. Johnson, D.B., Maltz, D.A.: Dynamic source routing in ad hoc wireless networks. In: *Mobile computing.* pp. 153–181. Springer (1996).
5. Perkins, C.E., Royer, E.M.: Ad-hoc on-demand distance vector routing. In: *Mobile Computing Systems and Applications, 1999. Proceedings. WMCSA'99. Second IEEE Workshop on.* pp. 90–100. IEEE (1999).
6. Haas, Z.J., Pearlman, M.R., Samar, P.: The zone routing protocol (ZRP) for ad hoc networks. *Draft. txt.* (2002).
7. Cerf, V., Burleigh, S., Hooke, A., Torgerson, L., Durst, R., Scott, K., Fall, K., Weiss, H.: Delay-tolerant networking architecture. *RFC 4838, April* (2007).
8. Shah, R.C., Roy, S., Jain, S., Brunette, W.: Data mules: Modeling and analysis of a three-tier architecture for sparse sensor networks. *Ad Hoc Networks.* 1, 215–233 (2003).
9. Zhao, W., Ammar, M., Zegura, E.: A message ferrying approach for data delivery in sparse mobile ad hoc networks. In: *Proceedings of the 5th ACM international symposium on Mobile ad hoc networking and computing.* pp. 187–198. ACM (2004).

10. Zhang, X., Neglia, G., Kurose, J., Towsley, D.: Performance modeling of epidemic routing. *Comput. Networks.* 51, 2867–2891 (2007).
11. Zhu, Y., Xu, B., Shi, X., Wang, Y.: A survey of social-based routing in delay tolerant networks: Positive and negative social effects. *Commun. Surv. Tutorials, IEEE.* 15, 387–401 (2013).
12. Liu, C., Wu, J.: Routing in a cyclic mobispace. In: Proceedings of the 9th ACM international symposium on Mobile ad hoc networking and computing. pp. 351–360. ACM (2008).
13. Chen, Y., Zhao, W., Ammar, M., Zegura, E.: Hybrid routing in clustered dtns with message ferrying. In: Proceedings of the 1st international MobiSys workshop on Mobile opportunistic networking. pp. 75–82. ACM (2007).
14. Whitbeck, J., Conan, V.: HYMAD: Hybrid DTN-MANET routing for dense and highly dynamic wireless networks. *Comput. Commun.* 33, 1483–1492 (2010).
15. Welte, H.: The netfilter framework in Linux 2.4. In: Proceedings of Linux Kongress (2000).

## Digital Chromatic Dispersion Equalization in Coherent Optical System

Celestino S. Martins<sup>1</sup>, Fernando P. Guiomar<sup>2</sup> and Armando N. Pinto<sup>2</sup>

<sup>1</sup> Faculdade de Engenharia da Universidade do Porto, Porto, Portugal

<sup>2</sup> Instituto de Telecomunicações, Campus Universitário de Santiago, Aveiro, Portugal  
{csmartins@av.it.pt, guiomar@av.it.pt, anp@ua.pt}

**Abstract.** The emergence of coherent optical transmission systems as the key technology for long-haul transmission of 100 Gb/s per channel and beyond, associated with ultra-fast digital signal processing (DSP) technology has revolutionized the optical communication systems. In this case, long-haul fully uncompensated links can be compensated at receiver-side. In this paper we show the feasibility of digital equalization of chromatic dispersion (CD) in coherent optical transmission systems using both time-domain (TD) and frequency-domain (FD) implementation. For TD and FD equalization we use the FIR filter and overlap-save algorithm, respectively. Besides, an overview of the both TD and FD implementation, we also evaluate their performance and computational effort considering a single channel QPSK long-haul optical link operating at 50 Gb/s, which in turn validates the feasibility of both algorithms. In addition, we demonstrate the hardware equalization of CD using FIR filter for single channel system operating at 50 Gb/s.

**Keywords:** Optical communications · coherent detection · digital signal processing · chromatic dispersion · TD · FD.

### 1 Introduction

Chromatic dispersion (CD) has traditionally been one of the most limiting impairments for the transmission reach and data rate of optical fiber systems [4, 16]. The use of dispersion compensating fibers (DCF) to inline compensate for CD in the optical domain has marked an era of long-haul optical communications. However, several disadvantages arise from the use of optical dispersion compensation, including signal-to-noise ratio (SNR) penalties due to enhanced noise and nonlinearities [5] and inflexibility to modifications on the fiber link and/or transmitted signal. The need for the spectral efficiency improvement in core networks has brought the coherent detection back as the key technology, in which combined with the advanced digital signal processing (DSP) technology, allow that the CD equalization (CDE) is fully performed in digital domain at receiver-side [6, 9], provided that the minimum sampling rate requirements are met. Although the CDE algorithms are well known case of study, the commercial deployment of these technologies still requires efficient and flexible hardware implementations. Thus, the analysis of CDE algorithms in terms of the hardware implementation is also of the crucial importance.

The digital CD equalization in coherent optical systems can be either implemented in time-domain (TD) [1, 2, 5, 12, 15, 16] or frequency-domain (FD) [3, 7, 8, 13]. The TD implementation can be performed using finite-impulse response (FIR) filters, resorting to either direct or transposed form, where the filter coefficients can be obtained a priori from the amount of accumulated CD, by applying a closed-form analytical formulation [12], or through a frequency-domain transfer function [15]. The infinite-impulse response (IIR) filters has also been proposed in order to reduce the number of the filter coefficients, however the feedback structure of IIR filters is a major drawback for real-time implementation [2]. The FD implementation is performed resorting to the use of fast Fourier transform (FFT) and inverse fast Fourier transform (IFFT), which makes FD equalization (FDE) more attractive regarding to the algorithms complexity. For an uncompensated long-haul fiber links, where the accumulated dispersion is large and high filter order is required, the FDE tends to be more computationally efficient than TD equalization (TDE) using FIR filter [14]. However, the use of FIR filter simplify the real-time implementation, since it avoids the use of block processing from FFT/IFFT. Therefore, several researches have been performed in both TDE and FDE in order to reduce the algorithm complexity [1, 3, 5, 13].

In this paper, an overview of TD and FD compensation techniques for chromatic dispersion is presented. Besides, an analysis of the algorithm complexity is also performed in terms of the number of real multiplications. Finally, the TD implementation, using FIR filter, is offline demonstrated in a field-programmable gate array (FPGA).

The structure of this paper is as follows. In section 2, the theoretical formulation behind CD is provided for both TD and FD. Section 3 refers to the numerical results where the performance and complexity of TDE and FDE are evaluated. In Section 4 the hardware implementation of TDE is presented, in addition with its performance analysis. Finally, in section 5, the main conclusions are presented.

## 2 Theoretical Formulation

Neglecting the effects of fiber nonlinearities, a noiseless optical fiber transmission system can be described in frequency domain as,

$$A_{rx}(\omega) = H_{CD}(\omega)A_{tx}(\omega), \quad (1)$$

where  $A_{tx}$  and  $A_{rx}$  correspond to the Fourier transforms of the transmitted and received signal as a function of the angular frequency, in rad/s.  $H_{CD}$  represents the chromatic dispersion transfer function, which, by neglecting higher-order dispersion terms, can be written as

$$H_{CD}(\omega) = \exp\left(-j\frac{\beta_2}{2}\omega^2 L\right), \quad (2)$$

where  $\beta_2$  represents the group velocity dispersion in  $\text{ps}^2/\text{km}$  and  $L$  is the fiber length in km. By analysing the  $H_{CD}(\omega)$  it can be noted that CD operates as an all-pass filter with gain one [2]. The time response can also be obtained easily by applying the IFFT to the chromatic dispersion transfer function.

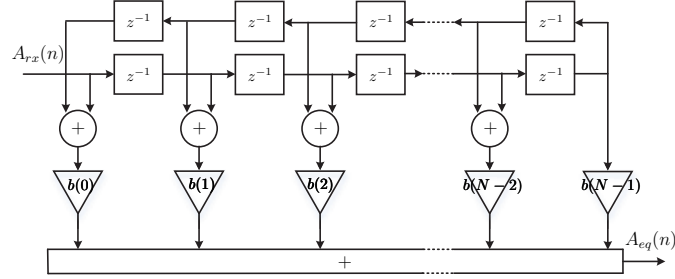


**Fig. 1.** Symmetric FIR filter implementation diagram.

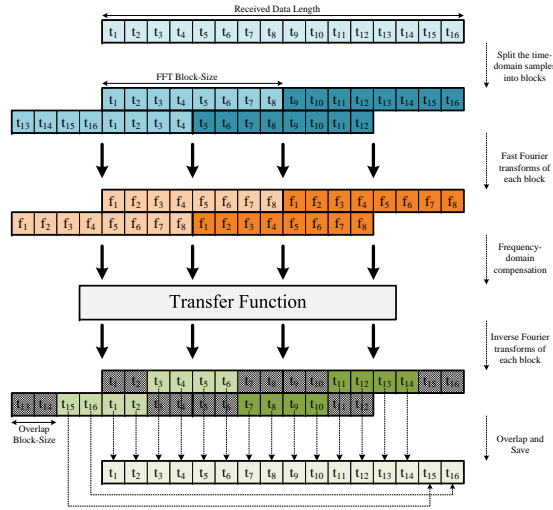


**Fig. 2.** Overlap-save algorithm implementation for CD equalization in frequency-domain.

### 2.1 TD Equalization of Chromatic Dispersion

Since the CD is a linear phenomenon it can be compensated by using a linear FIR or IIR filter, in time-domain. The goal of these filters is to apply the inverse effect of chromatic dispersion and consequently recover the desired signal without dispersion at the receiver. Therefore, using FIR filter the compensation of CD can be performed as

$$A_{eq}(n) = \sum_{k=0}^{N_{taps}-1} A_{rx}(n-k)b(k), \quad (3)$$

where  $b(k)$  corresponds to the FIR filter coefficients,  $N_{taps}$  is the required number of filter taps,  $A_{rx}$  is the received signal and  $A_{eq}$  is the equalized signal. For a static opti-

cal link in which the dispersion characteristics are a priori known, the tap weights of FIR filter can be determined from the inverse Fourier transform of the linear transfer function [12], defined in Eq. (2), as

$$b(k) = \sqrt{\frac{jcT^2}{D\lambda^2L}} \exp\left(\frac{-j\pi cT^2}{D\lambda^2L}k^2\right), \quad (4)$$

where  $T$  is the sampling period,  $D$  is the dispersion coefficient of the fiber,  $c$  is the speed of light,  $\lambda$  is the central wavelength of the transmitted optical wave and  $\lfloor \cdot \rfloor$  corresponding to the nearest integer. The value of  $N_{taps}$  is defined as the minimum number of taps required for CD compensation with negligible penalty and is given as

$$N_{taps} = 2 \left\lceil \frac{|D|\lambda^2 L}{2cT^2} \right\rceil + 1. \quad (5)$$

Eq. (5) clearly shows that the number of filter taps for TDE increases with the increase of accumulated dispersion, which in turn increases with  $L$ . Besides, we can note that the inverse of the impulse response of the dispersive fiber is symmetric about its center, thus implying that the filter coefficients are also symmetric. Therefore, taking into account the symmetry of the FIR filter taps, an example of direct form implementation of FIR filter with odd symmetry is shown in Fig. 1. However, the diagram of FIR filter with even symmetry can be also easily implemented.

## 2.2 FD Equalization of Chromatic Dispersion

From the Eq. (1) it becomes apparent that a zero-forcing equalizer with transfer function  $H_{cd}(\omega) = H^{-1}(\omega)$  can be employed to determine the equalized optical field envelope,  $A_{eq}(t)$ , at the expense of the received signal,  $A_{rx}(t)$ , as

$$A_{eq}(t) = \mathfrak{F}^{-1}\{H_{CD}(\omega)\mathfrak{F}\{A_{rx}(t)\}\}, \quad (6)$$

where  $\mathfrak{F}$  and  $\mathfrak{F}^{-1}$  represent the Fourier transform and inverse Fourier transform operator, respectively. Note that the direct implementation of Eq. (6) is not feasible in real-time processing, since it applies a circular convolution instead of the required linear convolution. However, this can be easily overcome by using overlap frequency domain equalization, where block processing is required, employing the well-known techniques, the overlap-add or overlap-save methods. Using this technique a large input stream to the filter is broken into blocks of shorter lengths. The outputs of successive blocks are computed and concatenated in a proper way to generate the total output [10]. An example of one of this methods is shown in Fig. 2. Taking into account this implementation, the length  $N_{FFT}$  of the FFT/IFFT operation must be defined. Usually, it is defined as a function of channel memory, which can be assumed as the length of the discrete impulse response of the equalizer,  $N_{taps}$ , and the minimum value of  $N_{FFT}$  is defined as the next power of two of  $N_{taps}$  [14]. The minimum value of  $N_{FFT}$  is defined in order to ensure the negligible performance penalty of FDE, nevertheless this parameter provides an additional degree of freedom that may be utilized to minimize the algorithm complexity. As it has been shown, the value of  $N_{FFT}$  can be optimized as [8]

$$N_{FFT} = KN_{taps}, \quad (7)$$

where  $K$  is an integer value which can take values between 4 and 10, and  $N_{taps}$  follows the Eq. (5).

### 2.3 TD and FD complexity analysis

In order to evaluate the computational effort of TD and FD algorithms, in this section we focus on the number of real multiplication operations to obtain an equalized sample. Although the main operations for the TD and FD equalization algorithms are additions and multiplications, it is known that the multiplications exceed by far the complexity of additions [14]. Therefore, we have measured the computational effort in terms of complex multiplications only. The complex multiplication is considered to be implemented with 4 real multiplications.

For TD implementation, using FIR filter, in which the impulse response of the filter is symmetric with length  $N_{taps}$ , the number of real multiplication required to obtain an equalized sample is given as

$$N_{rm} = 4 \left\lceil \frac{(N_{taps} - 1)}{2} \right\rceil. \quad (8)$$

For FD implementation, to obtain an equalized sample an FFT operation is required, followed by the multiplication of signal spectrum with the  $N_{FFT}$ -point transfer function of the equalizer, and finally an IFFT of the same length is carried out. From these operations it can be seen that the main complexity of FD equalization is associated with FFT/IFFT. As it is well known, there is a large diversity of different FFT algorithms implementation, however the most common one is the classical radix-2 algorithm, for which the length of the vector to be transformed needs to be equal to a power of 2 [8]. Taking into account these considerations, the number of real multiplication to obtain an equalized sample is given as

$$N_{rm} = N_{FFT} \left( \frac{4 \log_2(N_{FFT}) + 4}{N_{FFT} - N_{taps} + 1} \right), \quad (9)$$

## 3 Numerical Results

In this section, we have evaluated the performance and the complexity of TDE and FDE through the simulation results. Therefore we have considered the simulation setup as follows. A single channel quadrature phase-shift keying (QPSK) signal at 50 Gb/s is propagated over a several fiber spans with 80 km each. We have used a standard-single mode fiber (SSMF) with  $\beta_2 = -20.4 \text{ ps}^2/\text{km}$  and  $\alpha = 0.2 \text{ dB/km}$ . Fiber loss can be perfectly compensated at the end of each fiber span by an Erbium-doped fiber amplifier (EDFA) with 5 dB noise figure. The transmission system is first simulated in MATLAB, and the obtained distorted electrical signals are then fully post-processed also in MATLAB. The obtained electrical signals are then converted to digital signals, where a third-order Butterworth low-pass filter with cutoff-frequency at 80% of the symbol rate precedes the downsampling stage, and 2 samples per symbol are provided for the subsequent DSP algorithms. Chromatic dispersion equalization is performed using both TD

and FD chromatic dispersion equalizer. Since only a single polarization is considered in the simulation, the polarization demultiplexing is not required. Therefore, the phase estimation is performed and finally, symbol decoding is performed and the bit error rate (BER) is assessed.

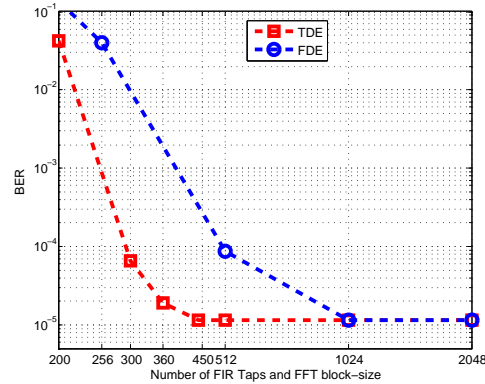


**Fig. 3.** Evaluation of the impact of number of FIR taps,  $N_{taps}$ , and FFT block-size,  $N_{FFT}$ , on the performance of TD and FD equalizer. The performance is evaluated in terms of BER.

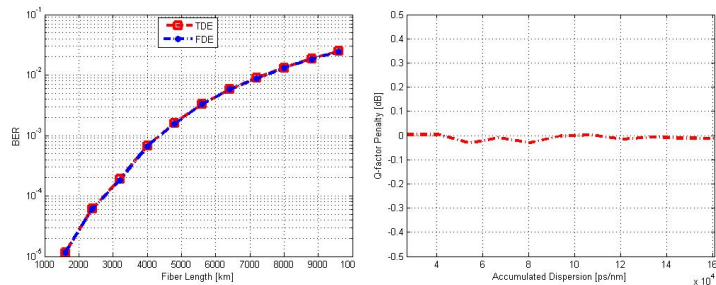


**Fig. 4.** Performance evaluation, considering BER as figure of merit, of TD and FD equalization for different values of fiber length, L; Performance evaluation, considering Q-factor penalty as figure of merit, in function of accumulated dispersion. The penalty is calculated over FD relatively to the TD equalization.

Initially, we start by evaluating the impact of number of FIR taps,  $N_{taps}$ , and FFT block-size on the performance of TD and FD equalizer, respectively. Hence, we have evaluated the evolving of BER in function of  $N_{taps}$  and  $N_{FFT}$  considering a fiber length,

$L = 1600\text{km}$ . This analysis allow us to determine the minimum values for  $N_{taps}$  and  $N_{FFT}$  which impose a negligible performance penalty for each implementation, Fig. 3. As it is shown in the Fig. 3, for the TDE the performance increases with the increase of  $N_{taps}$  and the stabilization (maximum performance) is achieved from the vicinity of theoretical value of  $N_{taps}$ , 513, which validates Eq. (5). Nevertheless, it should be noted that the value of  $N_{taps}$  can be still reduced at the cost of small penalty [11]. In a similar way, for the FDE the maximum performance is stabilized from the  $N_{FFT} = 1024$ , which is the next power of two of 513, according to the expectation, Eq. (7) for  $K = 1$ . Furthermore, note that from the minimum value of  $N_{taps}$  and  $N_{FFT}$  the performance does not increase with the increase of  $N_{taps}$  and  $N_{FFT}$ , instead remaining almost constant.

Moreover, we have evaluated the performance of TD and FD equalization in function of fiber length,  $L$ . As mentioned previously, for each value of  $L$  it is required to find the minimum value of  $N_{taps}$  and  $N_{FFT}$  that provides the minimal impact on system performance. According to the previous achieved validation, for the calculation of  $N_{taps}$  and  $N_{FFT}$  we have followed the Eq. (5) and Eq. (7), respectively. Following these considerations, we have evaluated the evolution of BER in function of fiber length, as illustrated in left Fig. 4. Note that each span corresponds to 80 km. As can be seen, by ensuring the lower bound value for  $N_{taps}$  and  $N_{FFT}$ , the performance of TD and FD implementations is almost the same, which validates the feasibility of digital post-compensation of chromatic dispersion in coherent optical system using the both implementations. We have also noted that considering the FEC limit of  $3.8 \times 10^{-3}$  an uncompensated link over 4000 km can be achieved. The same conclusion can be also taken by calculating the Q-factor penalty of FD implementation relatively to the TD implementation. From the right Fig. 4 we can note that the penalty is almost zero, for the considered fiber length range. Thus, we can conclude the behavior of TD and FD implementation are the same both for low BER as for high BER.

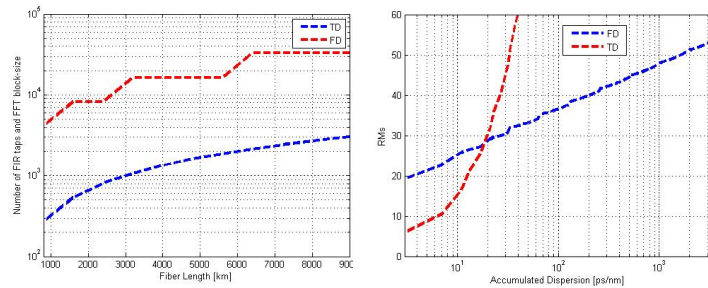


**Fig.5.** Calculation of  $N_{taps}$  and  $N_{FFT}$  for different values of  $L$  for a system operating at 50 Gb/s; Complexity analysis in terms of RMs in function of accumulated dispersion for a system operating at 50 Gb/s.

In left Fig. 5 we have presented the evaluation of  $N_{taps}$  and  $N_{FFT}$  for different values of fiber length,  $L$ . In order to ensure the penalty free of FDE, it has been considered that  $N_{FFT} = 4N_{taps}$ , although these values can still be better tuned in order to obtain the minimum computational effort for FD implementation. As expected, it can be seen that both,  $N_{taps}$  and  $N_{FFT}$  increase with  $L$ , which indicates that they increase with the increase of accumulated dispersion. Note also that, although the high increase of  $N_{taps}$  and  $N_{FFT}$  with  $L$ , while the increase of  $N_{taps}$  is regular, the increase of  $N_{FFT}$  is more abrupt. This fact is due to the power of two consideration in its calculation. Therefore, these results indicate that for high value of  $L$ ,  $N_{taps}$  and  $N_{FFT}$  are very high, which in turn imply a high computational effort for the hardware implementation of these algorithms. Nevertheless, it is already shown [11] that it is possible to reduce the number of taps by about 60% of the theoretical minimum value, given by Eq. (5), with a minimal impact on system performance. This number can be considered as the lower limit for an effective CDE, providing a reduction of the computational effort required by the TD and FD implementation.

In addition, we have also evaluated the complexity of TD and FD implementation. The comparison of these two implementations is performed in terms of real multiplications in function of  $N_{taps}$ , as illustrated right in Fig. 5. The values of  $N_{FFT}$  are obtained as  $N_{FFT} = 8N_{taps}$  in order to minimize the computational effort for FD implementation. It can be seen that for the very low values of  $L$  the TD implementation requires lower effort than FD implementation. However, as the fiber length increases the effort of FD implementation tends to approximate to the TD implementation, up to a point that it becomes to require lower effort. Therefore, becomes evident that the FD equalization requires less effort than TD equalization for high values of CD. Indeed, as it is already analysed [14], the complexity grows linearly with CD for the TD implementation, however it grows logarithmically for the FD implementation. Thus, for high bit rate and long-haul optical fiber link, where the accumulated CD is high, FD implementation is more efficient in terms of computational effort than TD implementation.

#### 4 Hardware Implementation

In order to show the feasibility of CD implementation, the hardware implementation has been performed in time-domain using the symmetric FIR filter following the Fig. 1. The implementation is performed using the hardware description language VHSIC Hardware Description Language (VHDL) and Xilinx Integrated Synthesis Environment

**Table 1.** Performance of CD using FIR filter in function on the input signal bit precision

Input Signal Bit Precision	BER	EVM
[3, 6]	0	20.98
[3, 5]	0	21.03
[2, 6]	1.1142e-02	31.42

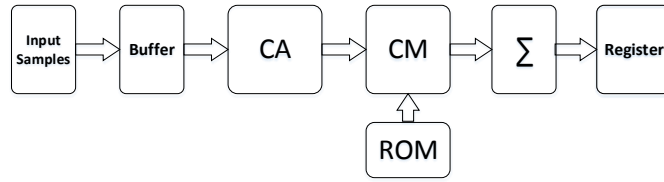


**Fig. 6.** Diagram flow of hardware implementation of FIR filter.

(ISE) design environment for FPGA. It is worth to highlight that the implementation is carried out only for TD since the aim of this section is only for the proof of concept, of digital CD implementation in hardware. Therefore, a brief hardware implementation structure, for single channel system is presented, as illustrated in the Fig. 6. Note that the Fig. 6 only shows the operations flow, bypassing the implementation details. We have used two buffers to store and shift the input samples. Considering the parallelization level of 1, for each clock cycle the buffer receives one sample and outputs  $N_{\text{taps}}$  samples. Then, it is used  $\frac{N_{\text{taps}}-1}{2}$  complex adders (CAs) which symmetrically sum  $N_{\text{taps}} - 1$  shifted input samples from the buffer. Next, we have used  $\frac{N_{\text{taps}}-1}{2} + 1$  complex multipliers (CMs) to multiply the outputs of CAs, considering also the middle sample which is not summed, with  $\frac{N_{\text{taps}}-1}{2} + 1$  coefficients, previously stored in a read only memory (ROM). Finally, the outputs of CMs are summed to obtain the equalized sample, which is then stored in a registers. To study the performance of hardware implementation of TDE, BER and error vector magnitude (EVM) has been evaluated as a function of the bit precision of input samples. Using the fixed-point representation, the input samples values are represented in the form  $[a, b]$  where  $a$  and  $b$  are the number of bits representing integer and fractional part of values, respectively. The simulation results are presented in Table 1, for a single channel system operating at 50 Gb/s, considering 21-taps FIR filter. Analysing the Table 1, we can validate the hardware implementation of CDE in TD. Besides, it is noted that the use of bit precision [3,5] yields a good compromise between performance and implementation complexity, for the considered simulation scenario.

## 5 Conclusions

In this work, we demonstrate that even for high value of accumulated dispersion, over long-haul optical link, the CD can be digitally compensated at receiver-side. We note that using the minimum values for  $N_{\text{taps}}$  and  $N_{\text{FFT}}$  the performance of TDE and FDE is practically the same, as analysed from Q-factor penalty. Nevertheless, the computational effort for FDE is much lower than the TDE, mainly for high value of accumulated dispersion. We have validated, in offline mode, the hardware implementation of TDE using FIR filter. We have noted that the input signal bit precision defines a compromise between performance and implementation complexity.

## References

- [1] Eghbali, A., Johansson, H., Gustafsson, O., Savory, S.: Optimal least-squares FIR digital filters for compensation of chromatic dispersion in digital coherent optical receivers 32(8), 1449–1456 (2014)
- [2] Goldfarb, G., Li, G.: Chromatic dispersion compensation using digital IIR filtering with coherent detection 19(13), 969–971 (2007)
- [3] Hauske, F.N., Xie, C., Zhang, Z., Li, C., Li, L., Xiong, Q.: Frequency domain chromatic dispersion estimation. In: Proc. Optical Fiber Communication Conf. and Exposition (OFC). JThA11 (2010), [http://ieeexplore.ieee.org/xpls/abs\\_all.jsp?arnumber=5465841&tag=1](http://ieeexplore.ieee.org/xpls/abs_all.jsp?arnumber=5465841&tag=1)
- [4] Ip, E., Kahn, J.M.: Digital equalization of chromatic dispersion and polarization mode dispersion 25(8), 2033–2043 (2007)
- [5] Jawad Munir, Amine Mezghani, I.S., Nossek, J.A.: Chromatic dispersion compensation using complex-valued all-pass filter 19(13), 969–971 (2013)
- [6] Kikuchi, K.: Fundamentals of coherent optical fiber communications. Lightwave Technology, Journal of PP(99), 1–1 (2015)
- [7] Kudo, R., Kobayashi, T., Ishihara, K., Takatori, Y., Sano, A., Miyamoto, Y.: Coherent optical single carrier transmission using overlap frequency domain equalization for long-haul optical systems 27(16), 3721–3728 (2009)
- [8] Leibrich, J., Rosenkranz, W.: Frequency domain equalization with minimum complexity in coherent optical transmission systems. In: Proc. Optical Fiber Communication Conf. and Exposition (OFC). OWV1, Optical Society of America (2010), <http://www.opticsinfobase.org/abstract.cfm?URI=OFC-2010-OWV1>
- [9] Li, G.: Recent advances in coherent optical communication. Advances in Optics and Photonics 1, 279–307 (2009)
- [10] Oppenheim, A., Schafer, R.: Discrete-Time Signal Processing. Prentice-Hall, New Jersey, US, 2nd edn. (1998)
- [11] Savory, S.J.: Digital coherent optical receivers: Algorithms and subsystems 16(5), 1164–1179 (2010)
- [12] Savory, S.J.: Digital filters for coherent optical receivers. Opt. Express 16(2), 804–817 (Jan 2008)
- [13] Slim, I., Mezghani, A., Baltar, L., Qi, J., Hauske, F., Nossek, J.: Delayed single-tap frequency-domain chromatic-dispersion compensation 25(2), 167–170 (2013)
- [14] Spinnler, B.: Equalizer design and complexity for digital coherent receivers 16(5), 1180–1192 (2010)
- [15] Taylor, M.G.: Coherent detection method using DSP for demodulation of signal and subsequent equalization of propagation impairments 16(2), 674–676 (2004)
- [16] Xu, T., Jacobsen, G., Popov, S., Li, J., Vanin, E., Wang, K., Friberg, A.T., Zhang, Y.: Chromatic dispersion compensation in coherent transmission system using digital filters. Opt. Express 18(15), 16243–16257 (Jul 2010), <http://www.opticsexpress.org/abstract.cfm?URI=oe-18-15-16243>

# Recognition of Banknotes in Multiple Perspectives Using Selective Feature Matching and Shape Analysis

Carlos M. Costa

Faculty of Engineering, University of Porto  
Rua Dr. Roberto Frias, s/n 4200-465 Porto, Portugal  
[carlos.costa@fe.up.pt](mailto:carlos.costa@fe.up.pt)

**Abstract.** Reliable banknote recognition is critical for detecting counterfeit banknotes in ATMs and help visual impaired people. To solve this problem, it was implemented a computer vision system that can recognize multiple banknotes in different perspective views and scales, even when they are within cluttered environments in which the lighting conditions may vary considerably. The system is also able to recognize banknotes that are partially visible, folded, wrinkled or even worn by usage. To accomplish this task, the system relies on computer vision algorithms, such as image preprocessing, feature detection, description and matching. To improve the confidence in the recognition results, the feature matching results are used to compute the contour of the banknotes using an homography, that later on is validated using shape analysis algorithms. The system successfully recognized all Euro banknotes in 80 test images, even when there were several overlapping banknotes in the same test image.

**Keywords:** banknote recognition · feature matching · computer vision · shape analysis

## 1 Introduction

Banknotes play a critical role in our trading society, and although digital currency is becoming popular, physical banknotes still account for a large amount of the local transactions. As such, systems that are able to recognize banknotes can be applied to aid in the manipulation of this type of currency. These kind of systems are critical for visually impaired people [9], since they allow them to be more independent while avoiding the help of untrusted people. Also, they can increase the security and reliability of ATMs [22], by making sure the maintenance operations are performed correctly and the valid banknotes are not replaced with counterfeits. Other less critical applications are related with automatic sorting and counting of banknotes to speedup transactions and money transfers. For these types of systems to be effective and useful, they must be able to recognize folded, wrinkled and worn banknotes in several perspective views, scale dimensions, and should also tolerate cluttered environments with different lighting conditions.

With these goals in mind, it was implemented a computer vision system capable of reliably recognize banknotes using a camera. It starts by preprocessing the input images in order to remove environment noise and improve contrast and brightness. Then relevant keypoints and their associated descriptors are computed, to later be used to find the best matching in a database of valid banknotes. The correct matching of keypoint descriptors is critical to ensure the proper recognition of the banknotes. As such, methods to filter the inliers from the matches are employed. There are several techniques to perform such filtering, such as the ratio test [14] and the homography outlier removal [3]. Although these techniques can yield very good results, a postprocessing shape analysis is applied to make sure the results obtained are really banknotes. This is related to the fact that the matching of several parts of wrinkle banknotes may result in the recognition of multiple instances of the same banknote. In addition, images similar to banknotes or from other countries currencies may yield incorrect partial matches. As such, this postprocessing phase is critical to ensure the correct recognition of the banknotes. This phase starts by computing the banknote contour using the retrieved homography, and then removes any banknote recognition result that has a convex contour, or has its area, circularity and aspect ratio outside the acceptable ranges for banknotes. To detect multiple banknotes in the same image, the inliers of the last recognized banknote are removed and the process presented earlier is repeated until there are no more valid matches.

In the following section it will be presented an overview of several approaches that can be used to perform banknote recognition. In Sect. 3 a detailed description of the implementation will be provided. In Sect. 4 the representative results of the recognition system will be given and in Sect. 5 it will be discussed the robustness and reliability of the system. Finally, the conclusions will be given in Sect. 6.

## 2 Related Work

There are several approaches that can be used to successfully recognize banknotes [17], and they range from simple but less robust techniques to more advanced and accurate systems [9]. Template matching is one of the simplest recognition methods, which tries to find the banknotes in an image by simple bitmap comparison. But this approach has the limitation that both the reference banknotes and its targets in the image must have the same size and perspective view. To mitigate this restriction, the comparison could be done in several scales and orientations, but it would not be very efficient. The dynamic template matching proposed in [16] could be used instead, but it still is not the best way to handle the recognition. Another way to tackle this problem would be to perform color and shape segmentation of specific parts of the banknotes, like the method proposed in [24]. But this leads to a very specific implementation that would require fine tuning for each banknote, and it would need a lot of effort to successfully recognize all banknotes from both sides. A more broad implementation

could use the size, color and texture of each banknote to perform the recognition [10], but like the previous case, it would require extensive parameterization to recognize each banknote, and would have to take in consideration the accuracy of the distance measurements, because several types of banknotes may have similar sizes. A more robust implementation could use Principal Component Analysis or even adapt the eigenfaces algorithm to try to recognize the banknotes [8], but this can have some problems when the perspective of the reference banknotes is very different from the ones in the image.

For detection of counterfeit banknotes, ultra violet or infra-red light could be used to highlight specific parts of the banknotes that are hard to duplicate and easier to recognize [12]. Other similar technique takes advantage of the fact that specific parts of the banknotes are highlighted when they are illuminated with LEDs with different colors and intensities [19]. Another approach takes in consideration the electromagnetic fields present in sections of the banknotes to perform the recognition [18]. But all these techniques require special hardware that is too expensive. Moreover, they are not meant to be used by visually impaired people.

Some of the most common techniques used to perform banknote recognition rely on machine learning algorithms, such as Support Vector Machines [25], Artificial Neural Networks [7], and Hidden Markov Models [11]. These techniques usually apply some sort of clustering of features before training the classifier, such as the Bag of Keypoints model [6], or try to extract relevant features from the reference images. After the training, the classifiers can be used to recognize the banknotes. Although this is a good approach for general recognition, it may not be very precise in calculating the exact location and contour of the banknotes.

### 3 Implementation

The following sections present the main processing stages of the implemented banknote recognition system (overview shown in Fig. 1). The C++ source code along with the complete results are available at <sup>1</sup>. To speed up development, the Open Source Computer Vision (OpenCV) library was used.

#### 3.1 Reference image database setup

In order for the system to be able to recognize the target banknotes, a database of valid instances must be computed. This database contains the descriptors associated with the keypoints for each preprocessed banknote (from both sides). To improve the detection of the relevant parts of the banknotes and to avoid the usage of sections that are similar across several banknotes, the keypoint detection algorithm is only applied inside the manually created masks associated with each banknote. Only relevant parts such as the banknote number and unique textures or patterns are included in the banknotes masks (only the white areas shown in Fig. 2 will be used to compute the keypoints of a 500 € banknote).

---

<sup>1</sup><https://github.com/carlosmccosta/Currency-Recognition>

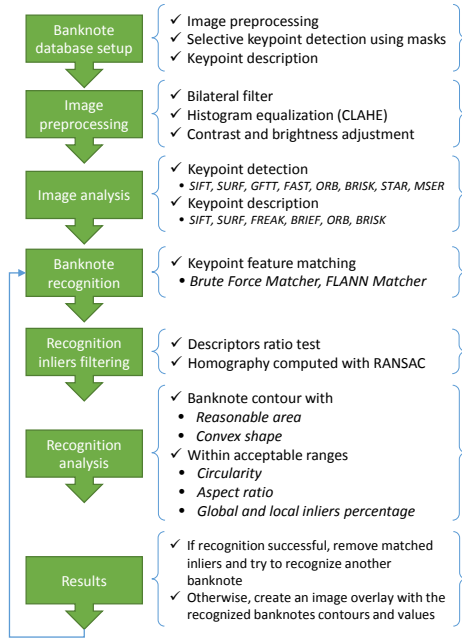


**Fig. 1.** Overview of the main processing stages of the banknote recognition system

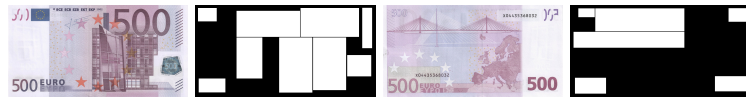


**Fig. 2.** Front and back of a 500€ banknote with associated feature detection masks

### 3.2 Preprocessing

To improve the detection of good features and ensure that the system has robust recognition even when the images have considerable noise, a preprocessing step is applied. In a first phase, most of the noise is removed using a bilateral filter. This filter was chosen because it preserves the edges of image blobs, which are very valuable structures in the detection of feature points. After the noise is reduced, a Contrast Limited Adaptive Histogram Equalization (CLAHE) is applied to increase the contrast. This can improve the recognition of the system when the images are taken in low light environments. This technique has better results over the simple histogram equalization because it can be applied to images that have areas with high and low contrast, and also limits the spread of the noise. Finally, it is also possible to manually tune the contrast and brightness. Figure 3 shows the impact of the preprocessing stage in an image which had camera sensor noise (left) and high brightness shifts (right) due to wrinkled plastic.



**Fig. 3.** Impact of preprocessing stage on two pairs of images (original image on the left, preprocessed image on the right)

### 3.3 Recognition

The recognition is the most critical phase in the system, in which the provided image is analyzed to extract the banknotes monetary value and their contour. The current implementation supports recognition of multiple banknotes in the same image, even if they are partially occluded. The system is able to recognize any type of banknotes. The Euro currency was selected for the computation of the results, but any other currency can be used. To setup the system for other currencies it is only necessary to replace the database images and masks with the intended currency images. To improve the robustness of the system, 3 levels of detail for each banknote are provided (with images having pixel width of 256, 512 and 1024 respectively). For an ideal banknote recognition result, the image resolution of both the reference and the target images should be the same. But converting a high resolution banknote database to the image banknotes resolution has a considerable processing overhead, and as such, to allow the system to be more efficient and able to run in real time, a compromise between precision and computation time was achieved by precomputing the reference images in 3 different scales. At run time, the appropriate level of detail is selected according to the resolution of the target image. The reason for several levels of detail is related to the fact that the geometry of the banknotes changes drastically from a low resolution to a high resolution banknote image. As a result, the computed keypoints and their associated descriptors will be considerably different and the recognition of the banknotes will likely fail. This can be clearly seen in Fig. 4. This approach mitigates this problem by selecting the most similar database image resolution in relation to the banknotes in the image being analyzed.



**Fig. 4.** Impact of image resolution when computing SIFT keypoints from a very low resolution image (left) to a high resolution image (right) of the hologram of a 500 € banknote

**Feature detection** Feature detection is the initial recognition step in which interesting keypoints for matching are identified in the image. These keypoints are normally selected by analyzing the edges, corners, blobs or even ridges. Also, the keypoints provide a condensed representation of the image, which significantly speeds up matching (compared to bitmap or blob matching). To allow fine tuning of the system, the implementation supports the usage of one of several feature detection algorithm, namely, Scale Invariant Feature Transform (SIFT) [14], Speeded Up Robust Features (SURF) [4], Good Features to Track (GFTT) [23], Features from Accelerated Segment Test (FAST) [20], Oriented FAST and Rotated BRIEF (ORB) [21], Binary Robust Invariant Scalable Keypoints (BRISK) [13], STAR [1] and Maximally Stable Extremal Regions (MSER) [15].

**Keypoint descriptor extraction** The feature description step associates to each keypoint a description of its surroundings, in order to allow the matching of keypoints. This normally involves the computation of n-jets or local histograms and the final result is a vector in an n-dimensional space characterizing each keypoint. In order to detect instances with different perspective views, these descriptors must be scale and rotation invariant. Also, they should tolerate different lightning conditions. There are several algorithms that can accomplish this task, and as such, they were included in the implementation and can be selected to fine tuning the system. It was included the SIFT [14], SURF [4], Fast Retina Keypoint (FREAK) [2], Binary Robust Independent Elementary Features (BRIEF) [5], ORB [21] and BRISK [13] feature descriptors.

**Descriptors matching** In order to detect multiple banknotes in the same image, a correct matching between the image descriptors and the reference banknotes descriptors must be established. This initial matching can be performed using either a brute force or a heuristic approach. In the brute force approach, each descriptor in the image is compared with all descriptors in the reference image to find the best correspondence. In the heuristic approach using the Fast Library for Approximate Nearest Neighbors (FLANN), several optimizations are employed to speed up the computations. These optimizations can be related to the appropriate selection of which keypoints to match and to the use of efficient data structures to speed up the search (such as k-d trees).

**Inliers filtering** After the initial matching, an inliers filtering phase is applied. It starts by applying a ratio test [14] and then refines the results with the computation of a homography. In the ratio test, each image keypoint descriptor is associated with the two best reference image descriptors. This allows to decide if the matching is correct or not, by computing the ratio between the distances of these keypoint descriptors. The rationale behind it is that if the ratio is close to 1 then there are two points with equivalent match probability, and as such, it is very likely that this is an incorrect match and should be discarded.

The refinement of the inliers is performed with the computation of a homography that allows the mapping of the positions in the database reference image

to the positions in the target image, in which the banknotes to be recognize reside. This is achieved by using the Random Sample Consensus (RANSAC) method to find the homography that best fits the detected keypoints. Since this is a RANSAC method, it iteratively tries to find better results by randomly selecting the supporting keypoints until there is a high confidence on the results (which occurs when the found homography transformation applied to the reference keypoints yields a high percentage of keypoints positions close enough to the target keypoints) or the maximum number of 5000 iterations is reached. The rationale behind using such method is that the geometry of the banknotes is planar, and if it is assumed that in most cases the banknotes that are going to be recognize have also planar geometry, then a homography can be used to analyze if a match is correct or not. This classification is performed by applying the transformation computed by the homography to each reference keypoint and check if a high percentage of the resulting points in the target image are close to the position of the matched keypoints.

Having the inliers, two approaches can be used to decide if a valid banknote was found or not. One technique relies in the computation of the global inliers ratio in relation to the number of keypoints, and considers that there was a correct match if this ratio is above a given threshold. This is the most appropriate method for most of the banknote recognition cases. Another method that may yield better results when the banknotes are partially occluded, is to consider a correct match when one of the components of the masks (shown in Fig. 2) have the local inliers ratio above a given threshold. The idea behind this approach is to consider each patch of the image represented in the mask as a unique identifier of a banknote. As such, if this local patch is correctly detected, then there is a high confidence that the recognition of that banknote was successful.

**Shape analysis** When a banknote matching is considered valid, it undergoes a postprocessing step in which its contour shape is analyzed. This step is crucial to avoid the multiple detection of the same banknote when it is wrinkled or folded. Also, it removes any recognition that have a contour shape that can not be associated with a banknote.

The initial filtering is performed by removing any result which have a contour with a very low area in relation to the whole image. In a second step, any result without a convex contour is also removed. This is applied because a banknote has a convex quadrilateral shape. It will never have a concave shape, even when it is folded. The reason for this is that the contour is not computed from the banknote borders. Instead a homography is used to map the 4 corners of the reference image to the positions in the image in which the banknotes reside. A final step removes any result that has a contour with a circularity or aspect ratio outside the acceptable bounds. These bounds are retrieved from a database of valid shapes (shown in Fig. 5).

**Detection of multiple banknotes** In order to recognize several banknotes in the same image, the steps presented in previous sections were performed to every

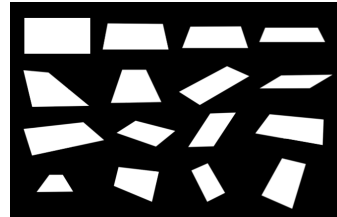


**Fig. 5.** Database of valid instances of banknote shapes

banknote reference image, and the best match was chosen. After the retrieval of the best match, its inliers were removed from the keypoint set, and these two steps were repeated again for every reference image, in order to find another banknote. This is done until no valid match is found.

Only the inliers were removed from the keypoint set in order to be able to successfully recognize partially occluded banknotes. A less robust method (not used), that will likely fail, removes the keypoints that are inside the banknote contour. Although it might require less computation time to perform, it will fail to detect banknotes that are on top of each other, because part of their keypoints will be removed when one of the banknotes is detected.

#### 4 Results

The system was tested with 80 test images (overview of banknotes value distribution shown in Table 1) that contained banknotes in the most common conditions, such as different perspective views, cluttered environments, partially occluded banknotes and also multiple banknotes per image (67 images had only 1 banknote, 11 images had 2 banknotes and 2 images had 3 banknotes).

With the proper selection of the keypoint detection and description algorithm (depending on the image contents), the system successfully recognized all the 95 banknotes in the 80 test images. The most successful configurations are shown in Table 2, which was built by manually inspecting each test image recognition results and selecting the configuration which successfully recognized all banknotes in the image and achieved better contour estimation.

In Fig. 6 to 9 are shown some representative results of the implemented banknote recognition system, showing detection of banknotes with background clutter, perspective distortion, folding and partial occlusion.

**Table 1.** Testing dataset overview

Banknote value	5 €	10 €	20 €	50 €	100 €	200 €	500 €
Nº of banknotes	15	12	19	19	6	9	15

**Table 2.** Selection of the configurations with the best recognition results (1 per image)

<i>Detector</i>	<i>Descriptor</i>	<i>Images with 1 banknote</i>	<i>Images with 2 banknotes</i>	<i>Images with 3 banknotes</i>
SIFT	SIFT	37	7	2
SURF	SURF	24	3	0
GFTT	SIFT	3	1	0
FAST	SIFT	1	0	0
BRISK	BRISK	1	0	0
ORB	ORB	1	0	0

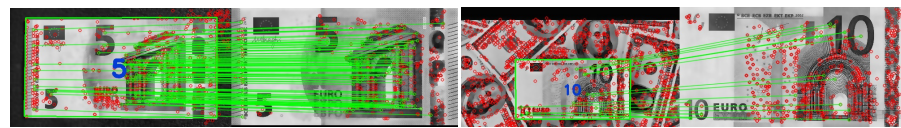


**Fig. 6.** Detection of a banknote in an ideal perspective view with and without background clutter (using SIFT detector, SIFT descriptors and BFMatcher)

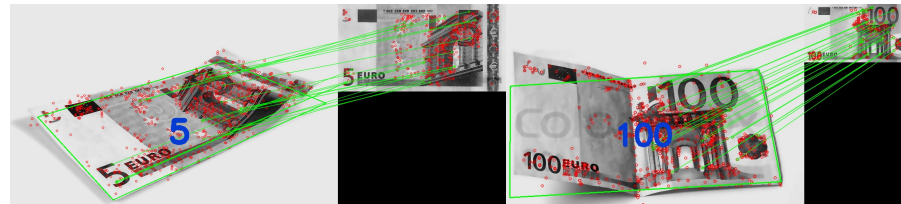


**Fig. 7.** Detection of banknotes with perspective distortion and folding (left image used SURF detector, SURF descriptors and BFMatcher while the right image used SIFT detector, SIFT descriptors and BFMatcher)

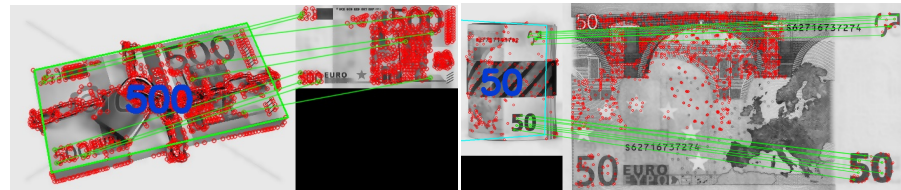


**Fig. 8.** Detection of partially occluded banknotes (left image used GFTT detector, SIFT descriptors and BFMatcher while the right image used SIFT detector, SIFT descriptors and BFMatcher)

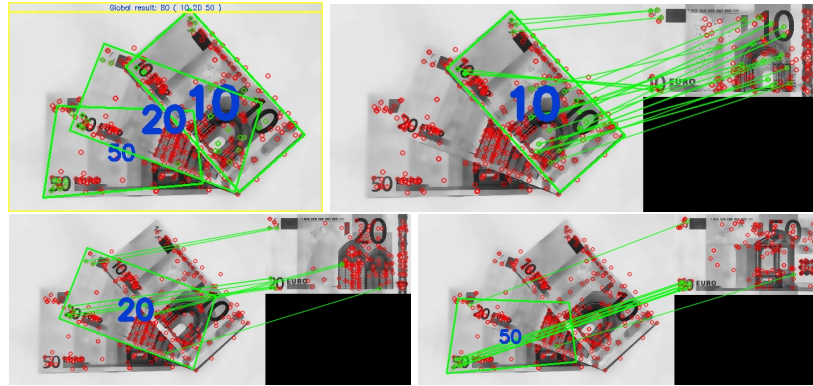


**Fig. 9.** Detection of overlapping banknotes (using SIFT detector, SIFT descriptors and BFMatcher)

## 5 Analysis of Results

Analyzing Fig. 6 to 9 it can be seen that the proposed recognition system managed to correctly detect the euro banknotes with perspective distortion and folding (shown in Fig. 7) and also with partial occlusion (presented in Fig. 8). Moreover, it was able to detect several overlapping banknotes in the same image (seen in Fig. 9). Optimal contour estimation was achieved with banknotes without folding and few perspective distortion (example in Fig. 6).

Several configurations were tested by combining different feature detectors with feature descriptors, and also using different approaches to perform the descriptor matching and inliers filtering. Analyzing Table 2 it can be seen that the configuration using SIFT as detector and descriptor in conjunction with a brute force matcher achieved best recognition results. The best performance of SIFT is mainly related to the fact that it can select feature points that can be reliably detected even if the objects are in different perspective views. Moreover, it can compute descriptors that are robust to different lighting conditions. For real-time use, the SURF feature detector and descriptor are more suitable, since they achieve similar results with significant less computation time. This is achieved mainly due to the simplification of the computations by using integral images. The brute force matcher, although slower than FLANN, achieved better results because unlike the heuristic approach, it matches all descriptors in order to find the best correspondences. However, if the system is to be used in real time, FLANN can be employed with very similar results and lower computation time. In relation to the inliers filtering method, the best results were achieved when the best matched reference image was selected based on the global inliers ratio. However for test images in which most of the banknotes regions were occluded, the local inliers ratio performed better. This occurred because the local matching of patches avoids the removal of recognition results that have low inliers ratio.

## 6 Conclusions

The proposed recognition system successfully recognized the 95 banknotes in the 80 test images, even when they had significant perspective distortion or were partially occluded. It was also robust enough to handle folded and wrinkled banknotes with different kinds of illumination. This was achieved by carefully identifying the regions of the banknotes that had unique features in order to avoid the usage of structures that were similar between banknotes. This technique in conjunction with the usage of reference images with several levels of detail were crucial to improve the correct matching of keypoints descriptors and ensure the correct recognition of the banknotes. The system was configured to recognize Euro banknotes, but can easily be reconfigured to detect other currencies. The achieved results make it a viable option to be used by visually impaired people or to improve automatic banknote counting machines and even increase the security of Automated Teller Machines (ATMs) by detecting counterfeit banknotes.

Future work would include the test of the system using the banknotes under ultra-violet and infra-red light in order to detect with higher confidence counterfeit banknotes and also integrate the system with a speech synthesizer in order to be usable by blind people.

## References

1. Agrawal, M., Konolige, K., Blas, M.: Censure: Center surround extrema for real-time feature detection and matching. In: Computer Vision – ECCV 2008, Lecture Notes in Computer Science, vol. 5305, pp. 102–115. Springer Berlin Heidelberg (2008)
2. Alahi, A., Ortiz, R., Vandergheynst, P.: Freak: Fast retina keypoint. In: IEEE Conference on Computer Vision and Pattern Recognition (CVPR). pp. 510–517 (June 2012)
3. Baggio, D.L., Escriva, D.M., Mahmood, N., Shilkrot, R., Emami, S., Levgen, K., Saragih, J.: Mastering OpenCV with practical computer vision projects. Packt Publishing (2012)
4. Bay, H., Tuytelaars, T., Van Gool, L.: Surf: Speeded up robust features. In: Computer Vision – ECCV 2006, Lecture Notes in Computer Science, vol. 3951, pp. 404–417. Springer Berlin Heidelberg (2006)
5. Calonder, M., Lepetit, V., Strecha, C., Fua, P.: Brief: Binary robust independent elementary features. In: Computer Vision – ECCV 2010, Lecture Notes in Computer Science, vol. 6314, pp. 778–792. Springer Berlin Heidelberg (2010)
6. Csurka, G., Dance, C.R., Fan, L., Willamowski, J., Bray, C.: Visual categorization with bags of keypoints. In: Workshop on Statistical Learning in Computer Vision (ECCV). pp. 1–22 (2004)
7. Gai, S., Yang, G., Wan, M.: Employing quaternion wavelet transform for banknote classification. Neurocomputing 118, 171–178 (2013)
8. Grijalva, F., Rodriguez, J., Larco, J., Orozco, L.: Smartphone recognition of the u.s. banknotes' denomination, for visually impaired people. In: IEEE ANDESCON. pp. 1–6 (September 2010)

9. Hasanuzzaman, F., Yang, X., Tian, Y.: Robust and effective component-based banknote recognition for the blind. *IEEE Transactions on Systems, Man, and Cybernetics, Part C: Applications and Reviews* 42(6), 1021–1030 (November 2012)
10. Hassanpour, H., Yaseri, A., Ardeshiri, G.: Feature extraction for paper currency recognition. In: 9th International Symposium on Signal Processing and Its Applications (ISSPA). pp. 1–4 (February 2007)
11. Hassanpour, H., Farahabadi, P.M.: Using hidden markov models for paper currency recognition. *Expert Systems with Applications* 36(6), 10105–10111 (August 2009)
12. Kim, B.K., Lee, E.C., Suhng, B.M., Ryu, D.Y., Lee, W.H.: Feature extraction using fft for banknotes recognition in a variety of lighting conditions. In: 13th International Conference on Control, Automation and Systems (ICCAS). pp. 698–700 (October 2013)
13. Leutenegger, S., Chli, M., Siegwart, R.: Brisk: Binary robust invariant scalable keypoints. In: IEEE International Conference on Computer Vision (ICCV). pp. 2548–2555 (November 2011)
14. Lowe, D.G.: Distinctive image features from scale-invariant keypoints. *International Journal of Computer Vision (IJCV)* 60(2), 91–110 (2004)
15. Matas, J., Chum, O., Urban, M., Pajdla, T.: Robust wide-baseline stereo from maximally stable extremal regions. *Image and Vision Computing* 22(10), 761–767 (2004), *british Machine Vision Computing 2002*
16. Nishimura, K.: Banknote recognition based on continuous change in strictness of examination. In: ICCAS-SICE. pp. 5347–5350 (August 2009)
17. Pawade, D., Chaudhari, P., Sonkambale, H.: Comparative study of different paper currency and coin currency recognition method. *International Journal of Computer Applications (IJCA)* 66(23), 26–31 (March 2013)
18. Qian, S., Zuo, X., He, Y., Tian, G., Zhang, H.: Detection technology to identify money based on pulsed eddy current technique. In: 17th International Conference on Automation and Computing (ICAC). pp. 230–233 (September 2011)
19. Radványi, M., Solymár, Z., Stubendek, A., Karacs, K.: Mobile banknote recognition: Topological models in scene understanding. In: Proceedings of the 4th International Symposium on Applied Sciences in Biomedical and Communication Technologies (ISABEL). pp. 185:1–185:5. ACM (2011)
20. Rosten, E., Drummond, T.: Machine learning for high-speed corner detection. In: Computer Vision – ECCV 2006, Lecture Notes in Computer Science, vol. 3951, pp. 430–443. Springer Berlin Heidelberg (2006)
21. Rublee, E., Rabaud, V., Konolige, K., Bradski, G.: Orb: An efficient alternative to sift or surf. In: IEEE International Conference on Computer Vision (ICCV). pp. 2564–2571 (November 2011)
22. Sako, H., Watanabe, T., Nagayoshi, H., Kagehiro, T.: Self-defense-technologies for automated teller machines. In: International Machine Vision and Image Processing Conference (IMVIP). pp. 177–184 (September 2007)
23. Shi, J., Tomasi, C.: Good features to track. In: IEEE Computer Society Conference on Computer Vision and Pattern Recognition (Proceedings CVPR). pp. 593–600 (June 1994)
24. Solymár, Z., Stubendek, A., Radványi, M., Karacs, K.: Banknote recognition for visually impaired. In: 20th European Conference on Circuit Theory and Design (ECCTD). pp. 841–844 (August 2011)
25. Yeh, C.Y., Su, W.P., Lee, S.J.: Employing multiple-kernel support vector machines for counterfeit banknote recognition. *Applied Soft Computing* 11(1), 1439–1447 (January 2011)

# Optimizing Network Calls by Minimizing Variance in Data Availability Times

Luis Neto

SYSTEC-FoF, Faculdade de Engenharia, Universidade do Porto,  
Rua Dr. Roberto Frias, 4200-465 Porto, Portugal  
[lcneto@fe.up.pt](mailto:lcneto@fe.up.pt)  
<http://systec-fof.fe.up.pt>

**Abstract.** Smart Nodes are intelligent components of sensor networks that perform data acquisition and treatment, by the virtualization of sensor instances. In this work, we present a methodology to improve the number off calls a Smart Node makes to the network. The paper exposes and explains the Smart Node internal structure, formally describing the problem of minimizing the number of calls Smart Nodes make to Cloud Services, by means of a combinatorial *Constraint Satisfaction Problem* and using a *Constraint Satisfaction Solver*. Considering this methodology to solve the problem, expected results are presented and conclusions are formulated.

**Keywords:** Sensor Simulation ·Combinatorial Optimization ·Time Synchronization ·Smart Nodes

## 1 Introduction

In this context, a Smart Node is a gateway. Those cyber-physical components are sink nodes for *Wireless Sensor Networks* that have enhanced data process and do have collaborative capabilities [9]. Considering a scenario that comprises a reasonable number of these components, in which:

- Gateways are in constant synchronization with Intra/Inter Enterprise Cloud systems.
- Gateways perform collaborative tasks by talking over the network.
- Human Machine Interface devices proceed to on demand requests to the Smart Nodes.

A large number of messages is expected caused by a large number of devices and services present.

Gateways collect data from different sensor types (eg: humidity, current, pressure). These cyber-physical components aim is to be coupled to industrial machines, along with several sensors, which collect data from the machine operations; finally, collected data is treated and synchronized with Cloud systems

that performs business intelligence. The majority of sensors coupled to industrial machines are sampling data at very different rates and synchronizing the collected data with the Smart Node, in the respective sampling frequency. A Smart Node can embed a set of different data treatment modules. These modules can be instantiated to provide different ways of treating sensors data in a graph arrangement.(Fig. 1) A gateway internal logic arrangement is represented using a *directed acyclic graph (DAG)*. The graph structure can be divided in three levels, each with a different color assignment: the Sensor Level includes sensor instances (bottom level, orange nodes), providing data to the gateway; the data treatment level (middle level, blue nodes), includes nodes representing instances of algorithms embedded at the gateway that can treat information in several ways (eg: perform a mean calculation, perform trend analysis); the Network Level (top level, green nodes) includes nodes where the flux resulting from the inferior level nodes can be redirected to subscribing hosts in the network. This internal structure can be dynamically rearranged: new sensors and data modules can be loaded into the Smart Node; the connections between nodes can be reformulated to synchronize and treat data in new ways. A problem of

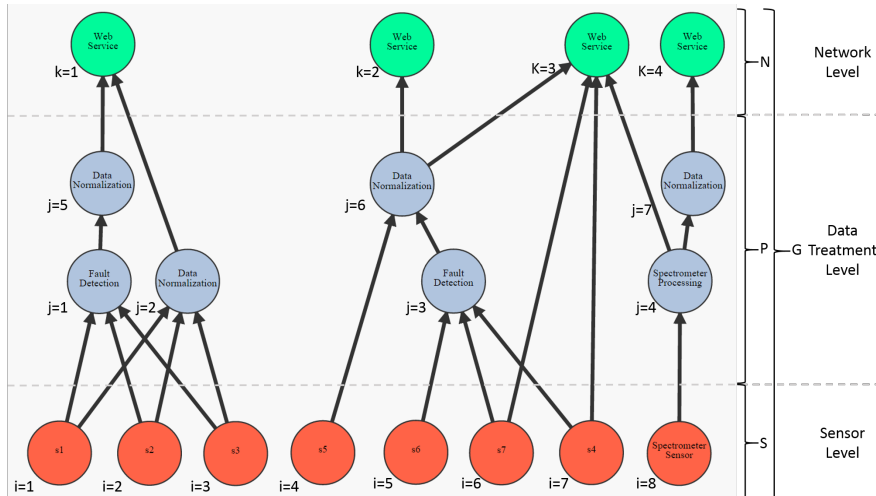


**Fig. 1.** Internal Gateway configuration.

efficiency emerges due to the different rates at which the data is gathered from the different sensors. When collected data reaches the Network Level nodes, it is immediately sent to the subscriber, a network Cloud service. Slight time differences in data availability to be sent lead the Network Level nodes to perform new and individual calls. If those time differences were eliminated, Network Level nodes would be synchronized and data from the different nodes could be packed together, decreasing the total number of calls made and reducing the network

traffic heavily. To accomplish synchronization among Network Level nodes, data buffers for all the edges connecting descending nodes from a Network node, must be resized to compensate: (1) the time elapsed in Data Treatment level nodes, since each treatment module takes different time to process data; (2) different sampling rates of sensors, imply same number of samples to be accumulated at different times.

Taking advantage of the DAG gateway representation, we formulated and proposed a solution to the problem as a combinatorial *Constraint Satisfaction Problem* (CSP).

In section 2, problem's formal definition is presented. Section 3, shows literature review, the problem formulation basis. Section 4, the solving process is detailed along with assumptions, constraints and technology that can be used. In sections 4 and 5, respectively, expected results and conclusions are presented.

## 2 Problem Definition

Each arc in the graph (see Fig. 1) has an associated buffer  $b$ . Given the fact that sensors are sampling at different frequencies  $freq$ , these buffers are filled at different rates. We define  $G$  as the set of nodes in a particular Gateway instance; three subsets of nodes are contained in  $G$ :  $N \subset G$  is the subset of Network Nodes (green nodes);  $P \subset G$  is the subset of data Processing Nodes (blue nodes);  $S \subset G$  is the subset of Sensor Nodes (orange nodes). The subsets obey to the following conditions:

$$G = N \cup P \cup S; N \cap P = \emptyset; P \cap S = \emptyset; N \cap S = \emptyset \quad (1)$$

Nodes in  $N$  can be classified as consumers; nodes in  $S$  are exclusively producers; nodes in  $P$  are both producers and consumers. Connections between nodes can be defined as:

$$x_{n,m} = \begin{cases} 1 & \text{if } n \text{ is consumer of } m : n \neq m; m \in P \cup S \text{ and } n \in N \cup P \\ 0 & \text{otherwise} \end{cases} \quad (2)$$

As an example, we can observe in Fig. 1 that node  $j = 6$  consumes from  $i = 4$  (sensor level) and  $j = 3$  which is in same level (network-level) and all the  $k$  nodes only consume from inferior levels. To help in the definition of this problem, two additional subsets of nodes, containing the connections of a given node, are defined as follows:

$$W_n = \{j : j \in P \wedge x_{n,j} = 1, n \in N \cup P\} \quad (3)$$

Equation 3 defines a subset of nodes in  $P$ , which are producers for the given node  $n \in N \cup P$ . For illustration purposes, in Fig. 1, those are the nodes with index  $j$ , in Data Treatment Level (blue nodes), from which other blue nodes and green nodes consume. As an example (Fig. 1), for  $n = j_6 : W_{j_6} = \{j_3\}$ ; for  $n = k = 3 : W_{k_3} = \{j_6, j_4\}$ ; and for  $n = j = 3 : W_{j_3} = \{\emptyset\}$  since it does not consumes from any Data Processing nodes.

$$X_n = \{i : i \in S \wedge x_{n,i} = 1, n \in N \cup P\} \quad (4)$$

Defines a subset of nodes in  $S$ , which are producers for the given node  $n \in N \cup P$ . In Fig. 1, are the nodes  $i$  in the Sensor Level (orange nodes), from which blue nodes and green nodes consumes. As an example (Figure 1), for  $n = k = 3 : X_{k_3} = \{i_6, i_7\}$ ; for  $n = k = 1 : W_{k_1} = \{\emptyset\}$  since it does not consume from any Sensor Level node and for  $n = j = 6 : W_{j_6} = \{i_4\}$ . A processing node in  $P$ , applies an algorithm to process the data of the associated producers. The generated data in the sensor level is delivered to the processing nodes as a batch, which contains the number of samples equal to the size of the buffer for the corresponding edge. In order to the processing to be possible, the number of elements in each collection must be the same. This constraint must be applied to the subsets  $W_n$  and  $X_n$  of a given node  $n$  in  $N \cup P$ ; for that constraint to be respected, the size of every buffer  $b_n$  associated to each element of  $W_n$  and  $X_n$  must be the same. Formally this constraint can be represented as:

$$\forall j \in W_n, \forall i \in X_n : |b_{n,j}| = |b_{n,i}| \quad (5)$$

Where  $|b_{n,m}|$  represents the size of the given buffer  $b$  for the given connection  $x_{n,m}$ .

The size of the buffer  $b$  is adjustable and can vary from 1 to 1000. The objective of this problem is to arrange a combination of values to parameterize the size of every buffer  $|b|$ , for every arc in the graph, that minimizes the differences between times at the Network Nodes in which data is available to send to the network. To calculate the time that takes data to be available at every node  $j \in N$ , times for all its providers in the graph must be calculated. As data comes in collections (sets of single values), let us define *burst* as the exact time at which data is sent from one provider node to a consumer node and represent the *burst* of a node  $n$  as  $B_n$ .

The *burst* of a Sensor Node  $i$ , is defined by its sampling frequency. That way, every time a sample from a sensor is collected, that sample is sent, which corresponds to a *burst* of a Sensor Node, and is formally represented by the expression:

$$B_i = freq(i), \forall i \in S \quad (6)$$

For a Data Processing Node, the burst time must contemplate all the burst times from its providers and the time that takes the associated function to treat one collection of data. The expression which determines burst time for a Data Processing Node  $j$  is defined as:

$$B_j = \max_{i \in W_j, n \in X_j} (B_i, B_n) + T(f_j) \times (|W_j| + |X_j|) \quad (7)$$

We assume that the growth in time complexity of the function  $T(f_j) : j \in P$  is linear with the number of collections to process. Since the size of each producer buffer is equal, we multiply the total number of producers of  $j$ , to the cost of treating a single producer collection. To calculate the *burst* for  $j = 1$  (see Fig. 1), we take the max *burst* of  $X_{j_1}$  and sum the multiplication of  $T(f_{j_1})$  (time to process one sensor sample) with the number of elements in  $X_{j_1}$  (which correspond to the producers  $i_1, i_2$  and  $i_3$ ).

Finally, to calculate the *burst* of a Network Node  $k : k \in N$ , the expression to consider is:

$$B_k = \max_{i \in X_k, j \in W_k} (B_i, B_j) \quad (8)$$

Using the expression to calculate the *burst* for each Network Node, the objective is to minimize the variance of *burst* for all the Network Nodes. By varying the size of the buffers in the graph, the variance of all burst times for Network Nodes is minimized:

$$\min_{k \in N} \hat{V}(B_k) \quad (9)$$

Using a Constraint Satisfaction Solver (CSV), by assigning values to the sizes of every buffer, a configuration which minimizes the variance of *bursts* in the Network Level is achieved. With a minimized variance for the bursts at the Network Level nodes, all data produced can be sent to the Cloud using the same call. In comparison with individual calls strategy - a call made every time a burst at the Network Level occurs - is expected that the number of calls to the Cloud is minimized as a consequence.

### 3 Background and Related Work

The theoretical background behind this problem has a large spectrum of application. The problem of modeling buffer sizes is mostly applied to network routing, where [6],[1][2] are examples. As we are not interested in dealing with networks intrinsic characteristics and these problems are not modeled as graphs,

those buffer optimization problems can hardly be extrapolated to this work. The domain of Wireless Sensor Networks (WSN) is another scope of application of buffer modeling optimization, with relevant literature in this domain; the section of *Routing* problems in [5] covers a great number of important works regarding Flow Based optimization models, for data aggregation and routing problems. WSN optimization models care with constraints that this problem modulation does not cover, such as: residual energy of nodes, link properties, network lifetime, network organization and routing strategies.

A relevant work in WSN revealed to be of the major interest for this work. The authors presented and solved the problem of removing inconsistent time offsets, in time synchronization protocols for WSN. [7] The problem presented has an high degree of similarity with the case we are dealing. The problem is represented by a *Time Difference Graph (TDG)*, each node is a sensor, every sensor has local time and every arc has an associated cost time given by a function. The solution to the problem is given by a CSP approach. For every arc in the graph exists an *adjustment variable* (analogous to the buffer size in this case), assignments are made to the variables to find the largest consistent subgraph, ie. a sub-graph in which inconsistent time offsets are eliminated.

Focusing the search in literature domain of CSP problems, several works were revealed in the sub-domain of balancing, planning and scheduling activities that can be related to this application [3][4],[11],[8][10]. Namely, models of combinatorial optimization for minimizing the maximum/total lateness/tardiness of directed graphs of tasks with precedence and time constraints [3][10]. These problems are analogous to this work, and due to a simplified formulation with the same constraints (precedences and time between nodes), can be easily extrapolated to our case.

## 4 Problem Solution

To solve the problem, a base graph configuration was tested using both the optimized version and the non-optimized, for comparison purposes. The version of the internal logic configuration is illustrated in Fig. 2.

### 4.1 Problem Assumptions

To test the implementation of the problem, a sensors simulation was built in the course of this work. The simulation application allows to deploy several sensors sampling with a desired frequency. The virtual sensors uses a normal distribution to generate data in a float format. The Smart Node application has several interfaces for real sensors, ranging from radio frequency to cable protocols. In tests using the simulation, data was transmitted over *WiFi*, using *HTTP* as the application protocol. By using this scheme to transmit data, we assume no interference or noise of any type can cause disturbance in the sampling frequency. In a real case scenario, a sensor could enter in an idle state by a variety of reasons. In that case, data would not be transmitted at all, causing the transmission of

data to the Cloud to be postponed for undefined time, waiting for the Network Level node burst depending on the idle sensor. Using the simulator we assume a sensor never enters an idle state.

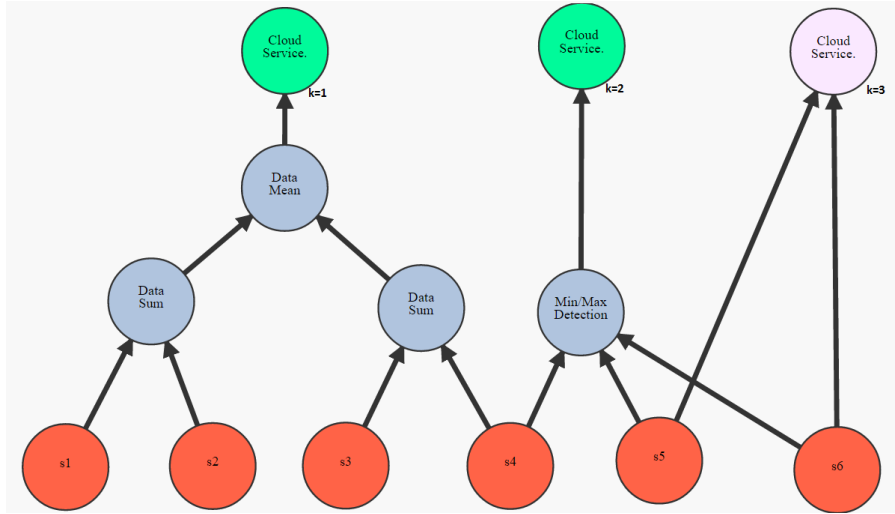


**Fig. 2.** Internal Gateway configuration for tests.

The data processing function times used in the configuration (Fig. 2), are illustrated in Table 1. The results were obtained by applying the functions to exactly one collection of data, collected from one sensor. Is assumed that the time that takes to treat one collection of data will increase linearly for more than one collection, as it was stated in (7) for  $T(f_j)$ .

**Table 1.** Data processing elapsed time for one collection of data.

Processing Module	Time (s)
DataSum	1.90084E-4
DataMean	4.33539E-4
MinMax	3.83043E-4

A number of tests dealing with a great number of configurations could be make. In this case, the frequencies adopted for tests are shown in Table 2. The index of sensors in the table corresponds to the sensors index in Fig. 2.

**Table 2.** Sensors sampling frequency for simulation.

Sensor Index	s1	s2	s3	s4	s5	s6
Frequency Time (s)	0.4	0.5	0.6	0.7	0.8	0.9

#### 4.2 Constraint Satisfaction Problem solver

There are several free CSP solvers available, but, as the Smart Node is coded in *Java*, we opted to use *OptaPlanner*<sup>1</sup>. This solver is a pure *Java* constraint satisfaction program that is maintained by the *RedHat* community, and it can be embedded with the Smart Node application to execute and provide on demand solutions to this optimization problem. Because of the reconfigurable property of the Smart Node internal structure, each time the structure is rearranged, the solution obtained to the problem instance prior to the reconfiguration becomes infeasible. The integration (see Fig. 3) between the two technologies is accomplished by defining the problem in the OptaPlanner notation: (1) *Buffer Size* class corresponds to the *Planning Variable*, during the solving process it will be assigned by the different solver configurations; (2) *Edge* class is the *Planning Entity*, the object of the problem that holds the *Planning Variable*; (3) *SmartNodeGraph* class is the *Planning Solution*, the object that holds the problem instance along with a class that allows to calculate the score of problem instance. The score is given by implementing Equation 9; the best score is 0, which corresponds to null variance between the Network Levels nodes.

The search space of this problem is huge, since the domain of the variable *Buffer Size* ( $b$ ), can vary from 1 to 1000. The search space can be determined by  $E^n$ , where:  $E$  is the total number of edges in the graph and  $n$  is the *Buffer Size* size domain (1000 for this case). Since the search space is exponential, heuristics can be implemented to help the *OptaPlanner* solver to determine the easiest buffers to change. The implemented heuristic sorts the buffers from the easiest to the hardest. The sorting values are given by the number of ancestors of a given edge, an edge with a greater number of ancestors is more difficult to plan. Also, if an edge leads to a Network Node, is considered more difficult to plan and its score is penalized. *OptaPlanner* offers a great variety of algorithms to avoid the huge search space of the majority *CSPs*. These algorithms can be consulted in the documentation<sup>2</sup> and configured to achieve best search performances.

### 5 Expected Results

Results obtained by a fully functional solution can be evaluated by a direct comparison between the number of calls performed by a non-optimized version with the optimized one. The total number of calls for an optimized version should be far less than the ones of the non-optimized version. Using the configuration

<sup>1</sup> URL: <http://www.optaplanner.org/>

<sup>2</sup> URL: <http://docs.jboss.org/optaplanner/release/6.3.0.Final/optaplanner-docs/pdf/optaplanner-docs.pdf>

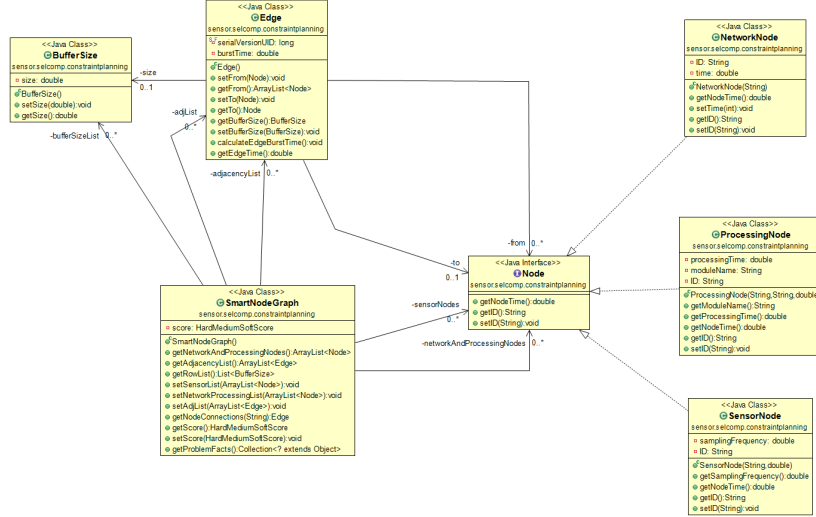


**Fig. 3.** UML for Smart Node and OptaPlanner integration.

illustrated in Fig. 2, with the parameters shown in Table 1 and Table 2, the values in seconds for *burst* in the Network Nodes are (Table 3): Assuming that

**Table 3.** Burst times studied Smart Node configuration.

Network Node	Burst (s)	Number of packets (1 min.)
k=1	2.80	21
k=2	3.60	17
k=3	1.80	33

an optimized version would achieve a solution in which *burst* for  $k = 1$  and  $k = 3$  is equal to  $k = 2$ , the difference in the total number of packets sent would be (Table 4):

**Table 4.** Comparison for the number of packets sent.

	Optimized	Non-Optimized
Total Number of Packets (1 min.)	17	71

## 6 Conclusions

An additional constraint to this problem could be the introduction of a minimum of two samples for providers of a Processing Node. If a variance value of 0 for the *bursts* in the Network Level nodes could not be found, it would imply the creation of a time window - to wait for all *bursts* - with the size of the variance; if that occurs, an upper bound of time must be imposed. In the case *bursts* occurs after the upper bound, the correspondent data should be sent in another call. This can imply the solution to be as costly compared with a non-optimized version of the same problem instance. In a case in which a single or several sensors are producing data with an higher priority, this problem can not be applied. But the problem can be easily reformulated to embrace that kind of situation modifying the objective function (Equation 9). Since the solution is hard to obtain due to the search space, a feasible solution was not found at the time this paper was written.

## References

1. Avrachenkov, K., Ayesta, U., Altman, E., Nain, P., Barakat, C.: The effect of router buffer size on the tcp performance. In: In Proceedings of the LONIIS Workshop on Telecommunication Networks and Teletraffic Theory. Citeseer (2001)
2. Avrachenkov, K., Ayesta, U., Piunovskiy, A.: Optimal choice of the buffer size in the internet routers. In: Decision and Control, 2005 and 2005 European Control Conference. CDC-ECC'05. 44th IEEE Conference on. pp. 1143–1148. IEEE (2005)
3. Blazewicz, J., Kubiak, W., Martello, S.: Algorithms for minimizing maximum lateness with unit length tasks and resource constraints. Discrete applied mathematics 42(2), 123–138 (1993)
4. Gacías, B., Artigues, C., Lopez, P.: Parallel machine scheduling with precedence constraints and setup times. Computers & Operations Research 37(12), 2141–2151 (2010)
5. Gogu, A., Nace, D., Dilo, A., Meratnia, N.: Review of optimization problems in wireless sensor networks. InTech (2012)
6. Ioachim, I., Desrosiers, J., Soumis, F., Bélanger, N.: Fleet assignment and routing with schedule synchronization constraints. European Journal of Operational Research 119(1), 75–90 (1999)
7. Jadliwala, M., Duan, Q., Upadhyaya, S., Xu, J.: On the hardness of eliminating cheating behavior in time synchronization protocols for sensor networks. Tech. rep., Technical Report 2008-08, State University of New York at Buffalo (2008)
8. Malapert, A., Guéret, C., Rousseau, L.M.: A constraint programming approach for a batch processing problem with non-identical job sizes. European Journal of Operational Research 221(3), 533–545 (2012)
9. Neto, L., Reis, J., Guimaraes, D., Goncalves, G.: Sensor cloud: Smartcomponent framework for reconfigurable diagnostics in intelligent manufacturing environments. In: Industrial Informatics (INDIN), 2015 IEEE 13th International Conference on. pp. 1706–1711. IEEE (2015)
10. Patterson, J.H., Albracht, J.J.: Technical noteassembly-line balancing: Zero-one programming with fibonacci search. Operations Research 23(1), 166–172 (1975)
11. Rustogi, K., et al.: Machine scheduling with changing processing times and rate-modifying activities. Ph.D. thesis, University of Greenwich (2013)

## Visible Light Communication - A Brief Overview

Stephen O. Ogodo

Faculdade de Engenharia da Universidade do Porto, Porto, Portugal  
up201406661@fe.up.pt

**Abstract.** The advent of wireless and mobile communication has redefined the telecommunication landscape. Consequently, the data traffic is growing in geometric proportion, pushing the available spectrum to its limit. This development has necessitated many efforts towards finding an alternative or, other means to complement the already saturated radio frequency (RF) spectrum in order to keep pace with the data-hungry modern age. One of such promising and viable modes of communication is the visible light communication (VLC). This paper briefly survey some advances made in recent years, in the emerging field of VLC with emphasis on the challenges facing mainstream adoptions of VLC and open issues for research in order to fully harness its abundant potentials.

**Keywords:** RF · VLC · OFDM · LED · communication · optical

### 1 Introduction

The ever growing demand for wireless access, triggered by the proliferation of smart mobile devices, has made the RF spectrum to be highly congested, sometime resulting in low data rate, leading to packet delay and sometime packet loss. Plethora of innovations aimed at increasing the spectral efficiency of the available RF spectrum such as in multiple-input multiple-output (MIMO) system, massive MIMO, cooperative MIMO, advance data modulation scheme like orthogonal frequency division multiplexing (OFDM), MIMO-OFDM has yielded tremendous results. However, there is need to consider other mode of communication such as VLC, in order to meet up with the exponentially rising demand for bandwidth.

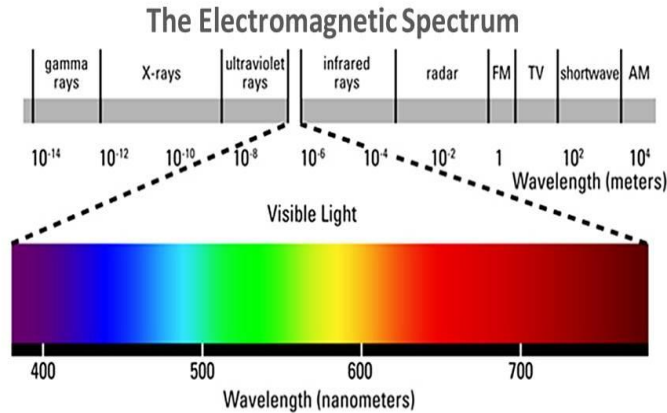


**Fig. 1.** The electromagnetic spectrum showing the visible light region [1]

VLC is data communication through visible light between 400 and 800 THZ (780-375nm) in the electromagnetic spectrum as shown in fig1. The inherent potentials of VLC make it worthwhile to expend research effort in the field. The virtually unlimited and unregulated bandwidth (nearly 400THz) covered by the visible light region of the electromagnetic spectrum is mind blowing compared with the conventional RF spectrum.

VLC serves dual purposes of illumination and communication simultaneously [2] making use of light emitting diodes (LEDs) as the transmitters and photodiodes (PDs) as the receivers. Light possesses no electromagnetic interference as opposed to the RF, which make VLC the preferred candidate in application where sensitive electronic devices are used, such as airplane, hospitals and nuclear plants. Also, no fear of harmful radiation from the visible light as usually is the case with the RF especially at high transmitting power.

Furthermore, communication using VLC is very secure without the possibility of eavesdropping as light doesn't penetrate through walls, partitions and opaque objects as the case is with the RF. This factor also affords VLC in an indoor scenario additional benefit of spatial frequency reuse. A secured communication is highly desired in sensitive areas like military applications and financial transaction. Other factors that favour the deployment of VLC is the fact that readily available and cheap devices like off the shelf LEDs and PDs can be used with little modification as optical transmitters and receivers [3]. Moreover, research has shown that over 70 per cent of communication takes place in the indoor environment where VLC is most applicable

These compelling benefits and inherent potentials of VLC has inspired many research work in the field of VLC in other to surmount the teething challenges of this technology and fully harness its abundant potentials. Modern research in optical wireless communication (OWC) can be traced back to 1979 when an indoor OWC system was presented by G. feller and Bapst [4]. They were able to interconnect a cluster of

terminals to a common cluster control using diffuse optical radiation. In their system, diffuse optical radiation in the near-IR region was utilized to interconnect a cluster of terminals located in a room to a common cluster controller. In 2003, research on VLC using LED was set up at Nakaguwa Laboratory in Keio University, Japan. Visible light communication consortium (VLCC) was also founded that same year [5] which has given rise to increasing wide spread curiosity in VLC.

In [6], a group of researchers from Centre for information and communication technology research (CICTR) at Penn State proposed the ideal of combining power line communication (PLC) with VLC to provide broadband access for indoor applications in 2006. They aimed at using PLC for backhaul data transmission while employing VLC to provide local (LAN).

The Europe Union OMEGA project was a three years project spanning January 2008 to March 2011. OMEGA "hOME Gigabit Access" was developed, and it implemented a 1 Gigabit/second data rate employing interior lighting system [7]. The project presented the results of its work in February 2011 which included exhibition of the VLC systems and infrared systems, which achieved data rate of 100Mbit/s and 280Mbit/s respectively [8].

In 2010, Jelena Vučić et al at Fraunhofer institute for telecommunication, Germany, achieved a point to point communication link with a gross transmission rate of 513Mbit/s with off line signal processing. The link was based on a commercial thin film-high power phosphorescent white LED as the light source and an avalanche photo diode (APD) as the receiver [9].

In July 2011, Professor Harald Hass of the University of Edinburgh demonstrated the transmission of a high definition video using a standard LED lamp at the TED Global conference [10].

In October 2014, Axrtek launched a commercial full duplex RGB LED VLC system called MOMO having equal uplink and downlink speed of 300Mbit/s within a range of 25 feet. The MOMO VLC system is PLC compatible and can handle 256 users simultaneously it also support session initiation protocol (SIP).for fast video teleconferencing [11].

In May 2015, Philips collaborated with supermarket giant Carrefour, to deliver VLC location based services to shoppers' smart phones in a hypermarket in Lille, France [12].

With this introduction, the rest of the paper is structured as follows: section 2 deals with the overview of VLC system, areas of application of VLC is considered in section 3 , while some challenges and open research areas in VLC is the focus of section 4. The conclusion is presented in section 5.

## 2 Overview of VLC system

Like any other communication systems, the VLC communication link consists of the LEDs as the light source, the propagating channel (the visible light) and the receivers (PDs).

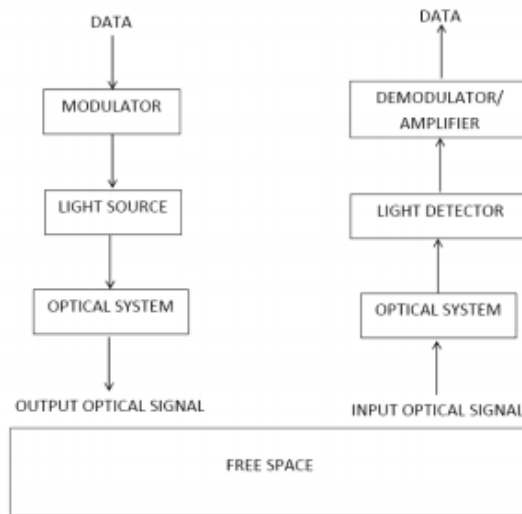


**Fig. 2.** Basic block diagram of a VLC link

### 2.1 Light source (LED)

It has been established from various research findings that LED is the best source of light for optical signal transmission in an indoor environment. Some of the properties of LEDs that make it the preferred choice are that it's durability, bright, energy efficient, ability to switch it on and off at very high frequency, lower path loss and dispersion over short range which enhances its bandwidth [13]. Both monochromatic standard LED and trichromatic RGB LED can be employed in VLC with RGB LED using wavelength division multiplexing (WDM) to achieve higher throughput than the standard LED. Signals are transmitted by means of intensity modulation and direct detection (IM/DD) as shown in the fig.2. In this way, the intensity of the LED is modulated with the baseband data signals to be transmitted. The optical output power of the LED is proportional to the DC biasing current. Usually the LED is biased in the linear region to avoid non linearity and modulated at high enough frequencies to avoid flickering [14].

## 2.2 VLC Channel model and Noise

J. M. Kahn and J. R. Barry characterized the optical wireless channel far back as 1997 for infra red (IR) communication [15], but it can be applied to visible light communication also. The received signal  $Y(t)$  is given by:

$$Y(t) = RX(t)*h(t) + N(t) \quad (1)$$

Where  $R$  is the responsivity (sensitivity) of the PD,  $X(t)$  is the modulating signal power, the channel model  $h(t)$  is the baseband linear system and  $N(t)$  is the combination of shot noise as a result of the ambient light sources and the thermal noise in the electronic circuitry.

## 2.3 Optical Receiver

Photo diodes convert the incident optical power into proportionate electrical current. Two types of optical receivers used in VLC are PIN PD and APD. While APD is reputed for its higher gain, it's however susceptible to shot noise [16]. The PIN PD on the other hand has high temperature tolerance and it's cheaper. This made the latter preferred especially when the intensity of the incident light is, at least, moderately high.

## 2.4 Modulation

The simplest forms of modulation are achieved when the Modulating signals are used to switch the LED at the frequencies of interest which contain information to be transmitted. This is called single carrier (SC) modulation and it includes on-off keying (OOK), pulse amplitude modulation (PAM) with its variants, pulse position modulation (PPM) and its variants and recently colour shift keying (CSK) [17]. However, to avoid long strings of 1s and 0s which can result in flickering, a controlling sequence is usually incorporated with the SC modulation. In order to achieve higher data throughput which SC modulation cannot offered, multi-subcarrier modulation schemes such OFDM have been adapted to VLC for greater throughput.

## 2.5 OFDM in VLC

OFDM is the modulation choice for applications that require high data rate [18] because of its spectral efficiency and its ability to drastically reduce inter symbol interference (ISI) suffered at high data rates by signals. OFDM is also robust against channel dispersion. However, OFDM must be properly adapted bearing in mind the peculiar features of optical signals [19, 20]. For instance, electric signals needs to be real-valued and positive (unipolar) for IM/DD. Therefore, to ensure that OFDM time domain is real-valued, Hermitian symmetry must be satisfied. Another constrain is that the LED must be biased in the linear region, but high PAPR required to convert the bipolar OFDM to unipolar OFDM [21]. DC biased optical OFDM (DCO-OFDM) uses DC bias to achieve non-negativity, while asymmetrically clipped optical OFDM

(ACO-OFDM)] is able to perfectly recover odd subcarriers since the clipping of negative signals forms distortion only in the even subcarriers [21].

### **3 Potential Application areas of VLC**

#### **3.1 Indoor Visible light Positioning**

This entails using visible light to locate objects within an indoor environment. This is somehow similar to global positioning system (GPS) for outdoor application. This was demonstrated In May 2015, when Philips collaborated with supermarket giant Carrefour, to deliver VLC location based services to shoppers' smart phones in a hypermarket in Lille, France [10]. The retailer giant is transmitting digital information from LED lamps to customers' smart phones, using VLC. The system is similar to one pioneered by US retailer Target. This was an innovative way of steering shoppers straight to discounts and products in its stores: via lights in the shop ceiling.

#### **3.2 Underwater Communication**

VLC is been considered as a means of underwater communication. Though underwater communication has been around lately, the industrial, scientific and Medical (ISM) RF band being used suffers so much attenuation. VLC can provide the means to establish high speed optical network at a range of up to several hundred meters in deep see environments, while also providing illumination for Divers [22].

#### **3.3 Vehicular communication**

Many cars are already fitted with LED lamps. Traffic signage, traffic lights, and street lamps are adopting the LED technology so there are massive applications opportunities here.

#### **3.4 Hazardous environments**

Industrial gas plant, petrochemical plants and nuclear plant are not safe for the RF, VLC is the appropriate technology for such places.

#### **3.5 Aviation**

As RF interferes with the onboard electronics, each reading lamp over each seat can be an access point for internet connectivity for passenger.

## 4 Challenges and Open issue

Great feats have been achieved by the community of researchers in the field of VLC technology as a result of growing interest in this emerging technology that promises to revolutionize communication. However, some of issues that needed to be addressed for commercialization of this technology are discussed in this section.

### 4.1 Modulation bandwidth of LED

One of the most critical limitations to achieving higher throughput in VLC is the LED modulation bandwidth. The modulation bandwidth of the commercial LED is limited to 2 MHz. The primary challenge is to increase the modulation bandwidth of commercial phosphorescent white LED, and then a very high throughput is the direct consequence. There will neither be need for equalization of transmitter/receiver response [23] nor the use of a blue filter to remove the phosphor slow response, to increase the bandwidth [24].

### 4.2 LED non linearity

The LED introduces non linearity distortion to the VLC system especially when OFDM modulation scheme is used. DC biasing current and OFDM signal power to modulate the LED intensity must be carefully chosen in order to control the LED nonlinearity induced distortion. However, in order to achieve non negativity in the optical signal, relatively high Peak-to-average-power is required and this consequently leads to Non linearity distortion as discussed under section 2.4 in [25], the authors, proposed a technique for mitigating non linearity under average power constrain.

### 4.3 Dimming

In VLC, it is desired to maintain the communication link when a user mistakenly turn off or dim the light or the light is switch in the day as may be the case, communication link will disappear, because the VLC requires that light source is remains on [26]. Dimming support is one of the main challenges for VLC. There is need for more research about the dimming of the LED.

### 4.4 Up Link Data

VLC is naturally suited for broadcast application. Several ways have been suggested in the literature and/or experimented to create a bi-directional connection. Mainly, the techniques suggested in [26] try to isolate the uplink and downlink in wavelength, wavelength division Duplex (WDD) using infrared IR as the uplink, or in time, time division duplex (TDD) and also by spatial or optical isolation .Employing RF signal for the uplink is another choice proposed in [27].This area requires further study.

## 5 Conclusion

This work has provided a brief overview of the VLC with some great accomplishment that has been recorded both experimentally and in demonstration. Basic VLC transmission and reception was explained, potential application areas and the open research issues were also outlined. Indeed, VLC is very promising but there are some areas that still require more research work in order to commercialize the technology.

## Reference

1. Electromagnetic spectrum, [https://en.wikipedia.org/wiki/Visible\\_light\\_communication](https://en.wikipedia.org/wiki/Visible_light_communication).
2. Sevincer, A., Bhattacharai, A., Bilgi, M., Yuksel, M., Pala, N.: LIGHTNETs: Smart LIGHTing and Mobile Optical Wireless NETworks #x2014; A Survey. *Commun. Surv. Tutorials, IEEE*. 15, 1620–1641 (2013).
3. Jovicic, A., Li, J., Richardson, T.: Visible light communication: opportunities, challenges and the path to market. *Commun. Mag. IEEE*. 51, 26–32 (2013).
4. Gfeller, F.R., Bapst, U.: Wireless in-house data communication via diffuse infrared radiation. *Proc. IEEE*. 67, 1474–1486 (1979).
5. Visible light communication consortium, <http://www.vlcc.net>.
6. Kavehrad, M., Amirshahi, P.: Hybrid MV-LV Power lines and white light emitting diodes for triple-play broadband access communications. *IEC Compr. Rep. Achiev. Triple Play Technol. Bus. Model. Success.* 167–178 (2006).
7. Home Gigabit Access, <http://www.ict-omega.eu/>.
8. OMEGA News, [http://www.ict-omega.eu/fileadmin/documents/newsletter/Omega\\_News\\_008\\_March\\_2011.pdf](http://www.ict-omega.eu/fileadmin/documents/newsletter/Omega_News_008_March_2011.pdf).
9. Vucic, J., Kottke, C., Nerrerter, S., Langer, K.-D., Walewski, J.W.: 513 Mbit/s Visible Light Communications Link Based on DMT-Modulation of a White LED. *Light. Technol. J.* 28, 3512–3518 (2010).
10. Global TED talk, [http://www.ted.com/talks/harald\\_haas\\_wireless\\_data\\_from\\_every\\_light\\_bulb](http://www.ted.com/talks/harald_haas_wireless_data_from_every_light_bulb).
11. Carrefour guides shoppers to in-store discounts via the ceiling lights, <http://luxreview.com/article/2015/05/carrefour-guides-shoppers-to-in-store-discounts-via-the-ceiling-lights>.
12. KULLER, R., LAIKE, T.: The impact of flicker from fluorescent lighting on well-being, performance and physiological arousal. *Ergonomics*. 41, 433–447 (1998).
13. Karunatilaka, D., Zafar, F., Kalavally, V., Parthiban, R.: LED Based Indoor Visible Light Communications: State of the Art. *Commun. Surv. Tutorials, IEEE*. 17, 1649–1678 (2015).
14. Kahn, J.M., Barry, J.R.: Wireless infrared communications. *Proc. IEEE*. 85, 265–298 (1997).
15. Hranilovic, S.: *Wireless Optical Communication Systems*. Springer New York (2006).
16. Elgala, H., Mesleh, R., Haas, H., Principe, B.: OFDM Visible Light Wireless Communication Based on White LEDs. In: *Vehicular Technology Conference, 2007. VTC2007-Spring. IEEE 65th*. pp. 2185–2189 (2007).
17. Tsonev, D., Sinanovic, S., Haas, H.: Novel Unipolar Orthogonal Frequency Division Multiplexing (U-OFDM) for Optical Wireless. In: *Vehicular Technology Conference (VTC Spring), 2012 IEEE 75th*. pp. 1–5 (2012).

18. Armstrong, J., Schmidt, B., Kalra, D., Suraweera, H.A., Lowery, A.J.: SPC07-4: Performance of Asymmetrically Clipped Optical OFDM in AWGN for an Intensity Modulated Direct Detection System. In: Global Telecommunications Conference, 2006. GLOBECOM '06. IEEE. pp. 1–5 (2006).
19. Mesleh, R., Elgala, H., Haas, H.: LED nonlinearity mitigation techniques in optical wireless OFDM communication systems. *Opt. Commun. Networking, IEEE/OSA J.* 4, 865–875 (2012).
20. Armstrong, J., Schmidt, B.: Comparison of Asymmetrically Clipped Optical OFDM and DC-Biased Optical OFDM in AWGN. *Commun. Lett. IEEE.* 12, 343–345 (2008).
21. Das, A.K., Ghosh, A., Vibin, A.M., Prince, S.: Underwater communication system for deep sea divers using visible light. In: Photonics Global Conference (PGC), 2012. pp. 1–3 (2012).
22. Gutierrez, J.F., Hunt, C.E., Quintero, J.M.: Visible Light Communication LED based Luminaire for General Lighting : State of Art. XII Conf. Panam. Iluminacao -Lux Am. 163–170 (2014).
23. Grubor, J., Randel, S., Langer, K.-D., Walewski, J.: Bandwidth-efficient indoor optical wireless communications with white light-emitting diodes. In: Communication Systems, Networks and Digital Signal Processing, 2008. CNSDSP 2008. 6th International Symposium on. pp. 165–169 (2008).
24. Popoola, W.O., Ogunkoya, F.B., Sinanovic, S.: Mitigating nonlinearities under average power constraint in visible light communication. In: Wireless Communications and Mobile Computing Conference (IWCMC), 2014 International. pp. 815–820 (2014).
25. Bhalerao, M. V, Sonavane, S.S., Kumar, V.: A Survey of Wireless Communication using Visible Light. *Int. J. Adv. Eng. Technol.* 5, 188–197 (2013).
26. IEEE 802.15 WPAN Visible Light Communication Interest Group (IGvlc), <http://www.ieee802.org/15/pub/IGvlc.html>.
27. Hou, J., O'brien, D.: Vertical handover-decision-making algorithm using fuzzy logic for the integrated Radio-and-OW system. *Wirel. Commun. IEEE Trans.* 5, 176–185 (2006).



## Reconstruction Algorithms in Compressive Sensing: An Overview

André Luiz Pilastrini<sup>1,3</sup> and João Manuel R. S. Tavares<sup>1,2</sup>

<sup>1</sup> Faculty of Engineering - University of Porto,

Rua Dr. Roberto Frias s/n, 4200-465 Porto, PORTUGAL

<sup>2</sup> LAETA-Laboratório Associado de Energia, Transporte e Aeronáutica (FEUP),

<sup>3</sup> PIXEL Research Group - UNEMAT/BRAZIL,

{andre.pilastrini,tavares}@fe.up.pt

<http://goo.gl/tcg6S7>

**Abstract.** The theory Compressive Sensing (CS) has provided a new acquisition strategy and recovery with good in the image processing area. This theory guarantees to recover a signal with high probability from a reduced sampling rate below the Nyquist-Shannon limit. The problem of recovering the original signal from the samples consists in solving an optimization problem. This article presents an overview of reconstruction algorithms for sparse signal recovery in CS, these algorithms may be broadly divided into six types. We have provided a comprehensive survey of the numerous reconstruction algorithms in CS aiming to achieve computational efficiency.

**Keywords:** compressive sensing · reconstruction algorithms · signal recovery · image processing · sampling theorem

### 1 Introduction

In recent years, Compressive Sensing (CS) has attracted considerable attention in areas of applied mathematics, computer science, and electrical engineering by suggesting that it may be possible to surpass the traditional limits of sampling theory. CS is the theory of reconstructing large dimensional signals from a small number of measurements by taking advantage of the signal sparsity. CS builds upon the fundamental fact that we can represent many signals using only a few non-zero coefficients in a suitable basis or dictionary. CS has been widely used and implemented in many applications including computed tomography [9], wireless communication [40], image processing [8] and camera design [20].

Conventional approaches to sampling images use Shannon theorem, which requires signals to be sampled at a rate twice the maximum frequency. This criterion leads to larger storage and bandwidth requirements. Compressive Sensing (CS) is a novel sampling technique that removes the bottleneck imposed by Shannon's theorem. This theory utilizes sparsity present in the images to recover it from fewer observations than the traditional methods. It joins the sampling and

compression steps and enables to reconstruct with the only fewer number of observations.

This property of compressive Sensing provides evident advantages over Nyquist-Shannon theorem. The image reconstruction algorithms with CS increase the efficiency of the overall algorithm in reconstructing the sparse signal. There are various algorithms available for recovery as shown in section 3.

## 2 Historical Background

In the area of engineering the sampling theorem of Nyquist-Shannon has a tremendous role e it can be used frequently only for band-limited signals otherwise it requires larger storage space and measurements for high-dimensional signals [33]. However, practically reconstruction is even possible with fewer measurements and compression is also needed before storage [3]. These requirements can be fulfilled with CS. The field of CS has gained enormous interest recently. It is basically developed by D. Donoho, E. Candes, Justin Romberg and T. Tao [1,11].

In the framework of CS, the signals probed are firstly assumed to be sparse or compressible in some basis [1,10,12,31,43]. Consider a complex-valued signal  $x$  which itself may or may not be sparse in the canonical basis but is sparse or approximately sparse in an appropriate basis  $\Psi$ . That is,

$$x = \Psi\theta. \quad (1)$$

where  $\Theta$  is sparse or approximately sparse. A central idea of the CS theory is about how a signal is acquired: the acquisition of signal  $x$  of length  $n$  is carried out by measunring  $m$  projections of  $x$  onto sensing vectors  $\{\varphi_i^T, i = 1, 2, \dots, m\}$  :  $y_i = \varphi_i^T x$  for  $i = 1, 2, \dots, m$ . For sensing efficiency, we wish to collect a relatively much smaller number of measurements, that is, one requires that  $m$  be considerably smaller than  $n$  ( $m \ll n$ ), hence the name CS. This data acquisition mechanism is at the core of a CS system that marks a fundamental departure from the conventional data acquisition compression transmission decompression framework: the conventional framework collects a vast amount of data for acquiring a high-resolution signal, then essentially discard most of the data collected (in the  $\Psi$ domain) in the compression stage, while in CS the data is measured in a compressed manner, and the much reduced amount of measurements are transmitted or stored economically, and every bit of the measurements are then utilized to recover the signal using reconstruction algorithms. The data acquisition process in CS framework is described by

$$y = \Phi x. \quad (2)$$

According to Eq.(1) and Eq.(2) can be written as  $y = \Phi\Psi\theta$  (the size of the sparsifying basis or sparse matrix  $\Psi$  is  $n \times n$ ). The figure1 illustrates the relationship between the variables. Typically with ( $m < n$ ), the inverse problem

is ill-posed [29]. However, the sparest solution of Eq.(2) can be obtained by solving the constrained optimization problem

$$\text{minimize} = \|\Theta\|_0; \text{subject to : } \Phi\Psi\Theta = y. \quad (3)$$

where  $\|\Theta\|_0$  is the  $l_0$  norm defined as  $\|\Theta\|_0 = \sum_{i=1}^n |\Theta_i|^0 = \text{number of nonzero components in } \Theta$ .

Unfortunately, it turns out that Eq.(3) is a problem of combinatorial complexity: finding solution of Eq.(3) requires enumerating subsets of the dictionary to identify the smallest subset that can represent signal  $x$ , the complexity of such a subset search grows exponentially with the signal size  $n$  [10]. A key result in the CS theory is that if  $x$  is  $r$ -sparse, the waveforms in  $\{\varphi_i^T, i = 1, 2, \dots, m\}$  are independent and identically distributed random waveforms, and the number of measurements,  $m$ , satisfies the condition:

$$m \geq c \cdot r \cdot \log(n/r), \quad (4)$$

where  $c$  is a small positive constant, then signal  $x$  can be reconstructed by solving the convex problem

$$\text{minimize} = \|\Theta\|_1; \text{subject to : } \Phi\Psi\Theta = y, \quad (5)$$

where  $\|\Theta\|_1 = \sum_{i=1}^n |x_i|$  [1].

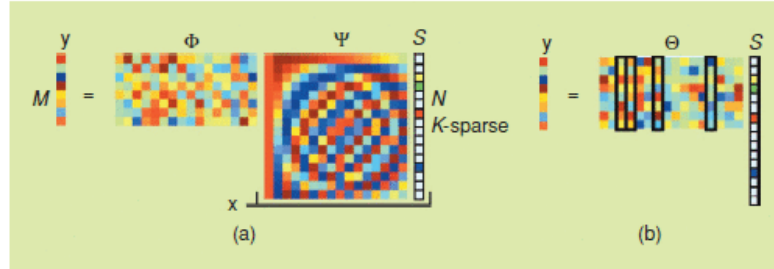


**Fig. 1.** (a) Compressive sensing measurement process with a random Gaussian measurement matrix  $\Phi$  and discrete cosine transform (DCT) matrix  $\Psi$ . The vector of coefficients  $s$  is sparse with  $K=4$ . (b) Measurement process with  $\Theta = \Phi\Psi$ . There are four columns that correspond to nonzero  $s_i$  coefficients, the measurement vector  $y$  is linear combination of these columns [1].

### 3 Reconstruction Algorithms

CS comprises a collection of methods of representing a signal on the basis of a limited number of measurements and then recovering the signal from these

measurements [35]. The problem of how to effectively recover the original signal from the compressed data plays a significant role in the CS framework. Currently, there exists several reconstruction algorithms which are defined either in the context of convex optimization, or greedy approaches, among them we can mention [1,6,10,12,35,37,42].

To present an overview of reconstruction algorithms for sparse signal recovery in compressive sensing, these algorithms may be broadly divided into six types as shown in Fig.2.

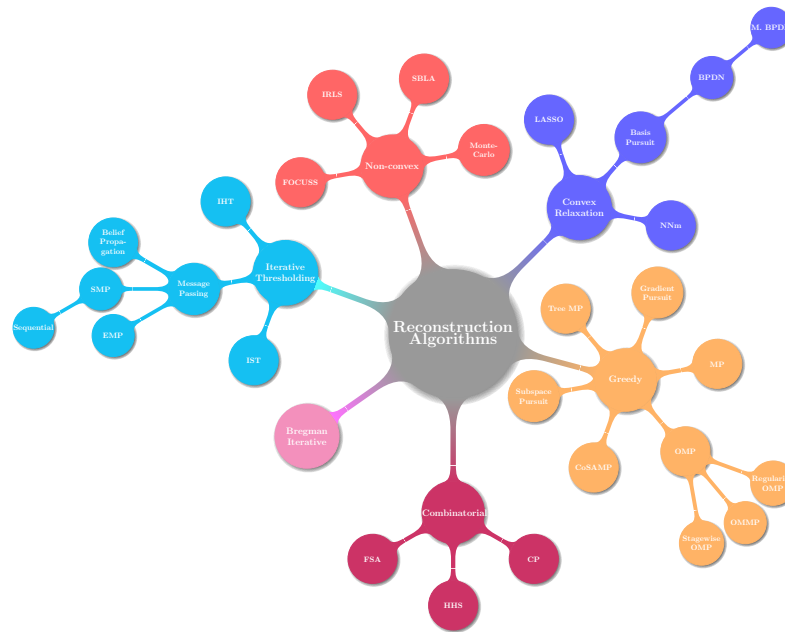


**Fig. 2.** Compressive Sensing: Reconstruction Algorithms and their Classification adapted from [37].

### 3.1 Convex Relaxation

With the development of fast methods of Linear Programming in the eighties, the idea of convex relaxation became truly promising. It was put forward most enthusiastically and successfully by Donoho and his collaborators since the late eighties [35,39].

This class algorithms solve a convex optimization problem through linear programming [12] to obtain reconstruction. The number of measurements required for exact reconstruction is small but methods are computationally com-

plex. *Basis Pursuit* [14], *Basis Pursuit De-Noising* (BPDN) [14], *Least Absolute Shrinkage and Selection Operator* (LASSO) [41] e *Least Angle Regression* (LARS) [21] are some examples of such algorithms. *Basis Pursuit* is a principle for decomposing a signal into an "optimal" superposition of dictionary elements, where optimal means having the smallest  $l_1$  norm of coefficients among all such decompositions.

*Basis Pursuit* has interesting relations to ideas in areas as diverse as ill-posed problems, abstract harmonic analysis, total variation denoising, and multiscale edge denoising. *Basis Pursuit* in highly overcomplete dictionaries leads to large-scale optimization problems. Such problems can be attacked successfully only because of recent advances in linear and quadratic programming by interior-point methods.

In the paper [41] *Lasso* ( $l_1$ ) penalties are useful for fitting a wide variety of models. Newly developed computational algorithms allow application of these models to large data sets, exploiting sparsity for both statistical and computation gains. Interesting work on the lasso is being carried out in many fields, including statistics, engineering, mathematics and computer science. Recent works show matrix versions of signal recovery called  $\|M\|_1$  Nuclear Norm minimization [38]. Instead of reconstructing  $x$  from  $\Theta x$ , Nuclear Norm minimization tries to recover a low rank matrix  $M$  from  $\Theta x$ . Since rank determines the order, dimension and complexity of the system, low rank matrices correspond to low order statistical models.

### 3.2 Non Convex Minimization Algorithms

Many practical problems of importance are non-convex, and most non-convex problems are hard (if not impossible) to solve exactly in a reasonable time. Hence the idea of using heuristic algorithms, which may or may not produce desired solutions.

In alternate minimization techniques, the optimization is carried out with some variables are held fixed in cyclical fashion and linearization techniques, in which the objectives and constraints are linearized (or approximated by a convex function). Other techniques include search algorithms (such as genetic algorithms), which rely on simple solution update rules to progress. There are many algorithm proposed in literature that use this technique like Focal Underdetermined System Solution (FOCUSS) [34], Iterative Re-weighted Least Squares [13], Sparse Bayesian Learning algorithms [44], Monte-Carlo based algorithms [27]. Non-convex optimization is mostly utilized in medical imaging tomography, network state inference, streaming data reduction.

### 3.3 Greedy Iterative Algorithm

Due to the fast reconstruction and low complexity of mathematical framework, a family of iterative greedy algorithms has been widely used in compressive sensing recently [19]. This class algorithms solve the reconstruction problem by finding the answer, step by step, in an iterative fashion.

The fast and accurate reconstruction algorithms has been the focus of the study of CS, they will be the key technologies for the application of CS. At present, the most important greedy algorithms include matching pursuit and gradient pursuit [18,19].

The idea is to select columns of  $\Theta$  in a greedy fashion. At each iteration, the column of  $\Theta$  that correlates most with  $y$  is selected. Conversely, least square error is minimized in every iteration. Most used greedy algorithms are *Matching Pursuit* [32] and its derivative *Orthogonal Matching Pursuits*(OMP) [42] because of their low implementation cost and high speed of recovery. However, when the signal is not much sparse, recovery becomes costly. For such situations, improved versions of (OMP) have been devised like *Regularized OMP* [36], *Stagewise OMP* [18], *Compressive Sampling Matching Pursuits*(CoSaMP) [35], *Subspace Pursuits* [15], *Gradient Pursuits* [22] and *Orthogonal Multiple Matching Pursuit* [30].

### 3.4 Combinatorial / Sublinear Algorithms

This class of algorithms recovers sparse signal through group testing. They are extremely fast and efficient, as compared to convex relaxation or greedy algorithms but require specific pattern in the measurements,  $\Phi$  needs to be sparse. Representative algorithms are Fourier Sampling Algorithm [24], Chaining Pursuit proper is an iterative algorithm [25], Heavy Hitters on Steroids (HHS) [26].

### 3.5 Iterative Thresholding Algorithms

Iterative approaches to CS recovery problem are faster than the convex optimization problems. For this class of algorithms, correct measurements are recovered by soft or hard thresholding [7], [16] starting from noisy measurements given the signal is sparse. The thresholding function depends upon number iterations and problem setup at hand.

The Iterative Hard Thresholding (IHT) algorithm for the first time was suggested by Blumensath and Davies for recovery in compressed Sensing scenario [7]. This algorithm can offer the theoretical guarantee with its implementation which can be shown in the particular one [23]. The basic idea of IHT is to chase a good candidate for the estimate of support set which fits the measurement. The IHT algorithm is an algorithm with a simple implementation.

*Message Passing*(MP) algorithms [17] are an important modification of iterative thresholding algorithms in which basic variables (messages) are associated with directed graph edges. A relevant graph in case of Compressive Sensing is the bipartite graph with  $n$  nodes on one side (variable nodes) and  $m$  nodes on the other side (the measurement nodes). This distributed approach has many advantages like low computational complexity and easy implementation in parallel or distributed manner. *Expander Matching Pursuits* [28], *Sparse Matching Pursuits* [5] and *Sequential Sparse Matching Pursuits* [4] are recently proposed algorithms in this domain that achieve near-linear recovery time while using  $O(s \log(n/s))$  measurements only. Recently, proposed algorithm of Belief Propagation also falls in this category [2].

### 3.6 Bregman Iterative Algorithms

Bregman method is an iterative algorithm to solve certain convex optimization problems. These algorithms provide a simple and efficient way of solving  $l_1$  minimization problem. [45] presents a new idea which gives exact solution of constrained problems by iteratively solving a sequence of unconstrained subproblems generated by a Bregman iterative regularization scheme. When applied to CS problems, the iterative approach using Bregman distance regularization achieves reconstruction in four to six iterations [45]. The computational speed of these algorithms are particularly appealing compared to that available with other existing algorithms. There are various algorithms available for recovery.

In the Table 1, we have listed some reconstruction algorithms complexity measures for Compressive Sensing.

**Table 1.** Complexity and Minimum Measurement requirement of Compressive Sensing Reconstruction Algorithms.

Algorithm	Complexity	Minimum Measurement
Basis Pursuit [14], [15]	$O(n^3)$	$O(s \log n)$
OMP [15], [36], [42]	$O(s m n)$	$O(s \log n)$
StOMP [18]	$O(n \log n)$	$O(n \log n)$
ROMP [35], [36]	$O(s m n)$	$O(s \log^2 n)$
CoSAMP [36]	$O(m n)$	$O(s \log n)$
Subspace Pursuits [15]	$O(s m n)$	$O(s \log (n/s))$
EMP [28]	$O(s \log (n/s))$	$O(s \log (n/s))$
SMP [5]	$O(s \log (n/s) \log R)$	$O(s \log (n/s))$
Belief Propagation [2]	$O(n \log^2 n)$	$O(s \log n)$
Chaining Pursuits [25]	$O(s \log^2 n \log^2 s)$	$O(s \log^2 n)$
HHS [26]	$O(s \text{polylog}(n))$	$O(\text{poly}(s, \log n))$

In paper [15] and [18], Basis Pursuit can reliably recover signals with  $n = 256$  and sparsity level up to 35, from only 128 measurements. The reconstruction algorithms OMP and ROMP can only be reliable up to sparsity level of 19 for same  $n$  and  $m$ . The performance of Basis Pursuit appears promising as compared to OMP derivatives from minimum measurements perspective.

## 4 Conclusion

Broadly speaking, the theory of Compressive Sensing sub-sample consists of a signal and then use a reconstruction algorithm based on optimization to rebuild it. This property of compressive Sensing provides evident advantages over Nyquist-Shannon theorem. The image reconstruction algorithms with CS increase the efficiency of the overall algorithm in reconstructing the sparse signal.

During the review process did the survey and identify six types of reconstruction algorithms classes. In this article, we have provided a comprehensive survey of the numerous reconstruction algorithms discusses the origin, purpose, scope and implementation of CS in image reconstruction and compares their complexity.

## 5 Acknowledgments

The author gratefully acknowledges "Conselho Nacional de Desenvolvimento Científico e Tecnologia - CNPq" for the scholarship provided during this research.

## References

1. Baraniuk, R.: Compressive Sensing [Lecture Notes]. IEEE Signal Processing Magazine 24(4), 118–121 (jul 2007), [http://ieeexplore.ieee.org/xpls/abs\\_all.jsp?arnumber=4286571&tag=1](http://ieeexplore.ieee.org/xpls/abs_all.jsp?arnumber=4286571&tag=1)
2. Baron, D., Sarvotham, S., Baraniuk, R.G.: Bayesian compressive sensing via belief propagation. IEEE Transactions on Signal Processing 58(1), 269–280 (2010), [http://ieeexplore.ieee.org/xpls/abs\\_all.jsp?arnumber=5169989](http://ieeexplore.ieee.org/xpls/abs_all.jsp?arnumber=5169989)
3. Bayar, B., Bouaynaya, N., Shterenberg, R.: Kernel reconstruction: An exact greedy algorithm for compressive sensing. In: 2014 IEEE Global Conference on Signal and Information Processing (GlobalSIP). pp. 1390–1393. IEEE (dec 2014), <http://ieeexplore.ieee.org/lpdocs/epic03/wrapper.htm?arnumber=7032355>
4. Berinde, R., Indyk, P.: Sequential sparse matching pursuit. In: 2009 47th Annual Allerton Conference on Communication, Control, and Computing, Allerton 2009. pp. 36–43. IEEE, Monticello, IL (2009), <http://ieeexplore.ieee.org/xpl/articleDetails.jsp?arnumber=5394834&tag=1>
5. Berinde, R., Indyk, P., Ruzić, M.: Practical near-optimal sparse recovery in the L1 norm. In: 46th Annual Allerton Conference on Communication, Control, and Computing. pp. 198–205. IEEE (2008), [http://ieeexplore.ieee.org/xpls/abs\\_all.jsp?arnumber=4797556](http://ieeexplore.ieee.org/xpls/abs_all.jsp?arnumber=4797556)
6. Blumensath, T., Davies, M.E.: Iterative Hard Thresholding for Compressed Sensing. Applied and Computational Harmonic Analysis 27(3), 265–274 (may 2008), <http://arxiv.org/abs/0805.0510>
7. Blumensath, T., Davies, M.E.: Iterative hard thresholding for compressed sensing. Applied and Computational Harmonic Analysis 27(3), 265–274 (nov 2009), <http://www.sciencedirect.com/science/article/pii/S1063520309000384>
8. Bobin, J., Starck, J.L., Ottensamer, R.: Compressed Sensing in Astronomy (feb 2008), <http://dx.doi.org/10.1109/JSTSP.2008.2005337>
9. Candès, E., Romberg, J., Tao, T.: Robust uncertainty principles: exact signal reconstruction from highly incomplete frequency information. IEEE Transactions on Information Theory 52(2), 489–509 (feb 2006), <http://ieeexplore.ieee.org/lpdocs/epic03/wrapper.htm?arnumber=1580791>
10. Candès, E., Romberg, J.: L1-magic: Recovery of Sparse Signals via Convex Programming (2005), <http://citeseerx.ist.psu.edu/viewdoc/summary?doi=10.1.1.212.9120>
11. Candes, E., Tao, T.: Near Optimal Signal Recovery From Random Projections: Universal Encoding Strategies? (oct 2004), <http://arxiv.org/abs/math/0410542>

12. Candès, E.J., Recht, B.: Exact matrix completion via convex optimization. *Foundations of Computational Mathematics* 9(6), 717–772 (2009), <http://link.springer.com/article/10.1007/s10208-009-9045-5>
13. Chartrand, R., Yin, W.: Iteratively reweighted algorithms for compressive sensing. In: ICASSP, IEEE International Conference on Acoustics, Speech and Signal Processing - Proceedings. pp. 3869–3872. Acoustics, Speech and Signal Processing, 2008. ICASSP 2008. IEEE International Conference on, Las Vegas, NV (2008), [http://ieeexplore.ieee.org/xpls/abs\\_all.jsp?arnumber=4518498](http://ieeexplore.ieee.org/xpls/abs_all.jsp?arnumber=4518498)
14. Chen, S.S., Donoho, D.L., Saunders, M.A.: Atomic Decomposition by Basis Pursuit. *SIAM Rev.* 43(1), 129–159 (2001), <http://dx.doi.org/10.1137/S003614450037906X>
15. Dai, W., Milenkovic, O.: Subspace pursuit for compressive sensing signal reconstruction. *IEEE Transactions on Information Theory* 55(5), 2230–2249 (2009), <http://ieeexplore.ieee.org/stamp/stamp.jsp?arnumber=4839056>
16. Donoho, D.L.: De-noising by soft-thresholding. *IEEE Transactions on Information Theory* 41(3), 613–627 (1995), <http://ieeexplore.ieee.org/xpl/articleDetails.jsp?arnumber=382009&newsearch=true&queryText=10.1109%2F18.382009>
17. Donoho, D.L., Maleki, A., Montanari, A.: Message Passing Algorithms for Compressed Sensing p. 6 (2009), <http://arxiv.org/abs/0907.3574>
18. Donoho, D.L., Tsaig, Y., Drori, I., Starck, J.L.: Sparse solution of underdetermined systems of linear equations by stagewise orthogonal matching pursuit. *IEEE Transactions on Information Theory* 58(2), 1094–1121 (2012), <http://citesear.ist.psu.edu/viewdoc/summary?doi=10.1.1.115.5221>
19. Du, L., Wang, R., Wan, W., Yu, X.Q., Yu, S.: Analysis on greedy reconstruction algorithms based on compressed sensing. In: 2012 International Conference on Audio, Language and Image Processing. pp. 783–789. IEEE (jul 2012), <http://ieeexplore.ieee.org/lpdocs/epic03/wrapper.htm?arnumber=6376720>
20. Duarte, M., Davenport, M., Takhar, D., Laska, J., Ting Sun, Kelly, K., Baraniuk, R.: Single-Pixel Imaging via Compressive Sampling. *IEEE Signal Processing Magazine* 25(2), 83–91 (mar 2008), <http://ieeexplore.ieee.org/lpdocs/epic03/wrapper.htm?arnumber=4472247>
21. Efron, B., Hastie, T., Johnstone, I., Tibshirani, R., Ishwaran, H., Knight, K., Loubes, J.M., Massart, P., Madigan, D., Ridgeway, G., Rosset, S., Zhu, J.I., Stine, R.a., Turlach, B.a., Weisberg, S., Hastie, T., Johnstone, I., Tibshirani, R.: Least angle regression. *Annals of Statistics* 32(2), 407–499 (2004), <http://arxiv.org/pdf/math/0406456v2.pdf>
22. Figueiredo, M.A.T., Nowak, R.D., Wright, S.J.: Gradient projection for sparse reconstruction: Application to compressed sensing and other inverse problems. *IEEE Journal on Selected Topics in Signal Processing* 1(4), 586–597 (2007), [http://ieeexplore.ieee.org/xpls/abs\\_all.jsp?arnumber=4407762](http://ieeexplore.ieee.org/xpls/abs_all.jsp?arnumber=4407762)
23. Foucart, S.: Sparse Recovery Algorithms: Sufficient Conditions in Terms of Restricted Isometry Constants. In: Approximation Theory XIII: San Antonio 2010, pp. 65–77. Springer New York (2012), [http://link.springer.com/10.1007/978-1-4614-0772-0\\_5](http://link.springer.com/10.1007/978-1-4614-0772-0_5)
24. Gilbert, A.C., Muthukrishnan, S., Strauss, M.: Improved time bounds for near-optimal sparse Fourier representations. In: Papadakis, M., Laine, A.F., Unser, M.A. (eds.) *Proceedings of SPIE*. vol. 5914, pp. 59141A–59141A–15. Proc. SPIE

- Wavelets XI (aug 2005), <http://citeseerx.ist.psu.edu/viewdoc/summary?doi=10.1.1.2.7187>
25. Gilbert, A.C., Strauss, M.J., Tropp, J.A., Vershynin, R.: Algorithmic linear dimension reduction in the L<sub>1</sub> norm for sparse vectors. In: 44th Annual Allerton Conference on Communication, Control, and Computing. Allerton 2006 (2006), <http://arxiv.org/pdf/cs/0608079v1.pdf><http://arxiv.org/abs/cs/0608079>
  26. Gilbert, A.C., Strauss, M.J., Tropp, J.A., Vershynin, R.: One sketch for all: fast algorithms for compressed sensing. Proceedings of the thirty-ninth annual ACM symposium on Theory of computing - STOC '07 pp. 237–246 (2007), <http://portal.acm.org/citation.cfm?doid=1250790.1250824><http://dl.acm.org/citation.cfm?id=1250824>
  27. Godsill, S.J., Cemgil, A.T., Févotte, C., Wolfe, P.J.: Bayesian computational methods for sparse audio and music processing. In: European Signal Processing Conference. pp. 345–349 (2007), <http://citeseerx.ist.psu.edu/viewdoc/summary?doi=10.1.1.330.5395>
  28. Indyk, P., Ružić, M.: Near-Optimal Sparse Recovery in the L<sub>1</sub> Norm. pp. 199–207 (2008), [http://ieeexplore.ieee.org/xpls/abs\\_all.jsp?arnumber=4690954](http://ieeexplore.ieee.org/xpls/abs_all.jsp?arnumber=4690954)
  29. Jalali, S., Maleki, A., Baraniuk, R.: Minimum Complexity Pursuit for Universal Compressed Sensing <http://arxiv.org/abs/1208.5814>
  30. Liu, E., Temlyakov, V.N.: The orthogonal super greedy algorithm and applications in compressed sensing. IEEE Transactions on Information Theory 58(4), 2040–2047 (2012), [http://ieeexplore.ieee.org/xpls/abs\\_all.jsp?arnumber=6092487](http://ieeexplore.ieee.org/xpls/abs_all.jsp?arnumber=6092487)
  31. Lustig, M., Donoho, D.L., Santos, J.M., Pauly, J.M.: Compressed Sensing MRI (2008)
  32. Mallat, S.G., Zhang, Z.: Matching pursuits with time-frequency dictionaries. IEEE Transactions on Signal Processing 41(12), 3397–3415 (1993), [http://ieeexplore.ieee.org/xpl/freeabs\\_all.jsp?arnumber=258082&abstractAccess=no&userType=inst](http://ieeexplore.ieee.org/xpl/freeabs_all.jsp?arnumber=258082&abstractAccess=no&userType=inst)
  33. Meenakshi, Budhiraja, S.: A Survey of Compressive Sensing Based Greedy Pursuit Reconstruction Algorithms. International Journal of Image, Graphics and Signal Processing 7(10), 1–10 (sep 2015), <http://www.mecs-press.org/ijigsp/ijigsp-v7-n10/v7n10-1.html>
  34. Murray, J., Kreutz-Delgado, K.: An improved FOCUSS-based learning algorithm for solving sparse linear inverse problems. Conference Record of Thirty-Fifth Asilomar Conference on Signals, Systems and Computers (Cat.No.01CH37256) 1, 347 – 351 (2001), <http://ieeexplore.ieee.org/xpl/articleDetails.jsp?arnumber=986949&abstractAccess=no&userType=inst>
  35. Needell, D., Tropp, J.A.: CoSaMP: Iterative signal recovery from incomplete and inaccurate samples. Applied and Computational Harmonic Analysis 26(3), 301–321 (may 2009), <http://www.sciencedirect.com/science/article/pii/S1063520308000638>
  36. Needell, D., Vershynin, R.: Uniform uncertainty principle and signal recovery via regularized orthogonal matching pursuit. Foundations of Computational Mathematics 9(3), 317–334 (2009)
  37. Qaisar, S., Bilal, R.M., Iqbal, W., Naureen, M., Lee, S.: Compressive sensing: From theory to applications, a survey. Journal of Communications and Networks 15(5), 443–456 (oct 2013), <http://ieeexplore.ieee.org/xpl/articleDetails.jsp?arnumber=6674179>
  38. Recht, B., Fazel, M., Parrilo, P.A.: Guaranteed Minimum-Rank Solutions of Linear Matrix Equations via Nuclear Norm Minimization. Society for Industrial and Applied Mathematics 52(3), 471–501 (2007), <http://arxiv.org/abs/0706.4138>

39. Rudelson, M., Vershynin, R.: Sparse reconstruction by convex relaxation: Fourier and Gaussian measurements (feb 2006), <http://arxiv.org/pdf/math/0602559.pdf>
40. Tauboeck, G., Hlawatsch, F., Eiwen, D., Rauhut, H.: Compressive estimation of doubly selective channels in multicarrier systems: Leakage effects and sparsity-enhancing processing <http://arxiv.org/abs/0903.2774>
41. Tibshirani, R.: Regression Shrinkage and Selection Via the Lasso. Journal of the Royal Statistical Society, Series B 58, 267—288 (1996), <http://statweb.stanford.edu/~tibs/ftp/lasso-retro.pdf>
42. Tropp, J.A., Gilbert, A.C.: Signal Recovery From Random Measurements Via Orthogonal Matching Pursuit. IEEE Transactions on Information Theory 53(12), 4655–4666 (dec 2007), <http://ieeexplore.ieee.org/lpdocs/epic03/wrapper.htm?arnumber=4385788>
43. Wang, L., Lu, K., Liu, P., Ranjan, R., Chen, L.: IK-SVD: Dictionary Learning for Spatial Big Data via Incremental Atom Update (2014)
44. Wipf, D.P., Rao, B.D.: Sparse Bayesian learning for basis selection. IEEE Transactions on Signal Processing 52(8), 2153–2164 (2004), [http://ieeexplore.ieee.org/xpl/freeabs\\_all.jsp?arnumber=1315936&abstractAccess=no&userType=inst](http://ieeexplore.ieee.org/xpl/freeabs_all.jsp?arnumber=1315936&abstractAccess=no&userType=inst)
45. Yin, W., Osher, S., Goldfarb, D., Darbon, J.: Bregman Iterative Algorithms for  $\ell_1$ -Minimization with Applications to Compressed Sensing. SIAM Journal on Imaging Sciences 1(1), 143–168 (jan 2008), <http://pubs.siam.org/doi/abs/10.1137/070703983>



## Robot Self-Localization Based on Sensor Fusion of GPS and iBeacons Measurements

Rui Pinto<sup>1</sup>, Filipe Neves dos Santos<sup>1,2</sup>, Armando Sousa<sup>1</sup>

<sup>1</sup> Faculty of Engineering, University of Porto, Porto, Portugal

<sup>2</sup> INESC TEC, Porto, Portugal

rpinto@fe.up.pt, fbsantos@inesctec.pt, asousa@fe.up.pt

**Abstract.** Autonomous robots must be able to navigate on a given unknown environment, which implies awareness of the environment and self-localization. Although the Global Position System (GPS) is widely used for localization, the position provided is not free of deviations, which increases when the environment conditions block the signal. Robots used for crop monitoring and harvesting require robust and accurate localization systems in order to navigate on harsh and challenging environment conditions. This work explored the use of artificial landmarks to increase the accuracy of a robot localization based on GPS data. Distance estimations were done using Received Strength Signal Indicator (RSSI) based approaches. By comparing the Empirical and Analytical models for wave propagation, it's expected to observe a better distance estimation for the Analytical model, because the Empirical one does not consider signal attenuation. Regarding the robot pose estimation, it's expected to be more accurate when fusing the GPS data and the estimated distances, instead of using only the GPS data.

**Keywords:** Outdoor Mobile Robot Localization · SLAM · Sensor Fusion · iBeacons · Wave Propagation · Path Loss Model

### 1 Introduction

Robot navigation is a key problem when developing autonomous robots. In order to be truly autonomous, the robot must be able to navigate freely on an unknown environment. For this to be true, the robot must be aware of the world around him and be capable to self-locate in that environment. Self-awareness and self-localization capabilities rely greatly on environment perceptions, which is possible due to the usage of sensors. These capabilities are challenging, because sensors aren't perfect and noisy sensor data leads to errors on the world representation and in bad position estimations. Moreover, inferring the robot position must be done by integrating sensor data from multiple sensors over time, using sensor fusion techniques [6, 9, 27], since one sensor is usually insufficient to do a good estimation. The problem becomes even more complex if the environment is highly dynamic or if the robot needs to represent a 3D world instead of a 2D.

Nowadays, the American Global Position System (GPS) [7, 11, 12] is widely used for outdoor localization, since the service is globally available, providing a good quality

3D position and the GPS receivers are relatively cheap. This system is limited to outdoor environments due to the signal blockage that occur when the receiver hasn't a clear sight of the satellites. But, even outdoor environments present challenges to the development of robot localization and mapping capabilities using only GPS signal. These may occur due to signal blockage, harsh atmospheric conditions or even tall buildings or mountains that cause multi-path interference, compromising the GPS accuracy and signal availability.

This work intends to improve robot outdoor self-location capabilities, when GPS data is compromised. It's expected to improve robot position estimation, by fusion GPS data and other sensor data, such as Odometry, distance observations to artificial beacons and beacon's mapping, by means of a Particle filter. Regarding the distance observations to the artificial beacons, RSSI methodologies were used to estimate the distances. A comparison between an Empirical and Analytical wave propagation models is performed, which is expected to obtain a better distance estimation using the Analytical model, because the Empirical one does not consider signal attenuation.

The paper is organized in four more sections. Section 2 gives an overview of what mobile robot localization is, describing how GPS works and its main limitations and the top challenges of wave propagation analysis. Section 3 describes the methodology of this work. Session 4 describes the tests performed and results. Session 5 finalizes the paper with conclusions and future work.

## 2 Mobile Robot Localization Strategies

There are no universal best solution regarding localization approaches. Each approach is fitted to a specific environment, such as indoor or outdoor spaces and the conditions in each environment, such as urban areas, forests, underwater, etc. Also, since the localization task depends greatly on sensor data, the sensors used on the robot for localization are chosen accordingly to the specific environment conditions. These sensors can be classified by how the interaction is made with the environment and what is the origin of the sensor data [18].

Known approaches for self-localization, without relying on external components, are the Dead Reckoning systems, which calculates one's current position using a previous known position, such as Odometry and Inertial Measurement Unit (IMU) [2]. These systems are based on the distance, orientation and speed of the robot motion by using accelerometers (motion sensors), gyroscopes (rotation sensors) and encoders connected to the motor or wheels. Accuracy may be compromised in these systems. A small deviation in the beginning will result in a big deviation after some iterations, invalidating the use of these techniques over a large period of time. For this reason, in order to avoid internal state cumulative errors, sensors must also measure the state of the environment.

The world around the robot can be measured using landmarks (both natural and artificial), which consists on specific spots in the worlds with known location. With these approaches, the robot must use sensors to detect the landmark in the environment and calculate its position related to the known position of the landmark, using triangulation and trilateration techniques [5, 15]. Natural landmarks [19], such as walls, doors or

trees can be detected using Light Detection and Ranging (LIDAR) sensors [10, 26] and Radio Detection and Ranging (RADAR) [1]. LIDAR and RADAR use respectively a laser scanner or radio waves to measure the distance to the landmark, calculated by the signal Time of Flight (TOF) [21], i.e., the time duration between signal emission and echo reception. Other wide used sensors are the optical sensors, which are based on vision systems such as RGB-D [29] and monocular/stereo vision algorithms [30].

Artificial landmarks can be passive, such as laser reflectors and computer vision patterns, or active, such as Radio Frequency (RF) beacons, Radio Frequency Identification (RFID) tags and WiFi/cellphone relays. There are several methods [15] to estimate the distance between the robot and a beacon, based on the RF signal time travel between beacon and robot or signal angle of arrival in the robot. Some of these methods are the previously mentioned TOF, Time Difference of Arrival (TDOA) [20] and Angle of Arrival (AOA) [14, 16]. Another method is the RSSI [1, 20, 25], which estimates the distance based on the strength of the RF signal received on the robot. In comparison with other methods, the RSSI method has the advantage of no extra hardware is required, other than a simple RF antenna. The disadvantage is the lower precision of measurements when signal noise and interference exist.

All the previous solutions are suitable (but not limited) to use on indoor environments, since first, there are controlled conditions regarding indoor environments and, second, on outdoor environments Global Navigation Satellite Systems (GNSS) [11] are widely used, in particular the GPS.

## 2.1 Global Position System

The GPS [7, 11, 12] was the first and still by far the most commonly used advanced satellite navigation system in the world. GPS is globally fully operational and it's assured to be free of cost to all users. The tremendous growth of GPS is driven by the enormous number of applications of this system, which are far beyond what was originally designed to be strictly U.S. military system. GPS is widely used on aviation, marine, space and vehicle navigation, mapping, locating and tracking of objects and people, for medical purposes and disaster management.

**Restrictions.** If the distance between the satellites and the receiver is known, together with the speed of light, the receivers can determine its location. The speed of light is approximately 300000 Km/s in vacuum, but the signal has to propagate through Earth's atmosphere, ionosphere and troposphere, which bend and slow the signal, causing position errors on the ground by making the satellites appear farther than they are. Although being the largest source of error, several other factors affect the accuracy of the GPS, such as accuracy of satellite and receiver clocks, position error on the satellites, atmospheric errors, multi-path interference in the signal and receiver internal errors (when computing the location).

**GPS Alternatives.** Currently, several countries launched or are developing their own navigation satellite systems, which are used regionally or globally. GPS is the American system, currently the world's most utilized satellite navigation system. The Russian Global Navigation Satellite System<sup>1</sup> (Glonass) also operates globally. The Chinese Beidou Navigation Satellite System<sup>2</sup> (BDS) and the Indian Regional Navigation Satellite System<sup>3</sup> (IRNSS) operate regionally, with the possibility of expanding their operation globally in the future. The Galileo<sup>4</sup> is European navigation system, currently being developed and with no predictions of being operational before 2020.

Systems based on Differential GPS (D-GPS) and Augmented GPS (A-GPS) currently exist in order to improve the quality and reliability of GNSS, by mitigating signal path distortions and satellite errors. Wide Area Augmentation System (WAAS) provides real time and continental augmentation, operating in North America and extended coverage into South America, the Atlantic and Pacific Oceans. Several other similar international systems exist, such as the Russian System for Differential Corrections and Monitoring (SDCM), the Indian GPS And Geo-Augmented Navigation (GAGAN), the Japanese Multi-functional Transport Satellite (MTSAT)-based Satellite augmentation System (MSAS) and the European EGNOS<sup>5</sup>.

## 2.2 Robot Localization based on RSSI

As mentioned previously, RF devices can be used as artificial landmarks. By receiving and extracting the RSSI value of the RF signal emitted by those devices, the robot is able to estimate the distance between them, using a wave propagation model.

A RF signal is an electromagnetic wave that propagates in every direction through space in a straight line. In the presence of obstacles, both direction of the wave propagation and its amplitude are modified, which represent deviations on signal reception.

**Wave Propagation.** It's very complex to characterize a wave propagation's behavior, because behavior changes are caused by random events. According to Alencar [3], several phenomena affect negatively the wave propagation [13], such as reflection, refraction, dispersion (shown on Fig. 1), diffraction and fading. There are advanced techniques, shown by He [28] that try to simulate the complex signal attenuation by having a 3D model of the world and simulating the reflections / refractions that a signal would be subject to before arriving to the receiver.

---

<sup>1</sup> Available in <https://www.glonass-iac.ru/en/>

<sup>2</sup> Available in <http://en.beidou.gov.cn/>

<sup>3</sup> Available in <http://www.isro.gov.in/irnss-programme>

<sup>4</sup> Available in <http://www.gsa.europa.eu/galileo/why-galileo>

<sup>5</sup> Available in <http://egnos-portal.gsa.europa.eu/>

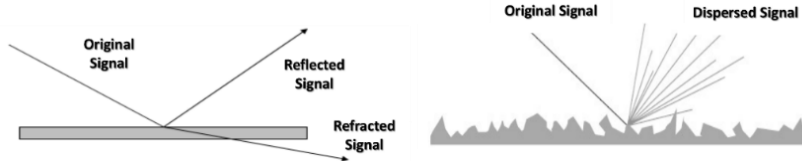


**Fig. 1.** Reflection, Refraction and Dispersion phenomenon on signal propagation

When a RF signal travels through an object with different density (often occurs on atmospheric variations), a part of the signal is refracted and another one is reflected, which is the number one cause for problems regarding multipath transmission. Dispersion/Spreading is a phenomenon that occurs when the RF signal reaches a rough surface object, dividing the signal into multiple one with different intensity and direction.

**Propagation Models.** Wave propagation models [13] try to estimate the RSSI at a given distance. Several models exist for different environment conditions, but they are all based on the Free Space propagation model [8, 22], which uses the Friis formula [24] to characterize the signal propagation when no obstacles are blocking the path between transmitter and receiver. Friis formula is valid only in situations where  $d$  (distance between the transmitter and the receiver) is at a minimum distance of the transmitter antenna, called the Fraunhofer distance  $d_f$ , represented on Eq. (1), where  $\lambda$  is the wave length of the RF signal.

$$d_f = \frac{2d^2}{\lambda}, \quad d_f \gg d \wedge d_f \gg \lambda \quad (1)$$

Since the Fraunhofer distance is not defined for  $D = 0$ , the model uses a reference distance  $d_0$ , represented by Eq. (2), where  $P_r(d_0)$  is the received signal strength of reference.

$$P_r(d)_{dBm} = P_r(d_0)_{dBm} + 20 \times \log\left(\frac{d_0}{d}\right), \quad d \geq d_0 \geq d_f \quad (2)$$

**Outdoor Path Loss Model.** Because there is no perfect conditions, the RF signal is normally attenuated due to the phenomenon described earlier, leading to deviations on the calculations [3, 13]. Signal noise and deviations are considered on Eq. (3), where  $\eta$  is the path loss coefficient,  $X_\theta$  is a normal random variable used to modulate and  $A$  is the signal attenuation. The path loss coefficient depends on the propagation environment and must be calculated according to the context (on outdoor the usual value is 2). By knowing  $\eta$ , is possible to linearize the relation between the RSSI ( $P_r(d)$ ) and the distance between the signal emitter and receiver ( $d_{i,j}$ ), represented on Eq. (4). The calculated distance is always associated with an ambiguity factor represented by a Gaussian distribution.

$$P_r(d)_{dB} = P_r(d_0)_{dB} + A - 10\eta \times \log\left(\frac{d_0}{d}\right) + X_\theta \quad (3)$$

$$d_{ij} = d_0 \times 10^{\frac{P_r(d_0) - P_r(d)}{10\eta}} \quad (4)$$

*Dual-Slope Model.* While the Path Loss model considers only the original wave that travels between the emitter and receiver, the Dual-Slope model considers also the resulting waves of reflection that reaches the receiver. The model is characterized by Eq. (5), where  $h_t$  and  $h_r$  are the heights of the transmitter and receiver related to the ground.

$$P_r(d) = P_t \times G_t \times G_r \frac{h_t^2 \times h_r^2}{d^4}, \quad d > \frac{4h_t h_r}{\lambda} \quad (5)$$

### 3 Methodology

Sensor fusion was used to improve the quality of a mobile robot (AGROB V14 platform [19]) localization. A Simultaneous Localization And Mapping (SLAM) technique was implemented, where GPS and RSSI data (from artificial RF beacons) were used to locate the robot and map the world. The robot location was improved by GPS data fusion with Odometry velocity, the beacons distance observations and the beacon's mapping.

Localization systems based on RSSI have three main components: distance estimation between the RF signal emitter and receiver, position calculation based on the distance estimations and localization algorithm.

#### 3.1 Beacons Distance Observation

iBeacons<sup>6</sup> are small Bluetooth devices used as artificial landmarks in the environment. The RF signals emitted were received by an Android mobile device connected to the robot, which used the RSSI value to estimate the distance to the beacon. The distance was first estimated by means of an empirical model that is described, in the Android Beacon Library<sup>7</sup>, by Eq. (6), where  $d$  is the estimated distance in meters,  $RSSI$  is the value received in the Android phone from one iBeacon,  $RefPower$  is the reference of the RSSI value (at a distance of 1 meter) and  $A$ ,  $B$  and  $C$  are constants to be adjusted according to the environment conditions where the iBeacons are being used. After several field tests,  $A$ ,  $B$  and  $C$  were derived from power regression against a table of distance/RSSI values (provided by the referred library), resulting on Eq. (7).

$$d = A \times \left(\frac{RSSI}{RefPower}\right)^B + C \quad (6)$$

$$d = 0.3534536 \times \left(\frac{RSSI}{RefPower}\right)^{14.8393466} + 0.7566785 \quad (7)$$

The empirical analysis has the advantage to consider every factor that influence the radio wave propagation on a given context. On the other hand, the equation obtained from regression may not work correctly on environments different from the one used

---

<sup>6</sup> Available in <https://developer.apple.com/ibeacon/>

<sup>7</sup> Available in <http://altbeacon.github.io/android-beacon-library/distance-calculations.html>

to collect data in the first place. Moreover, Eq. (6) may itself be source of deviations and noise. Also, the regression process is very dependent on the Android device used to obtain the data. The simple fact of using devices with different characteristics may lead to deviations and noise. For these reasons, analytical models, namely the outdoor path loss and dual-slope models mentioned before, for wave propagation were used in order to calculate the distance based on the RSSI values.

### 3.2 Robot Position Calculation

For a 2D position estimation, the robot needs at least three distance measurements to different beacons with known locations. Because the beacon's mapping is unknown and the robot location is estimated based on noisy GPS data, a SLAM approach is implemented, where the beacons are mapped at the same time as the robot position is calculated.

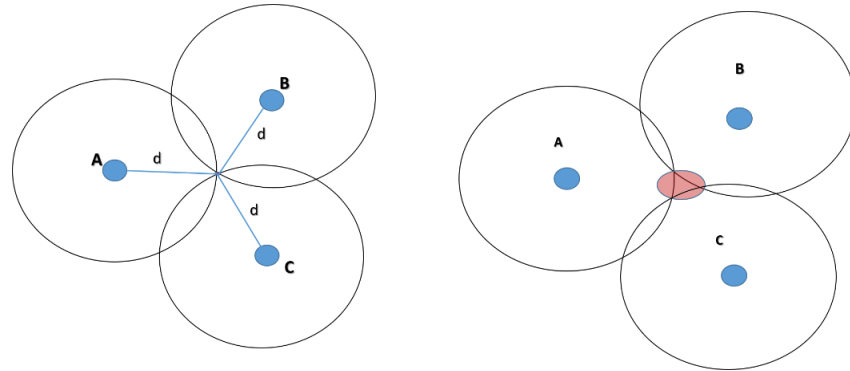


**Fig. 2.** Both theoretical and real triangulation results

Mapping the iBeacons is accomplished by estimating the beacons location in relation to the robot. By knowing the robot location and the distance between the robot and beacons, one can calculate the beacon position by using the trilateration method. Because only flat terrains were considered so far, the localization problem can be simplified to a 2D format, instead of 3D. At least three robot locations are represented graphically by circumferences, where the radius is the distance to the beacon. The resulting interception point of the three circumferences is the position of the beacon, as shown on Fig. 2 on the left.

### 3.3 Localization Algorithm

The uncertainties associated to the distances calculated and robot position, shown on Fig. 3 on the right, motivated the appearance of probabilistic approaches [17]. Instead of resulting in just one point, the interception of the circumferences, when using the

trilateration, results on a set of points, each one associated with a probability that represents the actual position of the beacon. These approaches are associated with filters [23], such as Kalman, Histogram and Particle filters, which increase the quality of the positioning process by decreasing the deviations of samples.

In this case, because robot localization is a highly nonlinear problem, the beacon mapping procedure developed on work [4] was used, which implements both a Particle and a Histogram filter. For a better estimation on the robot location, the Particle filter was used to fuse the GPS data, Odometry and beacon's distance estimation. The Histogram filter was applied to the robot location and distance estimation between robot and beacons (based on RSSI data), in order to map the beacons.

The Particle filter consists in spreading random points through space and associate to each one a probability of being in the actual beacon position. Every time a new GPS message arrives, the probability of each point is updated and the cloud of points gets concentrated, because points with lower probability are deleted and new points are generated close to the most likely ones.

$$P_t(x, y) = \frac{1}{\sqrt{2\pi}\sigma} e^{-(d-z_t)^2/2\sigma^2} \quad (8)$$

The Histogram filter consists on a discretization of a 2D space into a grid of cells (likelihood grid map), where the center of the grid is the robot location estimation. The goal is to calculate the grid's occupancy by assigning to each cell a probability of the beacon being located on that cell. The cell probability at time  $t$  ( $P_t(x, y)$ ) depends of the beacon distance ( $d$ ) and robot position ( $z_t$ ) estimation, as shown on Eq. (8), where  $\sigma$  is the deviation (on a normal distribution) that represents the sum of all uncertainties associated with the robot position and beacon distance estimation.

## 4 Tests and Results

Beacon distance estimation was tested by comparing the use of an empirical and analytical models for wave propagation. The algorithm for beacon mapping on [4] was tested, using data provided by the iBeacons Kontakt<sup>8</sup>.

### 4.1 Distance Estimation

Distance estimation based on RSSI techniques rely on modeling the beacons RF signal propagation. The empirical model identified on Eq. (6) and Eq. (7) is compared with the Outdoor Path Loss model, identified on Eq. (3) and Eq. (4). Because data is being post-processed and the ground true is unknown, the comparison is relatively to each approach and not absolute. RSSI values were collected and used on both models to calculate the distance to the corresponding beacon. Results are shown on Fig. 3.

---

<sup>8</sup> Available in <https://www.kontakt.io>

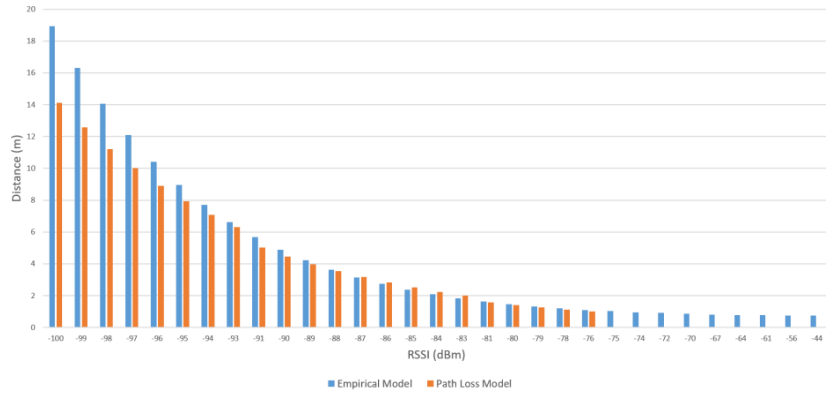


**Fig. 3.** Distance comparison between the Empirical Model and Path Loss Model approaches

The curve for the empirical model behaves exponentially, while the Path Loss model fits the empirical one (differences are lower than 1m) only between -95dBm and -75dBm, which corresponds closely to 8m and 1m of distance.

For RSSI values higher than -75dBm, the empirical model is more accurate, because 1m is the reference distance used in the Path Loss model. As said before, the reference distance is the minimum defined distance in this model, so results lower than 1m don't make any sense. On the other hand, the empirical model follows its exponential behavior until it reaches a distance very close to 0 on high RSSI values.

For RSSI values lower than -95dBm, a major difference is found between the Path Loss and the Empirical models. On the 8m distance mark, the RF probably suffers deviations, such as reflection and refractions, which weren't considered on the empirical model. Although being theoretically considered on the Path Loss model, the model lacks calibration regarding some parameters, such as signal attenuation and path loss coefficient, which may lead to less accurate modulation of the wave propagation. The static values considered of path loss coefficient is 2 (value defined for outdoor environments) and the signal attenuation is simplified to 1, but, for better accuracy on calculations, these variables should be dynamically calculated over each iteration. Still, 8m is already a big distance to be estimated, considering the problem context and the noise associated to signal propagation at this kind of distances. The accuracy will improve if distances higher then 8m are not considered for calculations.

#### 4.2 Algorithm for beacon mapping

As shown by Duarte [4], the beacons and robot position estimation have improved significantly when fusing the GPS data and the beacon's distance observation, by using a particle filter.



**Fig. 4.** Evolution of an iBeacon (id = 4903040350) Grid Map with 0.25meters/pixel resolution

In Fig. 4 is shown the obtained likelihood grid map for one beacon at four different time instances (0, 70, 200 and 330 seconds), on a test duration of 560. The grid map resolution is 0.25meters/pixel. The possible beacon position starts with a large circle, evolving to two small regions on stage two, which becomes one small region and ends with a very small spot.

#### 4.3 Robot Position

Google maps API was used for illustrating the robot estimated positions on different time instances. By using the particle filter, robot estimation was obtained from the fusion of GPS and odometry, considering the mapped beacons and beacons distance observation.



**Fig. 5.** Planned and estimated robot trajectory

Fig. 5 represents the tests performed for evaluating the robot position, by identifying the robot planned trajectory (on the left), which is considered to be the ground truth for comparison, the estimated trajectory using only GPS data (in the middle) and the estimated trajectory using the results from the sensor fusion described, considering the beacons mapping and distance to beacons (on the right).

## 5 Conclusions

The main goal of this work is to improve the robot self-localization capability by performing sensor fusion techniques on data from different sensors built in AGROB V14. It was proven in the previous work [4] that the robot location improves by fusing beacons distance information and mapping with GPS data.

The problem of improving the robot location may be approached on two levels: the first is to clean and improve individual noisy sensor data already used to estimate the robot location. The second is to add new (still noisy) sensor data to the sensor fusion approach, in order to get a better estimative of the robot location. The current work approaches the problem by improving the noisy data of the beacons distance observations before fusing it with GPS data. Empirical and analytical models for wave propagation (on RF signals) were considered and compared. Also, by fusing beacon's distance estimation calculated on the models and GPS data, is possible to correct the robot position.

For future work, noisy GPS data can be corrected, by using GPS Augmentation approaches. Regarding sensor fusion, the AGROB V14 is equipped with other important sensors that can be used for localization, such as a RADAR, IMU and a camera, which weren't used in the current work. These sensors' data can also be fused to the GPS data. Also, since several robot locations are required to estimate a beacon position, this work can be expanded by using multi-robot scenarios.

## References

1. Bahl, P., Padmanabhan, V.N., Balachandran, A.: Enhancements to the RADAR user location and tracking system. (2000).
2. Barshan, B., Durrant-Whyte, H.F.: Inertial navigation systems for mobile robots. Robot. Autom. IEEE Trans. 11, 328–342 (1995).
3. de Alencar, M.S.: Sistemas de comunicações. Érica (2004).
4. Duarte, M., dos Santos, F.N., Sousa, A., Morais, R.: Agricultural Wireless Sensor Mapping for Robot Localization. In: Robot 2015: Second Iberian Robotics Conference. pp. 359–370 (2016).
5. Esteves, J.S., Carvalho, A., Couto, C.: Generalized geometric triangulation algorithm for mobile robot absolute self-localization. In: Industrial Electronics, 2003. ISIE'03. 2003 IEEE International Symposium on. pp. 346–351 (2003).
6. Hall, D.L., Llinas, J.: An introduction to multisensor data fusion. Proc. IEEE. 85, 6–23 (1997).
7. Hofmann-Wellenhof, B., Lichtenegger, H., Collins, J.: Global positioning system: theory and practice. Springer Science & Business Media (2013).
8. Levis, C., Johnson, J.T., Teixeira, F.L.: Radiowave propagation: physics and applications. John Wiley & Sons (2010).
9. Li, Z., Ma, Y.-G.: A new method of multi-sensor information fusion based on SVM. In: Machine Learning and Cybernetics, 2009 International Conference on. pp. 925–929 (2009).
10. Lu, F., Milios, E.: Robot pose estimation in unknown environments by matching 2d range scans. J. Intell. Robot. Syst. 18, 249–275 (1997).
11. Madry, S.: Global Navigation Satellite Systems and Their Applications. Springer (2015).

12. Misra, P., Enge, P.: *Global Positioning System: Signals, Measurements and Performance* Second Edition. Lincoln, MA: Ganga-Jamuna Press (2006).
13. Molisch, A.F.: *Wireless communications*. John Wiley & Sons (2007).
14. Niculescu, D., Nath, B.: Ad hoc positioning system (APS). In: Global Telecommunications Conference, 2001. GLOBECOM'01. IEEE. pp. 2926–2931 (2001).
15. Patwari, N., Ash, J.N., Kyperountas, S., Hero III, A.O., Moses, R.L., Correal, N.S.: Locating the nodes: cooperative localization in wireless sensor networks. *Signal Process. Mag. IEEE.* 22, 54–69 (2005).
16. Priyantha, N.B., Miu, A.K.L., Balakrishnan, H., Teller, S.: The cricket compass for context-aware mobile applications. In: Proceedings of the 7th annual international conference on Mobile computing and networking. pp. 1–14 (2001).
17. Ramadurai, V., Sichitiu, M.L.: Localization in Wireless Sensor Networks: A Probabilistic Approach. In: International conference on wireless networks. pp. 275–281 (2003).
18. Robótico, F.: Arquitecturas de Sistemas Robóticos e Localização em Tempo Real Através de Visão, (2003).
19. Santos, F.B.N. dos, Sobreira, H.M.P., Campos, D.F.B., Santos, R.M.P.M. dos, Moreira, A.P.G.M., Contente, O.M.S.: Towards a Reliable Monitoring Robot for Mountain Vineyards. In: Autonomous Robot Systems and Competitions (ICARSC), 2015 IEEE International Conference on. pp. 37–43 (2015).
20. Savvides, A., Han, C.-C., Strivastava, M.B.: Dynamic fine-grained localization in ad-hoc networks of sensors. In: Proceedings of the 7th annual international conference on Mobile computing and networking. pp. 166–179 (2001).
21. Shang, Y., Rum, W.: Improved MDS-based localization. In: INFOCOM 2004. Twenty-third AnnualJoint Conference of the IEEE Computer and Communications Societies. pp. 2640–2651 (2004).
22. Singal, T.L.: *Wireless communications*. Tata McGraw-Hill Education (2010).
23. Thrun, S., Burgard, W., Fox, D.: *Probabilistic robotics*. MIT press (2005).
24. Ulaby, F.T., Moore, R.K., Fung, A.K., House, A.: *Microwave remote sensing: active and passive*. Addison-Wesley Reading, MA (1981).
25. Vandenbussche, K., others: Fine-grained Indoor Localisation Using Wireless Sensor Networks. *Signal.* 75, 70 (2005).
26. Vázquez-Martín, R., Núñez, P., Bandera, A., Sandoval, F.: Curvature-based environment description for robot navigation using laser range sensors. *Sensors.* 9, 5894–5918 (2009).
27. Zhao, X., Luo, Q., Han, B.: Survey on robot multi-sensor information fusion technology. In: Intelligent Control and Automation, 2008. WCICA 2008. 7th World Congress on. pp. 5019–5023 (2008).
28. He, D. et al.: A novel method for radio propagation simulation based on automatic 3D environment reconstruction. In: Antennas and Propagation (EUCAP), 2012 6th European Conference on. pp. 1445–1449 (2012).
29. Henry, P. et al.: RGB-D mapping: Using depth cameras for dense 3D modeling of indoor environments. In: In the 12th International Symposium on Experimental Robotics (ISER. (2010).
30. Wang, J., Wang, Y.Q.: A monocular stereo vision algorithm based on bifocal imaging. *Robot.* 33, 6, 935–937 (2007).

# A Multi-Agent System for Micro Grids Energy Production Management Supported by Predictive Data Analysis

Jonas Queiroz<sup>1,2</sup>, Paulo Leitão<sup>2,3</sup> and Artur Dias<sup>3</sup>

<sup>1</sup>Faculty of Engineering - University of Porto, Porto, Portugal,

<sup>2</sup>Artificial Intelligence and Computer Science Laboratory, Porto, Portugal

<sup>3</sup>Polytechnic Institute of Bragança, Bragança, Portugal

[jonas.queiroz@fe.up.pt](mailto:jonas.queiroz@fe.up.pt), {pleitao,a24744}@ipb.pt

**Abstract.** Micro grids comprise an emergent electrical paradigm, where several small, distributed and independent energy production and consumption units need to cooperate in order to achieve a local self-sustainability, by reducing their dependency from the main grid. The realization of the micro grid concepts requires the use of advanced information and communication technologies to design and implement systems capable to effectively manage the micro grids nodes and their elements. In this sense, multi-agent systems provide a suitable framework, where autonomous agents, endowed with predictive data analysis capabilities, take advantage of the large amount of data produced in these environments to predict the renewable energy production and consumption, contributing to the enhancement of the micro grid self-sustainability. In this context, this paper presents an agent-based system for the management of micro grids energy distribution, through the prediction of renewable energy generation. Some experiments were performed considering a simulation environment in a case study where predictive models were tested for forecasting the energy produced by renewable energy units.

**Keywords:** electrical micro grid · predictive data analysis · multi-agent systems · renewable energy generation prediction

## 1 Introduction

Smart grids envision an intelligent energy and information network of consumers and producers that promotes the integration and distribution of electrical resources, aiming an economically sustainable electrical grid, and also improving the control, quality of services, energy efficiency and the system reliability and stability [1-2]. Within this context, the micro grids are characterized by low voltage networks, comprehending a community of residential and commercial buildings, equipped with small renewable energy generation units, such those based on photovoltaic panels (PV) and wind turbines, as well as, consumption and power storage devices [3]. The main goal of the micro grids is to be able to operate isolated from the main grid (island mode, e.g. due

geographical constraints or to support outages) or with a minimal dependence, in order to achieve high levels of energy efficiency and self-sustainability [3].

Another characteristic of these electrical systems is related to the independence of each micro grid node, where each one has local autonomy to manage its own energy production, storage and consumption. In this context, to achieve high levels of energy self-sustainability, it is necessary the interaction and cooperation between the various micro grid nodes and their elements. These features make multi-agent systems (MAS) approach [4] suitable to deal with the challenges posed by micro grids [5]. In this sense, the micro grid nodes and their elements can be managed and controlled by one or more autonomous software agents, which are capable to take local decisions based on the combination of their information and the interaction with other agents. Therefore, the MAS approach provides the flexibility and scalability required by micro grids to support their components autonomy and dynamics.

Additionally, the fact that the renewable energy production entities are directly dependent on intermittent unstable weather conditions (e.g. solar irradiance and wind speed) further increases the system dynamics and consequently the complexity to manage the energy usage and distribution along micro grid nodes. This characterizes another challenge, requiring the design of accurate short and long term renewable energy prediction models. Either, the management of energy consumption and storage is not a simple and easy task, which usually depends on the prediction of consumer daily habits. In this context, predictive capabilities represent an important requirement to provide valuable information for the micro grid renewable energy management. On the other hand, in electrical grids, a large amount of data has been produced and collected from various sources, such as, smart sensors, meters and also electricity market transactions [1]. In this context, data analysis approaches, such those based on data mining and machine learning, can be used to understand and discover valuable information and knowledge from historical and streaming data, by building accurate descriptive and predictive models. This way, data analysis can contribute to achieve the micro grids goals, e.g., by predicting the renewable energy production, which can be used to improve the scheduling and planning of energy distribution and usage.

The goal of this work is to use data analysis to support an agent-based system for the micro grid management, through the prediction of energy production, consumption and storage. This paper focuses in the prediction models for the renewable energy production and in the MAS simulation environment used to test the proposed approach and predictive models, which was developed using JADE and WEKA frameworks, respectively. The paper is organized as follows: Section 2 overviews the state of the art and Section 3 describes the MAS approach for the management of micro grids supported by predictive data analysis. Section 4 presents the case study and the agent simulation approach, while Section 5 analyses the experimental results, taking into consideration the prediction of short and mid-term energy production of PV panels and wind turbines. Finally, Section 6 presents the conclusions and the future work.

## 2 State of the Art

Technological advances and cost reduction of devices with embedded sensors contributed for the increasing in their use in several domains and consequently in the amount of data retrieved and stored. The availability of large amount of heterogeneous data leveraged the interest in not only extract knowledge from raw data to better understand and explain events, but also to build predictive models to guide current actions taking in consideration what may happen in near future. Such interest in the value that can be extracted from the data has led to the emergence of the Big Data research field, characterized by the development of novel and advanced approaches and frameworks to support the data analysts in their tasks [6-7]. Big Data comprises basically the same algorithms, tools and infrastructures that are used for data mining and machine learning, but adapted and improved to support some data constraints, associated with the data volume, variety and velocity [6, 8]. Data analysis consists of the execution of tasks related to data gathering, integration, preprocessing, patterns identification, building and assessing descriptive and predictive analysis models [9]. This is a well consolidated research field supported by many different tools, frameworks and code libraries, such as WEKA and R, including some dedicated for Big Data, such as Apache Mahout, Apache Storm and others.

In the literature there are several works discussing issues regarding predictive data analysis in the context of electrical grids. In this context, artificial neural network algorithms were employed to forecast PV energy production [10] and load demand [11]. Also probabilistic models were employed to forecast the usage of household appliances [12], while data association mining algorithms were used to forecast the energy price and demand in smart grids [13].

The realization of micro grid vision, concerning the aspects of energy production and consumption, still depends on many technical and informational issues, related to the design of distributed and intelligent systems for the control and management of the micro grid nodes and their elements. In this context, MAS provides a suitable framework to support the design of flexible and scalable systems [4]. In the literature, the MAS approach has been used for several applications in the domain of electrical grids [5], such as for smart grid management [14], intelligent control of micro grid loads [15], implementation of real-time energy market [16] and simulating electric markets [17]. There are also some works that proposed MAS enhanced with predictive analysis for demand side management, by forecasting the energy consumption demand and the renewable energy production [14, 18].

Usually, such works give more attention to the control and management of the electrical loads than the renewable energy production units. In this context, the main issue faced by these systems is the forecasting of the dynamic and unstable weather condition. Therefore, a challenge explored in this work is the combination of MAS and predictive data analysis for improving the management of micro grid production units and the energy distribution, in order to achieve a more efficient and responsiveness system. These tasks are supported by the combination of historical and streaming data from multiple sources, such as the sensors of production units and meteorological weather web sites.

### 3 Micro grid agent-based system

In this work a micro grid is considered to be formed by a set of buildings that share the same low voltage energy distribution network, also connected to the main grid (Fig.1). In the micro grid each building represents a node that could be formed by energy consumer elements (electronics, home appliances and other electrical loads), energy producer elements (e.g., PV panels and wind turbines), and also by storage elements (e.g., battery banks). The micro grid agent-based system can be realized in such a way that each node of the micro grid can be represented by several distributed and autonomous agents (e.g., one for each node electrical element) that implement intelligent local strategies and interact with other agents to enhance the micro grid energy self-sustainability, by the management and optimization of its electrical element. For example, a building equipped with one PV panel, one wind turbine and one battery bank may have two PAs, one SA, and also some CAs to manage its electrical loads. Electrical vehicles can be managed by an agent performing both, consumer and storage roles.

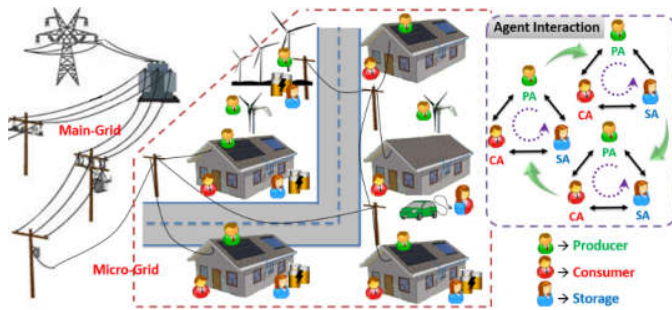


**Fig. 1.** A simplified representation of a micro grid and the agent-based system configuration.

In this sense, the agent-based system proposed in this work comprises a set of agents, which can perform three different roles [19]: Producer Agent (PA), Consumer Agent (CA) and Storage Agent (SA), see Fig.1. The autonomy of each micro grid node and the user interests, which could be represented by a set of agents, define some particular behaviors of agents, which are described in the following.

- PA – manages the energy production and distribution of energy generator units, supplying energy to consumers according to their demands or delivering the energy surplus to be stored in power storage devices. In order to attend local node energy requirements, PAs always tries, firstly, to satisfy local CAs, supplying the required demand, and SAs, supporting their desired load levels. Then, considering these priority order of energy negotiation and the micro grid self-sustainability requirements, PAs can negotiate produced energy with non-local agents. This negotiation has a cost that should be lower than main grid costs. In the case of the remaining energy surplus, it could be negotiated with the main grid.

- CA – manages the energy consumption of electrical loads, considering user profiles and micro grid sustainability requirements. CAs interact with PAs to negotiate current produced energy, and with SAs to require the energy supply that complement the energy demand not provided by current production. Like PAs, CAs also first negotiate with local agents considering user and micro grid sustainability requirements, which in this case could imply in CAs opting to save local SAs energy by consuming energy of non-local agents.
- SA – manages the charging and supplying of power storage devices, considering their electrical constraints and efficiency. Usually, these agents are associated with local CAs, supporting the energy demand not attended by current energy production, and local PAs, storing the energy that was produced but not consumed for attending future demands. When micro grid is connected with the main grid, SAs can buy energy in lower cost periods to use it in higher cost periods. Like PAs and CAs, these agents can negotiate energy with non-local agents, providing or storing energy with a cost that should be lower than main grid costs in order to attend micro grid requirements. For energy efficiency reasons, SAs should not negotiate energy with other SAs or sell energy for the main grid.

In the proposed approach, agents should implement several predictive capabilities, which are described below. In this work these capabilities are considered essential to support and enhance the control and management of the energy distribution through the micro grid elements.

- PA – can use prediction capabilities to obtain information, in advance about the amount of energy that will be produced in a mid and long term, in order to determine whether it will have production surplus, or the production will not be enough to attend the consumer demands. This information can be used to improve the energy distribution along the consumer and storage elements or even to sell it to the main grid. Also, long term prediction can be used to participate in energy markets in an effective way, while short term prediction can be used to correct imbalances, caused by the long term miss prediction, or provide information for CAs to reschedule and shift loads. Additionally, short term predictions could be used to detect any malfunction or performance degradation in the energy production units, e.g., by comparing if the energy produced is different from what was expected.
- CA – can use predictive models to obtain information about the energy demand of electrical loads, in short and mid term, in order to optimize the energy consumption by rescheduling and shifting loads, according with the current energy production. Mid and long term predictions, considering the users and loads profiles, could be used to negotiate energy, in advance, with production nodes and also effectively participate in energy markets. Electrical disturbances or outages could be predicted, in order to reduce their effects and to avoid the inoperability of the system.
- SA – can use prediction to determine how much and the better moments to charge or discharge loads, according to producers, consumers and main grid conditions. Like CAs, SAs can predict outages and other kinds of events that require extra energy demand, in order to maintain their load levels to satisfy user and micro grid needs in face of such conditions.

For this purpose, CAs, PAs and SAs need to embed proper data analysis methods based on different machine learning algorithms, such as artificial neural network (ANN). The choice of algorithms will depend on the scenario requirements, e.g., decision trees based algorithms use simpler approaches than ANN, taking less time and processing resources to process and analyze data, but they usually produce less robust models. They are built using historical data, and could be improved as new data is available. The data could be retrieved from several sources, such as, weather stations and web sites, sensors installed in micro grid elements, historical production and consumption records, energy markets and others. In this sense, the agents are also responsible to perform the tasks related to the data retrieval, preprocessing and integration.

## 4 Case study

The case study considered in this work focuses in the development of predictive models for PAs to manage the distribution of renewable energy production of micro grids. In order to develop such models it was used real data collected from some production elements (static PV panels and wind turbines) of an electrical grid installed in the Polytechnic Institute of Bragança (IPB), Portugal, which is part of the IPB renewable energy project (<http://vercampus.ipb.pt/>). Considering the characteristics of the micro grid and agents presented in the previous section, a small simulation environment was designed and developed for the deployment and test of the proposed MAS.

### 4.1 Dataset description

In this case study it was considered two data sources, where the main parameters used in the experiments are described in Table 1. The dataset of the IPB micro grid project are sampled in each 5 minutes, and the data set comprises historical data from the last 3 years. Also, it was used a set of meteorological data (historical and forecasts) obtained from weather web sites, such as openweathermap.org and wunderground.com. The data retrieved from the different sources required to be synchronized, which is done according with their timestamps. The data was preprocessed and cleaned by removing the missing values and outliers, such as, some periods not or wrong recorded by sensors. Moreover, it was used only data from daylight time and periods of the day that registered the power production.

### 4.2 MAS simulation environment

A MAS simulation environment was implemented using the agent framework JADE. In the experiments, was used a very simple configuration for the micro grid and the three different agent's roles, described in Section 3. As the focus of this case study is related with the prediction of the energy production, the energy consumption of loads and power storage were simulated based on simple static behaviors that follow some user load profiles and batteries charge and discharge functions, respectively.

In the following is described the behavior of agents in the simulation environment.

**Table 1.** List of data sources and parameters used for building predictive models.

Data Source	Parameter Description
<i>IPB Project</i>	<i>Electric power</i> (W) produced by electrical units.
	<i>Solar irradiance</i> (W/m <sup>2</sup> ) measured by production units sensors.
	<i>Environment temperature</i> (°C) measured by production units sensors.
	<i>PV modules temperature</i> (°C).
<i>Weather web sites</i>	<i>Wind speed</i> (m/s) measured at the energy units.
	<i>Environment temperature</i> (°C) provided by weather stations localized near the energy production units, registered for periods greater than 1 hour.
	<i>Cloud cover</i> (%) provided by the local weather stations.
	<i>Wind speed</i> (m/s) provided by the local weather stations.
	<i>Humidity</i> (%) provided by the local weather stations.

- PA – in this work, it is designed to present a passive behavior, waiting and attending energy request proposals from other agents. This agent cyclically performs the following tasks: 1) Predict the amount of energy to be produced; 2) Attend energy requests of local CAs; 3) Negotiate surplus to the local SAs; 4) Attend energy requests of non-local CAs and SAs; 5) Sell surplus to the network.
- CA – has an active behavior, taking the initiative to negotiate energy with other agents to satisfy its demand. This agent cyclically performs the following tasks: 1) Predict the energy demand of home appliances for next period (in this case study the prediction is based on static user profiles); 2) Request energy to the local PAs; 3) Negotiate energy with non-local PAs; 3) Request energy for local SAs; 4) Negotiate energy with non-local SAs; 5) Buy energy from the main grid.
- SA – has a passive behavior regarding the power supply, waiting for the proposals of CAs, and an active behavior regarding the energy acquisition, sending energy request proposals to PAs. This agent cyclically performs the following tasks: 1) Calculate the amount of energy to be acquired to supply local CAs demand and calculate the amount of energy that can be provided to non-local CAs (both based on local CAs historical requests); 2) Attend energy requests from local CAs; 3) Attend energy requests of local PAs to store energy surplus; 4) Attend energy requests from non-local CAs; Negotiate energy with non-local PAs; 5) Buy energy from main grid (if economic period).

The simulation environment was developed based on an artificial clock that emulate the real time in an accelerated speed, closer to asynchronous and real environments, instead of a round-based approach as in Repast agent simulation platforms. The simulation is based on time slots, where the agents perform the predictions and negotiate energy for each time slot of, e.g., 15 minutes or 1 hour interval. In order to reduce the complexity of agent interactions the time slots were divided into intervals dedicated for agents perform specific tasks (Fig.2-a).

In the simulation, the time slot division (e.g., 1 hour time slot as in Fig.2-a), could be as follows: the first 5 minutes are devoted for agents perform their computations and predictions. The interval from minute 5 to 25 can be used by CAs to negotiate with PAs, giving a priority for local PAs. The following interval (25 to 45) is reserved

for the negotiation of CAs with SAs and SAs with PAs. The last interval is reserved for agents to buy or sell extra demand or surplus from the main grid. In this approach the main grid always sell or purchase any amount of energy for a pre-established price, known by all agents, in order to support agents miss prediction. However, this price varies according to two periods of the day (Economic – lower prices and Normal – higher prices), which directly influence and determine the way agents negotiate energy and the prices practiced by them. For exempla, during economic period CAs prefer to buy energy from PAs or main grid than from SAs.

The local agents use the FIPA Request interaction protocols to negotiate energy, where an agent (e.g., a CA) request an amount of energy to other agent (e.g., PA), which will reply with the amount of energy it will provide. In the other hand, the negotiation between non-local agents is based on the FIPA Call for Proposal (CPF) protocol (Fig.2-b), where buyer agents send a call for proposal to seller agents with the desired amount of energy and price. Based on that, sellers make a proposal with an available amount of energy and a counter price. Buyer agents evaluate all the proposals and accept those required to supply their demands, by sending an accept proposal to sellers. When the sellers receive the accept proposals, if they do not have the total amount, but still have some, then they sell this amount, sending a message to the buyer, which accepts the negotiation result.

In addition to simulation infrastructure, some graphical user interfaces (GUI) were developed to enable the visual monitoring, analysis and management of the agents and their activities (Fig.3).

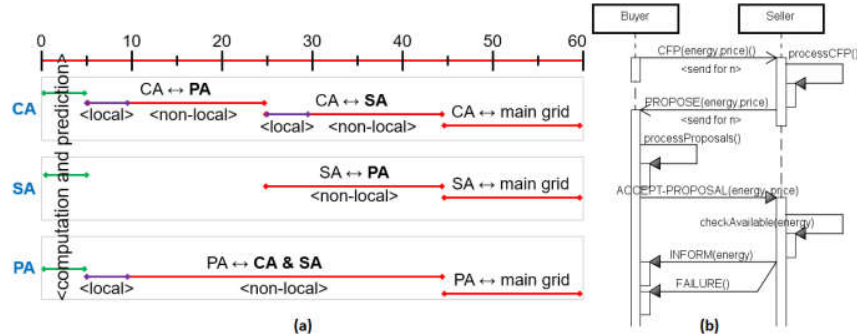
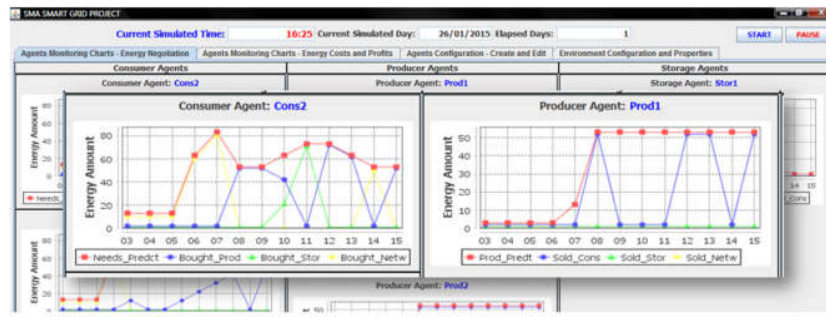


Fig. 2. An example of a 1 hour simulation time slot division.

## 5 Experimental results

Before the deployment of the predictive models in the PAs several experiments were performed to determine which machine learning algorithm, data sources and attributes produced better models in terms of the accuracy of the energy prediction. For the preliminary experiments were considered four algorithms provided by the WEKA framework (version 3.6): M5P (decision tree), M5Rules (rules), Linear Regression (linear function) and Multilayer Perceptron (ANN) [9]. The experiments were also

evaluated for some weather adversarial conditions, where the results for energy prediction showed better values for sunny days and moderate wind conditions, in the case of PV panels and wind turbines, respectively. In this sense, this section presents the preliminary experimental results of the data analysis performed for two scenarios: i) short term (5 and 15 minutes ahead) prediction, used by PAs for reducing imbalances in the energy production caused by the long term miss prediction, and ii) mid term (1 hour ahead) prediction, used by PAs for management of energy distribution along the micro grid, or even sell the energy surplus to the main grid.



**Fig. 3.** Simulation environment GUI. Charts represent the energy negotiated between agents.

### 5.1 Short term prediction experiments

This experiment focused on the prediction of the energy production for a 5 minutes interval to 5 and 15 minutes ahead. The predictive models in this experiment only considered the data measured and collected by the sensors attached in the production units. Different experiments were performed considering: all available data, only data from the last previous months, and also the combination of different attributes. The results showed that the PV energy production is mainly affected by the solar irradiance and temperatures, while the wind system by the wind speed. As weather web sites usually provide forecasts for periods of hours and days, in this experiment, the parameters used for the energy prediction were estimated based on the previous values registered by production units. This kind of forecast leads to high accurate values for PV system, mainly because parameters like temperature and solar irradiance do not vary too much in short intervals, but the same does not happen for wind system, as the wind speed usually presents high variability in short intervals.

The results of these experiments are showed in Table 2. The experiments were done using the same computational machine, thus the time taken to build models only illustrates the differences between the tested algorithms. The prediction values presented good performance, with low errors and high correlation, indicating the consistency of predictive models. As expected, the results for PV system were better than the wind system, which is affected by the very high wind instability. It is important to observe that the M5Rules method presented the best results but required more computational time to build the model than the other methods. Besides the time, the compu-

tational resources requirements also need to be evaluated, but if these are not critical issues, then M5P could be chosen since it presented very good results-time relation.

**Table 2.** Summary of energy production prediction analysis results

	Prediction for 5 minutes ahead							
	M5P		M5Rules		Liner Regression		Multi perceptron	
	PV	Wind	PV	Wind	PV	Wind	PV	Wind
Computational time (sec.)	8.9	7.91	121.63	55.78	0.17	0.09	41.39	15.03
Correlation coef.	0.991	0.839	0.991	0.841	0.989	0.837	0.990	0.840
Relative absolute error (%)	10.899	40.252	10.628	40.080	12.894	44.502	15.590	42.178
Prediction for 15 minutes ahead								
Computational time (sec.)	7.16	8	143.84	56.94	0.13	0.08	41.08	16
Correlation coef.	0.977	0.779	0.977	0.781	0.975	0.780	0.975	0.779
Relative absolute error (%)	15.723	46.128	16.150	46.034	16.924	49.015	18.315	47.579
Prediction of PV energy production for 1 hour ahead								
Computational time (sec.)	0.4		1.4		0.01		1.83	
Correlation coef.	0.951		0.952		0.858		0.926	
Relative absolute error (%)	25.997		25.555		49.852		37.003	

Fig.4 illustrates the values of PV energy production of three days compared with the values predicted for intervals of 5 minutes for 5 and 15 minutes ahead, by the M5Rules method. In this figure, the small distance between the real and predicted energy values indicates the accuracy of prediction models, which presented small relative absolute errors, leading to a prediction deviation of around 250W.

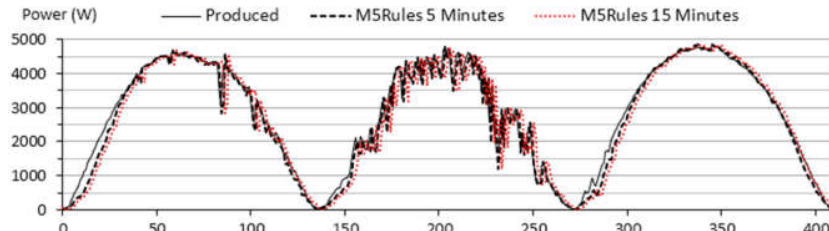


**Fig. 4.** The differences between the energy produced and predicted for short term of 3 days.

## 5.2 Long term for energy supply

This experiment focused on the prediction of the PV energy production for the next hour interval, based on the data provided by weather web sites. Such providers usually make forecasts for the environment temperature, wind speed, cloud cover, and others, however, the solar irradiance at surface, which is the main factor that influences the PV power production, is not forecasted. Thus in order to obtain an approximation for the value of this parameter, it was used the hourly extraterrestrial solar radiation, calculated according to the equations presented by [2]. This way, it is expected that machine learning algorithms be capable to learn how to approximate the

surface solar irradiance based on the calculated hourly extraterrestrial solar radiation and the cloud cover values, provided by the weather web sites.

The results of this experiment are summarized in the lower part of Table 2. The analysis of these values showed that the long term prediction was much worse than the previous ones, mainly due to the bad accuracy of the weather web site data. Considering these bad results, the experiments were not performed for wind system, which would present much worse results.

## 6 Conclusions

The paper presented an approach to enhance MAS with predictive data analysis for supporting the electrical micro grids management, aiming to improve the energy distribution and self-sustainability. In this sense, data mining and machine learning algorithms were used because their capabilities to build good models, when large amounts of sample data are available, while MAS was used since its autonomous and distributed nature provide an appropriate and powerful approach to address the micro grids organization and dynamics.

An agent-based simulation environment was designed and developed to test the proposed approach, considering a simple micro grid configuration. In the preliminary experiments this environment implements some simple and static agent behaviors and energy negotiation strategies. Additionally, some data analysis experiments were performed to predict the renewable energy production, using different machine learning algorithms and real data from different sources. Preliminary results showed that the short term prediction presented very accurate results for PV system, while the results for wind system were not so good, given the higher instability of wind speed. The long term prediction showed worse results, which were already expected given the higher variability of weather conditions in long term and the inaccuracy of meteorological data forecasts.

Future work aims to improve the simulation environment to support more micro grid features and agent negotiation strategies. Also, it will focus in the development of predictive capabilities for consumer agents.

## References

1. Fang, X., Misra, S., Xue, G., Yang, D.: Smart Grid - The New and Improved Power Grid: A Survey. *IEEE Communications Surveys & Tutorials* 14(4), 944–980 (2012)
2. Monteiro, C., Fernandez-Jimenez, L.A., Ramirez-Rosado, I.J., Munoz-Jimenez, A., Lara-Santillan, P.M.: Short-term Forecasting Models for Photovoltaic Plants: Analytical versus Soft-computing Techniques. *Mathematical Problems in Engineering* 2013 (2013).
3. Kojima, T., Fukuya, Y.: Microgrid System for Isolated Islands. *Fuji Electric Review* 57(4), 125–130 (2011)
4. Jennings, N.R.: An Agent-Based Approach for Building Complex Software Systems. *Communications of the ACM* 44(4), 35–41 (2001)

5. Kulasekera, A., Gopura, R., Hemapala, K., Perera, N.: A Review on Multi-agent Systems in Microgrid Applications. In: IEEE PES Innovative Smart Grid Technologies. pp. 173–177. IEEE (2011)
6. Sagiroglu, S., Sinanc, D.: Big Data: A Review. In: Int. Conf. on Collaboration Technologies and Systems. pp. 42–47. IEEE (2013)
7. Katal, A., Wazid, M., Goudar, R.H.: Big data: Issues, Challenges, Tools and Good Practices. In: 6th IEEE International Conference on Contemporary Computing (IC3'13). pp. 404–409. IEEE (2013)
8. Wu, X.D., Zhu, X.Q., Wu, G.Q., Ding, W.: Data Mining with Big Data. IEEE Transactions on Knowledge and Data Engineering 26(1), 97–107 (2014)
9. Witten, I.H., Frank, E., Hall, M.A.: Data Mining: Practical machine learning tools and techniques. Morgan Kaufmann, 3rd ed. (2011)
10. Brano, V.L., Ciulla, G., Falco, M.D.: Artificial Neural Networks to Predict the Power Output of a PV Panel. International Journal of Photoenergy 2014, 1–12 (2014)
11. Badri, A., Ameli, Z., Birjandi, A.: Application of Artificial Neural Networks and Fuzzy Logic Methods for Short Term Load Forecasting. Energy Procedia 14, 1883–1888 (2012)
12. Barbato, A., Capone, A., Rodolfi, M., Tagliaferri, D.: Forecasting the Usage of Household Appliances Through Power Meter Sensors for Demand Management in the Smart grid. In: IEEE International Conference on Smart Grid Communications. pp. 422–427. IEEE (2011)
13. Motamedi, A., Zareipour, H., Rosehart, W.: Electricity Price and Demand Forecasting in Smart Grids. IEEE Transactions on Smart Grid 3(2), 664–674 (2012)
14. Hernandez, L., Baladron, C., Aguiar, J.M., Carro, B., Sanchez-Esguevillas, A.J., Lloret, J., Chinarro, D., Gomez-Sanz, J.J., Cook, D.: A Multi-agent System Architecture for Smart Grid Management and Forecasting of Energy Demand in Virtual Power Plants. IEEE Commun. Mag. 51, 106–113 (2013)
15. Tao, L., Schwaegerl, C.: Advanced Architectures and Control Concepts for More Microgrids. EC Project - Sixth Framework Project for RTD, Tech. Rep. SES6-019864 (2009)
16. Gantenbein, D., Binding, C., Jansen, B., Mishra, A., Sundstrom, O.: EcoGrid EU: An Efficient ICT Approach for a Sustainable Power System. In: Sustainable Internet and ICT for Sustainability (SustainIT). pp. 1–6. IEEE (2012)
17. Vale, Z., Pinto, T., Praca, I., Morais, H.: MASCEM: Electricity Markets Simulation with Strategic Agents. IEEE Intelligent Systems 26(2), 9–17 (2011)
18. Kyriakarakos, G., Piromalis, D.D., Dounis, A.I., Arvanitis, K.G., Papadakis, G.: Intelligent Demand Side Energy Management System for Autonomous Polygeneration Microgrids. Applied Energy 103, 39–51 (2013)
19. Silva, R., Ferreira, A., Ferreira, A., Leitão, P.: Increasing Self-sustainability in Micro Grids using Load Prioritization and Forecasting Mechanisms. In: 10th IEEE Intern. Conf. on Industrial Electronics and Applications (ICIEA'15). pp. 1069–1074. IEEE (2015)

## Cooperative Spectrum Sensing with Energy Detection in Cognitive Radio Networks

A. U. Rehman

Faculdade de Engenharia da Universidade do Porto (FEUP), Porto, Portugal  
asad.rehman@fe.up.pt

**Abstract.** Spectrum sensing is a very important function of cognitive radio to prevent harmful interference with licensed user. In order to increase the usage level of the spectrum holes while maintaining seamless wireless connectivity spectrum sensing must be used. There are several techniques to sense the spectrum. In this paper, one of the popular technique energy detection is investigated. This involves multiple cognitive radios cooperation, coordination and collaboration to detect spectrum holes through energy detection. To achieve this, the optimal data fusion rule is derived. Optimal voting rule and detection threshold are investigated to minimizes the total error rate probability in cooperative spectrum sensing. The proposed method improves the performance of spectrum sensing and increases spectrum utilization.

**Keywords:** Cognitive Radio · Spectrum Sensing · Energy Detection

### 1 Introduction

Over the last decade the rapid growth of high data rate wireless devices, technologies and services create an increasing demand for a wireless spectrum. Globally, mobile networks face a wireless bandwidth crisis and mobile devices are only allowed to use certain frequencies. New emerging Voice and Video services on the internet required far more bandwidth than its available for the current networks. Further to that, On the platform of Software defined radio (SDR) in which modulation, coding, framing and processing are software based. The concept of cognitive radio emerges and an additional Module of Intelligence that can sense, learn and adapt is added to SDR platform and the technology is named as cognitive radio.

In cognitive radio it is possible to use all available frequencies and at the moment radio can communicate only with other radio of the same kind. Cognitive radio enables a new level of interaction and can communicate to any radio and it can quickly adapt to the unusual environment and ensure proper operation of the network [1]. However, the recent studies show that wireless networks today are characterized by a fixed spectrum assignment policy result in poor spectrum utilization. To address this problem cognitive radio technology is proposed that enable the access to the network when it is not occupied by a licensed user and can provide access to the other user in the intermittent period called spectrum

hole or white space. Thus, increases spectral efficiency. The basic task of the cognitive radio (CR) is to detect the licensed user in CR network also known as primary users (PU's). Once, the CR identifies the present or absent situation of PU's. It can improve spectrum utilization to borrow unused spectrum or share the spectrum with an unlicensed user known as Secondary user (SUs) by sensing the radio frequency environment. Moreover, The aim of this cognitive radio technology is to avoid harmful interference between primary and secondary users by utilizing spectrum holes for required throughput and quality of service (QoS).

The main parameters that can detect harmful interference in a cooperative spectrum sensing are probability of false alarm  $P_f$  and probability of detection  $P_d$ . The probability of a user declaring that PU is present when the spectrum is actually not occupied is the probability of false alarm  $P_f$ . In addition to that, the probability of a user declaring that PU is present when the spectrum is actually occupied is the probability of detection  $P_d$  [2]. Later, in the section 4 these terminologies are discussed in detail. Due to miss in the detection can cause the interference. To prevent this, an optimal data fusion rule is defined and the probability of detection is maximized for the constraint of false alarm.

The problem that needs to be addressed in spectrum sensing is hidden terminal, as CR is affected due to multipath fading and shadowing. There is good chance that at the time the primary user occupied the spectrum but it may be possible that CR can't recognize the presence of primary users (PUs). Due to this problem it can cause interference to the licensed user which is strictly not allowed. In order to resolve this issue a spatial diversity technique is exploited based on the location of CR users. The user can share their sensing information to make a combined decision rather than the individual decision of cooperative partner.

The rest of the paper is organized as follows. In Section 2 the roles and approaches of Knowledge-base (brain) in a cognitive radio are discussed, in the vicinity of cognitive radio networks. Section 3 and 4 describes the cooperative spectrum sensing through energy detection and address the hidden node problem in cognitive radio networks and proposed methodology that optimizes Cooperative spectrum sensing through energy detection. Particularly, In section 5 the results were simulated using MATLAB by applying optimal data fusion rule to facilitate cooperative spectrum sensing while satisfying a given error bound. Finally, Conclusions are given in section 6.

## 2 Brain of Cognitive Radio (Knowledge Base)

The Brain of cognitive radio act as a knowledge base. The database that stores all the information of the radio frequency environment in a centralized database as shown in Fig.1. The performance of cognitive radio depends on this knowledge base that contains all the information and characteristic of primary user(PU)such as traffic patterns, locations and power transmitted. This information is used to facilitate the detection processes of PU.

Knowledge base serves as two roles in cooperative sensing. Firstly, to enhance the detection performance by learning statistical models from database. Secondly, it alleviate the burden of cooperative sensing by retrieving the spectrum information such as a list of available PU's that occupied the channel from the given database. This improve spectrum utilization without harmful interference.

The Fig.3 shows knowledge Base of cognitive radio. The following knowledge Base approaches are discussed: Radio Environment Map, Received Signal Strength Profile, Power Spectral Density Maps and Channel Gain Maps. These approaches are useful to provide various information to detect primary user (PU).

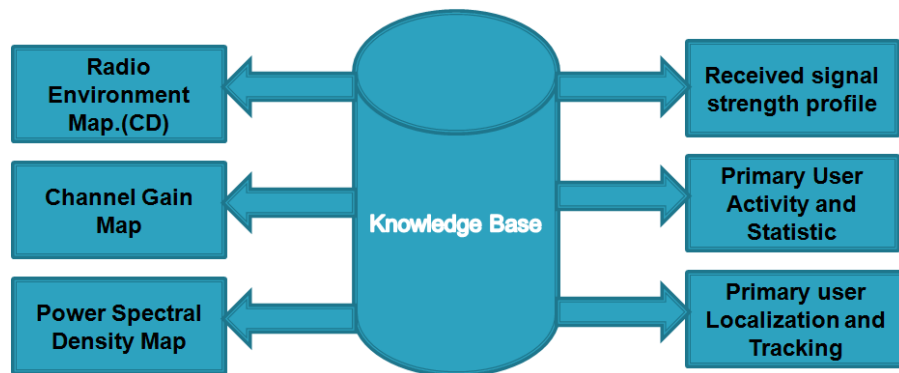


**Fig. 1.** Knowledge Base In CR Spectrum Sensing

## 2.1 Radio Environment Map

In CR networks, radio environment map is a centralized database that is used to access CR user information such as locations, available spectrum and primary user signal type [3]. Thus, it can improve detection performance in local and cooperative sensing. However, radio environment map contain large overhead due to the large information access and transfer between CR users.

## 2.2 Received Signal Strength Profile

In this module each cooperative user combines the received signal strength(RSS) sample and establish statistical distribution at each CR's locations. Moreover, each user estimates the noise power distribution for RSS profile. RSS profile is very important for the frequency and time variations.

### 2.3 Power Spectral Density Maps

In [4], a power spectral density (PSD) map is proposed based on distributed cooperative sensing. In this, CR users locally collect PSD map and exchange messages with on hop-neighbours. This method is adapted to the environment changes and with these maps user location power of the primary user transmitter can be tracked and justified.

### 2.4 Channel Gain Maps

In [5, 6], another techniques to track the primary User (PU) locations and their transmit power is proposed by using channel gain maps in a cooperative sensing environment. In this scheme, each CR user maintains the metric details of the parameters of the channels including shadowing, loss and fading. The Kalman Filtering is used in order to track fading at any point within the area.

## 3 Energy Detection

In this paper energy detection technique is selected in order to sense a spectrum and it is a very popular method for detection of the unknown signal [7]. The block diagram of energy detection is shown below:

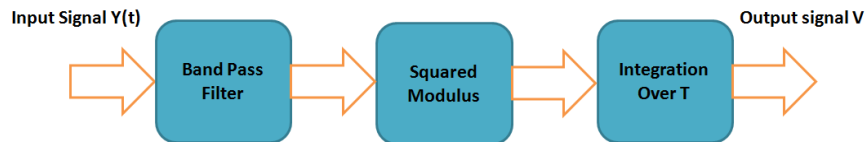


**Fig. 2.** Energy Detection in Spectrum sensing

Initially, Input signal  $Y(t)$  is filtered in order to limit noise and only permits a certain range of frequencies. Next to that, in the Fig.2. there is energy detector block that consist of squaring device and then in last finite time integrator. The output of the integrator at any time is the energy of the input to the squaring device over the interval  $T$  [8]. The output signal  $V$  from the integrator is given by (1):

$$V = 1/T \int_t^{t-T} |Y(t)|^2 dt \quad (1)$$

In last, this output signal V is compared to the threshold n in order to decide, whether a signal is present or not. The threshold is set according to statistical properties of the acquired output V.

As a matter of fact, several signal detection techniques are used in order to enhance the detection probability. The Energy detection method is optimal because of its simplicity and no priori knowledge of primary user (PU) signal is required. This method is also optimal for detecting any unknown Zero-mean constellation signals.

#### 4 Spectrum Sensing

One of the important requirement of the cognitive radio (CR) is to sense the radio frequency environment and identify spectrum holes. CR are designed in such a way that it learn and adapt the radio frequency environment quickly by detecting that the primary user is receiving data within the communication range of CR user. However, Practically it is not easy to estimate channel directly based on the local observation of CR Users [9]. To make most out of it, CR communication is performed before allowing the Unlicensed user to access a vacant licensed channel. The idea of the spectrum sensing is formulated as a binary hypothesis and the CR spectrum sensing is to be decide between the following given hypothesis (2):

$$X_i(t) = \begin{cases} n_i(t), & H_0 \\ h_i * s(t) + n_i(t), & H_1 \end{cases} \quad (2)$$

Where;  $\mathbf{X}_i(t)$  : Observed signal at the *i*th Cognitive radio.

$h_i$  : Complex Channel Gain between PU and *i*th Cognitive Radio.

$s(t)$  : PU Signal.

$n_i(t)$  : Additive White Gaussian Noise(AWGN).

$H_0$  : Primary user absent.

$H_1$  : Primary user operation presence absence statistics.

Moreover, the radio frequency energy in the channel is measured over a fixed bandwidth W and an observation time window T for the purpose of whether the channel is vacant or occupied. As shown in Fig.3. A scenario of cognitive radio networks composed of "K" cognitive radio (Secondary User) with the common receiver is illustrated. The common receiver act as a base station (BS) and manage information of cognitive radio networks and associated K cognitive radios.

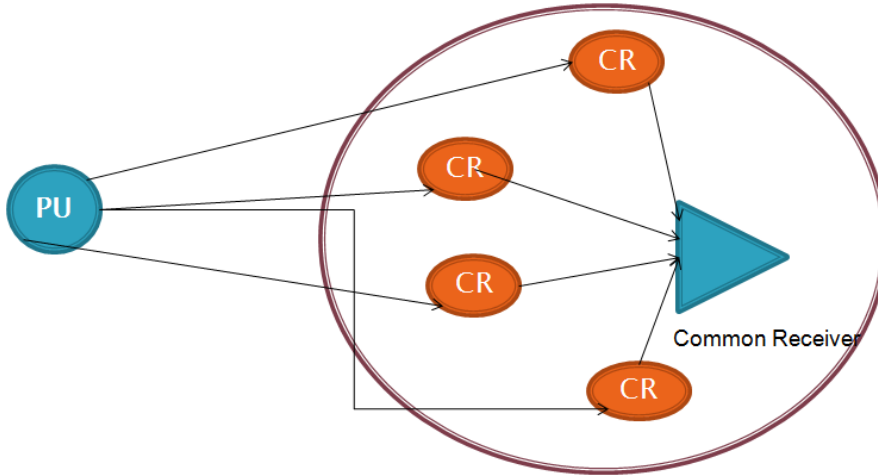


**Fig. 3.** Spectrum Sensing Configuration in Cognitive Radio Networks

It is also assumed that cognitive radio performs local spectrum sensing independently.

For the detection of performance the probabilities of detection and false alarm are defined as below:

$$P_d = P\{\text{decision} = H_1/H_1\} = P\{Y > \lambda/H_1\} \quad (3)$$

$$P_f = P\{\text{decision} = H_1/H_0\} = P\{Y > \lambda/H_0\} \quad (4)$$

Where: "Y" is the decision statistics and " $\lambda$ " is the decision threshold.

## 5 Cooperative Spectrum Sensing

As highlighted earlier on of the challenge of the spectrum sensing in cognitive radio is hidden node problem that is caused when the cognitive radio is shadowed. To resolve this issue multiple cognitive radio coordinate and then send

the decision to the common receiver by mutual cooperation and it can greatly increase the probability of detection because of the combined sensing decision rather than individual sensing. In a cognitive radio environment spectrum sensing is performed as [10]:

**Step 1:** Every cognitive radio  $i$  performs local spectrum sensing independently and then make decision  $D_i \in \{0, 1\}$  for all  $i = 1, \dots, K$ ;

**Step 2:** All Cognitive radios forward the binary decision to the common receiver. In the case of Cellular communication it forward the decision to the Base station (BS) .

**Step 3:** Based on step 2 the common receiver combines those binary decisions and makes a final decision  $H_0$  or  $H_1$  to infer the presence or absence of the primary User (PU) in the observed frequency band.

In the above step by step process of cooperative spectrum sensing each individual cognitive radio  $i$  make a binary decision based on its local observation and forward it to common receiver. At the common receiver, all 1-bit decision are fused together to the following logic rule:

$$Z = \sum_{i=1}^K D_i \begin{cases} \geq n, & H_1 \\ n <, & H_0 \end{cases} \quad (5)$$

Where: Z=Logic Rule

Data Fusion and Process of Result i.e  $D_i \in \{0, 1\}$ .

$H_0$  and  $H_1$  here denotes the inferences drawn by the Base station (BS) that the primary user (PU) signal is transmitted or not transmitted [11]. The Equation(5) demonstrates that BS infers the PU signal is being transmitted, i.e.,  $H_1$ . When there exist at least  $n$  out of  $K$  cognitive radios inferring  $H_1$ . Else, the BS decides that the PU signal is not being transmitted denoted by  $H_0$ . The OR and AND logic are applied which corresponds to the case of  $n=1$  and  $n=K$  respectively.

It is assumed here, that the distance between two cognitive radio is small as compared with the distance from any other cognitive radio to the primary transmitter. Therefore, the received signal at each cognitive radio experiences almost identical path loss [11].

Now, let us consider a scenario of Rayleigh fading with instantaneous SNR'S in independently and identical distributed(i.i.d)over RF environment. Moreover, it is also to be assumed here, that all the cognitive radio use the same threshold level  $\lambda$ .

This results in  $P_f$  being independent of  $i$  and denoted by  $P_f$ . In the case of an AWGN channel  $P_d$  is independent of  $i$  and denoted by  $P_d$ . However, in the

case of a Rayleigh fading channel it is assumed that  $P_d$  to be  $P_d$  and averaged over the statistics of instantaneous SNR's over time.

For the both kind of channel we get the expression(6) that define the average probability of miss detection stated below:

$$P_m = 1 - P_d \quad (6)$$

The probability of false alarm in cooperative spectrum sensing is given in (7) as a generalized Marcum Q-function:

$$\begin{aligned} Q_f &= \text{Prob}\{H_1/H_0\} \\ &= \sum_{l=n}^k \binom{k}{l} [\text{Prob}\{H_1/H_0\}]^l [\text{Prob}\{H_0/H_0\}]^{k-l} \\ Q_f &= \sum_{l=n}^k \binom{k}{l} P_f^l [1 - P_f]^{k-l} \end{aligned} \quad (7)$$

The missed detection probability of cooperative spectrum sensing is given in (8)as a generalized Marcum Q-function:

$$\begin{aligned} Q_m &= \text{Prob}\{H_0/H_1\} \\ Q_m &= 1 - \text{Prob}\{H_1/H_1\} \\ &= 1 - \sum_{l=n}^k \binom{k}{l} [\text{Prob}\{H_1/H_1\}]^l [\text{Prob}\{H_0/H_1\}]^{k-l} \\ Q_m &= \sum_{l=n}^k \binom{k}{l} P_d^l [1 - P_d]^{k-l} \end{aligned} \quad (8)$$

The  $Q_f$  and  $Q_m$  are generalized Marcum Q-function average over the SNR distribution and the total error rate is defined as the sum of  $Q_f$  and  $Q_m$ .

## 6 Simulation Results and Analysis

The main metric of sensing performance is to either minimize the miss detection probability for a target false alarm or in other case minimize the false alarm probability for a target miss probability. In this paper investigation of the total

error rate probability  $Q_f+Q_m$  in terms of several parameters has been carried out and simulation were performed in order to predict optimal data fusion rule and optimal energy detection threshold.

The investigation of the threshold level with total error probability is carried out to improve the spectrum sensing performance and to reduce the collision probability while cognitive radio user is functional in the energy detection spectrum sensing environment. The simulation was performed using MATLAB in order to determine the optimal data fusion rule, optimal energy detection threshold and the total number of cognitive radios required for cooperative spectrum sensing without any harmful interference.

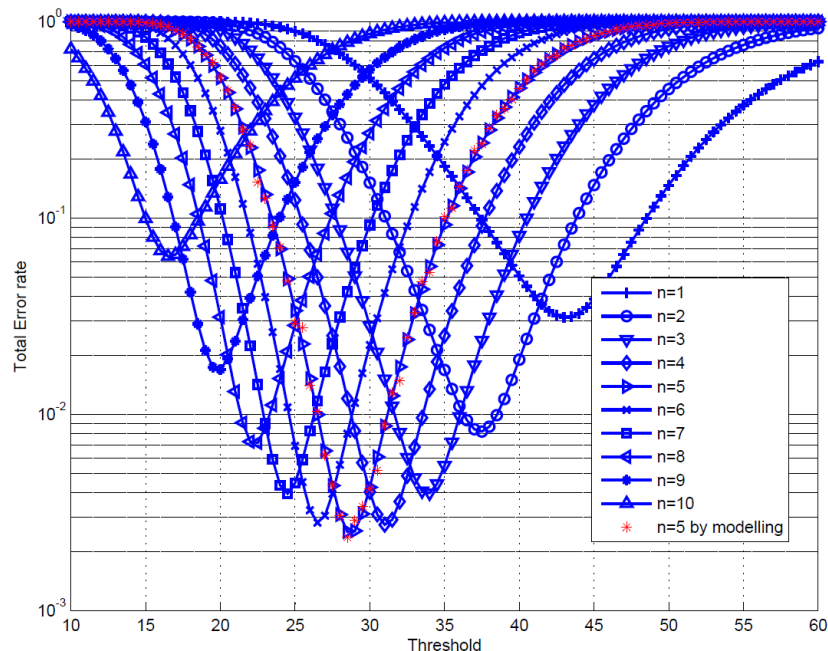


**Fig. 4.** Total error probabilities Vs detection threshold for various for  $n=1-10, K=10$  and SNR 10dB

Let us discuss some intuitive results shown in Fig.4.Which shows that the total error rate with respect to the detection threshold for various data fusion rules from  $n=1$  to  $n=10$  in cognitive networks with only 10 users. It is examined that the optimal voting rule over the all examined range of values of detection threshold is  $n=5$  . Although, for a very small fixed threshold level, the optimal is the AND rule i.e  $n=10$ .Similarly, for a large fixed threshold, the OR rule i.e

$n=1$ , consider to be optimal.

Further to that, in Fig.4. it can be also observed that the total error rate curve is a convex function of the detection threshold for any given value of  $n$ . Moreover, this refers to only one value of the threshold exists which is useful to minimize the total error bound. Therefore, the result obtained from Fig.4. satisfy the criteria of optimal fusion rule that will facilitate the cooperative spectrum sensing of the cognitive radio and determine the presence or absence of primary user(PU) in a real-time Radio frequency environment without any harmful interference. Thus, increases spectrum utilization through cooperative spectrum sensing of cognitive radios. As a result, the spectrum can be used more efficiently.

## 7 Conclusion

Cooperative Spectrum sensing through energy detection is a better technique to improve detection performance in a cognitive radio networks. In this study, it has been found that the optimal data fusion rule minimize the total error rate probability, while satisfying a given error bound. The proposed scheme provides better spectrum sensing performance under set optimal data fusion rule.

## References

1. T. Charles, Dynamic Spectrum Access In Cognitive Radio Networks, Thesis by Thomas Charles (2006).
2. D.Oh and Y.Lee , Energy Detection Based Spectrum Sensing for Sensing Error Minimization in Cognitive Radio Networks, International Journal of Communication Networks and Information Security (IJCNIS) Vol. 1, No. 1, pp.1-5,(2009).
3. Ian F et al., Cooperative spectrum sensing in Cognitive radio networks: A survey, Physical Communication 4, pp 40-62,(2011).
4. S.J. Kim, E. DallAnese, G. Giannakis, Sparsity-aware cooperative Cognitive radio sensing using channel gain maps, in: Conference Record of the Forty-Third Asilomar Conference on Signals, System and Computers pp. 518522,(2009).
5. S.J. Kim, E. DallAnese, G.B. Giannakis, Cooperative spectrum sensing for Cognitive radios using kriged kalman filtering, IEEE Journal of Selected Topics in Signal Processing, (2010).
6. A. Min, K. Shin, An optimal sensing framework based on spatial RSS profile in Cognitive radio networks, in: Proc. of IEEE SECON,pp. 19,(2009).
7. J.Nautiyal and R.Kumar,Spectrum Sensing In Cognitive Radio Using Matlab,International Journal of Engineering and Advanced Technology (IJEAT) ISSN: 2249-8958, Vol.2, Issue-5,pp 529-533,(2013).
8. M. Hossain,Energy Detection Performance of Spectrum Sensing in Cognitive Radio, I.J. Information Technology and Computer Science(IJITCS),pp 11-16, (2012).
9. W. Zhang et.al,Optimization of Cooperative Spectrum Sensing with Energy Detection in Cognitive Radio Networks, IEEE Transactions On Wireless Communications, VOL. 8, NO. 12, DECEMBER pp. 5761-5766(2009).
10. W. Zhang et.al,Cooperative Spectrum Sensing Optimization in Cognitive Radio Networks,ICC proceedings,pp 3411-3415(2008).
11. E. Peh and Y.-C. Liang, Optimization for cooperative sensing in cognitive radio networks, in Proc. IEEE Int. Wireless Communication. Networking Conf., Hong Kong, Mar. 11-15,pp 27-32(2007).

## Topic Modeling - A Case Study with Scientific Production

Rui Sarmento

Faculty of Engineering, University of Porto  
Rua Dr. Roberto Frias, s/n  
4200-465 Porto, Portugal  
[mail@ruisarmento.com](mailto:mail@ruisarmento.com)

**Abstract.** The automatic extraction of topics from text is an area of research with a fast evolution in recent years. We use two different methods for topic extraction, Latent Dirichlet Allocation (LDA), and Term Frequency-Inverse Document Frequency (TF-IDF) and compare them in several experimental situations. We also test the use of stemming processing of data in the context of our dataset and with topic extraction in mind. We study these methods by applying them to a dataset composed by scientific literature production. These documents are the 2014 work of researchers from the Czech Republic. The results obtained are conclusive and provide decision support for the choice between these methods with our dataset. TF-IDF provided better results when compared with LDA. Additionally, TF-IDF with clustering approached LDA with increasing size of analyzed text data. Finally, all methods increase quality when applying stemming to the data. The goal is to provide, in a near future, a complete prototype developed for the purpose of the study and visualization of affinity between authors and their topics of studies or research.

**Keywords:** NLP · Researchers Dataset · Topic Modeling

### 1 Introduction

Some authors, for example, Blei [3], emphasize that generative statistical and distribution models for text have the potential to make important contributions to the statistical analysis of large document collections. One example of these generative models is the topic model. These models enable the use of refined statistical methods to identify the structure that underlies a set of words combined in phrases. Topic models might use many of the key assumptions behind Latent Semantic Analysis (LSA) but enabling the identification of a set of interpretable probabilistic topics rather than a semantic space. Investigating these models provides the opportunity to expand both the practical benefits and the theoretical understanding of statistical language learning.

Our contribution with this work is the study of clustering and its implications when applied to the author's data. We experiment with the TF-IDF

matrix, and after applying cosine similarity to it. We aim to find representative elements in the cluster division of the obtained authors similarity data and their topics. We use these extracted topics from the exemplar or central element of the cluster to generalize to every cluster's element. We provide a comparison with a well-known benchmark method and obtain results for our dataset. We also test the application of stemming in topic extraction and provide results of this experiment.

Regarding the structure of this document, we start by including milestones and breakthroughs regarding topic model in 2. Topic modeling will be the main task regarding the goals of this research. Then, we also provide a brief statistical analysis of the dataset used for these experiment tasks in 3. We introduce the methodology for our experiments with topic modeling in 4. The results we obtained with our data are presented in 5 and finally, we conclude this document in 6 providing also some thoughts on the future work or necessary studies to improve this research.

## 2 Related Work

Several studies have already addressed Topic Modeling. This section first introduces related work with a more generic approach including an overview of research in this area. The selected publications imply milestones or novelties regarding this subject of Natural Language Processing (NLP) related research.

In a second subsection we introduce related work regarding Topic Modeling applied to scientific research data. Thus, we describe the previous NLP applications developed, focusing on research text data.

### 2.1 Topic Modeling - Milestones and Approaches

Lin and Hovy claim that only about 30% of topic keywords are not mentioned in the text directly [9]. The authors conclude that only about 30% of the humans' abstracts in this domain derive from some inference processes. They also conclude that in a computational implementation, only about the same amount has to be derived by processes yet to be determined with further research. The authors wrote that the titles contain about 50% of the topic keywords; the title plus the two most rewarding sentences provide about 60%, and the next five or so add another 6%. The authors, therefore, conclude that a fairly small number of sentences provides 2/3 of the keyword topics.

Lin and Hovy provide empirical validation for the Position Hypothesis. The authors also describe a method of deriving an Optimal Position Policy for a collection of texts within a genre, as long as a small set of topic keywords is defined with each text. The Precision and Recall scores indicate the selective power of the Position method on individual topics. Additionally, the Coverage scores indicate a kind of upper bound on topics and related material as contained in sentences from human-produced abstracts.

Lean and Hovy evaluations treat the abstract as ideal - the authors rest on the assumption that the central topic(s) of a text are contained in the abstract made of it. In many cases, this is a good assumption; it provides what one may call the author's perspective of the text. But this assumption does not support goal-oriented topic search, in which one wants to know whether a text pertains to some particular prespecified topics.

Topic models have also been extended to capture some properties of language, such as the hierarchical semantic relations between words [4], and the interaction between syntax and semantics [6].

Titov and McDonald [14] presented multi-grain topic models and claimed that they are superior to standard topic models when extracting ratable aspects from online reviews. According to the authors, these models are suited to this problem since they enable the identification of important terms, but also cluster them into consistent groups, which is a handicap of previously proposed methods.

AlSumait et al. [2], developed an online topic model for discrete data to model the temporal evolution of topics in data streams. The researchers used a non-Markov on-line LDA Gibbs sampler topic model (OLDA), in which the current model, along with the new data, guide the learning of a new generative process that reflects the dynamic changes in the data. They achieved this by using the generated model, at a given time, as a prior for LDA at the successive time slice, when a new data stream becomes available for processing. The weight of history in the generative process can be controlled by the weight matrix depending on the homogeneity of the domain. The authors claimed that the model results in an evolutionary matrix for each topic in which the evolution of the topic over time is captured. In addition, the authors proposed an algorithm to detect emerging topics based on the framework of OLDA. By processing small subsets of documents only, OLDA is claimed to enable the learning of meaningful topics, in some cases with higher quality than the LDA baseline. Additionally, the authors claim their method also outperforms LDA in detecting topics represented by a small set of documents at a certain point in time.

Sendhilkumar et al. [13], claim that their hPAM method is better to topic model research articles as the authors experienced better performance in terms of accuracy, precision and recall for retrieval of relevant documents. The authors include originality (inverse of similarity) as a parameter to define novelty in the documents. The described approach is not fully quantitative as it considers the semantics of concepts in the research article. The authors add they will be focused in further implementations and a qualitative approach for research articles, involving sentence importance and sentence contribution to novelty.

Gansner et al. [5], experiment streaming topic extraction with LDA and TF-IDF and argued that when extracting topics from short texts like twitter posts, the authors have better results with TF-IDF. Nonetheless, the authors did not experiment with the online version of LDA, the OLDA. According to the previous cited publication [2], when compared with LDA, OLDA presents better results than LDA for some use cases.

## 2.2 Topic Modeling of Scientific Production

The vast majority of the analysis of scientific production uses citations [12]. This includes the analysis of metrics as the frequency, patterns and graphs of citations in scientific written production like articles and books. Another approach already explored is the discovery of similarities between researchers. It was addressed by Price et al. [11], aiming to facilitate the process of paper distribution to reviewers. Their web-based methodology, called SubSift [11], retrieves researcher profiles based on their publications. These profiles enable a typical Information Retrieval task. The papers submitted to a scientific conference – playing the role of Query in IR – are compared with different profiles, in order to optimize the task of attributing articles for review.

Another approach was presented by Trigo et al. [15]. The authors present an Information Retrieval tool that facilitates the task of the user when searching for a particular information that is of interest to him. Trigo et al. [15] propose a system that processes a dataset of documents to produce a graph. This graph nodes represent documents and the links define similarities between nodes. The authors aim to offer the user a tool to navigate in the space of documents in an easy way. The authors present a case study that shows affinity groups based on the text production of researchers, beyond the previously established communities revealed by co-authorship. It characterizes the activity of each author by a set of automatically generated topics/keywords and by membership to a particular affinity group. The authors also provide validation methods of the most relevant information to be retrieved from researchers publications, analyse the impact of titles, abstracts and keywords on capturing the similarity between researchers.

Topic models such as LDA [4] and hierarchical models [8] have been successfully applied to various publications such as The American Political Science Review and Science. The work of Hall et al. [7] introduce the study of the history of ideas developments by using LDA and topic entropy. In [10] the authors extend over the work of Hall et al. [7] by adding two related fields (Linguistics and Education) and by employing various novel topic models for scientific research analysis.

## 3 Case Study

In this case study, we selected R&D publications from Czech Republic researchers. The dataset is publicly available in [1]. The dataset can be exported to a .html file or .xls. This dataset has a high amount of information including research area for each publication, authors, titles, abstracts, keywords, type of publication (which might include conference papers, book chapter, conference proceedings, patents, software, algorithms among many others), author's research institution and others. This is a complete source of information and there is information for dozens of years starting from around 1985 until 2015. The high quality and high organization of this structured data make it a good source for text mining or NLP tasks.

After exporting the data for 2014, we selected conference papers and book chapters only. Therefore, the number of publications was reduced from around 25000 to 5110 publications. For this amount of publications, we selected the titles and abstracts for our NLP tasks. In average, the titles have 11 words and the abstracts have 240 words. This amount of publications represents approximately 2800 different first authors.

Pre-processing the data is important in an information retrieval context since we are interested in reducing noise in data. Thus, by treating the text, we achieve less entropy in our models and achieve better results from automatic machine learning procedures. The pre-processing of data included the following sequence of procedures:

1. removal of whitespaces
2. removal of stopwords
3. removal of punctuation except hyphenated compounds
4. removal of numbering
5. convert every word to its lowercase version

This pre-processing was completely done with the *tm* package available for R language.

After text data pre-processing, there are 38544 terms in titles and 822888 terms in abstracts. It is visible that the titles have high sparsity with few words repeated many times and a high amount of words existing only one time. Fig. 1 representation of frequency distribution makes us conclude that it is approached by a power law distribution.

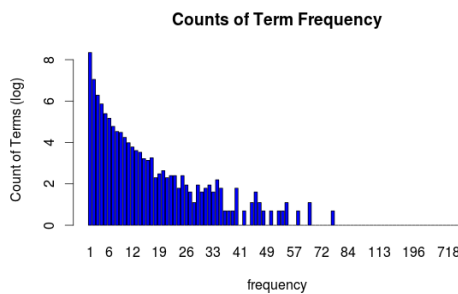


**Fig. 1.** Frequencies Counting for Titles Words

The distribution of words in abstracts is represented in Fig. 2. It is visible that the abstracts have high sparsity with few words repeated many times and a high amount of words existing only one time. Again, as previously with the titles, this representation of frequency distribution makes us conclude that it is

approached by a power law distribution. This is an expected characteristic when studying text data.

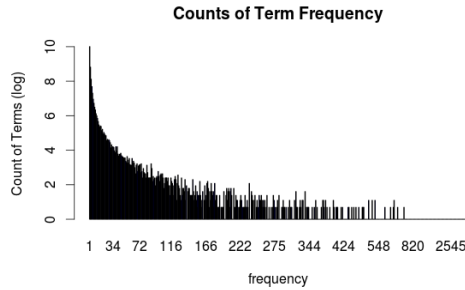


**Fig. 2.** Frequencies Counting for Abstracts Words

Both previous figures were smoothed by application of a logarithmic function to the values of frequency occurrences.

#### 4 Methodology

With the described data we are interested in finding topics in the documents available in the dataset. Our approach to the data has several possibilities. Succinctly, we can study:

- Titles of publications
- Abstracts of publications
- Titles and Abstracts concatenated

Additionally, the data available enables the use of the provided authors keywords to validate all experimented methods and their results. Since we have the goal to find an affinity between authors and topics, we are interested in finding the topics each author approaches in their publications. Thus, we concatenate every author's publications in one document for each author. This is true either for titles, abstracts or titles plus abstracts. To evaluate, we proceed to group all author's keywords in one document for each author.

The procedure used to extract the topics relies on experimenting with two distinct methods, LDA and TF-IDF. For these methods we find the similarity of the extracted topics/keywords with the keywords provided manually by the authors. In the end, we have the similarity/overlapping results for every author and regarding both methods. Additionally, we extend the TF-IDF method, by finding clusters of authors in the cosine similarity matrix, obtained from TF-IDF matrix. Then, we generalize the extracted topics of the central author (the

exemplar or centroid) in each cluster, for every author belonging to the individual cluster.

#### 4.1 Extraction of Topics

We used two different methods to extract the topics from the data. Following some related work we opted for LDA [4] and TF-IDF. For this task, we used the R language implementation of LDA from the package *topicmodels*. The TF-IDF method was applied to the data by using the package *tm* also for R language.

**4.1.1 LDA** The intuition behind LDA is that documents have multiple topics. Furthermore, knowing that the document blends those topics would help you situate it in a, for example, collection of scientific articles. LDA is a statistical model of document collections that tries to capture this intuition. It can be described by the generative process associated to this method. This process involves randomly selecting a model assumed to be one the documents arose from.

Blei et al. [3, 4] formally define a topic to be a distribution over a fixed vocabulary. For example, the *streaming* topic has words about streaming with high probability and the *clusterization* topic has words about clusterization with high probability. Then, for each document in the collection, the authors generate the words with a process involving two stages.

1. Randomly choose a distribution over topics
2. For each word in the document
  - (a) randomly choose a topic from the distribution over topics in step 1
  - (b) randomly choose a word from the corresponding distribution over the vocabulary

This statistical model reflects the intuition that documents exhibit multiple topics. Each document exhibits the topics in different proportion (step 1). Additionally, each word in each document is drawn from one of the topics (step 2b), where the selected topic is chosen from the per-document distribution over topics (step 2a).

The distinguishing characteristic of LDA is all the documents in the collection share the same set of topics. Nonetheless, each document exhibits those topics in different proportion.

**4.1.2 TF-IDF** TF-IDF is typically a computationally less complex option to calculate similarity using word counts. Since this counting can be biased toward common words in the documents, some adjustments have to be done. Thus, the term counting is weighted by the inverse of the number of appearances of the same term in the documents. We can mathematically formalize this the following way:

- Let  $D$  be the set of documents,  $d \in D$ , a document consisting of a sequence of words (terms), and  $t$  a particular term of interest in  $d$ . Then the scaled word count based on TF-IDF is

$$tfidf(t, d) = tf(t, d) * idf(t, D) \quad (1)$$

where  $tf(t, d)$  is the fraction of times the term  $t$  appears in  $d$ , and  $idf(t, D)$  is the logarithm of the inverse of the proportion of documents containing the term.

**4.1.3 TF-IDF with Clustering** The similarity of documents can then be calculated by cosine similarity of the TF-IDF vectors. After calculating similarity, we can extract the clusters presented in the author's list with the *apcluster* package for R language. Finding clusters, in this case, will signify that we have similar authors grouped together. We assume these authors are similar because they approach similar topics of studies. Then, for each cluster, we find the exemplar i.e. the central author, and assume the cluster topics is represented by the exemplar topics. We validate this assumption by iterating, for each cluster's authors, and then comparing the cluster's topics with the cluster's authors keywords.

## 4.2 Stemming

For further research about the results from both models, and since we are validating the models with the author's keywords, we are interested in finding the root of the words resulting from the automatic extraction and the root version of the keywords themselves.

It is commonly described that stemming is the term used in linguistic morphology and information retrieval to describe the process for reducing inflected or sometimes derived words to their word stem, base or root form. Frequently, the stem is not identical to the morphological root of the word. Additionally, it is usually sufficient that related words map to the same stem, even if this stem is not, in itself, a valid root.

For example, a stemming algorithm reduces the words "streaming", "streamed", and "streamer" to the root word, "stream". Another example, the words "endue", "endued", "endues", "enduing" reduce to the stem "endu". This last case exhibits a situation where the stem is not itself a word or root. By using stemming, we expect that both models increase the similarity with the keywords. This is a result of normal use by the authors of different forms for the same stem in different textual situations like, for example, in titles, abstracts or keywords. Further developments will be presented in the following sections.

For this task, the R language was used, more specifically the *tm* package. This package provides the possibility of executing stemming of a Corpus of documents.

### 4.3 Evaluation of topics/keywords generated

To validate and compare both LDA and TF-IDF results, we use a similarity measure to compare the author's keywords and the model results for topics extraction. The following formula describes the method to find this similarity:

$$\text{similarity} = \frac{\text{common}^2}{c(w_K) * c(w_M)} \quad (2)$$

where *common* is the intersection of both groups i.e. the number of words that appear in both the results and the keywords.  $c(w_K)$  and  $c(w_M)$  are the total number of words the author's keywords group has and the method (LDA or TF-IDF) provides, respectively. The values for the TF-IDF method similarity are calculated with the topics extracted from each author's TF-IDF matrix row, and by selecting every term with value superior to 0. Additionally, with LDA, we used all terms generated by the method for each author's topics.

## 5 Results

The results presented in this section were all obtained with the use of R language. The results are presented to provide a clear comparison between LDA and TF-IDF methods applied to our data. We provide a comparison of the LDA method and the TF-IDF method with and without clustering. Finally, we also provide the same experiments but applying stemming to the data in the validation process.

### 5.1 LDA vs TF-IDF

The average similarity results are presented here to provide a comparison for all methods. This average similarity is calculated with all first authors in the dataset.

**5.1.1 Without Clustering** In this section, we present a comparison between LDA and TF-IDF results for each author. Using only the titles, the average similarity for LDA is 0.176 and with TF-IDF is 0.217. For the abstracts, with LDA, the average similarity is 0.040. Additionally, with TF-IDF, the value is 0.105. Regarding the titles plus the abstracts, with the LDA method, the average similarity is 0.029. With TF-IDF, this value is 0.103.

**Table 1.** Average Similarity with LDA and TF-IDF without Clustering

Topic Extraction Method	Average Similarity		
	Titles	Abstracts	Titles + Abstracts
LDA	0.176	0.040	0.029
TF-IDF	0.217	0.105	0.103

Table 1 presents results that indicate TF-IDF is better than LDA in the extraction of topics when these topics are compared with the author's keywords.

**5.1.2 With Cluster Exemplars** In this section, we provide the comparison between LDA results for each author and the TF-IDF results obtained by generalizing the cluster's exemplar and its extracted topics.

**Table 2.** Average Similarity with LDA and TF-IDF Clustering Exemplars Generalization

Topic Extraction Method	Average Similarity		
	Titles	Abstracts	Titles + Abstracts
LDA	0.176	0.040	0.029
TF-IDF	0.066	0.029	0.029

Table 2 presents evidence the TF-IDF method equals LDA with more data in the studied dataset.

**5.1.3 Using Stemming - With and Without Clustering** In this section, we provide the results for LDA, TF-IDF with clustering and TF-IDF without clustering but using stemming when processing the extracted topics and also author's keywords.

**Table 3.** Average Similarity with stemming and for LDA and TF-IDF, with and without clustering

Topic Extraction Method	Average Similarity with Stemming		
	Titles	Abstracts	Titles + Abstracts
LDA	0.206	0.044	0.033
TF-IDF with Clustering	0.076	0.031	0.032
TF-IDF without Clustering	0.256	0.120	0.118

Comparing table 3 results with previous tables 1 and 2, we emphasize that, by stemming the topic extraction results and also the keywords, leads to better values of average similarity. This result suggests that topic extraction of this dataset improves by using stemming. This is true for every variant of the method or dataset (titles or abstracts, or even titles plus abstracts).

## 5.2 Discussion of Results

Our results indicate that TF-IDF is the best method to automatically extract topics with our dataset. Additionally, with the titles dataset, we obtain better

similarity values which indicate that both models extract more topics/keywords with less tentative provided terms. These topics have, therefore, higher similarity to the keywords provided by the authors. With abstracts or titles plus abstracts, the similarity values are lower. This happens because both models extract more terms and intersect less with the keywords provided by the authors.

Our results, by using clustering, were not conclusive to provide clear improvements in the extraction of topics when compared with the LDA method for each author. We stress that we have conducted a study with one year of data (2014). This short period of data might cause the clustering to have low density. Thus, the elements belonging to the same cluster might not have the expected similarity between them. Additionally, as the amount of data increased, for example, with titles plus abstracts the similarity decreased and is comparable to the similarity obtained with the LDA method. Thus, the exemplar or central element of the cluster might be representative of the cluster's generalization of topics if we had more data. Since we have only one year of data, we have less than 2 publications per year and by each author, which implies more variety of areas of research and, therefore, points in data clusters with higher dispersion. So, a question is, if we had more data, TF-IDF with clustering might be better than LDA?

Another interesting result we obtain from our experiments is the improvement exhibited by applying stemming to our extracted topics and keywords. This indicates that authors use different forms of words selected for keywords, and the same subject inside titles and abstracts text.

## 6 Conclusions and Future Work

This document provides an introduction to the subject of Topic Modeling. This NLP research area is an important task and can be a starting point to applications of NLP in need of documents clustering. In this work, we also do an introduction to the dataset we used in the testing of LDA and TF-IDF with and without clustering. The task to retrieve the topics with both methods from the titles and abstracts data was evaluated by using also the author's own keywords. Additionally, we also tested the methods with stemming processing experiments, to check if we obtain better topic modeling. Stemming proved to be useful when evaluating our model against the author's keywords.

As future work, we are expecting to improve experiments with more data. This might provide better results with the clustering TF-IDF method. The experimentation with LDA with clustering might also be needed to compare both methods. Additionally, we want to develop a prototype for visualization of networks of authors and their affinity regarding topics modeled from the dataset used for this task. We will eventually obtain a global matrix of authors and their affinities/similarity. As each author might be represented by their topics, we can obtain a method resulting in a graph to enable the visualization of the affinity between authors and topics. It is expected that the system will provide high intuitiveness or comprehensibility, in the knowledge or information extrac-

tion, from the visualization of results. Additionally, our goal is also enabling the system to be used with a streaming approach, and will be expected to provide scalability regarding large scale data and documents inputs.

## References

1. Published data from the r&d information system of the czech republic. <http://www.isvav.cz/>, 2015. Accessed: 2015-09-30.
2. Loulwah AlSumait, Daniel Barbará, and Carlotta Domeniconi. On-line lda: Adaptive topic models for mining text streams with applications to topic detection and tracking. In *ICDM*, pages 3–12. IEEE Computer Society, 2008.
3. David M. Blei. Probabilistic topic models. *Commun. ACM*, 55(4):77–84, April 2012.
4. David M. Blei, Andrew Y. Ng, and Michael I. Jordan. Latent dirichlet allocation. *J. Mach. Learn. Res.*, 3:993–1022, March 2003.
5. Emden R. Gansner, Yifan Hu, and Stephen C. North. Interactive visualization of streaming text data with dynamic maps. *J. Graph Algorithms Appl.*, 17(4):515–540, 2013.
6. T. L. Griffiths and M. Steyvers. Finding scientific topics. *Proceedings of the National Academy of Sciences*, 101(Suppl. 1):5228–5235, April 2004.
7. David Hall, Daniel Jurafsky, and Christopher D. Manning. Studying the history of ideas using topic models. In *Proceedings of the Conference on Empirical Methods in Natural Language Processing*, EMNLP ’08, pages 363–371, Stroudsburg, PA, USA, 2008. Association for Computational Linguistics.
8. Wei Li and Andrew McCallum. Pachinko Allocation: DAG-structured Mixture Models of Topic Correlations. In *Proceedings of the 23rd International Conference on Machine Learning*, ICML ’06, pages 577–584, New York, NY, USA, 2006. ACM.
9. Chin-Yew Lin and Eduard H. Hovy. Identifying topics by position. In *ANLP*, pages 283–290, 1997.
10. Michael J. Paul and Roxana Girju. Topic modeling of research fields: An interdisciplinary perspective. In Galia Angelova, Kalina Bontcheva, Ruslan Mitkov, Nicolas Nicolov, and Nikolai Nikolov, editors, *RANLP*, pages 337–342. RANLP 2009 Organising Committee / ACL, 2009.
11. Simon Price, Peter A Flach, and Sebastian Spiegler. Subshift: a novel application of the vector space model to support the academic research process. In *WAPA*, pages 20–27, 2010.
12. R. Rubin. *Foundations of Library and Information Science*. Neal-Schuman Publishers, 2010.
13. S. Sendhilkumar, Nachiyar S N, and G. S. Mahalakshmi. Novelty detection via topic modeling in research articles.
14. Ivan Titov and Ryan T. McDonald. Modeling online reviews with multi-grain topic models. *CoRR*, abs/0801.1063, 2008.
15. Luis Trigo, Martin Vita, Rui Sarmento, and Pavel Brazdil. Retrieval, visualization and validation of affinities between documents. In *KMIS 2015 - Proceedings of the International Conference on Knowledge Management and Information Sharing, part of the 7th International Joint Conference on Knowledge Discovery, Knowledge Engineering and Knowledge Management (IC3K 2015), Volume 3, Lisbon, Portugal, November 12-14, 2015*, pages 452–459, 2015.

## A Review of Recent Developments in Abstractive Summarization Techniques

Jaime Reis Silva<sup>1</sup>

<sup>1</sup>Faculty of Engineering, University of Porto, Porto, Portugal  
pro09008@fe.up.pt

**Abstract.** Abstractive summarization techniques have evolved during the previous years since extraction-based methods fail to achieve a series of requirements necessary for a summary to be efficient. Abstraction aims to mimic the process of summarization in order to make it feel as if it was made by humans. Its main feature is the ability to generate new sentences as a result of the summarization process. Recent approaches include concepts as information items, abstraction schemes, template extraction, summary revision, word graph, and timeline. These ideas are presented.

**Keywords:** Abstractive Summarization · Information Items · Abstraction Schemes · Template Extraction · Summary Revision · Word Graph · Timeline

### 1 Introduction

Summarization is a process that aims to resume, in a few words or sentences, the contents of a large text.

While this has been done manually for centuries, automatic text summarization began in the middle of the 20th century.

An extraction-based approach has been used by the majority of summarization systems. This method selects some original sentences from the source documents to create a short summary [1].

As, in this kind of systems, only a whole sentence of the input text may be selected, there may be some redundancy in the built summary. Compression-based methods deal with this issue by erasing words or phrases that might not add relevant information [2]. This approach still has, however, the limitation that it cannot join facts from different input sentences.

Human-written summaries are more abstractive, which can be regarded as a result of sentence aggregation and fusion [3]. Some researchers have worked on abstraction-based approaches that aim to build a sentence whose elements come from different source sentences.

Important features, such as sentence fusion, have been incorporated [4]. Other works [5, 6] use clustering on sentences in order to determine the salience of topical themes. Then, sentence fusion is applied inside each cluster to create a new sentence with the most relevant elements that may come from different parts of the input texts.

These abstractive methods analyze a whole text, which allows the new sentences to incorporate salient elements across sentence boundary.

This paper addresses recent techniques have been developed to enhance abstractive summarization methods.

## 2 Automatic Text Summarization

One of the most important techniques prior to the described abstraction-based approaches is the bottom-up snippet method.

This process aims to create the summary out of extracted sentences from the input sources. The basic steps of this process are, namely [7], content selection and information ordering.

### 2.1 Content selection

The content selection step focuses on choosing sentences to extract from the input documents. It has three main sub-steps: sentence segmentation, simplification and extraction.

**Sentence segmentation.** This process aims at dividing the text into its different sentences so that they can be more easily analyzed. There are some challenges to be solved; for instance, characters such as “!” and “?” are simple to interpret – they always mark the end of a sentence. “.” is not so obvious – it may or may not be a sentence boundary (e.g. Mr. or 5.87).

A binary classifier, like a decision tree, may be used to decide if the period means an EndOfSentence (EOS) or NotEndOfSentence (Not EOS). This classifier can use manual rules, regular expressions, or machine-learning techniques.

A simple decision tree for deciding whether a period is an EOS or Not EOS is illustrated in Fig. 1.

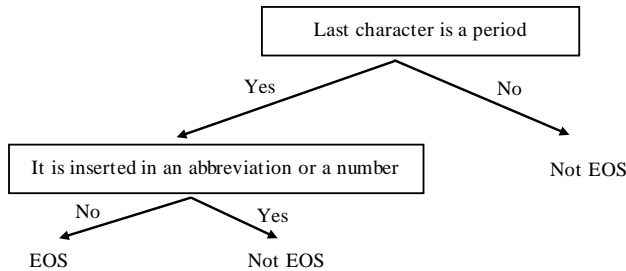


**Fig. 1.** A decision tree for sentence segmentation

More sophisticated features can be integrated in the decision tree, such as the case of the word before the period or the case of the word after the period. It is more likely,

if the period marks the end of a sentence, that the word before the period is lower-case and the word after the period is upper-case.

**Sentence simplification.** This process usually starts by parsing the sentences. Then it prunes some modifiers of the sentences. Modifiers that might be pruned are:

- appositives (e.g. "Paulo Reis, 27, based in Aveiro, made a statement about... ")
- attribution clauses ("Angela Merkel has previously said that..., according to a former adviser to Merkel")
- initial adverbials ("for instance", "for example", "as mentioned before")

**Sentence extraction.** After the previous steps have been taken, there is now a very redundant set of sentences, especially because they might come from different documents about the same event. So, the goal of this process is to select, out of all the sentences, which ones should be used.

This can be achieved using parameters such as maximal marginal relevance. This approach allows us to iteratively choose the best sentence to insert in the summary so far. This sentence should be relevant, having a high similarity to the user's query, and novel, having a low similarity to the summary that has so far been written.

Another way is to score each sentence with maximal marginal relevance and log-likelihood ratio. This allows us to prioritize sentences with words that occurred more than what we expect by chance and with words that occurred in the user's query.

## 2.2 Information ordering

This is the process of choosing an order to place the extracted sequences in the summary.

Chronological ordering is a commonly used method, especially for the summarization of news streams [8]. Coherence is also a criterion that may be used for ordering, allowing us to choose orderings that make neighboring sentences similar. This criterion can be measured by their cosine similarity. If the same entity is mentioned by various sentences that can also mean that there is a high level of coherence [9].

# 3 Abstractive Summarization Techniques

## 3.1 Information item based method

The authors propose a technique [10] where the contents of the summary are created from abstract representations of input documents, rather than of whole sentences from source documents. These information items consist of a subject-object-verb triple; they are the basic element of coherent information perceived in the analyzed text.

New sentences are generated with the information items using a language generator. They will then be scored and ranked according to their document frequency and at least the system builds the summary.

Fig. 2 shows the main steps of this method.

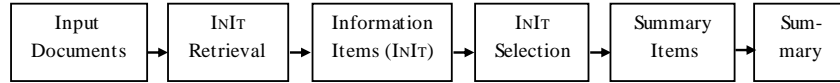


**Fig. 2.** The main steps of the information item based method

### 3.2 Abstraction scheme based method

This information extraction based approach selects abstraction schemes that will be the basic elements for the generation of new sentences [11]. These abstraction schemes consist of manually created rules for information extraction, content selection and generation patterns. Each one of these elements is theme-specific. This implies that the rules for two abstraction schemes will be equal or similar if they address related topics.

**Table 1.** Abstraction scheme paying

Information Extraction	SUBJ(pay,A) → WHO_PAID(A) OBJ(pay,B) → WHO_RECEIVED(B) SUBJ(give,A) → WHO_PAID(A) OBJ(give,B) → WHO_RECEIVED(B)
Content Selection	Selection of the best candidate for A, B and verb
Generation	A verb B

Table 1 shows one abstraction scheme. For the scheme paying, the information extraction rules would match A as the payer entity and B as a receiver entity for the following phrases: A paid B 500 euros, B was given 100 pounds by A.

### 3.3 Template extraction based method

A system that attempts to generate abstractive summaries for spoken meetings was proposed [12].

This method uses a template extraction algorithm, based on Multiple Sequence Alignment. This concept, introduced in biology, refers to the alignment of three or more biological sequences (protein or nucleic acid) of similar length. From the output, affinity can be inferred and the developmental relationships between the sequences studied.

This process is designed to work across a whole range of meeting domains (e.g. faculty meetings, student meetings, project group meetings). The technique's goal is to induce meeting domain-independent templates for the summarization process.

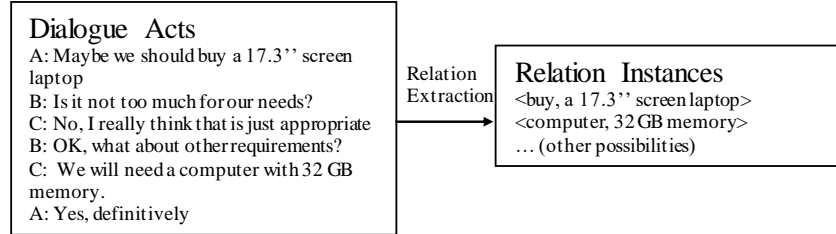


**Fig. 3.** The content selection module

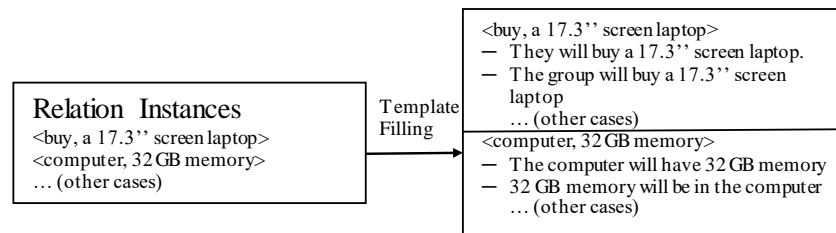


**Fig. 4.** The template filling module

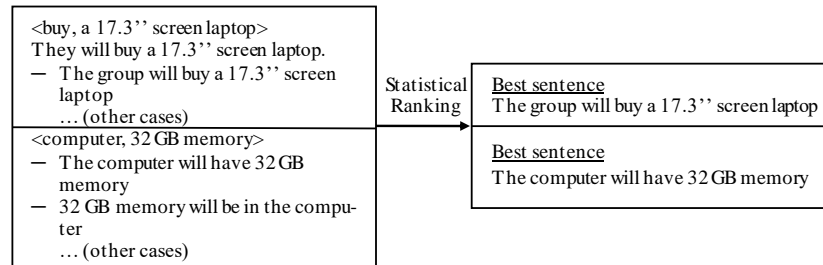


**Fig. 5.** The statistical ranking module

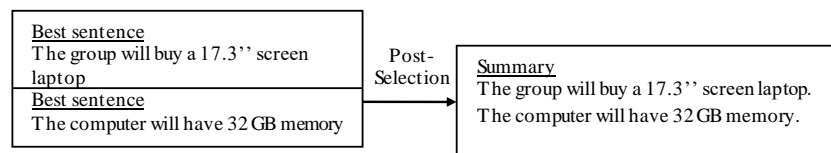


**Fig. 6.** The post-selection module

The summarizer consists of two main components. The first module (Fig.3) selects content by extracting relation instances out of the input dialogues.

The second module creates the summary. It is divided into three sub-steps. The first one (Fig.4) introduces the relation instances in the templates. The second sub-step (Fig. 5) selects the best sentence per relation instance, using a discriminative ranker based on Support Vector Regression. The third sub-step (Fig.6) processes the selected sentences to build the summary.

### 3.4 Summary revision based method

Summary revision was also investigated; this process consists of rewriting people references, phrases, or other features in the summaries [13].

Human written summaries were analyzed to develop a model for making references to people in news summarization. Based on this analysis, a set of rewrite rules was constructed.

Each time a person is mentioned for the first time, a discourse-new reference, the description is longer. Data from all the input documents will be used. When that person is further mentioned, a discourse-old reference, the description will be much shorter, using only the surname.

For a discourse-new reference, if the name of the person is the head of a noun phrase, the process will refer to it as the longest description ever made of that person of every analyzed text so far. If the name of the person is not the head of a noun phrase, the reference will not be rewritten.

A discourse-old reference will use only the person's surname.

This approach makes the summarization process closer to the way a human would do it.

The application of this algorithm allows the summary in Fig. 7 to be rewritten as the one of Fig. 8.

**Margaret Thatcher** was one the most influential personalities of the 1980s in Europe. The UK had, at the time, high unemployment rates. **Thatcher**, the former United Kingdom Prime Minister, became unpopular mainly because of her economic policies. It is remarkable, however, that during the 1980s, a decade dominated by **Thatcher**, personal wealth rose by 80 per cent in real terms.

**Fig. 7.** Example of a summary

**Former United Kingdom Prime Minister Margaret Thatcher** was one the most influential personalities of the 1980s in Europe. The UK had, at the time, high unemployment rates. **Thatcher** became unpopular mainly because of her economic policies. It is remarkable, however, that during the 1980s, a decade dominated by **Thatcher**, personal wealth rose by 80 per cent in real terms.

**Fig. 8.** Rewritten version of the summary from Fig. 7

### 3.5 Word graph based method

This approach is based on a graph-based framework and aims at achieving a high degree of concision in a context of elevated redundancy [14].

The authors propose the use of a graph representing the input text (Fig. 9). In the example, three sentences are graphed: "cable TV is great", "it is too expensive to have

cable TV", and "it is too expensive". Each node contains numbers that express the sentence identifier and the word identifier inside each sentence.

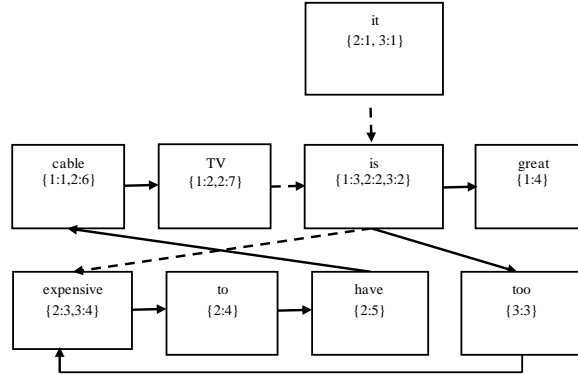


**Fig. 9.** A sample word graph

Three properties of the graph are employed to analyze the diverse subpaths upon which summary is built.

Redundancy capture is one of the properties. The phrase "cable TV" is mentioned in different parts of the sentences, but appears twice, and thus it suggests that its relevance is high.

The second one is gapped subsequence structure. "It is expensive" and "it is too expensive" express basically the same idea, so the word "too" might be ignored in the formation of the summary.

The third property refers to collapsible structures. The word "is" integrates various subpaths. So that fact can be used to merge sentences.

### 3.6 Timeline based method

This system uses timelines to improve the summarization task [15].

The process builds a timeline for each document. These timelines show the relation between events and time expressions. An event refers to a given action, while a time expression refers to a particular day or hour (e.g. "2015 January 1").

Out of each timeline, three features are derived.

The first feature is time span importance, related to the number of events that occur in a particular time interval. Another measurement is contextual time span importance, which takes into account the relevance of neighbor time intervals. The third feature is sentence temporal coverage density, that deals with the number of time intervals that events in a sentence refer.

These features measure the saliency of sentences, allowing the summary to be built upon the most relevant ones.

## 4 Results

The information item based system [10] got in the TAC 2010 summarization evaluation a 0.315 Pyramid score [16], which is better than the average of the automatic systems that participated in TAC 2010.

The abstraction scheme based system [11] generated two sentences for the cluster of documents D1001A-A that contain 8 Semantic Content Units (SCU) for a weighted total of 30 out of a maximum of 56. The respective Pyramid score is 0.54 which is much higher than the average score of 0.31 obtained for that cluster.

The template extraction based system [12] was scored using ROUGE-SU4 on two corpora from disparate domains: the AMI Meeting Corpus [17] and the ISCI Meeting Corpus [18]. The first one is a data set consisting of 100 hours of meeting records where groups of four people discuss a project while the other consists of several naturally occurring meetings, each one having 4 to 10 participants.

For the task of writing a decision summary, the system achieved a 0.07 score; at problem summary, that value was 0.06. It outperformed both two unsupervised baselines, one where the longest dialogue act in each cluster is selected in each summary [19] and another that picks the dialogue act with the largest TF-IDF similarity with the cluster centroid as the summary [20], and two state-of-the-art supervised extractive summarization systems, both based on Support Vector Machines [21],[22].

The summary revision based system [13] was evaluated in a manual way. Four persons analyzed a set of 44 documents. 39 preferences (89%) were for the rewritten summary, 4 (9%) were for the original summary and 1 (2%) has no preference.

The word graph based system [14], Opinosis, was compared to MEAD [23], an extractive multi-document summarizer based on cluster centroids. MEAD was chosen as a baseline. It selects the 2 most representative sentences as summaries. Opinosis has the best ROUGE-SU4 scores.

The timeline based system [15] was experimented, using another summarization system, SWING [23]. This is based on a supervised extractive method that ranks sentences based on several scores that are computed using a group of elements. While SWING alone gets a ROUGE-2 score of 0.1339, when it is used with the features proposed in this paper (time span importance, contextual time span importance, and sentence temporal coverage density), this score is improved by 4.1%.

## Conclusion

Abstractive based summarization research is a very dynamic field and has seen a whole lot of new ideas during the last years. The ability to mimic human behaviour seems to be one of its greatest strengths. As a result, automated summaries tend to be more cohesive, coherent, and less redundant.

This paper examined a set of relevant approaches, focusing on explaining their core points and using concrete examples for a better understanding of the processes.

## Acknowledgement

This research is supported by the Department of Informatics Engineering of FEUP at the University of Porto.

## References

1. Wan, X., Yang, J., Xiao, J.: Manifold-ranking based topic-focused multi-document summarization. In: IJCAI, pp. 2903-2908 (2007)
2. Li, P., Bing, L., Lam, W., Li, H., Liao, Y.: Reader-aware multi-document summarization via sparse coding. In: IJCAI (2015)
3. Cheung, J. C. K., Penn, G.: Towards robust abstractive multi-document summarization: A caseframe analysis of sententiality and domain. In ACL, pp. 1233-1242 (2013)
4. Barzilay, R., McKeown, K. R.: Sentence fusion for multidocument news summarization. Comput. Linguist., 31(3), pp. 297-328 (2005)
5. Filippova, K., Strube, M.: Sentence fusion via dependency graph compression. In EMNLP, pp. 177-185 (2008)
6. Filippova, K.: Multi-sentence compression: Finding shortest paths in word graphs. Proceedings of the International Conference on Computational Linguistics (COLING), pp. 322-330 (2010)
7. Jurafsky, D., Martin, J. H.: Speech and Language Processing: An Introduction to Natural Language Processing, Computational Linguistics, and Speech Recognition (2nd ed.). Pearson, Prentice Hall: Upper Saddle River (2008)
8. McKeown, K. R., Barzilay, R., Evans, D., Hatzivassiloglou, V., Klavans, J. L., Nenkova, A., Sable, C., Schiffman, B., Sigelman, S.: Tracking and summarizing news on a daily basis with Columbia's Newsblaster. Proceedings of Human Language Technology Conference (2002)
9. Barzilay, R., Lapata, M.: Modeling local coherence: An entity-based approach. Computational Linguistics, 34(1), pp. 1-34 (2008)
10. Genest, P.E., Lapalme, G.: Framework for abstractive summarization using text-to-text generation. Proceedings of the Workshop on Monolingual Text-To-Text Generation, pp. 64-73 (2011)
11. Genest, P.E., Lapalme, G.: Fully abstractive approach to guided summarization. In ACL, pp. 354-358 (2012)
12. Wang, L., Cardie, C.: Domain-Independent Abstract Generation for Focused Meeting Summarization. In ACL 2013, pp. 1395-1405 (2013)
13. Siddharthan, A., Nenkova, A., McKeown, K.: Information status distinctions and referring expressions: An empirical study of references to people in news summaries. Computational Linguistics, 37(4), pp. 811-842 (2011)
14. Ganeshan, K., Zhai, C., Han, J.: Opinosis: A graph-based approach to abstractive summarization of highly redundant opinions. Proceedings of the International Conference on Computational Linguistics (COLING), pp. 340-348 (2010)
15. Ng, J., Chen, Y., Kan, M., Li, Z.: Exploiting timelines to enhance multi-document summarization. In ACL, pp. 923-933 (2014)
16. Nenkova, A., Passonneau, R., McKeown, K.: The pyramid method: Incorporating human content selection variation in summarization evaluation. In ACM Trans. Speech Lang. Process., 4, May (2007)

17. Mccowan, I., Carletta, J., Kraaij, W., Ashby, S., Bourban, S., Flynn, M., Guillemot, M., Hain, T., Kadlec, J., Karaiskos, V., Kronenthal, M., Lathoud, G., Lincoln, M., Lisowska, A., Post, W., Reidsma, D., Wellner, P.: The AMIMeeting Corpus. Proceedings of the 5th International Conference on Methods and Techniques in Behavioral Research (2005)
18. Janin, A., Baron, D., Edwards, J., Ellis, D., Gelbart, D., Morgan, N., Peskin, B., Pfau, T., Shriberg, E., Stolcke, A., Wooters, C.: The ICSI Meeting Corpus. Proceedings of the ICASSP (2003)
19. Riedhammer, K., Favre, B., Hakkani-Tür, D.: Long story short – global unsupervised models for keyphrase based meeting summarization. *Speech Commun.*, 52(10), pp. 801-815 (2010)
20. Wang, L., Cardie, C.: Summarizing decisions in spoken meetings. Proceedings of the Workshop on Automatic Summarization for Differentt Genres, Media, and Languages, pp. 16-24 (2011)
21. Sandu, O., Carenini, G., Murray, G., Ng, R.: Domain adaptation to summarize human conversations. Proceedings of the 2010 Workshop on Domain Adaptation for Natural Language Processing, pp. 16-22 (2010)
22. Fernández, R., Frampton, M., Dowding, J., Adukuzyiyil, A., Ehlen, P., Peters, S.: Identifying relevant phrases to summarize decisions in spoken meetings. In INTERSPEECH, pp. 78-81 (2008)
23. Radev, D., Jing, H., Budzikowska, M.: Centroid-based summarization of multiple documents: Sentence extraction, utility-based evaluation, and user studies. In ANLP/NAACL Workshop on Summarization, pp. 21-29 (2000)
24. Ng, J., Bysani, P., Lin, Z., Kan, M., Tan, C.: Exploiting category-specific information for multi-document summarization. Proceedings of the International Conference on Computational Linguistics (COLING), pp. 2093-2108 (2012)

## Phase Conjugated Twin Waves Based Transmission in Few-mode Fibers

J. S. Tavares, L. M. Pessoa, and H. M. Salgado

INESC TEC, Campus da FEUP, Rua Dr Roberto Frias, 4200-465  
Porto, Portugal  
[{joana.s.tavares,luis.m.pessoa,hsalgado}@inesctec.pt](mailto:{joana.s.tavares,luis.m.pessoa,hsalgado}@inesctec.pt)

**Abstract.** In this paper we extend the concept of phase conjugated twin waves to spatial division multiplexed systems. Moreover, we further explore this technique by resorting to an orthogonal spatial path, rather than the orthogonal polarization, to propagate the twin wave. A numerical simulation model for nonlinear propagation was implemented by employing generalized Manakov equations for multimode fibers. System performance was assessed for different configurations and coupling regimes. Our numerical simulation results show that the PCTW technique is an effective means to overcome the nonlinear impairments arising in mode division multiplexed systems, improving performance by up to 10 dB, in the strong coupling regime. We also verified that the polarization-wise configuration is more effective at nonlinear cancellation than the mode-wise approach.

**Keywords:** fiber nonlinearity · multimode fiber · phase conjugated twin waves · space-division multiplexing

### 1 Introduction

The capacity of fiber-optic communication systems has been increased by three orders of magnitude over the last two decades [1], motivated by the demand of bandwidth-hungry data services which has been growing at a rate close to 60 per year [2]. A succession of technological breakthroughs, namely the development of low loss single mode fibers, Erbium Doped Fiber Amplifier (EDFA), Wavelength Division Multiplexing (WDM) and more recently the high spectral efficiency of Digital Signal Processing (DSP) based coherent optical transmission allowed the capacity of optical networks to cope with the exponential growth of capacity demand [3]. In the last years the scope for sending yet more information in optical networks is diminishing, since we are rapidly approaching the Shannon capacity limit [2]. This points to a SMF (Single Mode Fiber) capacity of no more than around 100Tbit/s of data, at a spectral efficiency of 10 bits/s/Hz [3] the ultimate limit being imposed by fiber nonlinearity.

In an effort to overcome this limit there have been extensive efforts attempting to break the Kerr nonlinear limit through nonlinearity compensation, either through mid-link optical phase conjugation (ML-PC) [4] or through transmitter

or receiver based digital back-propagation (BP) [5]. However, ML-PC requires the transmission link to be modified to include a phase conjugator in the middle of the link, which is impractical, whereas BP based schemes are known to be computationally complex to implement, even when the interchannel nonlinearities are known to the receiver [6].

Recently, new light was shed into this topic, when a group in Bell Labs-Alcatel Lucent proposed a novel method to perform nonlinearity mitigation [7]. The researchers proved that the nonlinear distortions experienced by a pair of mutually phase conjugated twin waves (PCTWs) are anti-correlated, so that the signal-to-signal nonlinear interactions can be cancelled by coherently superimposing both waves using a coherent receiver. This technique requires a symmetric dispersion map, which could be readily applied in a dynamic optical network environment, through the employment of electronic dispersion pre-compensation at the transmitter with a software defined optical architecture. It has been argued that the limit imposed by these single-mode transport systems, on the longer run, may still lead to a transport capacity shortage [8]. The solution of introducing multiple systems over parallel fibers suggests that transmission costs and power consumption scales linearly, which will likely be economically impractical [3]. The research community has generally agreed that the solution to the capacity growth is to employ spatial division multiplexing (SDM) [1–3] [8–10]. It has been shown that from an economical and energy consumption perspective the parallel transport solutions based on SDM are more attractive than the single-mode capacity scaling approach adopted so far [10]. This will allow for the reduction of the cost-per-bit since SDM provides enormous potential to facilitate integration [3,9]. However, similarly to single-mode fiber based modern telecommunication systems, the nonlinear penalties will eventually become the ultimate limiting factor in SDM systems, resulting from crosstalk effects in multimode or multicore fibers, which generate intramodal and intermodal nonlinearities.

In this paper we investigate the concept of PCTW as a means of overcoming the nonlinear impairments arising in SDM systems, in a practical and sustainable way, paving the way for optical transmission capacities beyond next-generation systems. Specifically, we investigate the application of the PCTW technique on three different SDM scenarios: 1) propagation of each pair of PCTWs on different spatial modes; 2) a single polarization (SP) generalization of PCTW that consists of using an orthogonal dimension (space) to transmit the twin wave; 3) and a dual polarization (DP) generalization of PCTW, assuming that the signal and its conjugated twin are polarization division multiplexed (PDM) signals propagating on orthogonal dimensions.

The remainder of this paper is organized as follows: in Section 2 we describe the principles of the single mode PCTW. In Section 2.1 we describe the proposed multimode PCTW scenarios. In Section 3 we present an overview of the numerical simulation model including simulation parameters. In Section 4 the obtained numerical simulation results are presented. Finally, conclusions are given in Section 5.

## 2 PCTW Principles

Single mode (SM)-PCTW-based transmission consists of co-propagating an optical signal and its complex conjugate on two orthogonal polarizations of the same optical carrier [7]. It has been demonstrated that if the dispersion map of the link is symmetric the nonlinear distortions experienced by the pair of twin waves are anti-correlated and the signal-to-signal nonlinear interactions are mitigated at the receiver after coherent superposition of the received twin waves. The symmetric dispersion map can be obtained by performing electronic dispersion pre compensation. The schematic of a SM-PCTW transmission link is shown in Fig. 1.

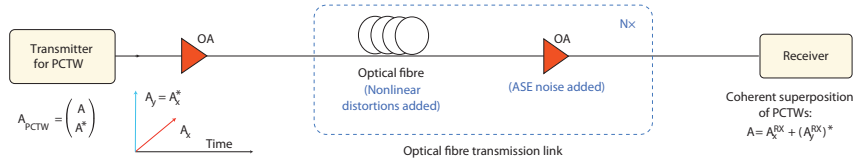


**Fig. 1.** SM-PCTW transmission link schematic (adapted from [7])

In the case of single mode fibers, the well-known Manakov-polarization mode dispersion (PMD) equations [11–13] can be used to describe the nonlinear propagation of PDM signals, as in Eq. (1).

$$\frac{\partial A_{pctw}}{\partial z} + i \frac{\beta_2}{2} \frac{\partial^2 A_{pctw}}{\partial t^2} = i \frac{8}{9} \gamma (|A_x|^2 + |A_y|^2) A_{pctw}, \quad (1)$$

where  $\beta_2$  is the group-velocity dispersion (GVD) and  $\gamma$  is the Kerr nonlinear coefficient. In this configuration  $A_{pctw}$  is the PDM signal containing the transmitted pair of PCTWs, i.e. two orthogonal polarization components, where the x-polarization is the transmitted optical field and the y-polarization is the complex conjugate of the x-polarization, as follows

$$A_{pctw} = (A_x, A_y)^T, \quad (2)$$

where

$$A_x = A \quad (3)$$

$$A_y = A_x^*. \quad (4)$$

At the receiver side, the original signal is recovered without nonlinear distortions after coherent superposition of the received signals, by employing

$$A_x^{RX} + (A_y^{RX})^* = 2A. \quad (5)$$

However, this technique incurs a spectral efficiency loss of one half, as denoted by Eq. (5).

## 2.1 SDM-PCTW scenarios

In this work we investigate three different multimode PCTW scenarios, which are summarized on Table 1, considering four spatial modes.

In the first scenario, which we call PDM-wise PCTW, each pair of PCTWs is propagated on a single spatial mode and different pairs are sent on four distinct spatial modes. This is a natural extension of the previous single-mode PCTW.

A different approach has been proposed in [14]. Instead of using an orthogonal polarization to transmit the complex conjugate of a signal as in the original PCTW concept, the twin wave is propagated on a different orthogonal dimension (i.e. space). It has been argued that this technique can be particularly beneficial to ensure secure communications [7]. This is described here as mode-wise SP-PCTW.

Additionally, Liu et al. also proposed the extension of the previous case to vector waves [14]. In this scenario the signal and its conjugated twin are PDM signals (consisting of two independent polarization components), propagating on orthogonal dimensions (i.e. space). This is described here as mode-wise DP-PCTW. However, no performance results have been given regarding the last two proposed scenarios.

**Table 1.** Overview of different SDM-PCTW scenarios

	PDM-wise PCTW	Mode-wise SP-PCTW	Mode-wise DP-PCTW
LP01			
LP11a			
LP02			
LP21a			

Eq. (1) cannot be used for multimode fibers since it does not include the intermodal nonlinear effects. However, a new set of Manakov equations which describe nonlinear propagation in multimode fibers has been derived in [8], where the authors also addressed a complex problem, which is the coupling strength between spatial modes, that can vary for different mode pairs, by considering

two extreme cases. In the weak coupling regime, linear coupling between spatial modes is neglected, while in the strong coupling regime it is assumed that all modes are strongly coupled. In both coupling regimes the two orthogonal polarization components are strongly coupled due to birefringence fluctuations. These Manakov equations include intramodal and intermodal nonlinear effects, random polarization birefringence, chromatic dispersion, differential mode group delay (DMGD) and fiber losses.

In the weak coupling regime [8], the nonlinear propagation in a multimode fiber is given by:

$$\begin{aligned} \frac{\partial \bar{A}_p}{\partial z} + \langle \delta \beta_{0p} \rangle \bar{A}_p + \langle \delta \beta_{1p} \rangle \frac{\partial \bar{A}_p}{\partial t} + i \frac{\beta_{2p}}{2} \frac{\partial^2 \bar{A}_p}{\partial t^2} \\ = i\gamma \left( f_{pppp} \frac{8}{9} |\bar{A}_p|^2 + \sum_{m \neq p} f_{mmpp} \frac{4}{3} |\bar{A}_m|^2 \right) \bar{A}_p, \end{aligned} \quad (6)$$

where  $\gamma$  is the Kerr nonlinear coefficient,  $\langle \delta \beta_{0p} \rangle$  is the propagation constant,  $\langle \delta \beta_{1p} \rangle$  is the DMGD and  $\beta_{2p}$  is the GVD. The nonlinear coefficient  $f_{lmnp}$  provides a relative weight among the nonlinear terms between the spatial modes and is defined by:

$$f_{lmnp} = \frac{A_1^{eff}}{(I_l I_m I_n I_p)^{1/2}} \iint F_l^* F_m F_n F_p^* dx dy, \quad (7)$$

where  $I_l, I_m, I_n$  and  $I_p$  represent the constants of normalization for the modal fields  $F_l, F_m, F_n$  and  $F_p$ .  $A_1^{eff}$  is the effective area of the fundamental mode, given by Eq. (8).

$$A_{eff} = \frac{\left( \iint |F(x, y)|^2 dx dy \right)^2}{\iint |F(x, y)|^4 dx dy} \quad (8)$$

In the strong coupling regime [8], we have

$$\frac{\partial \bar{A}}{\partial z} + i \frac{\bar{\beta}_2}{2} \frac{\partial^2 \bar{A}}{\partial t^2} = i\gamma\kappa |\bar{A}|^2 |\bar{A}|, \quad (9)$$

where the nonlinear coefficient  $\kappa$  is given by Eq. (10), where  $M$  is the number of spatial modes.

$$\kappa = \sum_{k \leq l}^M \frac{32}{2^{\delta_{kl}}} \frac{f_{kkll}}{6M(2M+1)} \quad (10)$$

### 3 Numerical Simulations

Our numerical simulations considered 32-Gbaud PCTW-QPSK signals, each signal consisting of  $2^{13}$  modulated symbols. The signals were filtered by a squared root raised cosine (SRRC) filter with a 0.1 roll-off factor and were pre-compensated for half of the fiber link dispersion.

The simulations were based on the standard symmetric split-step Fourier method [15] to solve the generalized Manakov equations for multimode fibers [8], using a simulation step of 1000 m. The transmission line consists of 10 100-km fiber spans, each span being followed by an erbium-doped fiber amplifier (EDFA) that compensates for the span losses. ASE (amplified spontaneous emission) noise was also added by each EDFA, with a noise figure of 5 dB. We considered a step-index few-mode fiber (FMF), with a core radius of 6  $\mu\text{m}$  and a fiber loss of 0.2 dB/km. The nonlinear coefficient, numerical aperture, and V parameter at 1550 nm used were  $1.4 \text{ W}^{-1}\text{km}^{-1}$ , 0.2, and 5, respectively. With this configuration six spatial modes are supported by the fiber (LP01, LP11a, LP11b, LP02, LP21a, and LP21b). Dispersion and differential mode group delay (DMGD) calculated for each mode are presented on Table 2 [16–20].

At the receiver side, the received signals were post-dispersion compensated for the rest of the transmission link, followed by SRRC filtering. After phase estimation, the received signals were coherently super-positioned, accordingly to the three configurations presented on Table 1. System performance was evaluated by calculating the average Q<sup>2</sup>-factor of the received signals after 1000 km fiber transmission, before and after superposition, and for different launch powers. Furthermore, weak coupling and strong coupling regimes are also evaluated for each case, using the corresponding Manakov equations as proposed in [8].

**Table 2.** Fiber dispersion and differential mode group delay for different spatial modes

	<i>LP<sub>01</sub></i>	<i>LP<sub>11</sub></i>	<i>LP<sub>02</sub></i>	<i>LP<sub>21</sub></i>
DMGD (ns/km)	0	6.5	9.9	12.4
D (ps/nm/km)	25.1	27.4	-2.5	20.9

### 4 Numerical Simulation Results

In this section we present the results of the performed numerical simulations considering the three proposed scenarios. In all our numerical simulations, multimode PCTW transmission consists of co-propagating four spatial modes (i.e. LP01, LP11a, LP02, and LP21a).

The attained results are presented in Fig. 2 to 7, regarding the weak and strong coupling regime.

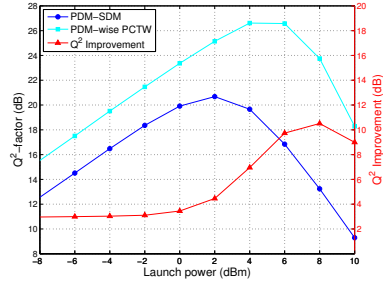


**Fig. 2.** PDM-wise PCTW in strong coupling

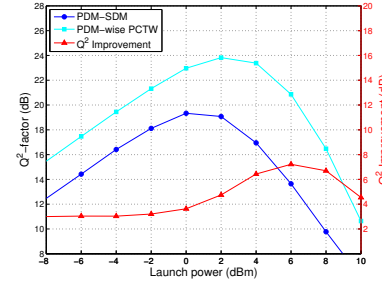


**Fig. 3.** PDM-wise PCTW in weak coupling

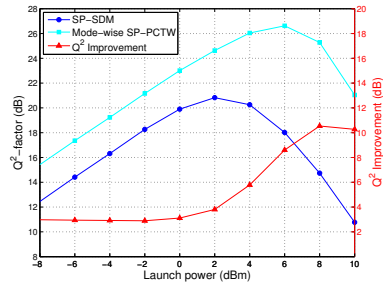


**Fig. 4.** Mode-wise SP-PCTW in strong coupling

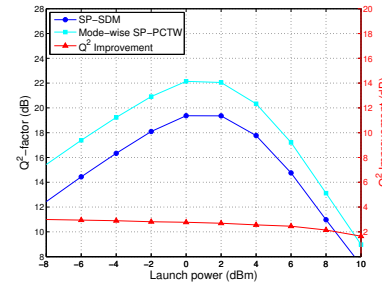


**Fig. 5.** Mode-wise SP-PCTW in weak coupling

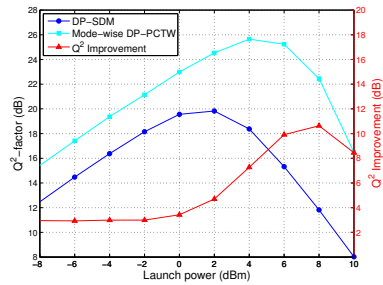


**Fig. 6.** Mode-wise DP-PCTW in strong coupling

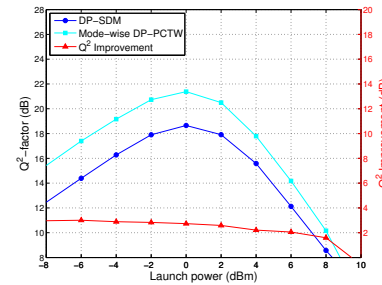


**Fig. 7.** Mode-wise DP-PCTW in weak coupling

For each case we present the average  $Q^2$ -factor calculated before and after coherent superposition, i.e., for the SDM (circles) and PCTW cases (squares), respectively. The right hand axis shows the  $Q^2$ -factor improvement (triangles).

These results show that in the strong coupling regime a performance improvement of  $\sim 10$  dB is achieved at 8 dBm of launched power, for all three scenarios. In the weak coupling regime the highest  $Q^2$ -improvement is  $\sim 7$  dB at 6 dBm in the first scenario and less than 3 dB in the other two.

Fig. 8 shows an overview of the results obtained before coherent superposition of the received signals (i.e. SDM signals), as well as the single mode PDM case. We verify that multimode propagation in the strong coupling regime performs better than in the weak coupling regime and also that system performance for multimode fibers is better than the single mode case, as expected [8].

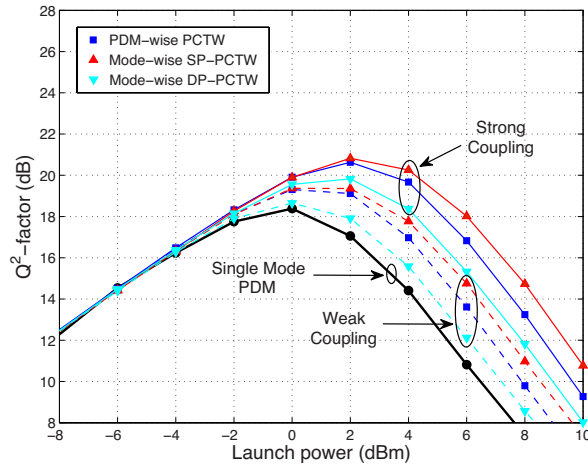


**Fig. 8.** Overview of the results obtained before coherent superposition of the received signals

Fig. 9 depicts the results after coherent superposition of the received twin waves and the single mode PCTW case. We verify that in the strong coupling regime, a performance improvement of  $\sim 10$  dB is achieved for PDM-wise PCTW and mode-wise SP-PCTW, and  $\sim 8$  dB for mode-wise DP-PCTW, compared to the single mode PCTW case. Regarding the weak coupling regime, performance improvement for PDM-wise PCTW is  $\sim 4$  dB, mode-wise SP-PCTW shows no improvement compared to the original PCTW, and lastly, mode-wise DP-PCTW shows a performance degradation of  $\sim 3$  dB.

The nonlinear distortions in a pair of PCTWs are anti correlated, therefore nonlinear distortion cancellation occurs after coherent superposition of the re-

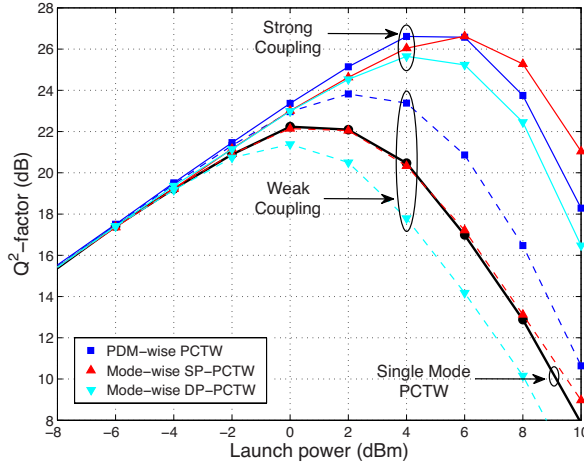


**Fig. 9.** Overview of the results obtained after coherent superposition of the received signals

ceived signals. When resorting to an orthogonal dimension rather than polarization, the same principle applies [7]. However, PDM-wise and mode-wise PCTW configurations presented different results. PDM-wise PCTW shows better results in both coupling regimes, due to the relatively strong coupling between polarization components. Mode-wise PCTW shows poorer performance, especially in the weak coupling regime. Since the phase conjugation is done resorting to orthogonal spatial paths, the benefit from this technique is diminished.

## 5 Conclusions

The performance of SDM systems in different PCTW scenarios and coupling regimes has been assessed numerically. The proposed multimode PCTW configurations show a performance improvement of up to 10 dB in the strong coupling regime and up to 4 dB in the weak coupling regime, compared to the single mode PCTW case. Best performance is achieved in the strong coupling regime in all scenarios. The PDM-wise case presented improved results due to the advantage from the relative strong coupling between polarization components, while the mode-wise configurations revealed inferior performance since the twinning is done resorting to different spatial modes, hence the benefit from this technique is diminished. Also, optimal launch power is increased in most cases. These results demonstrate the effectiveness of the PCTW within SDM systems, namely for FMF based propagation.

Additionally, this subject could be further explored by performing similar assessment regarding multicore fibers and also by studying spectrally efficient PCTW techniques in multimode and multicore fibers.

### Acknowledgments

This work was supported by FCT - Fundação para a Ciência e Tecnologia (Portuguese Foundation for Science and Technology) under the project TWAVE (EXPL/EEI-TEL/1748/2013) and in the framework of programme POCTI/FEDER with grant REEQ/1272/EEI/2005.

### References

1. R. Essiambre, A. Mecozzi, Capacity Limits in Single Mode Fiber and Scaling for Spatial Multiplexing, Optical Fiber Communication Conference (2012)
2. P. J. Winzer, G. J. Foschini, MIMO Capacities and Outage Probabilities in Spatially Multiplexed Optical Transport Systems, Optics Express, 19, p. 16680-16696 (2011)
3. D. Richardson, J. Fini, L. Nelson, Space-Division Multiplexing in Optical Fibres, Nature Photonics, 7, p. 354-362 (2013)
4. C. Xi, L. Xiang, S. Chandrasekhar, B. Zhu, R. W. Tkach, Experimental Demonstration of Fiber Nonlinearity Mitigation Using Digital Phase Conjugation, Optical Fiber Communication Conference and Exposition and the National Fiber Optic Engineers Conference (2012)
5. E. Ip, J. M. Kahn, Compensation of Dispersion and Nonlinear Impairments Using Digital Backpropagation, Journal of Lightwave Technology, 26, p. 3416-3425 (2008)
6. D. Rafique, A. Ellis, Scaling the Advantages of Intra-channel Nonlinearity Compensation in Future Flexible Optical Networks, European Conference and Exhibition on Optical Communication (2012)
7. X. Liu, A. Chraplyvy, P. Winzer, R. Tkach, S. Chandrasekhar, Phase-conjugated Twin Waves for Communication Beyond the Kerr Nonlinearity Limit, Nature Photonics, 7, p. 560-568 (2013)
8. S. Mumtaz, R. Essiambre, G. P. Agrawal, Nonlinear Propagation in Multimode and Multicore Fibers: Generalization of the Manakov Equations, Journal of Lightwave Technology, 31, p. 398-406 (2013)
9. P. J. Winzer, Challenges and Evolution of Optical Transport Networks, European Conference on Optical Communication (2010)
10. P. J. Winzer, Energy-efficient Optical Transport Capacity Scaling Through Spatial Multiplexing, Photonics Technology Letters, IEEE, 23, p. 851-853 (2011)
11. D. Marcuse, C. R. Menyuk, P. K. A. Wai, Application of the Manakov-PMD Equation to Studies of Signal Propagation in Optical Fibers with Randomly Varying Birefringence, Journal of Lightwave Technology, 15, p. 1735-1746 (1997)
12. P. Wai, C. Menyuk, Polarization Mode Dispersion, Decorrelation, and Diffusion in Optical Fibers with Randomly Varying Birefringence, Journal of Lightwave Technology, 14, p. 148-157 (1996)
13. P. Wai, C. R. Menyuk, H. Chen, Stability of Solitons in Randomly Varying Birefringent Fibers, Optics Letters, 16, p. 1231-1233 (1991)

14. X. Liu, S. Chandrasekhar, P. Winzer, R. Tkach, A. Chraplyvy, Fiber-Nonlinearity-Tolerant Superchannel Transmission via Nonlinear Noise Squeezing and Generalized Phase-Conjugated Twin Waves, *Journal of Lightwave Technology*, 32, p. 766-775 (2014)
15. G. P. Agrawal, *Nonlinear Fiber Optics*, Academic Press (2007)
16. D. Gloge, "Dispersion in weakly guiding fibers," *Applied Optics*, vol. 10, pp. 2442-2445 (1971)
17. D. Gloge, "Weakly guiding fibers," *Applied Optics*, vol. 10, pp. 2252-2258 (1971)
18. M. J. Adams, *An introduction to optical waveguides*: UMI Books on Demand (1981)
19. A. Ghatak and K. Thyagarajan, *Introduction to fiber optics*: Cambridge university press (1998)
20. K. Iizuka, *Elements of Photonics* vol. 2 (2002)

# Author Index

<b>A</b>	
Aguiar, Ana	73
Akingbade, Kayode F.	39
Almeida, Eduardo Nuno	1
Azuaje, Orangel	27
<b>B</b>	
Busari, Sherif A.	39
Brandão, Pedro	73
<b>C</b>	
Costa, Carlos M.	95
Costa, Valter	49
<b>D</b>	
Dias, Artur	151
Dias, João	1
Dunmoye, Abibat F.	39
<b>F</b>	
Faria, João Pascal	61
<b>G</b>	
Guimaraes, Fernando P.	85
<b>L</b>	
Leitão, Paulo	151
Lima, Bruno	61
Lima, Emanuel	73
<b>M</b>	
Martins, Celestino S.	85
Miguel Silva Antunes, Hugo	13
<b>N</b>	
Neto, Luis	107
Neves Dos Santos, Filipe	139
<b>O</b>	
Ogodo, Stephen	117
<b>P</b>	
Pessoa, L. M.	197
Pilastri, Andre	127
Pinto, Armando N.	85
Pinto, Rui	139
<b>Q</b>	
Queiroz, Jonas	151
<b>R</b>	
Rehman, Asad Ur	163
<b>S</b>	
Salgado, H. M.	197

Sarmento, Rui	175
Silva, Jaime	187
Sousa, Armando	139
<b>T</b>	
Tavares, J. S.	197
Tavares, João Manuel R. S.	127

ISBN 9789727521968



9789727521968